University of Southampton

Faculty of Medicine

Clinical Experimental Sciences

Determinants and Effects of Collagen Cross-linking Enzyme Dysregulation in Idiopathic Pulmonary Fibrosis

by

Christopher James Brereton

Thesis for the degree of Doctor of Philosophy

July 2021

University of Southampton

Abstract

Faculty of Medicine

Clinical Experimental Sciences

Doctor of Philosophy

Determinants and Effects of Collagen Cross-linking Enzyme Dysregulation in Idiopathic Pulmonary Fibrosis

by

Christopher James Brereton

Progressive accumulation of abnormal extracellular matrix (ECM) is a key pathologic event in idiopathic pulmonary fibrosis (IPF). Repetitive micro-injuries to a genetically susceptible alveolar epithelium are thought to incite an abnormal wound healing response, propagating fibrogenesis through the induction of pro-fibrotic signals of which TGFβ is considered the prototype. Beyond ECM deposition, alterations to collagen nanostructure such as increased pyridinoline cross-linking are critical to the loss of ECM compliance in IPF, resulting from upregulation of collagen cross-linking enzymes such as lysyl hydroxylase 2 (PLOD2) and the lysyl oxidase-like (LOXL) family.

It was hypothesised that pathological remodelling and increased tissue stiffness in IPF involves aberrant expression of these collagen cross-linking enzymes, caused by dysregulation of core upstream signalling pathways. The aims of this study were therefore to identify the cellular provenance of key 'bone-type' collagen cross-linking enzymes, the upstream regulatory pathways which promote their expression, and the biomechanical consequences of their dysregulation.

Through human tissue analyses integrating regionally selective RNA sequencing *LOXL2* was established as the LOX(L) enzyme with greatest expression in IPF fibroblastic foci, and a strong correlation between *LOXL2* and *PLOD2* expression was observed, with co-localisation identified through *in-situ* mRNA hybridisation. Hypoxia Inducible Factor (HIF) pathway stabilisation was found to be a potent inducer of these 'bone-type' collagen cross-linking enzymes using 2D *in vitro* experiments, and exhibited synergistic effects with TGFβ signalling. Yet HIF pathways, rather than TGFβ signalling, disproportionately induced collagen cross-linking expression compared to collagen fibrillogenesis. The presence of HIF pathway activation within IPF tissue was confirmed through immunohistochemical analysis, correlating to areas of *PLOD2* and *LOXL2* mRNA expression. Using an *in vitro* 3D fibroblastic focus model, HIF pathway stabilisation was observed to profoundly alter collagen structure-function, with increases in pyridinoline collagen cross-linking and matrix stiffness, and a reduction in collagen fibril diameter, that were comparable to changes seen within IPF tissue. Gene silencing of *HIF1/2α* or *LOXL2*, and catalytic inhibition of LOX(L) activity, was capable of modulating the pathogenetic HIF-mediated changes to ECM stiffness, suggesting these pathways may offer novel therapeutic targets.

In summary HIF pathway stabilisation is a key regulatory promoter of 'bone-type' collagen cross-linking and, in conjunction with TGFβ signalling, may act as a 'second-hit' insult to drive pathological remodelling of ECM within the IPF lung. Therapeutic applications which target HIF pathways could normalise these matrix changes and prevent progressive fibrosis.

Table of Contents

Table of Tables

Table of Figures

Research Thesis: Declaration of Authorship

Print name: Christopher James Brereton

Title of thesis: Determinants and Effects of Collagen Cross-linking Enzyme Dysregulation in Idiopathic Pulmonary Fibrosis

I declare that this thesis and the work presented in it are my own and has been generated by me as the result of my own original research.

I confirm that:

1. This work was done wholly or mainly while in candidature for a research degree at this University;
2. Where any part of this thesis has previously been submitted for a degree or any other qualification at this University or any other institution, this has been clearly stated;
3. Where I have consulted the published work of others, this is always clearly attributed;
4. Where I have quoted from the work of others, the source is always given. With the exception of such quotations, this thesis is entirely my own work;
5. I have acknowledged all main sources of help;
6. Where the thesis is based on work done by myself jointly with others, I have made clear exactly what was done by others and what I have contributed myself;
7. Parts of this work have been published as:

Hypoxia-inducible factor pathway activation promotes bone-type collagen cross-linking in Idiopathic Pulmonary Fibrosis. Christopher J Brereton, Liudi Yao, Joseph Bell, Franco Conforti, Aiman Alzetani, Aurelie Fabre, Ben G Marshall, Luca Richeldi, Donna E Davies, Yihua Wang, Mark G Jones. European Respiratory Journal Sep 2019, 54 (suppl 63) PA2424; DOI: 10.1183/13993003.congress-2019.PA2424

HIF pathway activation is a core regulator of collagen structure-function in lung fibrosis. Christopher J Brereton, Robert Ridley, Franco Conforti, Liudi Yao, Aiman Alzetani, Ben Marshall, Sophie V Fletcher, Luca Richeldi, Yihua Wang, Donna E Davies, Mark G Jones. European Respiratory Journal Sep 2020, 56 (suppl 64) 4323; DOI: 10.1183/13993003.congress-2020.4323

Signature: ..... Date: 14/07/21

Acknowledgements

I would like to acknowledge the friends, family and colleagues who supported me in every step of my Southampton journey.

Within the Brooke lab I am indebted to Rob Ridley, Lizzie Davies and Joe Bell, who assisted me with my experiments and provided insight and camaraderie through the many highs and lows of experimental research.

In the School of Biomedical Science I would like to deeply thank Yihua Wang and Liudi Yao for lending me their time, resources and knowledge in the science and art of studying HIF pathways.

In the Biomedical Research Centre I would like to acknowledge the support of Tim Wallis, Kat Pontoppidan and the entire research nursing team, who made the difficult balance of clinical demands and laboratory research not just tolerable, but a rewarding and memorable experience.

Finally, to my parents Jeff and Narelle and parents-in-law Ben and Janet, who were pillars of support throughout our entire UK adventure.

I dedicate this thesis to the people who made everything possible:

To Donna and Mark, for your wisdom, guidance and unwavering dedication.

To Sophie, for your mentorship, as well as your untiring and resolute support.

To Franco, for your generosity and selfless commitment to my training

To Lara, for your boundless love and patience

Abbreviations

4-OHT.....4-hydroxytamoxifen

αSMA .....Alpha Smooth Muscle Actin

A2.....Phospholipase A2

ABC.....Avidin Biotin Complex

ACTA2 .....Actin Alpha 2

AGE .....Advanced Glycation End Products

AKAP13 .....A-Kinase Anchoring Protein 13

APS.....Ammonium persulfate

AT1.....Alveolar Type 1

AT2.....Alveolar Type 2

BAL.....Bronchoalveolar Lavage

BCA.....Bicinchoninic Acid

BSA.....Bovine Serum Albumin

bHLH .....basic Helix-Loop-Helix

C1.....Channel 1

C2.....Channel 2

Ca9 .....Carbonic Anhydrase 9

CAS9.....CRISPR-Associated 9

CFA.....Cryptogenic Fibrosing Alveolitis

CREB.....Cyclic-AMP Response Element Binding

CRISPR.....Clustered Regularly Interspaced Short Palindromic Repeats

Ct.....Cycle threshold

CT .....Computed Tomography

DAB .....Tetrahydrochloride 3,3'-Diaminobenzidine

dapB.....4-hydroxy-tetrahydrodipicolinate reductase

DAPI .....4',6-diamidino-2-phenylindole

Abbreviations

dH_2O ..... de-ionised H_2O

DHLNL..... Dihydroxylysinonorleucine

DMAB ..... 4-(dimethylamino)benzaldehyde

DMEM ..... Dulbecco's Modified Eagles Medium

DMOG ..... Dimethyloxalylglycine

DMSO ..... Dimethylsulfoxide

DNA ..... Deoxyribonucleic Acid

dNTP..... Deoxynucleoside Triphosphate

DPD ..... Deoxypyridinoline (lysyl pyridinoline)

dsDNA ..... Double Stranded DNA

DSP ..... Desmoplakin

Dt..... Deoxythymidylic

ECM ..... Extracellular Matrix

EGF ..... Epidermal Growth Factor

EGFR ..... Epidermal Growth Factor Receptor

EMT ..... Epithelial Mesenchymal Transition

FBS..... Foetal Bovine Serum

FDA ..... Food and Drug Administration (US)

FFPE ..... Formalin-Fixed Paraffin-Embedded

FIH ..... Factor Inhibiting HIF

FGF ..... Fibroblast Growth Factor

FVC ..... Forced Vital Capacity

GAPDH..... Glyceraldehyde 3-phosphate dehydrogenase

gDNA ..... genomic DNA

GOI ..... Gene of Interest

GTP ..... Guanosine Triphosphate

HAS..... Hyaluronan Synthase

H&E ..... Haematoxylin and Eosin

HBSS.....Hank's Balanced Salt Solution

HEPES.....4-(2-hydroxyethyl)-1-piperazineethanesulfonic Acid

HHL .....Histidinohydroxylysinorleucine

HIF.....Hypoxia Inducible Factor

HKG .....House Keeping Gene

HLNL.....Hydroxylysinonorleucine

HRCT .....High Resolution CT

HRE.....Hypoxia Response Element

HRP .....Horseradish Peroxidase

HRU .....Histochemical Research Unit

hTERT .....Human Telomerase Reverse Transcriptase

IIP .....Idiopathic Interstitial Pneumonia

IL .....Interleukin

ILA .....Interstitial Lung Abnormality

ILD .....Interstitial Lung Disease

IPF .....Idiopathic Pulmonary Fibrosis

IOX2 .....N-[[1,2-Dihydro-4-hydroxy-2-oxo-1-(phenylmethyl)-3-quinolinyl]carbonyl]-glycine

JNK .....c-Jun N-terminal kinases

kPa .....kilopascal

LAP .....Latency Associated Peptide

LCMD.....Laser Capture Microdissection

LH .....Lysyl Hydroxylase

LNL .....Lysinorleucine

LT .....Large-tumour

LOX.....Lysyl Oxidase

LOX(L).....Lysyl Oxidase-Like

LTBP .....Latent TGFβ Binding Peptide

LTQ ..... Lysyl Tyrosyl Quinone

LW1 ..... long wave 1

MAP..... Mitogen Activated Protein

MDT..... Multidisciplinary Team

M-MLV..... Moloney Murine Leukaemia Virus

MMP..... Matrix Metalloproteinases

NAC ..... N-acetylcysteine

NaP ..... Sodium Pyruvate

NBCS..... New Born Calf Serum

NEAA ..... Non-Essential Amino Acids

ODDD ..... Oxygen dependent degradation domain

OTU ..... Operational Taxonomic Unit

PAF ..... Population Attributable Fraction

PARN ..... Poly(A)-Specific Ribonuclease

PAS ..... Per-Arnt-Sim

PBS ..... Phosphate-Buffered Saline

PBS/T ..... PBS with 0.01% Tween-20

PCR ..... Polymerase chain reaction

PDGF..... Platelet Derived Growth Factor

PFA ..... Paraformaldehyde

PFKFB3..... 6-phosphofructo-2-kinase/fructose-2,6-biphosphatase 3

PHD ..... Prolyl Hydroxylase

PLIN2 ..... Perilipin 2

PLOD2..... Procollagen-lysine, 2-Oxoglutarate 5-Dioxygenase 2

PO_2 ..... Partial Pressure of Oxygen

POLR2A..... RNA Polymerase II Subunit A

PPIB ..... Peptidyl-prolyl Cis-trans Isomerase B

ProSP-C..... Pro-Surfactant Protein C

PSG.....Penicillin Streptomycin Glutamate

P-Smad.....Phosphorylated-Smad

PVDF.....Polyvinylidene Difluoride

PYD.....Pyridinoline (Hydroxylysyl Pyridinoline)

qPCR.....quantitative Polymerase Chain Reaction

RAS.....Rat Sarcoma

RNA.....Ribonucleic Acid

ROCK.....Rho Kinase

ROS.....Reactive Oxygen Species

RTEL1.....Regulator of Telomere Elongation Helicase 1

RTqPCR.....Real time quantitative PCR

SFTPC.....Surfactant Protein C

siRNA.....short-interfering RNA

SNP.....Single Nucleotide Polymorphism

TBS.....Tris-Buffered Saline

TBS/T.....TBS with 0.01% Tween-20

TEMED.....Tetramethylethylenediamine

TERC.....Telomerase RNA Component

TERT.....Telomerase Reverse Transcriptase

TKI.....Tyrosine Kinase Inhibitor

TLCO.....Transfer Capacity of Carbon Monoxide

TG2.....Transglutaminase 2

TGFβ.....Transforming Growth Factor Beta

TGFβR.....Transforming Growth Factor Beta Receptor

TNFα.....Tumour Necrosis Factor Alpha

TRIS.....Trisaminomethane

TRITC.....Tetramethylrhodamine

UBC.....Ubiquitin

UIP ..... Usual Interstitial Pneumonia

VEGF ..... Vascular Endothelial Growth Factor

VHL ..... Von Hippel-Lindau

Wnt ..... Wingless/integration site

YAP ..... Yes-associated Protein

ZEB ..... Zinc-finger enhancer binding

Chapter 1 Introduction

1.1 A clinical overview of idiopathic pulmonary fibrosis

1.1.1 Definition and incidence

The interstitial lung diseases (ILDs) are a broad group of disorders characterised by cellular infiltration and proliferation within the pulmonary interstitium. Changes in the quantity and quality of extracellular matrix (ECM), the non-cellular portion of tissue comprised predominantly of proteins, polysaccharides and water, is a critical component of many ILDs. Fibrosis is the accumulation of excessive and often abnormal ECM within tissue, often as a wound healing response to injury. ILDs may occur with or without subsequent fibrosis and by definition are not the result of either infection or malignancy[1].

On a practical level, ILD is an umbrella term which encompasses specific diseases of the lung parenchyma that can be subcategorised based on their aetiology, pathophysiology, clinical features and outcomes **(Figure 1.1)**. Idiopathic interstitial pneumonias (IIPs) are one such category, historically delineated by the lack of a clearly identifiable or wholly attributable inciting agent. IIPs are further stratified by clinical acuity and have specific clinical, radiographic and histopathologic patterns, with a multidisciplinary approach considered the gold standard for diagnosis[2,3]. ILDs which do not meet any of the diagnostic criteria, either due to insufficient, discordant or indeterminate information, are deemed unclassifiable[2].

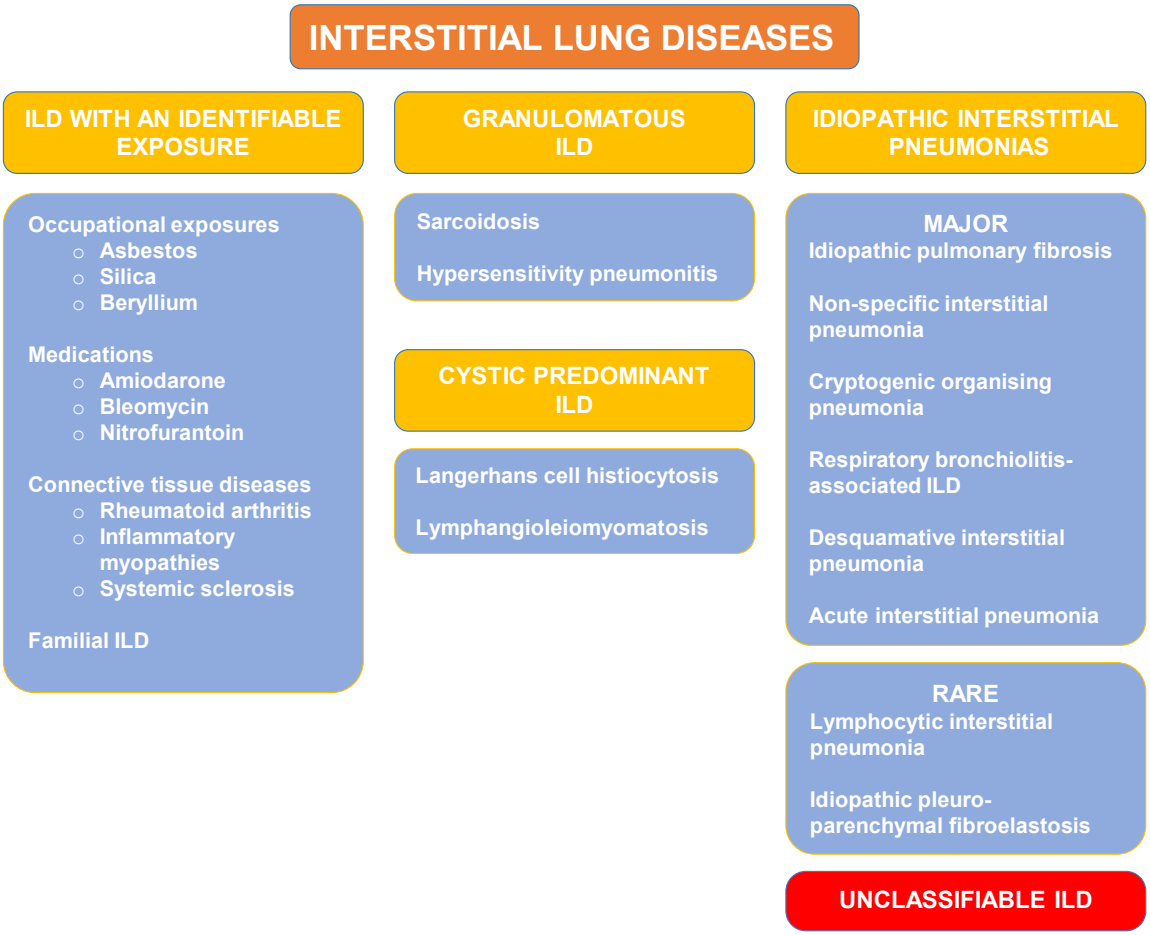

Figure 1.1: Classification of interstitial lung diseases. A commonly used system for categorising ILDs based broadly on a combination of aetiology, clinical, radiologic and pathologic findings[2,3].

Idiopathic pulmonary fibrosis (IPF) is the prototypical progressive fibrotic ILD, characterised by a usual interstitial pneumonia (UIP) pattern of fibrosis either on radiology or histopathology, in the absence of an identifiable underlying cause[4]. While IPF is a diagnosis of exclusion the diagnostic criteria are still rigidly applied, an important point which differentiates this disease from a large, heterogeneous cohort of patients who do not meet any specific disease criteria and are subsequently labelled "unclassifiable ILD".

While it is considered a rare lung disease, there are over 30,000 people with IPF in the UK alone, with roughly 6000 new IPF diagnoses made each year[5]. Indeed, with estimates of between 4.6 and 8.65 new diagnoses per 100 000 people per year the UK has one of the highest incidence rates of IPF within Europe[6]. Furthermore the number of new diagnoses appears to have risen over time[7]. It should be noted however that any comparison of incidence either temporally or internationally is limited by variances in detection rates and methods of identifying IPF cohorts.

1.1.2 The evolving terminology around IPF

IPF is a relatively modern clinical diagnostic label which has enabled significant progress over the past two decades in mechanistic studies exploring pulmonary fibrosis pathophysiology. Prior to this evolution in disease terminology, patients with what we now consider IPF were cohorted with a multitude of other ILDs, leading to misleading findings that distracted from the true nature of the fibrotic process.

While terms such as “chronic interstitial pneumonia” and “diffuse interstitial fibrosis” have been reported as far back as the late 19th and early 20th century, IPF did not emerge as an established entity until the 1960s[8]. However the diagnosis was broadly applied to a variety of cases including paediatric and acute pathologies, and used interchangeably in Europe and other regions with the label “cryptogenic fibrosing alveolitis” (CFA). Further developments such as a pathological classification of UIP by Averill Liebow in 1968 and the introduction of chest computed tomography (CT) in the 1970s and 1980s led to refinement of the IPF/CFA criteria. IPF became the preferred nomenclature over CFA in the new millennium, possibly driven by a growing consensus that fibrosis, rather than inflammation, was the key underlying mechanism of disease.

More recently the Fleischner society revised the high resolution (HR)CT diagnostic criteria for UIP in a 2018 white paper[9]. A key recommended change was to make a working diagnosis of IPF in the absence of honeycombing (provided both the radiology and clinical picture were otherwise in keeping with IPF). Reflecting this softened stance, the intermediate diagnostic category of “possible UIP” was replaced by the term “probable UIP”. While the 2018 ATS/ERS/JRS/ALAT Clinical Practice Guidelines adopted the changes in nomenclature, they grouped the category with “indeterminate for UIP” and “alternative diagnosis” and maintained a conditional (very low quality of evidence) recommendation for surgical lung biopsy in these instances[4].

Debate continues on the appropriateness of the current IPF definition, with some authors describing the classification of IPF as a “moving target”[10]. However despite ongoing desires to either further sub-stratify, or conversely, to group ILDs together, the crystallisation of our current definition for IPF has enabled greater coherence in our investigation of the underlying pathophysiological mechanisms in this disease. Advancements in our understanding may filter back into diagnostic guidelines, as well as aid in the development of novel therapeutic strategies.

1.1.3 Clinical features, diagnosis and prognosis

The clinical course of IPF is characterised by the insidious onset of dyspnoea and cough which advances with fibrosis progression. The onset of these symptoms is often ascribed by the patient

to a previous chest infection or period of relative inactivity and lack of fitness, leading to delays in seeking medical attention[11]. Clues on examination include digital clubbing and bibasal inspiratory crackles on auscultation of the chest[12]. Restrictive spirometry, characterised by a preserved spirometric ratio and reduced forced vital capacity (FVC), should alert the clinician away from more commonly seen respiratory disorders such as asthma and chronic obstructive pulmonary disease. Reductions in the transfer capacity of carbon monoxide (TLCO) are seen as the disease progresses. A chest X-ray may detect lower zone predominant reticular changes however chest HRCT is more sensitive and the gold standard imaging modality for diagnosis of UIP.

The radiological pattern of UIP on HRCT includes a bilateral and subpleural fibrotic process, typically affecting the lower zones to a great extent than the upper zones, resulting in architectural distortion of the lung parenchyma and abnormally dilated airways (traction bronchiectasis), with or without honeycombing (cystic changes reflecting bronchiolisation of the alveolus)[9] **(Figure 1.2 A-B)**.

Occasionally patients with IPF disease do not have typical features of UIP on HRCT and receive their diagnosis from lung biopsy. Pathologically, UIP is characterised by a heterogeneous interstitial infiltration of dense ECM with adjacent areas of relatively unaffected lung parenchyma[13]. A key feature within affected areas of tissue is the fibroblastic focus – a cluster of mesenchymal cells convexly protruding into an adjacent alveolar space and lined by epithelial cells that are often morphologically altered **(Figure 1.2 C)**.

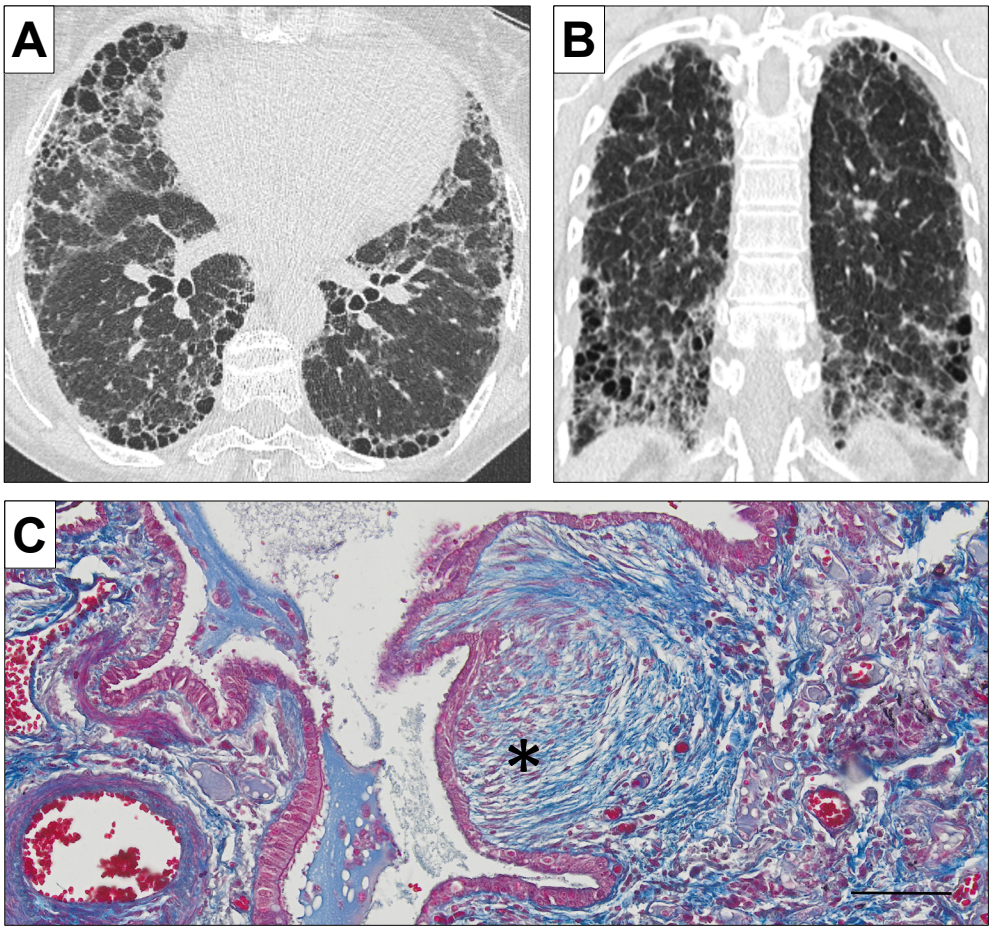

Figure 1.2: Usual interstitial pneumonia on radiology and histopathology. (A) Axial and **(B)** coronal chest HRCT images for a patient with IPF demonstrating a radiological pattern of definite UIP, as defined by subpleural fibrosis and traction bronchiectasis in an apicobasal gradient, and honeycombing. **(C)** Massons trichrome staining (pink – cellular contents, blue – ECM) of a histological section from a patient with IPF demonstrating a fibroblastic focus (star), a key feature in the histopathological diagnosis of UIP. Scale bar 100µm.

Taken together, the diagnosis of IPF is made by clinical assessment and identification of a pattern of UIP on radiological or histopathological criteria as set out by international consensus guidelines[4]. This is recommended to occur through multi-disciplinary team (MDT) discussion of the clinical, radiological and histopathological evidence.

The prognosis for IPF is poor with an average life expectancy of 2-4 years from diagnosis, although emerging evidence suggests that treatment with anti-fibrotic medications may improve survival[14-16]. Most patients with IPF will die from the disease itself, with inexorable progression of the fibrosis culminating in overt hypoxaemic respiratory failure. In a subset of patients the clinical trajectory is complicated by an acute exacerbation (either idiopathic or triggered by a

superimposed disease process), while others will succumb to associated co-morbidities such as cardiovascular disease and lung cancer[17].

1.1.4 Current and future treatments

Although lung transplant remains the only cure for IPF, the management strategy to stabilise disease progression has undergone significant change in the past two decades. An increasing understanding of the underlying pathophysiological process has elicited a transition away from immunosuppressive strategies towards disease modifying therapies that target fibrotic pathways[14,17].

The conventional approach for treating IPF, as with many ILDs, had been with corticosteroids and other immunomodulatory agents such as azathioprine or cyclosporine. The concept of "triple therapy" arose from the IFIGENIA study in 2005 which observed a slower rate of FVC decline when N-acetylcysteine (NAC) was added to a "standard of care" treatment of prednisone plus azathioprine[18]. The hazards of using two treatment groups that had not been robustly tested against placebo did not emerge until 2012, when a prematurely terminated arm of the PANTHER study revealed that the 'triple therapy' regimen incorporating prednisone, azathioprine and NAC left the IPF patient at least ten times more likely to be deceased or hospitalised after 15 weeks than placebo, with no significant differences in lung function[19]. Continuation of the NAC-only arm revealed that, whilst NAC did not appear overtly harmful, it failed to have any benefit in lung function preservation compared to placebo, suggesting the positive results of the earlier IFIGENIA study may have resulted from protective effects of NAC against the harmful effects of immunosuppressive regimens[20]. This protective effect of NAC does not appear to extend to any clinical benefit when given to patients treated with current anti-fibrotic strategies[21].

Shortly after the triple therapy results of the PANTHER study, in landmark clinical trials for IPF treatment, two mechanistically distinct anti-fibrotic agents (nintedanib and pirfenidone) emerged as effective disease modifiers, each capable of slowing the rate of FVC decline by approximately half[22-24].

Nintedanib is a tyrosine kinase inhibitor (TKI) which broadly targets pro-fibrotic pathways including fibroblast growth factor (FGF), vascular endothelial growth factor (VEGF) and platelet derived growth factor (PDGF) [24,25]. It was originally developed to treat solid organ tumours (namely non-small cell lung cancer) but repurposed into pulmonary fibrosis following the observation that its target receptors were implicated in the mechanisms of pulmonary fibrosis and inhibition of these pathways had shown promise in animal models[25-27].

Following an earlier phase 2 study (TOMORROW) which had demonstrated the safety of nintedanib in IPF as well as trends to reduction in FVC decline and acute exacerbations, two replicate phase 3 studies – INPULSIS 1 and 2 – were undertaken to establish the efficacy of nintedanib in IPF[24,28]. After recruiting a total of 1066 participants both studies met the primary outcome of a significant reduction in the annual decline of FVC, with a mean decline of 115mls and 114mls in the nintedanib arm of INPULSIS 1 and 2 respectively, compared to 240mls and 207mls respectively for the placebo groups. Additionally, and despite heterogeneity between the individual twin trials, a pooled analysis of the rate of IPF exacerbations using centrally adjudicated criteria demonstrated a significant reduction of 68% in probable or confirmed exacerbations.

Longer-term data from both the TOMORROW and INPULSIS trials have since demonstrated both a sustained preservation of FVC as well as a potential beneficial effect on survival[15,29,30]. More recently the scope of nintedanib to treat lung fibrosis has extended even further, with the SENSCIS trial demonstrating similar efficacy of nintedanib for patients with ILD associated with systemic sclerosis while the INBUILD study found nintedanib to delay FVC decline across a range of ILDs with a "progressive fibrotic" phenotype, in particular those with a UIP pattern[31,32].

Pirfenidone, a synthetically manufactured pyridine and the only other approved anti-fibrotic agent for IPF to date, has broad anti-inflammatory and anti-fibrotic effects which are generally attributed to inhibition of the downstream actions of transforming growth factor (TGF)-β1 such as fibroblast proliferation and collagen synthesis[14,33]. Transcriptomic analysis of lung fibroblasts and whole lung homogenates from IPF patients treated with or without pirfenidone suggest a particular influence of pirfenidone on fibroblast migration, activity and production of ECM, as well as a non-fibroblast effect on innate and adaptive immune regulation[34].

Following on from two earlier and promising studies centred in Japan, the CAPACITY trials were undertaken to evaluate the efficacy of pirfenidone in IPF over 72 weeks[23,35,36]. The results of the two trials were conflicting, with CAPACITY 004 demonstrating an FVC decline of 12.4% for placebo and 8% for pirfenidone 2403mg/day (a statistically significant relative benefit of 4.4%) while CAPACITY 006 showed a decline of 9.6% for placebo and 9% for pirfenidone. After being declined approval from the United States' Food and Drug Administration (FDA) a third trial was undertaken[37]. With a 52 week duration ASCEND was shorter than the CAPACITY trials yet it met the primary endpoint, with a mean decline from FVC baseline of 428mls for placebo compared to 235mls for the pirfenidone group[22].

Pooled analysis from the CAPACITY and ASCEND trials revealed an overall reduction by 43.8% in the number of patients that died or suffered a 10% decline in FVC[38]. Pirfenidone, along with Nintedanib, was subsequently approved by the FDA for use in IPF in October 2014[37]. Further

studies of pirfenidone in other ILDs are either inconclusive or still underway, largely due to issues with trial design and recruitment[39,40].

The broad targets of both nintedanib and pirfenidone are postulated to be an important aspect of their anti-fibrotic efficacy but also result in a range of adverse effects, such as photosensitive rash (pirfenidone), increased bleeding risk (nintedanib) and gastrointestinal symptoms (both). Accumulating evidence from longer-term, open-label studies of these drugs have found no new safety concerns but reinforce the significant burden of these adverse effects[30,41,42]. While often mild, adverse effects such as diarrhoea and weight loss are occasionally serious enough to require reduction or cessation of treatment. This problem, coupled with the relatively modest effects on FVC decline that anti-fibrotics exert, highlight the importance of ongoing research to develop more effective and tolerable treatments.

Alternative therapeutic interventions in IPF have proven elusive. A rationale for anticoagulation arose from the findings of increased thrombotic rates in patients with IPF suggesting a dysregulated clotting cascade[43]. However the placebo-controlled ACE-IPF trial using the vitamin K antagonist warfarin was ultimately terminated following just over 50% recruitment after review of the safety and outcome data revealed a low likelihood of efficacy and an increase in mortality with the treatment group[44]. Similarly, large studies investigating the use of vasodilatatory compounds such as the phosphodiesterase-5 inhibitor sildenafil and the endothelin-1 receptor antagonist bosentan were unable to show benefits in their primary outcomes[45,46]. Other treatments which have failed to elicit clinically meaningful differences include subcutaneously delivered interferon gamma-1β, the TKI imatinib and the tumour necrosis factor (TNF)α inhibitor etanercept[47-50].

In 2017 results were published from a phase 2 clinical trial using a monoclonal antibody (Simtuzumab) against the collagen cross-linking enzyme lysyl oxidase-like 2 (LOXL2). After recruitment of 544 participants the study was terminated following the second interim analysis when no positive difference was detected in progression-free survival[51]. Yet significant limitations with the study design have left questions over the reasons behind a lack of treatment response. To begin with, it remains unclear if the monoclonal antibody achieved its target effect as no markers of target engagement were identified or measured. By aiming to target LOXL2 alone it was also unclear whether redundancies within the 5 member LOXL family may have compensated for Simtuzumab's inhibitory effect. Finally, LOXL2 has numerous established intracellular and non-catalytic functions which Simtuzumab, as an extracellular-based monoclonal antibody, would have failed to influence[52-59]. Overall these limitations raise significant questions on the suitability of Simtuzumab as an appropriate candidate for targeting matrix dysregulation in IPF.

The cautionary results of the PANTHER trial, the success of nintedanib and pirfenidone, and the limitations of the multitude of negative studies to date highlight the fundamental importance of understanding the subtleties in IPF pathophysiology when pursuing development of novel anti-fibrotic agents. Through the mechanistic dissection of pathways which initiate, propagate and drive lung fibrosis is the potential to better understand how this disease develops, as well as identify targets of interest which may assist in diagnostic or therapeutic intervention.

1.1.5 Physiological changes in lung fibrosis

The pulmonary interstitium is the anatomic space located at the working interface of the lung between the alveolar epithelium and capillary endothelium. It is composed predominantly of ECM, with a scaffolding of type I and type III collagen fibrils that maintain the alveolar-capillary surfaces in close proximity[60]. Tensile strength within these collagenous structures is necessary to resist architectural distortion with fluctuating pressure gradients during minute ventilation.

As the key anatomical impediment between the alveolar epithelium and capillary endothelium, lung interstitium must also be thin enough to enable effective passage of gases from one surface to another. Healthy pulmonary interstitium averages 300μm in breadth, which is thin enough for oxygen to diffuse rapidly from the alveolar surface to the bloodstream.

Finally, a healthy interstitium imbues the lung parenchyma with a high degree of compliance, enabling effective respiration. While expiration at rest in a healthy human is passive due to elastic recoil, inspiration is an energy-requiring process. As the average person will respire 12 to 16 times per minute, or around 20,000 times per day, efficient respiration is important for energy conservation.

These three physiological properties of the interstitium are disrupted in the patient with IPF. Lung architecture is progressively and heterogeneously altered, with infiltration of the interstitial space leading to distortion and eventually obliteration of alveolar sacs, capillary networks and conducting airways. Altered lung structure leads to increased dead space ventilation and subsequent mismatches in ventilation/perfusion relationships for patients with IPF.

Expansion of the interstitial compartment with altered ECM also reduces the diffusive abilities of the lung, particularly that of oxygen from the alveolar compartment to the capillary bloodstream[61]. Changes in alveolar membrane diffusive conductance (DM_{CO}) significantly correlate with fibrotic disease severity[62]. Carbon dioxide, 20 times more soluble than oxygen, diffuses more easily from the bloodstream to the alveolar space and therefore hypercapnic respiratory failure is invariably less relevant

As the interstitial compartment is progressively altered in IPF, changes to both alveolar membrane conductance and ventilation/perfusion relationships lead to an increased gradient in alveolar-arteriolar oxygen tension gradients (P_AO_2-P_aO_2), with the end-result being progressive hypoxaemic respiratory failure, initially on exertion only but ultimately at rest[61].

Changes in both volume and composition of interstitial proteins along with other alterations such as surfactant composition leads to a reduction in lung compliance[63]. By increasing the force required to inspire and ventilate the lung, a defective interstitium can significantly increase work of breathing. The extent of fibrotic infiltration strongly correlates with pulmonary compliance, and as the disease progresses the patient will experience a reduction in total lung capacity and increasing respiratory work effort[64]. As a result of this, basal caloric energy requirements in patients with ILD can rise by over 100%[63].

1.2 Our emerging understanding of IPF pathophysiology

1.2.1 The current paradigm of IPF research

The evolution of criteria to define and cohort IPF stems largely from the strong demand for further clinical trials to study novel anti-fibrotic agents. Yet in parallel has emerged improved access to biological material and translational research methodologies to investigate the heterogeneous mechanisms which underlie the disease process.

For two decades the fundamental mechanistic hypothesis for IPF disease is proposed to be a repetitive environmental or intrinsic injury in a genetically vulnerable individual with a consequent maladaptive and dysregulated wound healing response[65,66]. Yet this complex and multifactorial process has been extensively expanded upon and refined, enabling a level of detail sufficient to identify new target pathways and novel therapeutic strategies.

1.2.2 Genetic susceptibility to pulmonary fibrosis

Predisposing genetic traits are increasingly implicated in the initiation and progression of pulmonary fibrosis **(Table 1)**[67]. Case-control genome wide association studies have identified variants in at least 11 different genetic loci associated with IPF[68-70]. Some, such as the *MUC5B* promoter variant, are relatively common but with low penetrance, increasing the risk of sporadic IPF in a substantial cohort of individuals. Other, such as telomere mutations, are rare but have high penetrance and contribute to a small but important subpopulation of familial disease. Beneath these individual polymorphisms also lies a range of gene expression and epigenetic risk

factors linked with the disease, highlighting the complex and often multifactorial pathways in IPF genetics[71-74].

Arguably the strongest genetic association with sporadic IPF is the single nucleotide polymorphism variant of the *MUC5B* gene promoter – rs35705950 – which confers a 3-fold increased risk of developing IPF and is found in over 30% of patients with the diagnosis[75]. Now increasingly associated with other ILDs including rheumatoid arthritis-ILD and early subclinical disease (termed interstitial lung abnormalities, ILAs) the *MUC5B* promoter presents the strongest evidence for a pathogenetic influence behind central mechanisms of pulmonary fibrosis[76,77]. *MUC5B* encodes a mucin glycoprotein responsible for immune and mucociliary regulation, and is overexpressed in the IPF bronchoalveolar epithelium, leading some to propose IPF as primarily a disease of the small airways[78]. Several mechanisms are proposed to explain a causal link between overexpression of *MUC5B* and the development of pulmonary fibrosis, including the sustained injuries arising from mucociliary impairment and failure to clear the small airways of debris, coupled with a disruption in normal reparative responses, leading to fibro-proliferative remodelling and honeycombing in the affected area[78].

A number of other genetic associations provide clues to the pathogenetic origins of pulmonary fibrosis within the respiratory epithelium. One of the earliest associations with familial pulmonary fibrosis was a mutation in the gene encoding surfactant protein C (*SFTPC)*, a component of alveolar surfactant produced by type II alveolar cells to maintain alveolus integrity[79]. Variants of the desmoplakin (*DSP*) gene, which encodes an essential desmosomal protein that anchors intermediate filaments to desmosomal plaques, are associated with sporadic IPF, suggesting failure in cell-to-cell adhesion and loss of epithelial barrier integrity may be an important precipitant for progression of disease[68]. Overexpression of A-Kinase Anchoring Protein (*AKAP)13*, identified in an independent study as a sporadic IPF risk factor, has been sourced primarily to epithelial cells in both healthy and IPF lung tissue, and is postulated to increase TGFβ signalling through Rho kinase upregulation of the mechanoreceptor αvβ6 integrins[70].

Telomere length is increasingly implicated in pulmonary fibrosis. Telomeres are the protective nucleotide sequences which cap the ends of chromosomes and will progressively shorten with each cycle of cell division until the cell either becomes apoptotic or undergoes cell cycle arrest (termed senescence)[80]. Short telomere length can be found in a quarter of sporadic IPF and over a third of familial cases, supporting the role for cellular senescence and impaired wound healing in early pathogenesis[81]. In a Mendelian randomisation study, Duckworth and colleagues argue the link between telomeres and IPF is not merely an association but causal[82]. They analysed two cohorts (the UK Biobank with up to 1369 cases of IPF against 435866 controls, and an IPF

replication cohort with 2668 cases and 8591 controls) and found meta-analysis of the two groups statistically inferred shorter telomeres to cause IPF, with an overall odds ratio of 5.81. Mutations of genes involved in the regulatory telomerase complex such as Telomerase Reverse Transcriptase *(TERT)*, Telomerase RNA Component *(TERC)*, Poly(A)-Specific Ribonuclease *(PARN)* and Regulator of Telomere Elongation Helicase 1 *(RTEL1)* result in shorter telomere length and whilst rare have a significant impact on the likelihood of pulmonary fibrosis development and progression[83].

Table 1: Genes associated with an increased risk of developing familial or sporadic IPF

Gene	SNP	Locus	Odds Ratio	Reference
MUC5B	Rs35705950	11p15	2.43 - 4.51	[68], [69]
MUC2	Rs7934606	11p15	1.61	[68]
TOLLIP	Rs5743894	11p15	1.49	[69]
TOLLIP	Rs111521887	11p15	1.48	[69]
MDGA2	Rs7144383	14q21	1.44	[69]
DSP	Rs2076295	6q24	1.43	[68]
TERC	Rs6793295	3q26	1.3	[68]
FAM13A	Rs2609255	4q22	1.29	[68]
DPP9	Rs12610495	19q13	1.29	[68]
AKAP13	Rs62025270	15q25	1.27	[70]

1.2.3 Environmental exposures as potential disease triggers

IPF is classically associated with male gender and advancing age however there is an increasing number of environmental exposures which are associated with disease incidence and progression. These exposures are frequently inhalational in nature and may account for early triggers in the disease process.

Cigarette smoking is generally regarded as a risk factor for the development of IPF, and the incidence of tobacco smoking is consistently increased in IPF cohorts, although a robust dose-effect relationship has not been established[84]. The chance of developing IPF for ever-smokers is nearly twice as high as non-smokers, while even maternal smoking presents an independent and

significant risk[85]. Current and ex-smokers have more rapid progression of disease than non-smokers[86].

Also frequently associated with IPF are other possible inhalational exposures such as wood dust, metal dust and silica, as well as agricultural activities such as working with livestock and birds[87]. A significant proportion of these inhalation injuries are likely to be experienced through workplace exposures. In an ATS/ERS position statement on the occupational burden of non-malignant respiratory diseases, Blanc et al concluded a substantial proportion of IPF disease may be associated with occupational exposures[88]. Across 11 case-control studies the authors calculated pooled population attributable fractions (PAFs) using the odds ratios and proportion of cases exposed in each relevant study, reporting PAFs of 8% for metal dusts, 4% for wood dusts and 3% for silica. It should be noted however that the definition of IPF excludes an identifiable pneumoconiosis and therefore the proportion of environmental exposures in a population may vary depending on how rigorously an alternative diagnosis was sought. Furthermore it is likely that many of these workplace exposures will be confounded by other shared and possibly occult exposures (such as asbestos).

Gastro-oesophageal reflux is one of the most common co-morbidities in IPF, and among pooled analyses of case control studies it is observed with an increased incidence in cases compared to healthy controls[89,90]. A popular theory is that chronic micro-aspiration of gastric contents could provide the elusive trigger for pathological changes in many IPF patients where no other clearly identifiable cause is found. However reflux is common in the general population, and the presence of confounders such as smoking means the true underlying relationship remains unclear[90]. The use of antacid therapy for treatment of asymptomatic reflux in IPF is another source of controversy despite a weak recommendation from the ATS/ERS guidelines on IPF management[91]. Across numerous observational cohort studies the results for antacid use have been mixed and some flawed by bias, while a recent larger population-based prospective study that took account of these biases found no treatment effect[92,93]. Randomised trials are currently in progress which will hopefully address this question definitively.

Air pollution is associated with the development of subclinical ILD as well as a risk factor for IPF disease progression. Using a range of air quality data sources and residential history from over 3000 participants who received whole lung CT scans, the MESA cohort study identified a heightened risk of ILAs with increasing exposure to nitrous oxides and fine particulate matter[94]. Specific traffic gases may also lead to clinical worsening of pulmonary fibrosis. A cohort of 436 IPF patients with air pollutant exposure data based on the nearest available monitoring station demonstrated an increased incidence of acute exacerbation with higher levels of nitrogen dioxide

and ozone, but not sulphur dioxide or carbon monoxide[95]. A larger study of 1114 patients with IPF demonstrated a 17% increase in mortality with a 10 parts-per-billion increase in nitrogen dioxide levels[96]. Short term exposure to ozone and long term exposure to inhalable particulate matter was found in a separate study to be associated with increased mortality in 135 IPF patients[97,98].

In summary a range of environmental exposures are associated with IPF and could potentially catalyse the early disease process in a genetically susceptible individual.

1.2.4 Alterations in the respiratory microbiome

Despite long-held hypotheses regarding causal infections, limitations with traditional culture-dependent methods have previously restricted efforts to study the impact of micro-organisms on pulmonary fibrosis. A number of viruses, such as hepatitis C and Epstein-Barr virus, have been associated with IPF but no robust relationships have been demonstrated[99-101]. The development of non-culture techniques such as DNA and RNA sequencing have substantially improved the ability to detect and sub-type organisms, resulting in an ever-growing understanding of the complex community of both pathogenic and commensal micro-organisms within the respiratory tract collectively termed the microbiome.

Garzoni and colleagues report being the first to analyse the microbial populations within the upper and lower respiratory tracts of an ILD cohort using 16S ribosomal RNA sequencing, a culture-independent technique that is reliable, time-efficient and sensitive due to highly conserved regions for primer binding and highly variable, organism-specific regions that can be used for species identification[102]. However the individual cohorts were small and despite detecting a range of organisms within the IIP sub-cohort (namely Prevotellaceae, Pasteurellaceae, Neisseriaceae and Streptococcaceae) they did not find any differences in the diversity or abundances compared to either control or other disease cohorts (such as sarcoidosis). Similar techniques were employed to examine the respiratory microbiome in bronchoalveolar lavage (BAL) samples from 55 IPF patients in the Correlating Outcomes with biochemical Markers to Estimate Time-progression (COMET)-IPF biobank. While there was no control group to enable healthy comparison, this study found disease progression was strongly associated with a high relative abundance of one specific sub-species each of staphylococcus (Operation Taxonomic Unit [OTU]1348) and streptococcus (OTU1345)[103].

Shortly thereafter a robust comparison of the respiratory microbiome in 65 IPF and 44 control patients was reported, and found patients with IPF had both differences in species abundance and an overall higher bacterial burden, the latter being the most consistent finding amongst

subsequent microbiome studies[104]. Notably however, the median age of the control cohort was nearly a decade younger than the IPF cohort. A strong association was identified between microbial burden and risk of disease progression and death, which is possibly independent of the extent of fibrosis and lung parenchymal destruction as determined by radiological assessment[105].

Intriguingly a correlation was also made with the presence of the MUC5B rs35705950 polymorphism, suggesting an interplay between microbial populations and host immunity that could generate alveolar injury and drive disease[104]. A relationship has subsequently been identified between specific genes pertaining to host immunity and defence (such as NLRC4) and an increased microbial burden, BAL neutrophilia and lung function decline[106]. Dysregulation of alveolar inflammation has been identified in BAL samples from IPF patients with reduced bacterial diversity, with increases of pro-inflammatory cytokines such as interleukin (IL)-1Ra[107]. Efforts to remodel this host-microbial interaction through antimicrobial agents such as co-trimoxazole showed early promise however a larger study has not elicited any significant differences in outcome modification, suggesting there is a way to go before the advances in knowledge of the respiratory microbiome translate into positive outcomes for patients with IPF[108,109].

1.2.5 Injury and impaired regeneration of the alveolar epithelium

The currently accepted paradigm for IPF pathogenesis, introduced at the turn of the millennium, purports that repetitive micro-injuries to the alveolar epithelium trigger a fibrogenic cascade which is sustained and dysregulated **(Figure 1.3)**[65,110]. Emerging data using advanced methodologies firmly place the alveolar epithelium in a central role for inciting lung fibrogenesis[111].

The alveolar barrier is formed by type 1 (AT1) epithelial cells, readily identified morphologically due to their thin, plate-like cytoplasm which enables efficient gas exchange and together encompass 96% of the alveolar surface[112]. Due to limited AT1 self-repair abilities, regeneration of the alveolar barrier and gas exchange surface following cellular injury requires proliferation and trans-differentiation from a pool of cuboidal, multipotent and highly plastic type 2 alveolar (AT2) cells, which have a similar population size to AT1 cells despite only comprising the remaining 4% of the alveolar surface. Despite AT1 cells originating from AT2 cells, the two cell types have broadly divergent roles in the immune response to inhalational pathogens and foreign material, with AT1 cells possessing pro-inflammatory functionality while AT2 cells (in health) having broadly more anti-inflammatory actions[113]. AT2 cells are also responsible for generating pulmonary surfactant, a lipoproteinaceous amalgam essential for lowering surface tension in the alveolus to

avoid collapse at low volumes. This function is lost when AT2 cells transdifferentiate into AT1 cells, as reflected by differences in gene expression such as *SFTPC*[114].

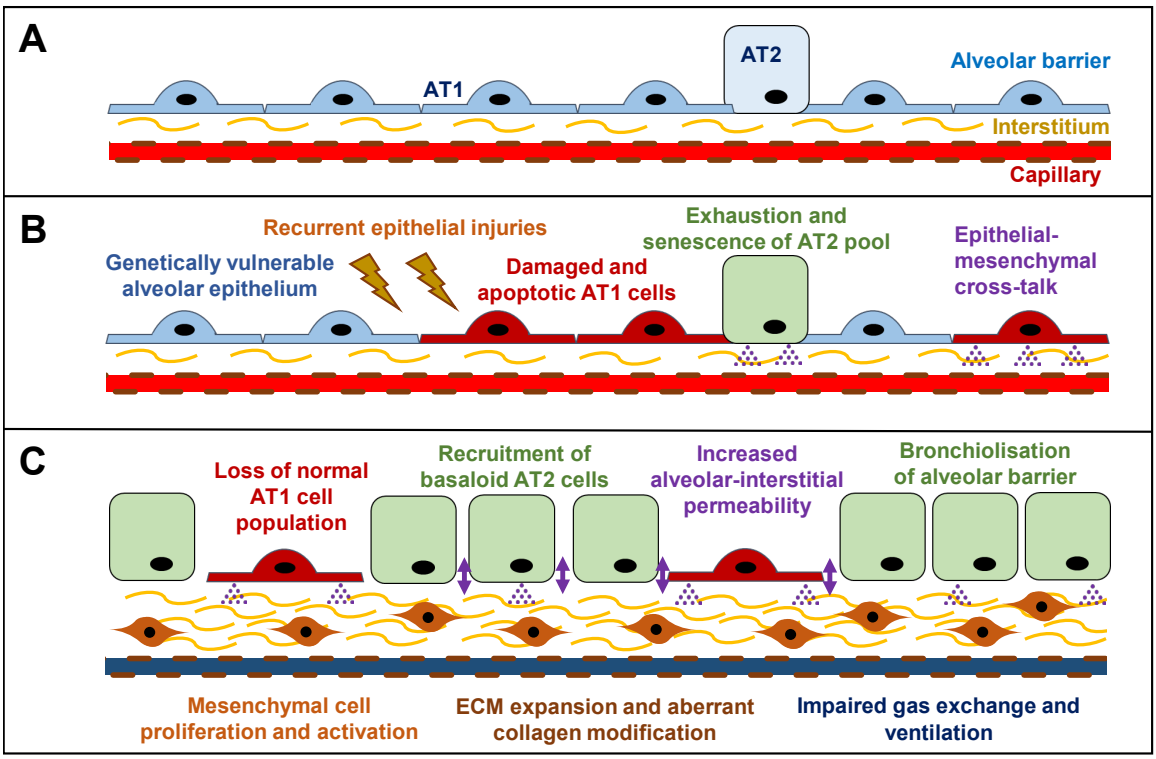

Figure 1.3: Mechanisms through which pulmonary fibrosis is proposed to develop. **(A)** The healthy lung unit with an alveolar epithelial barrier (blue) composed of flattened AT1 and cuboidal AT2 stem cells overlying a thin interstitial layer (yellow) comprised predominantly of collagen and elastin, which separates it from the capillary network (red). **(B)** Recurrent injuries to a genetically vulnerable alveolar barrier leads to epithelial apoptosis, increased cell turnover, stem cell exhaustion and senescence, with subsequent recruitment of "basaloid" stem cells from bronchial airways (green). **(C)** Breakdown of the alveolar barrier from maladaptive and senescent basaloid cells leads to increased permeability of exogenous exposures into the interstitium, epithelial-mesenchymal cross-talk, and mesenchymal cell recruitment and activation within the underlying interstitial compartment. This results in ECM expansion and aberrant modification, resulting in impairment of both ventilation and gas exchange[65].

Epithelial mesenchymal transition (EMT) is another important process in both normal epithelial tissue development and wound healing responses, and dysregulation of this process is seen in disease states including IPF. EMT is typified by a loss of epithelial traits such as apicobasal polarity and intercellular connectivity and an upregulation of mesenchymal properties such as increased

migratory and invasive behaviour as well as increased matrix production and apoptosis resilience[115]. This process is driven by master transcription factors such as *SNAIL1* and *SNAIL2*, Zinc-finger enhancer binder (*ZEB*)1 and *TWIST1*, resulting in a broad range of effects in gene and protein expression such as downregulation of cadherin cell-cell adhesion proteins (such as cadherin-1, encoded by *CDH1*), and upregulation of the mesenchymal filament protein vimentin (encoded by *VIM*).

A hyperplastic and dysfunctional alveolar epithelium may arise in IPF from both depletion and dysregulation of AT2 cells[111,116]. The repetitive injuries to the alveolar barrier are thought be the precipitant for AT1 and AT2 cell apoptosis, occurring through multiple pathways including endoplasmic reticulum stress and mitochondrial dysfunction[117,118]. Progressive epithelial cell loss leads to an exhaustion of the AT2 stem cell pool, resulting in reduced numbers seen in the IPF lung[65]. This effect may be exacerbated by a shortening and/or dysfunction of AT2 telomeres, which promotes cellular senescence rather than proliferation and growth, and is associated with progressive fibrosis in animal models[119,120].

The residual senescent AT2 cells are dysregulated in activity, reverting to developmental signalling axis such as Wingless/integration site (Wnt), Notch, Hippo, and hedgehog pathways and lacking important markers of self-renewal and lung repair such as hyaluronan and Toll like receptor 4[116,121]. Through single cell RNA-sequencing, subsets of IPF AT2 cells have been identified which express conducting airway-associated genes such as MUC5B and SOX2, suggesting the recruitment of more proximal airway stem cells to sites of peripheral damage that may drive the remodelling and *"*bronchiolisation*"* of the alveolar compartment[121]. Larger single cell RNA-sequencing studies have confirmed this observation and even proposed the "basaloid" airway cell characteristics to be a common theme linking the two pathological endpoints of pulmonary fibrosis – honeycomb cysts and fibroblastic foci[122,123].

These studies as well as earlier work have identified markers of EMT as another key signature within IPF alveolar cells yet the specific role in IPF pathobiology remains controversial. Hypotheses purporting EMT as a source of mesenchymal cells within the fibroblastic foci have become less favoured to a more communicative function, relaying pro-fibrotic signals from the alveolar surface to myofibroblast progenitors within the interstitial compartment[124].

A failing alveolar epithelial barrier results in disruption and loss of integrity in the underlying basement membrane. The injured and dysfunctional epithelial lining initiates a fibrogenic response by recruitment and activation of proliferating myofibroblasts through both autocrine and paracrine means of epithelial-mesenchymal cross-talk[116,125]. Hyperplastic AT2 cells overlying fibroblastic foci are thought to be a significant source for these growth factors, with both animal

and human studies demonstrating their pro-fibrotic capabilities[111,122]. In another mouse model, TGFβ signalling was identified in AT2 cells exposed to increased mechanical tension to catalyse a typical UIP pattern periphery-to-centre fibrosis[126]. Mechanical stress is likely to compound alveolar barrier dysregulation, with typical longitudinal and circumferential forces of respiration having been demonstrated to slow re-epithelialisation[127].

1.2.6 Mesenchymal cell recruitment and activation

Fibroblasts reside in the ECM, contributing to matrix homeostasis and providing a diverse range of tissues with organ-specific needs of compliance and water content[128]. Despite being first identified by Vichow in the 19th century they remain poorly understood due to relatively low numbers in health and significant heterogeneity across tissue types, although single-cell RNA sequencing studies in mice and humans are revealing important insights into their molecular composition, gene expression and inter-organ heterogeneity[128]. In general, fibroblasts are highly responsive to both the mechanical and chemical environment, and are capable of differentiating from a passive and relatively inactive phenotype into migratory, secretory and contractile forms (with a wide range of terms including mesenchymal, activated or myofibroblast). In this study, 'lung mesenchymal cells' will be used in reference to histochemical work with IPF tissue and 'lung fibroblasts' in reference to *in vitro* studies, in recognition of phenotypical and behavioural differences between cells grown *in vitro* compared to those found in their native matrix

In IPF lung tissue, activated mesenchymal cells can often be readily identified by their location within an aggregate of ECM (collectively termed a fibroblastic focus), convexly protruding from the interstitium into the alveolar compartment. They are also notable for their spindle morphology and contractile phenotype, and will often express mesenchymal markers such as α-smooth muscle actin (α-SMA)[129]. By producing excessive and pathologically altered matrix that disrupts normal lung structure and function these mesenchymal cells are widely attributed as the principal effector cells of the IPF condition[122,123,130].

Fibroblastic foci are thought to represent areas of active fibrogenesis within the IPF lung[14]. Initially proposed to be interconnected networks representing a wave of active fibrogenesis, micro-CT analysis has now characterised them as complex but morphologically discrete structures which arise geographically independently from one another[131]. Significant heterogeneity in shape and size are seen between individual foci, with the largest displaying volumes up to 100 times the smallest. Although the reason for this variation is unclear, they have been hypothesised to represent different levels of injury and response, or alternatively reflect foci as differing stages of development. Hypothesised to originate within the interstitial compartment, fibroblastic foci are

frequently identified beyond the remains of basal lamina, protruding into the alveolar spaces and disrupting normal lung structure-function[132].

Emerging evidence from single-cell RNA sequencing suggests IPF mesenchymal cells are not one single entity, but rather a heterogeneous population, likely comprised of a spectrum of active and relatively inactive phenotypes. In one study the least differentiated mesenchymal cells were found in the perimeter of the fibroblastic focus, contrasting to a population of well differentiated myofibroblasts in the focus core[130]. These less-differentiated mesenchymal cells expressed highly proliferative and developmental genomic signatures, most significantly the pro-fibrotic TGFβ pathway. A separate analysis found multiple distinct fibroblast phenotypes, each with an individual pattern of expression and regional location[123]. For example fibroblasts expressing hyaluronan synthase 1 (*HAS1*) were found in subpleural areas, demonstrated markers of cellular stress such as IL4, and co-localised with collagen I (COL1A1) on histochemical analysis of IPF lung tissue. By contrast perilipin 2 (*PLIN2*)-expressing lipofibroblasts – lipid-laden cells thought to be important for fibrosis resolution[133] – were located diffusely throughout the lung parenchyma, and actin alpha 2 (*ACTA2*)-expressing myofibroblasts were localised to sub-epithelial regions of conducting airways and honeycomb cysts. An independent study published simultaneously also identified a spectrum of lung mesenchymal cells in IPF tissue however these were broadly split into *HAS*-expressing fibroblasts and *ACTA2*-expressing myofibroblasts[122]. The authors proposed this dichotomy could represent the co-existence of healthy and disease-related mesenchymal cell populations within IPF lungs. Differences in observations between RNA sequencing studies on mesenchymal cells highlight the importance of further work to validate these findings and dissect the mechanisms and purpose of these individual mesenchymal phenotypes.

Despite our growing understanding of the heterogeneity of lung fibroblast phenotypes in IPF, the sources of active mesenchymal cells capable of producing the abundant ECM remain controversial. Resident fibroblasts and lipofibroblasts recruited locally to sites of injury are traditionally thought to be the primary pool of mesenchymal cell progenitors[134]. Other research has pointed towards circulating blood fibrocytes which, under the influence of cytokines such as PDGF, migrate to regions of injury and contribute to the fibrotic process[135,136].

Finally EMT, the process of an epithelial cell losing cell-cell contacts and becoming more motile, is increasingly implicated in lung fibrosis although the precise mechanisms remain to be clearly delineated[115,124]. Rather than directly forming myofibroblasts, some argue that the EMT phenomenon promotes epithelial-mesenchymal crosstalk to indirectly drive fibrogenesis[134]. An observation which favours this theory is that many classically pro-fibrotic cytokines such as TGF-

β1, members of the Rat sarcoma (RAS) and Wnt families, and hypoxia-inducible factors (HIFs) are also potent promoters of EMT[115].

1.2.7 Signalling pathways which regulate fibrogenic responses

Numerous cell signalling pathways have been implicated in the aberrant wound repair response in the IPF lung. While TGFβ is widely considered the classic signalling peptide for organ fibrosis, there is increasing focus on alternative pro-fibrotic pathways such as canonical and non-canonical Wnt signalling, the tyrosine kinases, and hypoxia inducible factors.

TGFβ was first reported to promote fibroblast proliferation and collagen synthesis in the 1980s[137,138]. It is manufactured by cells as a latent precursor and bound to latent TGFβ-binding protein (LTBP) for extracellular secretion where it is predominantly sequestered within ECM **(Figure 1.4)**. Cleavage of the LTBP and latency associated peptide (LAP) converts it to the active unit. It has three isoforms of which TGFβ1 is considered the most abundantly expressed, however all three isoforms operate through common TGFβ receptor (TGFβR) signalling pathways. In canonical signalling, TGFβR phosphorylation leads to SMAD protein phosphorylation and subsequent dimerisation, exerting wide-ranging downstream effects at the cell nucleus. TGFβR activation also invokes a variety of non-SMAD signalling effects including the promotion of guanosine triphosphate (GTP)-binding proteins such as Ras and RhoA, and upregulation of mitogen activated protein (MAP) kinase subunits such as c-Jun N-terminal kinases (JNK) and ERK1/ERK2.

TGFβ expression is upregulated in a range of different cell types within fibrotic lung, including alveolar epithelial cells and mesenchymal cells[139]. Single-cell RNA sequencing has identified strong expression of TGFβ signalling pathways in IPF epithelium, particularly in cells with an undifferentiated or basaloid phenotype[121]. In a separate analysis characterising gene expression patterns of mesenchymal cell differentiation in IPF, TGFβ was observed to be one of the top 5 upstream regulators of this mesenchymal transcriptomic signature[130]. The striking potency of TGFβ signalling to promote lung fibrosis has been demonstrated using a rat model with adenoviral vector-mediated transfer of porcine TGFβ1 to the rat lung[140]. The temporary expression of active TGFβ1 produced a profound interstitial fibrosis characterised by a proliferation of mesenchymal cells and extensive ECM deposition. This effect was not seen with the latent form of TGFβ1. Compared to the bleomycin model – perhaps the most commonly used animal model of lung fibrosis – the TGFβ1 adenoviral vector model resulted in a more severe and sustained fibrotic process with a relative absence of the acute epithelial injury and inflammatory process that is typified in bleomycin studies, and is more consistent with the pathological process seen in IPF.

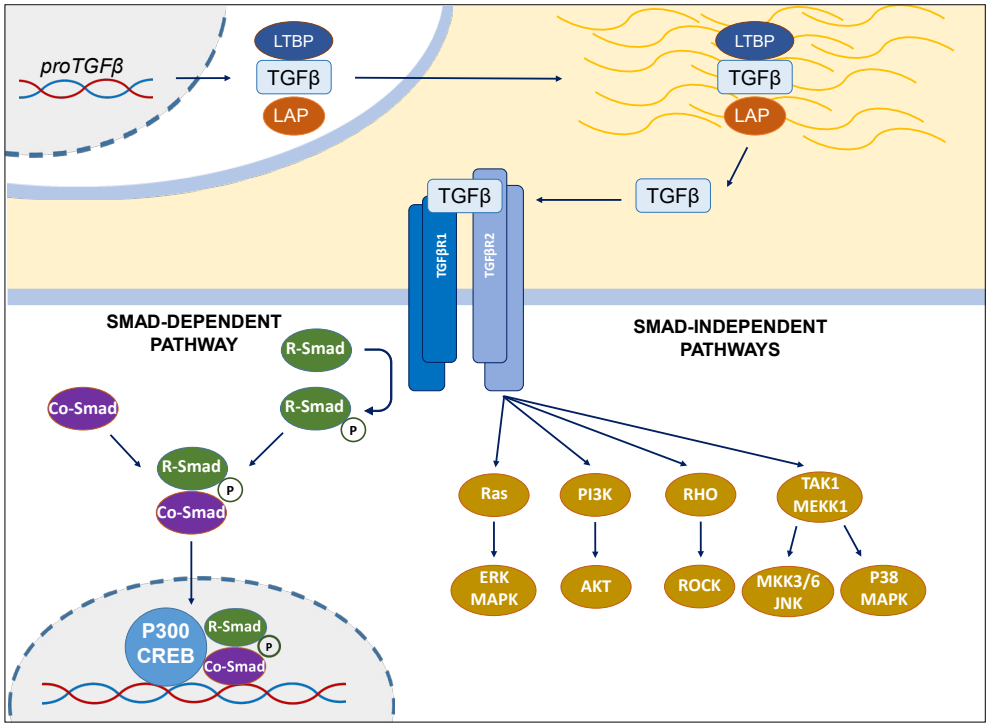

Figure 1.4: Transforming growth factor β signalling pathways. Following translation of the TGFβ homodimer and interaction with the Latency Associated Peptide (LAP) and Latent TGFβ-Binding Protein (LTBP), the latent TGFβ complex is secreted into the ECM. Cleavage of the LAP and LTBP occurs through numerous mechanisms such as oxidation, mechano-signalling and acidification, releasing active TGFβ that is capable of binding to TGFβ receptors (TGFβR1 and TGFβR2). Smad-dependent signalling occurs through the phosphorylation of receptor-activated (R)-Smads (Smad2/3) and recruitment of common (Co)-Smads (Smad4) before binding with other co-activators such as P300 or cyclic-AMP response element binding (CREB)-binding protein at the nucleus. Non-canonical (Smad-independent) TGFβ signalling also occurs through numerous pathways such as Ras/ERK/MAPK and RHO/ROCK[141].

The mechanisms by which TGFβ signalling exerts a pro-fibrotic effect are well established and include fibroblast growth factor (FGF)-driven recruitment and proliferation of fibroblasts, activation of myofibroblasts through SMAD-mediated α-SMA expression, stimulation of cellular collagen production, and induction of alveolar epithelial cell apoptosis[138]. Pirfenidone, one of the anti-fibrotic drugs to be broadly approved for IPF treatment, is believed to exert at least some of its action through inhibition of these TGF-β-mediated effects on fibroblast activity and ECM remodelling[23].

Numerous other pro-fibrotic signalling pathways have been implicated in driving pulmonary fibrosis. Tyrosine kinases are an important superfamily of cellular signalling proteins and include Epidermal Growth Factor (EGF), VEGF and PDGF[142]. EGF, through dimerisation of the EGF receptor

(EGFR), is capable of triggering a complex cascade of cellular signalling pathways including RAS/MEK/ERK and mTOR pathways which have been implicated in promoting fibroblast activity[143,144]. VEGF promotes ECM remodelling through induction of matrix metalloproteinases, and VEGF levels are positively and strongly correlated with fibrotic disease severity on HRCT[145]. It is notable that Nintedanib, the second anti-fibrotic treatment in IPF, is an inhibitor of multiple tyrosine kinases including VEGF, PDGF and FGF.

An increasingly recognised pathway in pulmonary fibrosis centres on Wnt signalling, which plays an important role during embryonic development. Traditionally Wnt signalling has been divided into canonical pathways which promote cytosol accumulation of non-phosphorylated β-catenin (for example Wnt3a), and non-canonical pathways which act independently of β-catenin (of which Wnt5a is one of the most researched members). Upregulation of both canonical and non-canonical pathways has been identified in IPF[146,147]. Sustained Wnt expression facilitates aberrant repair at the injured alveolar epithelium, which may propagate the underlying fibrotic process[148]. Furthermore Wnt signalling is capable of promoting fibroblast differentiation and proliferation[146]. ICG-001, a compound which essentially prevents canonical Wnt signalling by blocking β-catenin interactions with cyclic-AMP response element binding (CREB) protein, was demonstrated to be capable of preventing and even reversing fibrosis in a bleomycin mouse model[149]. However despite the promise of Wnt-interfering therapy for targeting fibrosis pathways, to date no such treatments have successfully translated into positive clinical trials.

Finally, hypoxia and its effects through hypoxia-inducible factor (HIF) pathways are an emerging area of interest in pulmonary fibrogenesis. HIFs function as heterodimers, with an oxygen-dependent HIFα subunit and oxygen-independent HIFβ subunit that together exert their effect at the nucleus **(Figure 1.5)**[150]. The three HIFα isoforms – HIF1α, HIF2α and HIF3α – are thought to have different roles, with HIF1α more often present in the acute phase of hypoxia while HIF2α expression increases with hypoxia chronicity. HIF3α is likely to be a regulatory protein involved in a negative feedback loop to control and dampen HIF pathway activity[151].

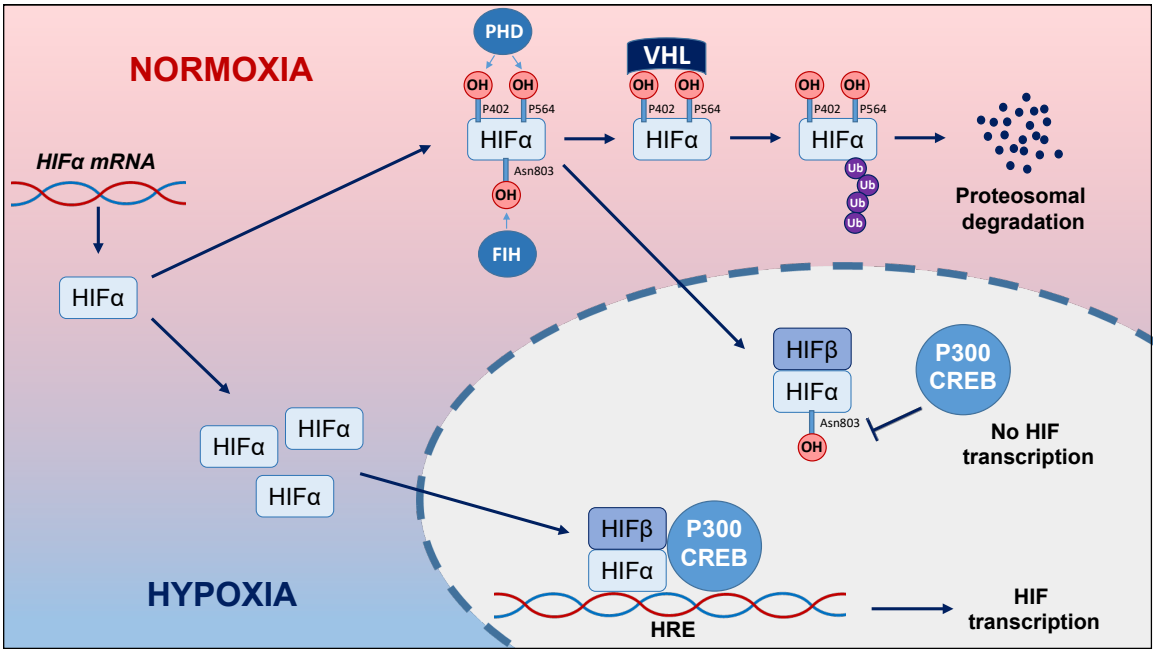

Figure 1.5: Hypoxia inducible factor pathways. In normoxia the accumulation of HIFα is prevented by hydroxylation of two proline residues (P402 and P564) by the oxygen-dependent HIF-prolyl hydroxylases (HIF-PHDs). This enables recognition and binding of the HIFα protein by the von Hippel-Lindau (VHL) E3 ubiquitin ligase complex for ubiquitination and subsequent proteosomal degradation. PHD activity is reduced in hypoxia, enabling HIFα accumulation and dimerisation with HIFβ for downstream transcriptional effects at hypoxia response elements (HRE). A second mechanism for HIF pathway downregulation occurs through hydroxylation of an aspariginyl residue (Asn803) by the di-oxygenase Factor Inhibiting HIF (FIH) enzyme, which prevents interaction between HIFα/HIFβ and the P300/CREB transactivating complex at the HRE, thereby inhibiting downstream transcription[150].

Reduced oxygen tension in the cellular microenvironment inhibits the enzymatic activity of oxygenases such as prolyl hydroxylases (PHDs) which would otherwise target HIFα for proteosomal degradation. The subsequent accumulation of HIFα enables coupling with HIFβ and downstream expression of hypoxia pathways[150,152]. Within IPF tissue HIF expression is increased and capable of promoting IPF fibroblast proliferation[153]. Hyperplastic alveolar epithelial cells within IPF tissue have been observed to express increased levels of HIF1α, and hypoxia is thought to be a key driver of ER stress within IPF tissue[154]. Furthermore HIF activation has been demonstrated to drive EMT-mediated pro-fibrotic gene expression[155]. Together with TGFβ1, HIF pathway activation synergistically increases the expression of myofibroblast markers such as αSMA and fibronectin[156].

In summary there is a complex network of signalling pathways which co-ordinate a fibrogenic response, which in the IPF lung is dysregulated and maladaptive. The product of this response, and the primary determinant behind the deranged physiological effects in IPF, is the manufacture of pathologically altered ECM. This abnormal ECM is often misunderstood to be a static end-product of the disease process yet emerging evidence suggests the contrary; it is a complex and adaptive interface which not only responds to pro-fibrotic stimuli but in a particular environment may induce further fibrogenesis. Therefore the study of how these pathways interfere with ECM homeostasis is of particular significance to understanding IPF pathogenesis.

1.2.8 Structure and function of the extracellular matrix

ECM is a mixture of complex molecules including over 300 different types of protein such as collagen, elastin, glycoproteins, fibronectin and proteoglycans[157]. The relative proportions of these proteins in the ECM impart different properties which are organ specific.

Within pulmonary tissue, the ECM can be divided into the epithelial and endothelial cell basement membranes, thin layers which separate epithelium from underlying stroma, and the interstitial ECM. Interstitial ECM is comprised predominantly of fibrillar collagen (type I and type III) and elastin[158]. Cross-linked elastin proteins form the central core of elastic fibres and thereby imbue lung parenchyma with elasticity, enabling stretch of greater than 250% of initial fibre length[159]. Glycoproteins such as fibrillin make up the outer layers of the elastic fibres, while the hydrogel-forming proteoglycans contribute to the overall pulmonary viscoelasticity[158].

By contrast, the rigidity and tensile strength of collagen provides the stress-bearing foundation that ties the alveolar-capillary network together as well as limiting parenchymal distension at the height of inspiration. The fibrillar type I and type III collagens are most represented, while lesser quantities of other fibrillar and non-fibrillar collagens such as collagen V and VI are seen and have regulatory roles in addition to providing a structural scaffold.

Rather than being inert or static, ECM is highly dynamic, with a continuous balance between matrix synthesis and degeneration. Animal studies have shown protein turn-over in pulmonary ECM to be particularly high, with an estimated synthesis rate for non-collagen proteins of 35% per day compared to other tissues such as muscle, skin and heart which demonstrate a range of turnover between 11% and 22% per day[160]. Collagen proteins in the lung also display a higher turnover (10% per day) than other organs (muscle 3% per day, skin 4 % per day, heart 5% per day).

Matrix degradation in humans is primarily co-ordinated through targeted cleavage by the 23-member family of matrix metalloproteinases (MMPs), extracellularly secreted zymogens that are then activated by oxidation or proteolytic cleavage[161]. Most MMPs are collagenases, although only MMP1, 8, 13 and 14 are reported to cleave the triple helix within fibrillar collagen types I, II and III[162]. In healthy lung tissue MMP production and activity is low, with increased activity seen at sites of tissue injury and repair.

The functions of the ECM extend beyond merely a cellular scaffold, with ECM signalling mechanisms proposed to be important determinants of cell behaviour[163]. Cells interact with the ECM through cell adhesion receptors, namely the transmembrane integrins[164]. As a family of heterodimeric proteins there are at least 18 α and 8 β integrin subunits in human and mice genomes, with a total of 24 α/β combinations that have individual and specific roles. Integrins provide cellular connection to, and communication with, ECM ligands, enabling structural changes within the cell as well as activation of signalling pathways to change cell behaviour.

The ECM also serves as a repository for growth factors, which bind to ECM proteins and are later released upon matrix degradation or presented directly from the ECM domain[157]. TGFβ signalling is regulated in this way, with the inactive precursor isoforms binding to other ECM proteins such as fibronectin[163]. Activation of the TGFβ isoforms occurs when the LAP is cleaved upon degradation of the ECM protein, triggering downstream TGFβ signalling. Mechanical strain within the ECM network also triggers integrin binding to the LAP, changing the LAP conformation and thereby activating the TGFβ molecule.

1.2.9 The extracellular matrix in pulmonary fibrosis

Pulmonary fibrosis is characterised by an expansion of the interstitial compartment with abnormal, functionally disruptive ECM. An imbalance caused by excessive collagen fibrillogenesis and reduced collagen degradation was conventionally considered the underlying pathological mechanism. However a number of other ECM proteins including proteoglycans and fibronectin are also increased. Furthermore, collagen content normalised to overall protein is similar between non-fibrotic and fibrotic lung tissue and less relevant to tissue structure-function than post-translational modifications to the collagen molecule[165]. Contrary to the conventional theory of reduced matrix resorption, increased MMP activity and collagen turnover have been identified in IPF cohorts and increased turnover by MMPs of collagen 1, 3, 5 and 6 was associated with increased mortality over 3 months[166,167]. The relevance of MMPs to pulmonary fibrosis is further complicated by their broader roles in matrix metabolism such as the release of growth factors (TGFβ, osteopontin) and facilitation of cellular migration[166].

Rather than being an end-product and passive bystander of the fibrotic cascade, this altered and dysfunctional ECM is hypothesised to be a highly disruptive medium which propagates further pro-fibrotic changes **(Figure 1.6)**[64]. Booth and colleagues demonstrated this through the decellurisation and fibroblast re-seeding of healthy and IPF lung tissue. They found the decellularised IPF ECM strongly upregulated a mesenchymal phenotype within seeded fibroblasts compared to the healthy donor ECM[168]. Another study seeded healthy lung fibroblasts into a polyacrylamide gel with titratable stiffness and demonstrated that an increase in the matrix stiffness was capable of upregulating fibroblast α-SMA expression through polymerisation of fibroblast cytoskeletal actin filaments[169]. In both these studies the changes were observed to be independent of TGFβ, highlighting the potency of ECM to directly influence fibroblast activation.

Aside from the well described integrin pathway, increases in matrix stiffness trigger other mechano-sensitive pathways such as the GTPase RhoA and downstream Rho kinase (ROCK), as well as the Yes-associated protein (YAP)1 and miR-21 to promote further ECM production[170]. Dysregulation of these pathways promotes a positive feedback loop, stimulating fibroblast contractility, proliferation and survival, leading to a vicious cycle of matrix accumulation and remodelling **(Figure 1.6)**[171-173]. Pathological increases in ECM stiffness may also create a mechanical gradient which promotes cellular migration towards the diseased area in the process of durotaxis[158].

In addition to the production of abnormal ECM, mesenchymal cells in IPF tissue are capable of exerting direct mechanical strain on the matrix. In the aforementioned study by Booth et al, the "decellularisation" of healthy donor lung tissue had no appreciable influence on tissue elastance measured by atomic force microscopy[168]. Conversely however, donor IPF tissue was significantly less stiff after decellularisation (yet persistently stiffer than the donor healthy tissue). The contractile phenotype of the IPF myofibroblast may at least partially explain this observation. Expression of α-SMA on these cells leads to cytoskeletal re-organisation and increased formation of stress fibres[174]. These changes enable myofibroblasts to generate contractile forces through myosin light chain phosphorylation and contribute directly towards tissue stiffness. Myofibroblast contractile activity is chiefly regulated through RhoA, a GTPase of the Ras superfamily which, through downstream ROCK, inactivates myosin light chain phosphatase.

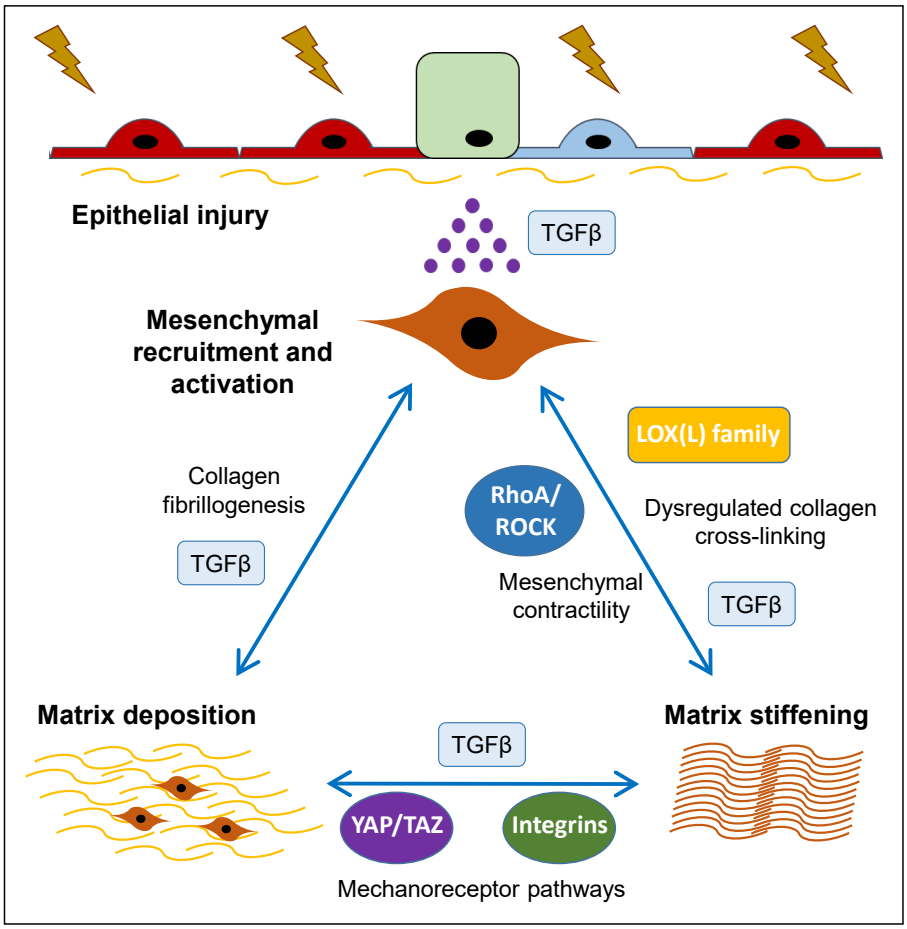

Figure 1.6: A conventional model of extracellular matrix remodelling in fibrosis, and the central role of transforming growth factor β. Pro-fibrotic pathways (namely TGFβ1) mediate mesenchymal activation and proliferation, as well as alterations to matrix quantity and quality. In a vicious cycle, changes to matrix stiffness driven by collagen modification and mesenchymal contractility trigger mechanoreceptor pathways such as Yes associated protein (YAP)1 and integrins, generating further fibroblast activation and matrix remodelling[170].

Tissue stiffness in fibrotic lung matrix can be determined by measuring the relationship between stress and strain[175]. Within this model, strain is the term ascribed to the deformative change in shape for an applied force, such as the expansion in lung volume on inspiration. Stress can be described as the oppositional force which occurs when an elastic material has a force applied to it, such as the rising negative transthoracic pressure which occurs within lung parenchyma during inspiration. Stress and strain have a proportional association termed Young's modulus, which can be used to provide estimates of tissue compliance/stiffness in kilopascals (kPa). Healthy lung is relatively compliant with values generally less than 5kPa[165,168]. Given the heterogeneity of the disease process, measurements of tissue stiffness in IPF are highly variable and range from healthy-equivalent levels to much higher (with one study showing a mean stiffness of 17kPa and peak areas of stiffness greater than 100kPa)[28]. These discrete areas of stiffness correlate to

deposition of fibrotic ECM, and significant research efforts are aimed at understanding the biological processes which alter the ECM in IPF to produce these changes in pulmonary compliance.

Taken together these observations suggest ECM mechano-physiology may contribute to progressive disease by propagating the fibrotic cascade, and highlight the need for further analysis into the mechanisms by which pathological modification of ECM occurs.

1.3 Collagen modification in the fibrotic lung

1.3.1 Synthesis and hydroxylation of collagen

Collagen forms the architectural scaffold across a spectrum of tissues ranging from skin through to bone, and differences in collagen synthesis and modification have an enormous impact on the imparted mechanical properties.

The collagen molecule is synthesised as a pro-peptide composed predominantly of the amino acids glycine, proline and lysine[176]. It subsequently undergoes intracellular post-translational modifications beginning with the ascorbic acid-dependent hydroxylation of lysine and proline peptides through lysyl and prolyl hydroxylases respectively, resulting in formation of the triple helix molecule **(Figure 1.7)**.

The degree of lysine hydroxylation in a collagen molecule is highly variable, and will ultimately affect the type of collagen being formed. As will be discussed in more detail below, organs with compliant ECM such as skin are predominantly comprised of collagen with lysine-aldehyde based cross-links, while stiffer tissue such as bone have more hydroxylysine-aldehyde based cross-links (such as pyridinoline)[176]. Furthermore, individual lysyl hydroxylase family members have specific regional activity, with lysyl hydroxylase 1 (LH1) targeting the triple helical lysine residues on collagen molecules. Conversely lysyl hydroxylase 2, encoded by the gene procollagen-lysine, 2-oxoglutarate 5-dioxygenase 2 (*PLOD2*), is responsible for hydroxylation of collagen lysine residues at the collagen telopeptide. Notably, it is the formation of hydroxylysine residues at the telopeptide which promote the formation of the stiffer pyridinoline-type cross-links[177]. It therefore follows that increases in PLOD2 activity have been associated with a number of fibrotic processes[178]. Further intracellular collagen modification occurs through glycosylation of some of the hydrolysine residues, and while the purpose of these changes are unclear they may influence the level of mineralisation and degree of downstream cross-linking[176].

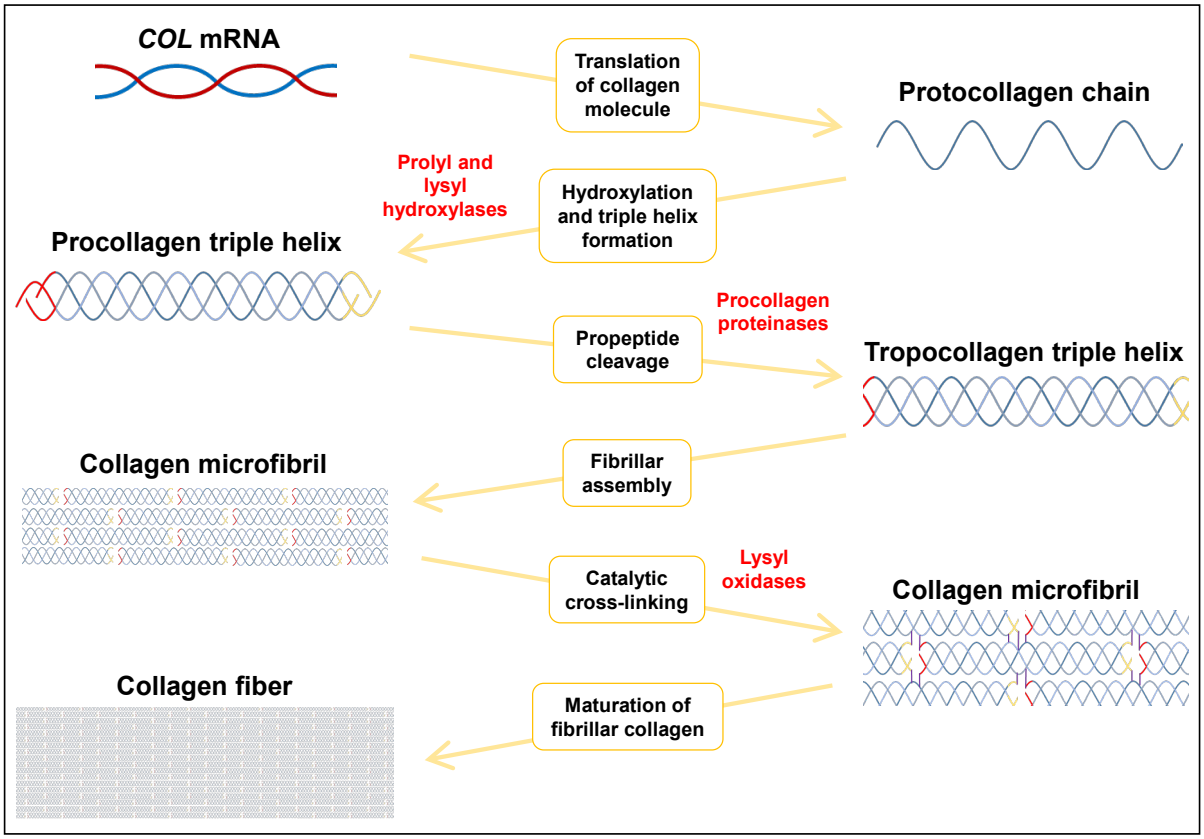

Figure 1.7: Collagen manufacture, post-translational modification and fibrillogenesis. Following translation of protocollagen alpha peptides, ascorbic acid-dependent hydroxylation of prolyl and lysyl residues within three collagen alpha chains leads to the formation of a procollagen triple helix. The procollagen is extracellularly secreted before undergoing N- and C-terminal propeptide cleavage to form tropocollagen. Self-alignment and assembly of individual tropocollagen molecules results in the formation of collagen microfibrils, which are subjected to LOX(L)-mediated oxidation of lysine/hydroxylysine residues, producing aldehydes along the collagen microfibrils. This promotes spontaneous condensation and cross-linking between aldehydes and lysine/hydroxylysine residues, forming the collagen fibril[176].

1.3.2 Collagen cross-linking and fibrillogenesis

The strength of fibrillar collagen lies at least partially in the covalent inter and intra-molecular cross-links which knit collagen fibrils together. Following lysyl hydroxylation, generation of a triple helix and extracellular secretion, the pro-collagen molecule undergoes post-translational modifications to enable fibril assembly. An integral step in this process is the oxidative deamination of specific telopeptide lysine and hydroxylysine residues by lysyl oxidases (LOXs) to facilitate covalent collagen cross-linking[176].

The LOX family consists of five members, LOX and LOX-like peptide (LOXL) 1, 2, 3 and 4, which all possess similar catalytic activities due to their highly conserved C-terminals **(Figure 1.8)**. However while the N-terminus of LOX and LOXL1 is a basic propeptide, LOXL2, 3 and 4 contain four scavenger receptor cysteine rich (SRCR) domains instead. The purpose of these SRCR units remains an area of active research however it is postulated they have non-catalytic roles including trafficking, protein-to-protein interactions, and the regulation of binding to collagen substrates[179,180].

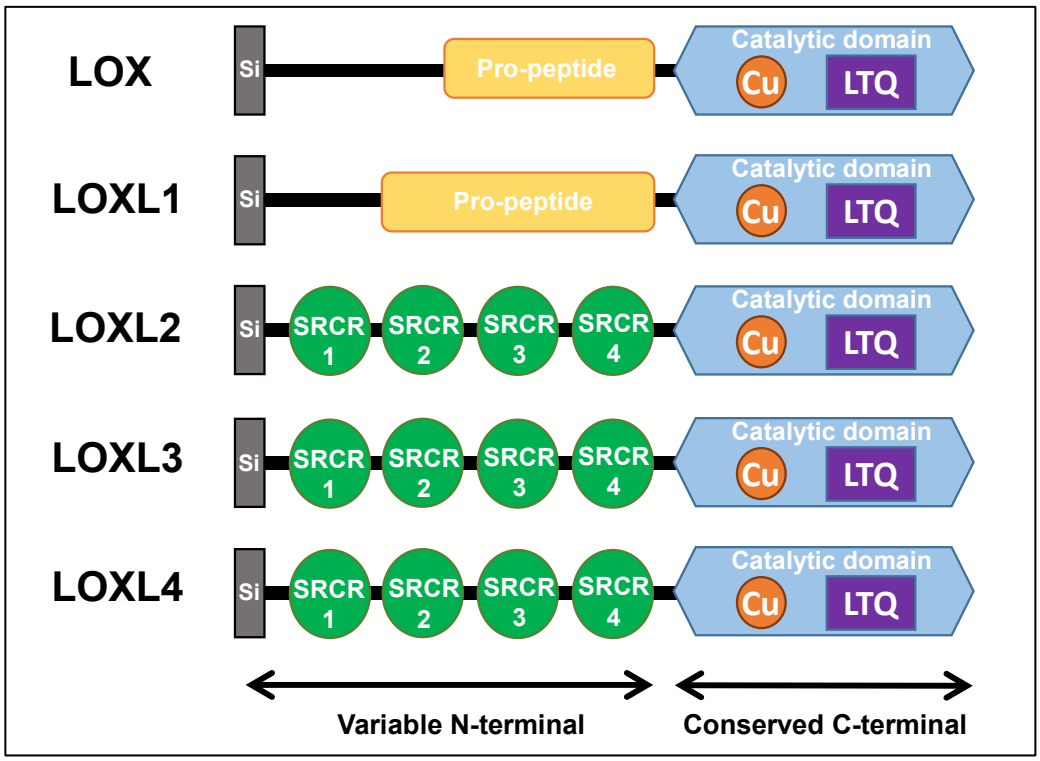

Figure 1.8: The lysyl oxidase-like family. All five LOX(L) members contain a highly conserved C-terminus which requires copper (Cu) to form the co-factor lysyl tyrosyl quinone (LTQ) for catalytic amine oxidation. The N-terminus of LOX and LOXL1 are basic pro-peptides while LOXL2, LOXL3 and LOXL4 have four scavenger receptor cysteine rich (SRCR) domains thought to be relevant to protein trafficking and substrate interactions. Signal peptides (Si) at the N-terminus facilitates extracellular secretion of the enzymes[181].

LOX and LOXL1, but not LOXL2-4, are extracellularly secreted as a soluble, but inactive, pro-enzyme before undergoing modification by procollagen C-proteinases to produce an active (and less soluble) mature enzyme that targets the ε-amino groups on telopeptide lysine and hydroxylysine residues[180,182]. As part of a larger group of amine oxidases, the LOX(L) family requires copper to generate lysyl tyrosyl quinone (LTQ), an essential cofactor for oxidation of its amine substrates[183]. Schiff base production with LTQ at specific telopeptide lysine and hydroxylysine residues leads to the formation of aldehydes. Spontaneous reactions between two

aldehyde groups or between an aldehyde group and an unmodified lysine or hydroxylysine residue ε-amine group on parallel collagen molecules produces an immature (divalent) collagen cross-link.

Different types of immature cross-links are formed depending on the permutations of lysine and hydroxylysine groups in the neighbouring collagen molecules. More compliant tissue such as skin will have lower levels of lysyl hydroxylation, and therefore an increased proportion of lysine aldehyde reactions results in a greater number of lysine aldehyde-derived divalent cross-links to produce aldimines such as lysinonorleucine (LNL)[184]. Conversely in stiffer tissue such as cartilage and bone, higher levels of lysyl hydroxylation lead to greater hydroxylysine-aldehyde reactions and the formation of ketoimines, namely hydroxylysinonorleucine (HLNL) and dihydroxy-lysinonorleucine (DHLNL)[184].

Over time many of the immature divalent cross-links undergo further reactions, developing into mature, trivalent cross-links. The pyridinolines (hydroxylysyl pyridinoline [PYD] and lysyl pyridinoline [DPD]) are comprised of two hydrolysyl-aldehyde residues with either a helical hydroxylysyl or lysyl residue respectively and are predominantly seen in areas of high lysyl hydroxylase activity such as cartilage and bone[184]. Conversely a lower level of lysyl hydroxylation and formation of aldimines in more compliant tissues such as skin and tendon favours the formation of alternative trivalent cross-links such as histidinohydroxylysinorleucine (HHL) and pyrrole **(Figure 1.9)**.

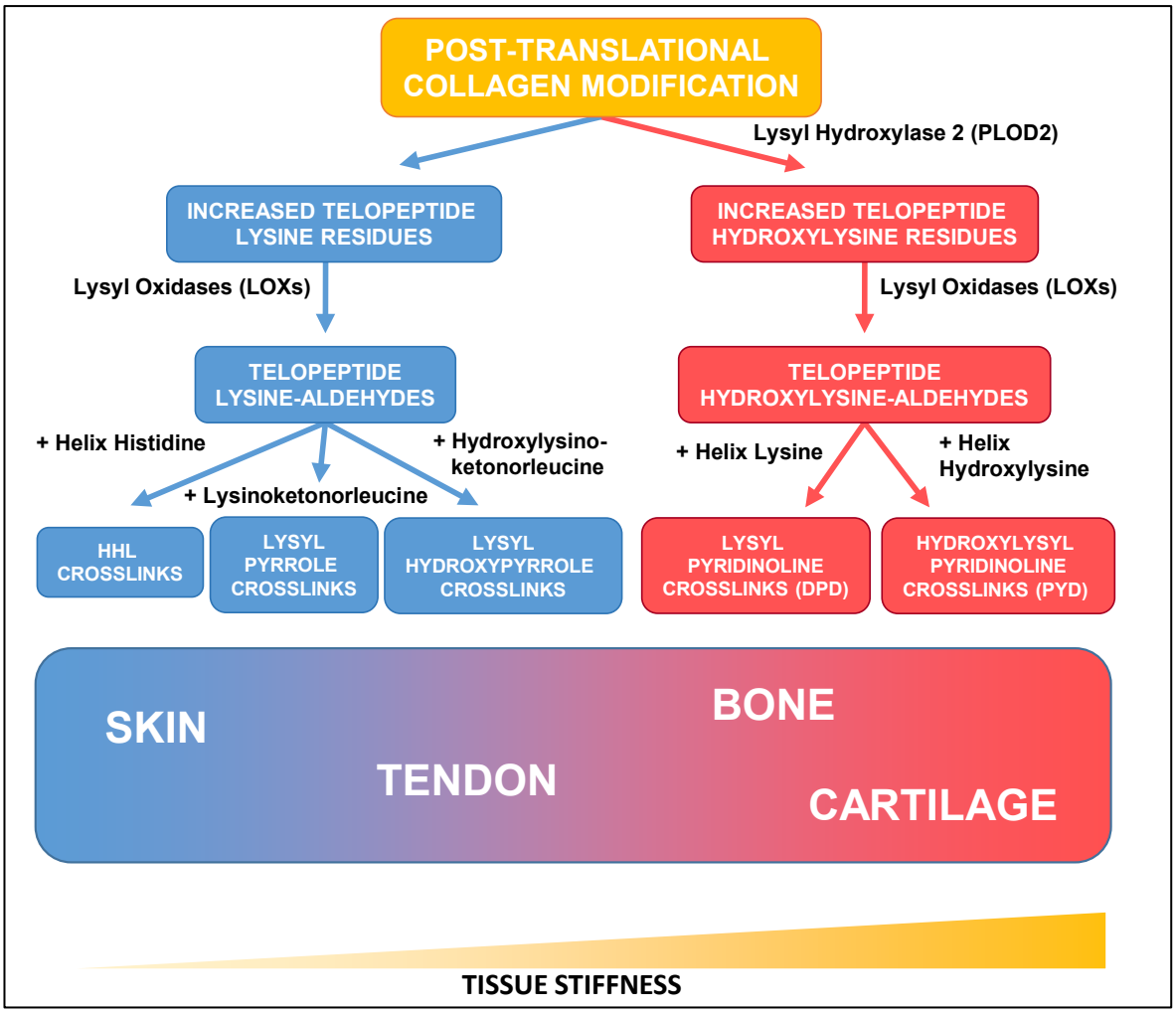

Figure 1.9: The proportion of lysine and hydroxylysine residues at collagen telopeptides determine the type of collagen cross-links and tissue compliance. Softer tissue such as skin has more lysine cross-links, while stiffer tissue such as bone and cartilage has more hydroxylysine cross-links. HHL: Histidinohydroxylysinorleucine. Adapted from Eyre D.R., Wu JJ. Collagen Cross-Links. In: Brinckmann J. et al, Collagen. Topics in Current Chemistry, vol 247. Springer, Berlin, Heidelberg[185].

Other forms of collagen cross-linking occur independently of lysyl oxidases. For example, tranglutaminases are a family of nine highly conserved and calcium-dependent enzymes of which eight are catalytically active but only one (transglutaminase 2, TG2) is broadly expressed across different tissues and cellular compartments[186]. TG2 has important roles in matrix stabilisation during tissue repair by creating protein-protein cross-links through transamidation between glycine and lysine residues to generate an isopeptide bond in a broad range of substrates[187]. Additionally TG2 produces isopeptide covalent bonds between adjoining monomers of individual collagen molecules to enhance stability within the existing structure[186].

1.3.3 Changes to collagen in lung fibrosis

While IPF is classically considered a disease of excessive ECM deposition, the specific changes to the most prevalent protein component – collagen – are less clear. In the early 1980s Fulmer and colleagues published results from a study of IPF versus control lung tissue whereby no difference was observed in collagen concentration (normalised to dry lung tissue weight) and proposed the hypothesis that the type, quality and location of collagen may have more bearing on the disease process[188]. Controversially however another group observed significant increases in normalised collagen concentration in IPF lung, postulating that the inter-study discrepancies may have arisen from the heterogeneity of disease within IPF lung and therefore the sites of sample selection[189]. Kirk et al also found an increase in mean collagen concentration across 14 autopsy and 7 open-lung biopsy samples from patients with IPF compared to 17 controls[190]. Yet when adjusting for autopsy versus open-lung biopsy IPF samples it was evident that the autopsy samples were significantly more collagen-rich than the lung biopsy samples, and the lung biopsy samples had similar collagen concentrations to control. This suggests that discrepancy in the literature could reflect not just sampling variation but also stages of disease, with an earlier cellular fibrotic process eventually giving way to an advancing front of dense acellular matrix accumulation.

A more recent study by Jones and colleagues, including this author, found no difference in collagen concentrations normalised for either total protein or dry weight, yet a significant increase in mean tissue stiffness in IPF lung[165]. The conclusion from this study was that factors other than collagen concentration were capable of influencing the compliance of lung tissue. Changes in collagen cross-linking in fibrotic lung tissue were first described by JA Last and colleagues, who observed a shift in the ratio of immature DHLNL to HLNL crosslinks in acute respiratory distress syndrome as well as increases in mature pyridinoline content in “chronic lung fibrosis”[191]. The observation of increased divalent and trivalent cross-links was confirmed in IPF tissue, alongside an increase in lysyl hydroxylation and lysyl oxidase activity by Jones et al[165]. This study found the proportion of immature hydroxylysine cross-links to be greater than the mature trivalent cross-links (possibly implying an increase in collagen metabolism), and yet it was the mature pyridinoline cross-links which closely correlated to tissue stiffness.

Increased pyridinoline cross-link formation, driven by over-hydroxylation of lysine residues at collagen telopeptides, is considered a common pathway in fibrotic disease[192]. The mechanisms by which pyridinoline cross-linking density impacts on tissue stiffness are incompletely understood, however likely stem from tighter collagen molecule proximity leading to reduced fibril hydration and smaller, more-dense fibrils[165]. In keeping with this hypothesis it was noted that IPF collagen fibrils were smaller in diameter than control fibrils. Increased pyridinoline cross-links have also

been shown to render fibrotic ECM more resistant to proteolytic degradation by MMPs, thereby promoting progressive accumulation and possibly explaining both the increased MMP activity and associated mortality seen in IPF disease[162,167].

1.3.4 Pathological collagen modifiers in IPF

Given the correlation between pyridinoline cross-link density and IPF tissue stiffness, factors which promote these mature bone-type cross-links warrant particular attention.

Members of the LOX(L) family appear to be key pathological modifiers of collagen structure. Through oxidative deamination of the PLOD2-derived hydroxylysine residues at the collagen telopeptides these copper-dependent enzymes promote formation of "bone-type" pyridinoline cross-links to enhance fibril and matrix stiffness. While heavily implicated with pulmonary fibrosis, the LOX(L) family's cause-or-effect nature remain a topic of great debate. TGFβ is a central promoter of LOX(L) expression, suggesting core pro-fibrotic responses inevitably end in the upregulation of LOX(L) activity. Other pro-fibrotic mediators such as PDGF, FGF and hypoxia have also been demonstrated to increase *LOX(L)* expression[193].

Certain LOX(L) family members are more strongly associated with pulmonary fibrosis than others, however the level of functional overlap between the individual family members remains unclear. *LOXL2* has the strongest association and is the most researched, with expression increased in both lung tissue and serum from IPF patients, and high LOXL2 serum levels correlating with increased risk of hospitalisation, lung function decline and mortality in IPF patients[194]. Pre-clinical studies using an anti-LOXL2 monoclonal antibody in bleomycin-exposed mice demonstrated improvement in lung fibrosis scores[195]. Yet the aforementioned phase 2 randomised, placebo-controlled clinical trial using Simtuzumab, a LOXL2 monoclonal antibody, failed to show efficacy in a large cohort of IPF patients, raising important questions about the specific role of LOXL2 and its family members in this disease[51].

Aside from limitations with the monoclonal antibody, an important question is whether inhibiting LOXL2 alone was enough. In a biomechanical analysis of collagen post-translational modification in IPF tissue, Jones et al identified *LOXL2 and LOXL3* to be most significantly upregulated of the LOX(L) family in IPF compared to control tissue[165]. Furthermore, the selective inhibition of LOXL2 / LOXL3 with a small molecule inhibitor on human *in vitro* and rat *in vivo* models of lung fibrosis resulted in normalisation of tissue stiffness. This could suggest some redundancy between LOX(L) family members, implying the need for broader inhibition to inhibit the pathogenic matrix remodelling.

PLOD2, the gene responsible for lysyl hydroxylase 2 which drives the switch towards hydroxylysine-derived cross-links, is increased in IPF tissue and therefore has been put forward as another important pathological promoter of bone-type cross-linking in IPF matrix[165,196]. PLOD2 expression is increased in the IPF samples, along with increases in the density of hydroxylysine-derived immature and mature collagen cross-links, suggesting a PLOD2-mediated switch to produce stiffer matrix in IPF lung tissue[165].

Upregulation of *PLOD2* occurs through a number of pro-fibrotic pathways, however the specific drivers of PLOD2 dysregulation in IPF remain unknown. The archetypal pro-fibrotic mediator TGFβ is perhaps the best known promoter of *PLOD2* induction, mediated through SMAD interactions with the *PLOD2* promoter[197]. Yet TGFβ1 is not the only candidate, with emerging evidence from cancer research suggesting a number of other key regulators. For example *PLOD2* dysregulation has been correlated with EGFR phosphorylation in non-small cell lung cancer, leading to the discovery of an EGFR-PI3K/AKT-FOXA1-PLOD2 axis. Another promising candidate is the hypoxia protein HIF1α, which is reported to modify *PLOD2* induction in a number of malignant cells, most likely through direct modulation of the hypoxic response element within the *PLOD2* promoter[198].

Taken together, core regulatory enzymes such as the LOX(L) family and PLOD2 are responsible for altering the types of collagen cross-links formed in fibrotic lung tissue, although more research is required to identify the cellular sources and characterise expression patterns.

1.4 Summary

IPF is characterised clinically by progressive respiratory failure secondary to loss of lung function, and pathologically by progressive deposition of abnormally modified ECM. These two features are likely intertwined, with matrix accumulation distorting normal lung architecture, inhibiting compliance and impairing gas exchange.

The underlying mechanisms which promote this dysregulated matrix remodelling are being increasingly elucidated. In the genetically predisposed individual, damage to the alveolar epithelium from recurrent exogenous and/or endogenous exposures leads to maladaptive changes including AT2 stem pool exhaustion and senescence, epithelial-mesenchymal transition, proliferation of a basaloid airway epithelial cell population and bronchiolisation of the alveolar compartment. Disruption to the basement membrane from these repetitive injuries and inadequate barrier formation enhance epithelial-mesenchymal cross-talk, leading to the recruitment, proliferation and activation of fibroblasts with active mesenchymal phenotypes in the interstitial compartment.

This cross-talk is mediated through a myriad of pro-fibrotic signalling pathways of which TGFβ, with broad ranging actions on fibroblast proliferation and behaviour, is considered the prototype. However there is increasing evidence for the roles of a variety of other signalling pathways, including tyrosine kinases, canonical and non-canonical Wnt signalling, and HIF pathways.

The aberrant IPF fibroblasts produce excessive and abnormal ECM which is poorly compliant, at least in part because of enhanced post-translational collagen modification. This is important because alterations in matrix stiffness not only affect respiratory mechanics, but through mechano-signalling and durotaxis are likely to promote further fibroblast activity and thereby sustain a progressive fibrogenic response.

Within the IPF ECM, an increase in density of mature trivalent "bone-type" pyridinoline collagen cross-links is the result of enhanced PLOD2-mediated hydroxylysine formation at collagen telopeptides, followed by subsequent increases in lysyl oxidase-mediated aldehyde formation. Changes to pyridinoline cross-link density, rather than the amount of collagen, correlate with IPF tissue stiffness. LOXL2 and LOXL3 appear particularly relevant to this process, with increased expression seen in IPF lung tissue, and selective inhibition demonstrating normalisation of tissue stiffness using *in vitro* and *in vivo* models.

1.5 Hypothesis and aims

1.5.1 Hypothesis

The roles of collagen post-translational modifying enzymes such as *PLOD2* and members of the *LOX(L)* family in the development and progression of IPF remain poorly understood. In particular, the cellular origins and mechanisms of dysregulated *PLOD2* and *LOX(L)* family expression which result in downstream "bone-type" pyridinoline collagen cross-links in the IPF lung have not been explored. Furthermore the upstream signalling pathways which drive aberrant expression of these post-translational collagen modifying enzymes remain unclear.

I hypothesise that pathological remodelling and increased stiffness in idiopathic pulmonary fibrosis involves aberrant expression of collagen cross-linking enzymes, and this is determined by dysregulation of core upstream signalling pathways.

A better understanding of the cellular origins of collagen cross-linking enzymes and the upstream pathways which lead to their dysregulation in IPF lung will provide an important platform for further study into matrix homeostasis in IPF, with substantial therapeutic implications. Localisation of the sources of these enzymes and their upstream regulatory processes will

facilitate the development of better disease models as well as identify novel targets for inhibition of pathological matrix remodelling. Normalisation of tissue stiffness could not only improve respiratory mechanics and physiology, but through inhibition of the disease-propagating mechano-sensitive pathways may impede disease progression.

1.5.2 Aims

I propose to investigate the core regulatory processes of collagen post-translational modification IPF which result in pathologically altered ECM. To achieve this my aims are:

i) To compare the expression patterns and cellular sources of collagen cross-linking enzymes in healthy and IPF lung tissue.
ii) To determine core signalling pathways which control collagen cross-linking enzyme expression and are dysregulated in IPF.
iii) To use a 3D *in vitro* model of a fibroblastic focus to determine the importance of these dysregulated pathways in promoting post-translational collagen modifications and increased matrix stiffness.

Chapter 2 Materials and Methods

2.1 Obtaining clinical material

Human lung tissue from healthy and IPF donors was obtained from University Hospital Southampton under the "Pathophysiological Mechanisms of Pulmonary Fibrosis" study led by Dr Mark Jones in collaboration with Dr Aimen Alzatani from the Southampton Department of Cardiothoracic Surgery. Ethical approval for the study was provided by Mid and South Buckinghamshire Local Research Ethics Committee (LREC#: 07/H0607/73).

Healthy lung tissue samples were obtained from macroscopically normal sites in patients undergoing clinically indicated lung resection for suspected malignancy. IPF lung tissue samples were obtained from clinically indicated surgical lung biopsy for the diagnosis of their ILD (subsequently confirmed to be IPF at a radiological/histopathological MDT).

In both groups the subjects were provided with a participation information sheet before giving written consent.

Samples were processed for either live cell culture by Dr Franco Conforti and Dr Rob Ridley (as described below) or for histochemical analysis by the Southampton Histochemical Research Unit (HRU). For histochemical analysis, samples were fixed for 48 hours in neutral buffered formalin and embedded in paraffin wax. 4 micron thick serial sections were cut from the formalin-fixed paraffin-embedded (FFPE) blocks and mounted on glass histology slides.

2.2 Laser capture micro-dissection

Laser capture micro-dissection (LCMD) was employed to obtain tissue from discrete regions of healthy and IPF lung, which were then further analysed using RNA sequencing to identify regional patterns of collagen cross-linking enzyme expression **(Figure 2.1)**. LCMD was performed by Dr Mark Jones using a Leica ASLMD laser microdissection microscope. 4 micron thick sections (mounted on Leica membrane slides) stained with Paradise PLUS staining solution (Life Technologies, UK, catalogue number KIT0312S) were examined under live microscopy, and the region of interest outlined prior to dissection using an ultraviolet laser and displacement from the tissue into a sample container.

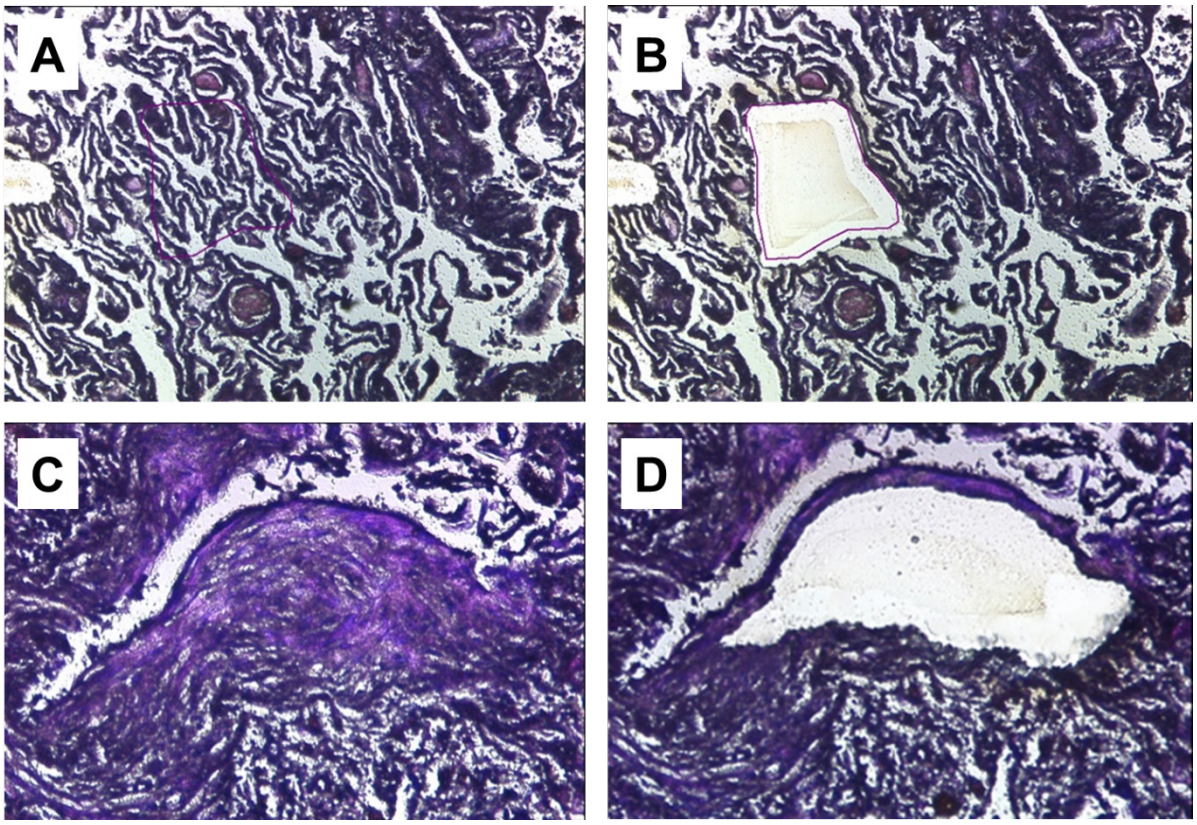

Figure 2.1: Use of laser capture micro-dissection to obtain region-specific samples of IPF tissue for RNA sequencing. (A) An area of alveolar septae in lung tissue from an IPF donor. **(B)** Residual section following LCMD-mediated removal of a discrete region of alveolar septae for subsequent analysis. **(C)** A fibroblastic focus (centre) in lung tissue from a donor with IPF. **(D)** The remaining tissue section after LCMD-removal of the fibroblastic focus. Images courtesy of Dr Mark Jones.

RNA from dissected samples was isolated using Micro Filter Cartridges from RNAqueous-Micro Total RNA Isolation Kit (Invitrogen, UK, AM1931) according to the manufacturer's instructions, and the Ion Ampli-Seq-transcriptome human gene expression kit (Life Technologies, UK, A26325) was used to prepare cDNA libraries as per the manufacturer protocol. The cDNA libraries were sequenced using Ion Torrent Proton Sequencing by Dr Milica Vukmirovic and Dr Naftali Kaminski at the Yale School of Medicine, Connecticut, USA. The reference genome University of California and Santa Cruz (UCSC) hg19 was used for mapping reads and Fragments per Kilobase of exon per Million (FPKM) values were calculated using Cufflinks[199]. FPKM data was provided to, and analysed, by Dr Mark Jones and myself.

2.3 RNA *in-situ* hybridisation

To observe the cellular sources and patterns of collagen cross-linking expression *in situ*, duplex RNA *in-situ* hybridisation (RNAscope, Biotechne, UK) was performed on healthy and IPF lung

tissue as per the manufacturer protocol (RNAscope 2.5 Duplex Detection protocol for FFPE tissues, 322500-QKG). This method has superior sensitivity and specificity over earlier non-radioisotopic techniques due to the use of a double oligonucleotide Z target probe (Z probe pair) conjugated to an enzyme label **(Figure 2.2)**[200]. Both of the Z probes within the Z probe pair must hybridise to the target sequence in order for signal amplification. Z probe pairs target mRNA with > 300 base pairs, and a signal is achieved after hybridisation of the target mRNA with a minimum of 6 Z probe pairs. The RNAscope methodology employs similar steps to conventional immunohistochemistry and allows for labelling and amplification of single RNA molecules with minimal background staining.

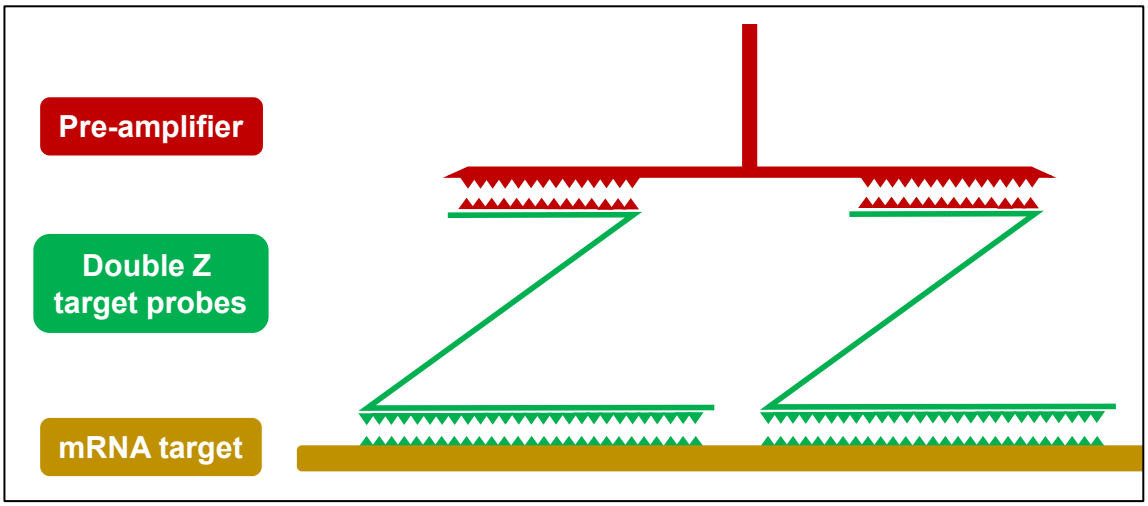

Figure 2.2: RNA in-situ hybridisation uses double Z target probes to bind target mRNA with high sensitivity and specificity. Target probes each have an 18-25 base sequence (the bottom of the Z) that is complimentary to the target mRNA, enabling hybridisation. The top of each Z probe is a 14 base sequence specific to the pre-amplifier. After hybridisation of both Z probes to the mRNA, the combined 28 base sequence binding site is available for hybridisation of the pre-amplifier. Multiple sites on the pre-amplifier enable binding of amplifiers, followed by binding of the chromogenic enzyme to the amplifiers to enable a signal[200].

RNAscope assays were performed according to manufacturer's instructions. Briefly, 4 micron thick histopathological sections were baked for 1 hour at 60°C, deparaffinised in xylene and rinsed twice in 100% ethanol before being left to air dry. The slides were then incubated in RNAscope hydrogen peroxide solution for 10 minutes to neutralise endogenous peroxidases and rinsed in water. Target retrieval was performed by incubating slides for 15 minutes in pre-heated RNAscope 1X Target Retrieval Solution at >95°C using a manufacturer-recommended food steamer. RNAscope protease plus was then applied to each section and incubated for 30 minutes

in the RNAscope HybEZ Oven (all steps incorporating the RNAscope HybEZ oven were performed at 40°C).

The RNAscope duplex probes were subsequently applied in combination and hybridised for 2 hours in the HybEZ oven. *LOXL2* was detected by a channel 1 (C1)-probe (Probe-Hs-LOXL2-C1, 311341) and *PLOD2* was detected using a channel 2 (C2)-probe (Probe-Hs-PLOD2-C2, 547761-C2). On adjacent serial sections *LOX* was detected using a C1-probe (Probe-Hs-LOX-C1, 311341) and *LOXL3* detected using a C2-probe (Probe-Hs-LOXL3-C2, 547761-C2). Premixed RNAscope positive duplex controls (*PPIB* in C1 and *POLR2A* in C2, 321641) and negative duplex controls (*DapB* in both C1 and C2, 320751) were used to confirm true tissue staining **(Figure 2.3)**.

Six probe amplification steps were then performed to detect the red (C2) signal by applying RNAscope amplification reagents 1 through 6 (150µL of each per slide) for between 15 and 30 minutes each, with wash steps in between using RNAscope 1x wash buffer. The red signal was detected by adding RNAscope AP Fast Red to each section and incubating for 10 minutes at room temperature. Four more amplification/wash steps were then performed before detection of the green (C1) signal using RNAscope HRP Green to each section and incubating for 10 minutes at room temperature. Sections were counterstained with 50% Gill's Haemtoxylin in dH_2O for 30 seconds and then mounted with coverslips using Vectamount permanent mounting medium (Vector laboratories, H-5000).

On visualising samples, individual mRNA molecules were identified by discrete points of chromagen. When mRNA expression is high these distinct spots coalesce to form dense regions of colour **(Figure 2.3 A)**. The RNAscope probes are highly specific and therefore no staining is observed in regions which do not express the gene of interest (GOI). Negative controls were used throughout the mRNA in-situ hybridisation experiments to confirm chromagen staining was specific for the GOI **(Figure 2.3 B)**.

Slides were imaged using the Olympus Batch Dotslide VS110. To confirm significant results the staining patterns were analysed by Prof Aurelie Fabre, Dublin, an independent expert histopathologist in the field of interstitial lung disease.

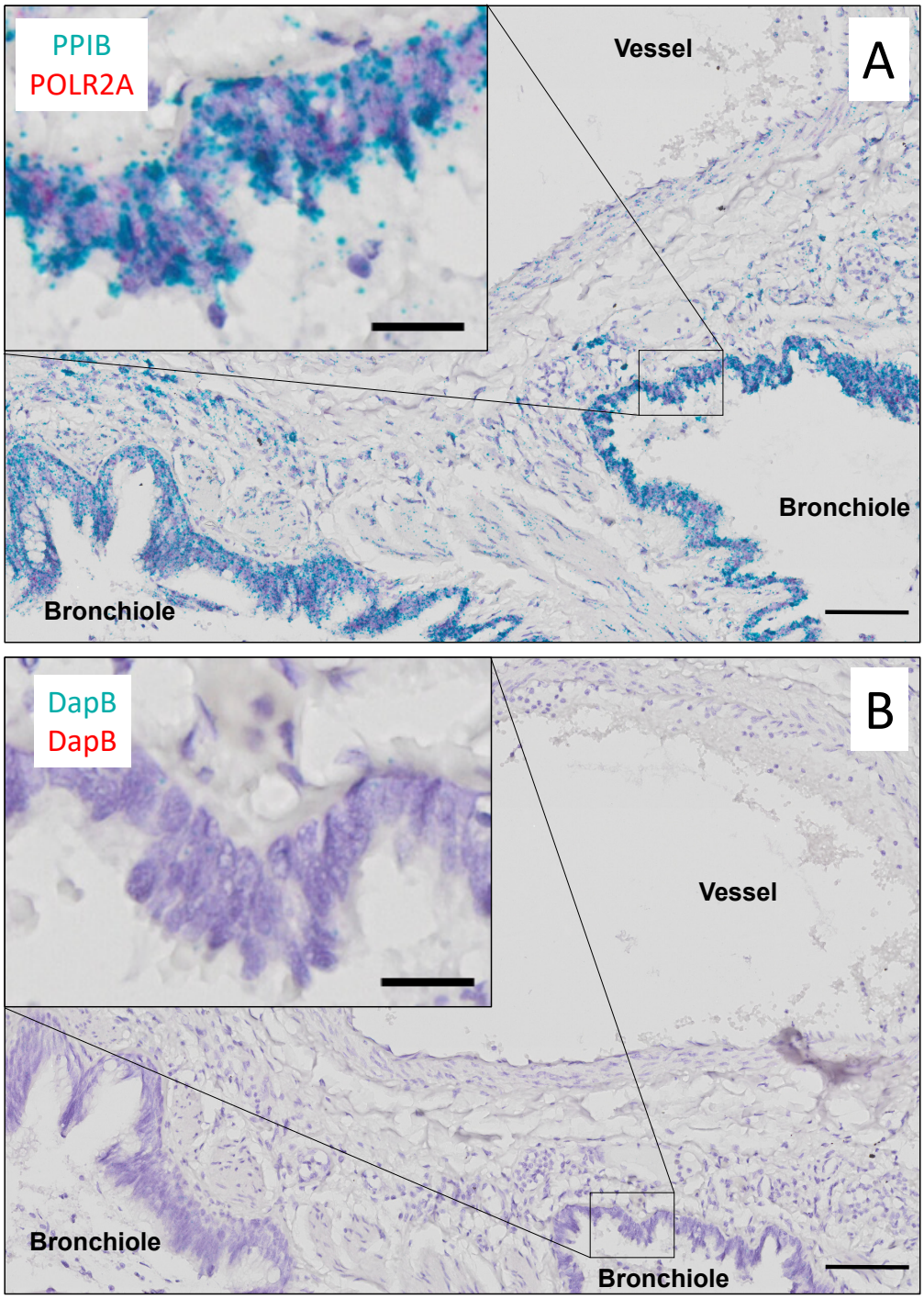

Figure 2.3: RNA in-situ hybridisation of IPF tissue with positive and negative controls.

Representative RNA in-situ hybridisation images of **(A)** the ubiquitously expressed positive control genes peptidyl-prolyl cis-trans isomerase B (*PPIB* - green arrows) and RNA polymerase II Subunit A (*POLR2A* - red arrows). As described by the manufacturer, *PPIB* expression in bronchial epithelium is typically high while *POLR2A* expression is typically low-medium. **(B)** Duplex negative control genes using 4-hydroxy-tetrahydrodipicolinate reductase (*dapB* – a gene from *Escherichia coli* bacteria), in both channels which confirm no staining. Macro scale bar 100µm and inset scale bar 20µm.

2.4 Cell culture

2.4.1 Primary lung fibroblast cell lines

Fibroblast experiments were performed using primary human lung fibroblasts from three different “healthy” donors between passages 4-6, and six different IPF donors between passages 4-6.

Pulmonary fibroblasts were outgrown from lung tissue taken at surgical biopsy by Dr Franco Conforti and Dr Rob Ridley, School of Medicine, University of Southampton using established methodologies[201] before being passaged, cleaned of debris with media changes, testing for mycoplasma (MycoFluor Mycoplasma Detection Kit, Life Sciences UK, M7006) and subsequent cryopreservation (methodology discussed below).

For all monolayer experiments primary lung fibroblasts were cultured in Dulbecco’s Modified Eagle Medium (DMEM, Gibco 41965039) with 10% Fetal Bovine Serum (FBS, Gibco 10500064), 1% penicillin-streptomycin (PS, Gibco 15070063), 1% Non-Essential Amino Acids 100x (NEAA, Gibco 11140035), 1% L-glutamine 200mM (Gibco 11140-035) and 1% Sodium Pyruvate (NaP, Gibco 11360070).

2.4.2 Immortalised alveolar epithelial cell line

Epithelial cell experiments were primarily performed using an immortalised alveolar epithelial type 2 (AT2) cell line ($AT2^{ER:KRASV12}$) provided by Dr Yihua Wang of the School of Biological Sciences at the University of Southampton. The cell line’s immortalised state is a result of being retrovirally transduced with human telomerase reverse transcriptase (hTERT) and two mutants of large-tumour (LT – U19 and tsA58)[202]. This cell line was originally derived from AT2 cells obtained from human lung resection samples, and expresses several alveolar epithelial cell markers including surfactant protein C[143].

The cell line also stably expresses the 4-hydroxytamoxifen (4-OHT)-inducible chimeric protein ER:KRAS:V12[203,204]. This results in RAS pathway activation upon exposure to 4-OHT, enabling a specific mechanism for RAS activation with negligible off-target effects.

$AT2^{ER:KRASV12}$ cells were cultured in DCCM-1 serum free media (Biological Industries 05-010-1A) with 10% FBS and 1% Penicillin-Streptomycin-Glutamate (PSG, Gibco 10378016).

2.4.3 Primary alveolar type 2 epithelial cells

Primary AT2 cells were outgrown by Dr Franco Conforti from lung tissue taken at surgical biopsy, as previously described, and subsequently cryopreserved[201,205].

Cells were subsequently thawed and seeded onto collagen-coated plates in pre-warmed media containing DCCM-1, 10% Newborn calf serum (NBCS, Gibco 16010159) and 1% PSG. Cells were cultured for 6 days with media replacement every 48 hours prior to the introduction of experimental conditions.

2.4.4 Cellular thawing, passage, and cryopreservation

For cryopreservation, cells were chilled on ice and then suspended in chilled complete media with 10% dimethyl sulfoxide (DMSO, Sigma D2650). 1mL aliquots were placed in cryovials and frozen slowly using "Mr Frosty" freezing containers at -80°C. After 24 hours the cells were transferred for long-term storage in liquid nitrogen (-196°C).

For thawing from cryopreservation, cells were removed from liquid nitrogen and thawed in a 37°C water bath under direct observation until almost completely thawed. The de-frosted cell suspension was then rapidly added to 5mL of pre-warmed complete media (either DCCM-1 for immortalised AT2 cells, or DMEM for lung fibroblasts) before centrifuging at 300xg and careful discarding of the DMSO-containing supernatant. The cell pellet was re-suspended in 1-3mLs of complete media before use as required.

Cells were passaged after reaching a confluence of between 70-80%, usually following two to three days incubation. The medium was discarded and the monolayer rinsed with pre-warmed Hank's Balanced Salt Solution (HBSS without calcium and magnesium, Gibco 14170112) to remove residual FBS. Trypsin-EDTA 0.05% (Gibco, 25300054) was added in an appropriate volume (1mL for a 75cm^2 monolayer) and the flask incubated for 5 minutes at 37°C. Following confirmation of cellular detachment from the plastic base by microscopic examination, the trypsin was deactivated with 5-7mLs of complete media. A 10µL aliquot was taken for counting with a haemocytometer while the remaining cell suspension was spun at 300xg for 5 minutes and the media/trypsin removed, before resuspension of the cell pellet in 3mLs of fresh complete media.

2.4.5 Pro-fibrotic condition reagents

A variety of pro-fibrotic conditions were used for both monolayer and 3D transwell culture experiments.

EGF (R&D systems, 236-GMP-200) was reconstituted as per manufacturer protocol using sterile phosphate buffered solution (PBS), and used at 10ng/mL in both monolayer time course experiments and 3D fibroblastic focus model experiments.

TGFβ1 (R&D systems, 240-GMP-010) was reconstituted as per manufacturer protocol using 4mM HCl, and used at 10ng/mL in monolayer time course experiments and at 3ng/mL for 3D fibroblastic focus model experiments.

Dimethyloxallylglycine (DMOG, Merck, CAS89464-63-1) was reconstituted in DMSO as per manufacturer protocol and used at 0.1-1mM in monolayer and 3D fibroblastic focus model experiments.

Recombinant Wnt3a (R&D systems, 5036-WN) and Wnt5a (R&D systems, 645-WN) were reconstituted as per manufacturer protocol using sterile PBS with 0.1% bovine serum albumin (BSA). They were used at 100ng/mL in monolayer experiments.

The selective PHD2 inhibitor N-[[1,2-Dihydro-4-hydroxy-2-oxo-1-(phenylmethyl)-3-quinolinyl]carbonyl]-glycine (IOX2, Tocris, 4451) was reconstituted in DMSO as per manufacturer protocol and used at 50-250μM in both monolayer and 3D fibroblastic focus model experiments.

2.4.6 Short-interfering RNA transfection

Transfection of short-interfering (si)RNA was performed to silence select gene expression within lung fibroblasts and alveolar epithelial cells in order to examine downstream effects. SiRNA are formed from longer double-stranded RNA by endoribonuclease Dicer, an RNase enzyme[206]. They can be delivered into the cell through a variety of carriers, broadly divided into viral and non-viral vectors. Reverse transfection involves the transfection of siRNA during passage of the cells (while they are still in suspension), while in forward transfection the cells are already adherent to the plate when the siRNA is delivered. RNA interference occurs through the cell's RNA-induced silencing complex (RISC), which binds to the siRNA before targeting the specific mRNA of interest. The mRNA is subsequently cleaved by RISC protein, thereby preventing its expression.

In monolayer experiments both AT2 cells and lung fibroblasts were reverse transfected with either control (On-Targetplus Non-targeting pool, D-001810-10-05), HIF1α (On-Targetplus Human HIF1A, L-004018-00-0005), HIF2α (On-Targetplus Human EPAS1, L-004814-00-0005) or LOXL2 (On-Targetplus Human LOXL2, L-008020-01-0005) siRNA using RNAimax lipofectamine transfection reagent (ThermoFisher, 13778030).

Briefly, for every 2mls of culture media used in the experiment 2.5µL of siRNA and 7.5µL of RNAimax lipofectamine were added to separate 250µL aliquots of Opti-MEM culture media (Gibco, 31985062) and warmed to room temperature before combining together and incubating for 20 minutes at room temperature. Cell density and media volume was pre-determined by the size of the wells used for the experiment. Cells were incubated in trypsin, spun and resuspended in the required amount of media before combining with the siRNA/lipofectamine media (500µl of siRNA mixture for every 2mls culture media) and aliquotting into experimental wells. Plates were incubated overnight in the culture media and siRNA before replacing with fresh media within 24 hours

In the 3D fibroblastic focus model, cells were initially reverse transfected as described above. After 6 days of cell culture (24 hours prior to spheroid formation and application of experimental treatments), a second forward transfection was performed. For every 2mLs of required culture media, 500µL of siRNA mixture was prepared as described above and the combined siRNA culture media was warmed to 37°C before replacing the pre-existing culture media in the fibroblast model. Cells were subsequently incubated in the siRNA culture mixture for 24 hours prior to replacement with fresh media containing experimental treatments.

Silencing efficacy was confirmed by examining mRNA and protein expression of the target gene within lysed samples. Aliquots of media were also obtained from individual samples at harvest and blotted to examine the level of extracellularly-secreted LOXL2, an indirect measure of silencing efficacy for LOXL2 or upstream pathways within samples.

2.4.7 Inhibitors of HIF and LOX(L) enzymes

Dose-finding experiments were performed on primary lung fibroblasts using three different HIF-inhibiting compounds. Digoxin (Sigma, D6003-100MG) was prepared as per the manufacturer protocol to a 2mM working stock by reconstituting in DMSO. Echinomycin (Sigma, 330175-1MG-M) was prepared as per manufacturer instructions by reconstituting in DMSO for a 1mM working stock. NSC124754 (Merck, 400086) was prepared as per manufacturer protocol by reconstituting in DMSO for a 10mM working stock. Vehicle controls with DMSO were included in all experiments and treatment conditions had an adjusted DMSO concentration to that of the highest dose.

The LOXL2,3 selective inhibitor PXS-S2A (a gift from Wolfgang Jarolimek, Pharmaxis, Australia) was used in the 3D fibroblastic focus model at concentrations selective for LOXL2/3 inhibition only (0.1µM) and doses which were capable of inhibiting pan LOX(L) expression (10µM)[165]. It was reconstituted as per the manufacturer protocol to a working stock of 10mM using DMSO. All experiments with PXS-S2A contained vehicle controls for DMSO content.

2.4.8 3D fibroblastic focus model culture

The *in vitro* 3D fibroblastic focus model uses primary lung fibroblasts from IPF donors to form spheroids of cells within endogenously-produced ECM that morphologically and biomechanically reflect the fibroblastic foci seen in IPF lung tissue. This system is already in use to investigate mechanisms of lung fibrosis and test novel anti-fibrotic compounds, and the methods for the 3D fibroblastic focus model have been described previously[165]. Briefly, lung fibroblasts were seeded in complete DMEM at 15,000 cells per well using transwells on 24-well plates. The following day the complete DMEM media was replaced with an optimised 3D fibroblastic model media containing the necessary compounds for fibroblast synthesis of ECM **(Appendix A)**. The 3D model media was replaced in both the apical and basal compartments of the transwell 3 times per week for the duration of the experiment. After 1 week of culture in 3D media, the experimental treatments were added. Thus a pilot 3D model experiment which lasted 2 weeks had 1 week of experimental treatment, while a full 6 week experiment had 5 weeks of experimental treatment.

After completion of the pilot or full experiments the samples were processed accordingly. For protein analysis, the spheroids and their surrounding outgrowth sheets of cells and ECM were each incubated in 200µL of 2x Laemmli buffer and underwent mechanical lysis using the TissueLyser LT (Qiagen, 85600) for 6 x 1 minute intervals at 50 hertz. For mRNA extraction, samples were submerged in 300µL of RNA protection reagent (Monarch, T2010) and treated with 45µL of proteinase K solution (Monarch, T2019L) and incubated at 55°C for 30 minutes as per the manufacturer protocol (Monarch total RNA extraction for fibrous tissue). Samples were subsequently mechanically homogenised using the TissueLyser LT (6 x 1 minute intervals at 50 hertz) before RNA was isolated as per the manufacturer's instructions (described below). For collagen biomechanical analysis the samples were enclosed in sterilised aluminium foil parcels and flash frozen in liquid nitrogen before storage at -80°C. For tinctorial stains the samples were fixed in 4% paraformaldehyde (PFA) and embedded in paraffin blocks (courtesy of the HRU, University Hospital Southampton). For electron microscopy the samples were fixed in 3% glutaraldehyde in 0.1 M Cacodylate buffer at pH 7.4 (courtesy of the Biomedical Imaging Unit (BIU), University Hospital Southampton). For second harmonic generation imaging the samples were fixed in 4% PFA and stored in PBS with 0.05% Sodium Azide.

2.5 Immunohistochemistry

Immunohistochemistry enables the identification of specific proteins of interest within sections of clinical tissue using antibodies directed against specific antigens of interest, followed by amplification and labelling of the antibody with a chromagen or fluorophore.

Immunohistochemistry was used within the study to analyse the expression of HIF pathways and downstream markers of hypoxia in lung tissue from healthy and IPF donors. A streptavidin biotin-peroxidase system was used for amplification followed by detection with the chromogenic tetrahydrochloride 3,3'-Diaminobenzidine (DAB) as per the manufacturer protocols.

In detail, sections were deparaffinised through Clearene solvent (Leica biosystems 3803600, two x 10 minutes incubation) and rehydrated through gradated alcohols to a final bath of distilled water (dH_2O). Antigen retrieval was performed using microwave heating (50% power for 20 minutes) with samples in a citrate buffer (0.01M, pH 6). Endogenous peroxidase was nullified by incubating sections in 3% hydrogen peroxide in dH_2O for 15 minutes, followed by a PBS rinse.

Non-specific antigen binding was blocked by incubating slides for 20 minutes in serum from the animal species that the secondary antibody was raised in (for both HIF1α and Ca9 this was goat serum, Dako, X090710-8). Goat blocking solution was prepared by diluting neat goat serum to a concentration of 0.015% in TBS-0.1% Tween 20 (TBS/T). Blocking solution was then tapped off before addition of the primary antibody (150µL per slide) and incubation overnight at 4°C.

HIF1α (Cayman, 10006421, IgG raised in rabbit) or Ca9 (Novus Bio, NB100-417, IgG raised in rabbit) were diluted to a concentration of 0.2% (1:500) in goat blocking solution. Isotype controls were performed with polyclonal immunoglobulins of the animal species that the primary antibody was raised in (Rabbit IgG, Dako, X090310-8) at an equivalent concentration to the primary antibodies, to exclude non-specific staining **(Figure 2.4)**.

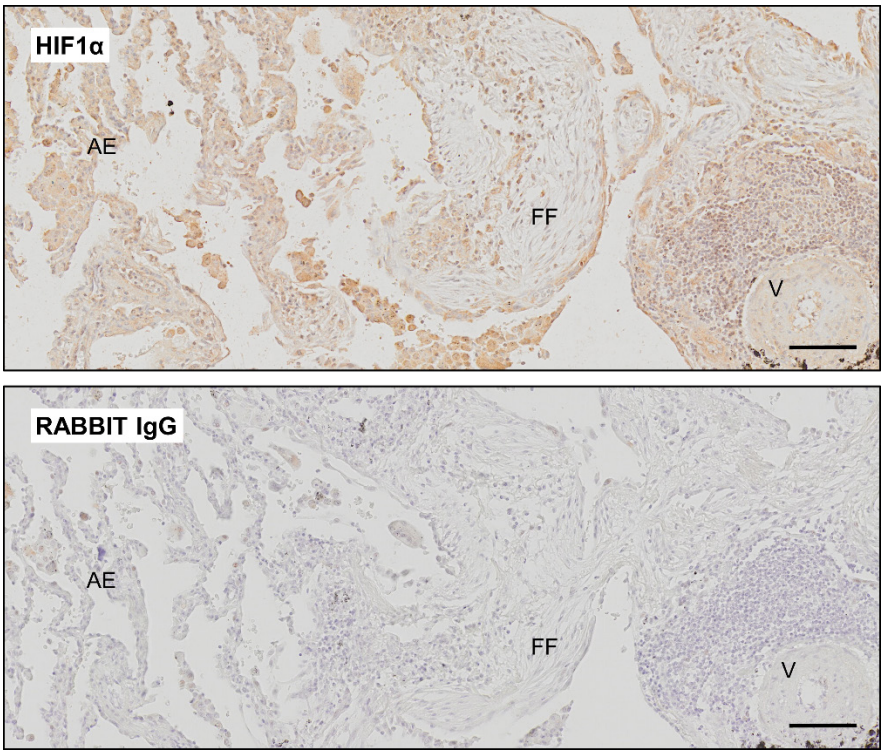

Figure 2.4: Immunohistochemistry staining of IPF tissue with HIF1α and isotype control. IHC staining of serial sections from a donor with IPF demonstrating alveolar epithelium (AE), a fibroblastic focus (FF) and a blood vessel (V), staining for HIF1α (top) and an isotype control using Rabbit IgG in an equivalent concentration (bottom). Scale bar 100µM.

The following day the primary antibody was gently tapped off and three TBS rinses (5 minutes each) were performed before addition of the secondary antibody (biotinylated goat anti-rabbit, Dako, E0432, dilution 1:500 in PBS, 150µL per slide) and incubation for 20 minutes at room temperature. 3 x TBS rinses (5 minutes each) were performed before application of the Avidin Biotin Complex (ABC) reagent (Vectastain, Elite ABC Kit, PK6100, 150µL per slide) and incubation for 30 minutes at room temperature. 3 further TBS rinses (5 minutes each) were subsequently undertaken followed by addition of DAB diluted in the imidazole substrate buffer (DAB+ substrate chromagen system, Dako, K3468, 150µL per slide) and incubation for 5 minutes.

Sections were then rinsed in TBS, bathed in running water for 2-3 minutes, counterstained in Mayer's haematoxylin (Sigma, MHS32) for 1 minute, rinsed for a further 2 minutes in running water and dehydrated through gradated alcohols to clearene (Leica biosystems 3803600, two x 10 minutes incubation) before applying pertex and a coverslip.

Sections were left to dry for 24-48 hours and then imaged using the VS110 Batch Dotslide scanner.

2.6 Hypoxia chamber

In addition to other methods, HIFs were stabilised through atmospheric hypoxia using a HypoxyLab bench-top workstation (Oxford Optronix). The sealed chamber was temperature and humidity controlled to ensure optimal culture conditions for cells incubated over several days. The PO_2 within the unit was controlled automatically by adjusting the ratio of nitrogen, air and oxygen from attached cylinders.

Prior to the hypoxia chamber experiment, cells were seeded and incubated for 24 hours, and media was changed to conditioned media just prior to introduction to the hypoxia chamber. The hypoxylab was first turned on and allowed to equilibrate to the pre-specified temperature (37°C), humidity (80%), CO_2 (5%) and PO_2. All hypoxia experiments were performed at a PO_2 of 8mmHg (equating to approximately 1% oxygen at sea level)[207].

Cells were lysed at the completion of the experiment while still in the hypoxia chamber, in order to stabilise HIFα RNA and protein prior to sample exposure to a normoxic environment. Samples were subsequently processed in the same way as non-hypoxia chamber experiments.

2.7 RNA extraction, reverse transcription and real time quantitative polymerase chain reaction

2.7.1 RNA isolation

Formation of mRNA occurs during transcription of nuclear DNA, and facilitates genomic instructions for cytoplasmic protein formation by ribosomal translation. Thus mRNA can be detected and quantified using methods such as RTqPCR in order to understand cellular expression at a transcriptional level.

To isolate RNA for analyses the Total RNA Miniprep Kit (Monarch, T2010S) was used as per the manufacturer's protocol. In detail, the cell monolayer was lysed with Monarch lysis buffer (300µL per well for a 6 well plate) before being transferred to the genomic (g)DNA removal column and centrifuged to trap gDNA in the membrane. All centrifuge steps were performed at 16000g for 30 seconds. The flow-through was collected and 300µL of 100% ethanol was added and gently mixed before the sample was transferred to the RNA purification column and centrifuged. The trapped RNA was treated with the wash buffer, the DNAse pre-treatment, the priming buffer and several further washes (all supplied in the Monarch kit), with centrifugation of the column between steps and discarding of the flow-through. Finally the clean, bound RNA was released from the silicon

membrane of the spin column with nuclease-free water (30-100µL) into an RNAse-free 1.5mL eppendorf tube.

The wavelength absorbance of the RNA samples at 230, 260 and 280nm was measured using the NanoDrop ND-1000 Spectrophotometer to estimate RNA quantity and purity. The aromatic base moieties within RNA enable the absorption of UV light at 260nm, which can be used to quantify the amount of RNA in a sample (measured in ng/µL). The presence of proteins within the sample can be estimated through their aromatic amino acid side chains which have strong absorbance at 280nm. Other contaminating compounds such as phenol and salts have high absorbance at 230nm. Therefore the purity of RNA could be estimated using both the 260/230 and 260/280 ratios. High quality RNA was considered to have been produced with 260/280 and 260/230 ratios >1.8.

2.7.2 Reverse transcription

Reverse transcription of the RNA was performed using the Precision nanoScript2 Reverse Transcription Kit (Primer Design, UK) as per the manufacturer protocol. Briefly, in the annealing phase a predetermined amount of RNA (usually 1µg) was added to a mastermix of supplied random hexamer primers, oligo deoxythymidylic (dt) primer and deoxynucleoside triphosphate (dNTP) mix in thin-walled 200µL containers. The solution was made up to 10µL using RNAse-free H_2O. The samples were then incubated for 5 minutes at 65°C and rapidly cooled using an ice bath. In the extension phase a 10µL mastermix of Moloney Murine Leukaemia Virus (M-MLV) reverse transcriptase enzyme, 5x M-MLV buffer and RNAse free H_2O was added to each of the samples which were subsequently incubated in the BioRad T100 thermal cycler for 10 minutes at 37°C and then 1 hour at 42°C. The resulting cDNA was diluted in RNAse free H_2O at a ratio of 1:10 and stored at -20 °C.

2.7.3 Quantitative polymerase chain reaction

The polymerase chain reaction utilises thermostable DNA polymerase to amplify DNA fragments through a series of thermal cycles. In real time quantitative PCR (RTqPCR) a fluorescent label is incorporated into the amplified DNA, and the changing intensity of fluorescence during each cycle enables calculation of the DNA quantity. Specific regions within the DNA are selected using primers, complimentary sense and anti-sense strands which are designed to target the GOI. Both the fluorescent dye-based SybrGreen primers and the hydrolysis (“Taqman”) primers were used for RTqPCR in this project. SybrGreen is a dye which fluoresces when bound to double-stranded (ds)DNA, both from specific and nonspecific PCR products. During the qPCR process, amplification

of the target sequence creates further dsDNA to which the SybrGreen binds, resulting in a proportionate increase in fluorescent signal. Because SybrGreen binds to all dsDNA PCR material it is considered less specific than the TaqMan method. The TaqMan method involves a fluoregenically-labelled probe with a reporter dye, a quencher dye and *Taq* DNA polymerase. In the presence of the target sequence the probe is cleaved by *Taq* nuclease activity, thereby removing the quencher dye from the reporter dye's proximity and enabling a signal. As the qPCR amplification continues more TaqMan probes are cleaved by the target sequences, leading to increased signal.

Housekeeping genes, observed to be stably expressed across a broad range of conditions, were used to compare against the expression of specific GOI[208]. For alveolar type 2 cells these were Glyceraldehyde 3-phosphate dehydrogenase (*GAPDH)* and ubiquitin (*UBC)*, while for fibroblasts these was *UBC* and phospholipase A2 (*A2)*. Notably hypoxia is recognised to induce changes in the expression of commonly used housekeeping genes such as *GAPDH*[209]. Therefore in experiments incorporating hypoxia only stable genes such as *UBC* and *A2* were utilised.

As per the manufacturer protocol, for each target gene 2.5µL of pre-prepared 1:10 cDNA (in RNAse-free water) was added to a 96-well plate in duplicates along with 5µL of Precision IC/SybrGreen, 2µL of RNAse-free H_2O and 0.5µL of the GOI primer (total 10µL).

RTqPCR was performed using the BioRad CFX96 system, consisting of alternating thermal cycles of amplification. Briefly, PCR enzyme activation and DNA denaturation was achieved by heating the samples to 95°C for 135 seconds, followed by annealing of the GOI primers to the single-stranded sample DNA by cooling to 50°C for 45 seconds. Subsequently in the extension phase the samples were heated to 72°C for 10 seconds to enable DNA polymerisation before reading of the fluorescent signal intensity and repeat cycling.

The cycle threshold (Ct) is calculated from the qPCR amplification curve, measuring the intensity of the fluorescent signal at the end of each cycle until it exceeds the predetermined threshold. The lower the value of the Ct, the earlier the threshold was reached and therefore the higher the expression of the GOI. The Δ Ct method was employed to compare relative gene expression to that of the housekeeping gene. Subsequently, the fold change in expression was determine by comparing the normalised Ct values between test conditions and the control (ΔΔ Ct). Where Ct values were of a similar threshold between donors or repeat experiments an average of the control samples was taken for normalisation, in order to allow comparison of mRNA expression across the entire experiment. However using an average of control Ct values was not suitable when significant variation was seen between individual donors, in which case the fold change in

expression was determined against the individual control samples per donor or repeat experiment.

For SybrGreen assays a melt curve analysis was also performed by heating the dsDNA amplicon and measuring the point at which 50% is denatured. If the samples contained predominantly amplified DNA from the GOI then it would produce similar dissociation curves with a single peak. Melt curves for samples which contained multiple peaks, or which did not align with the other sample melt curves of the same GOI, were likely to contain other amplified products. This assisted in confirming the specificity of the SybrGreen primer, and the presence of possible contamination.

2.8 Protein quantification and western blotting

2.8.1 Obtaining protein and quantification

While mRNA quantification can indicate cellular expression at a transcriptional level, this does not always reflect cellular activity at a protein level. Therefore measurement of protein expression plays an important role in understanding the cellular function and regulation. A widely used method to analyse protein expression is the Western Blot, described below.

Cell lysate for protein analysis was obtained by adding 2x Laemmli buffer to experiments (200uL per well in a 6 well plate) and sonicated for 3 x 10 seconds prior to use or storage at -80°C. Protein from cell lysate was quantified using a bicinchoninic acid (BCA) protein assay (Thermo Scientific Micro BCA protein assay, 23235). Protein standards were first created in duplicate using serial dilution of 2µg/µL BSA in dH_2O (from 20µg to 0.313µg). For the conditions, 5µL of each sample were then added in duplicate to 145µL dH_2O **(Figure 2.5)**.

Working reagent was prepared using reagent A, B and C in a ratio of 25:24:1 and 150µL of this mastermix added to each of the wells, making the total volume in each well 300µL. After incubation at 37°C for 60 minutes the plates were analysed using colorimetric analysis on a spectrophotometer plate reader at 560nm. A standard curve was created using either Microsoft Excel or Graphpad Prism and the linear trendline obtained from the standard to calculate the condition protein concentrations.

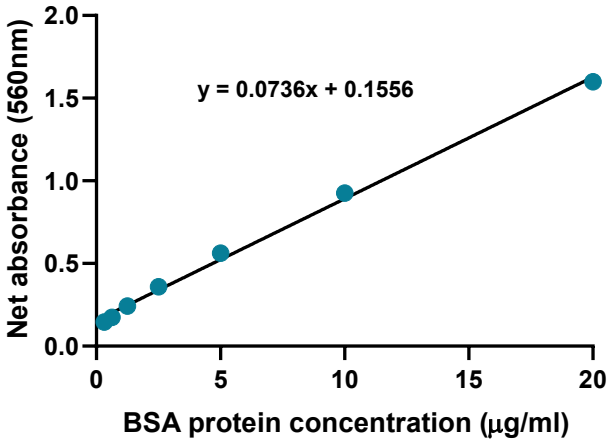

Figure 2.5: Standard curve for a protein quantification assay. Protein quantification for an experiment examining primary fibroblasts under a range of pro-fibrotic conditions. A line of best fit equation was obtained from the standard curve to estimate the protein concentration within the sample conditions.

2.8.2 Sodium dodecyl sulphate polyacrylamide electrophoresis

To separate proteins based on molecular weight samples undergo sodium dodecyl sulphate polyacrylamide electrophoresis (SDS-PAGE). Briefly, polyacrylamide stacking and separation gels were pre-prepared using Biorad 1.5mm protean III gel casts **(Appendix A – polyacrylamide gels)**. The percentage of acrylamide was determined by the molecular weight of protein under study, ranging from 7.5% for high molecular weight proteins (such as LOXL2 and HIF1α) to 15% for low molecular weight proteins (such as β-actin). The gels were immersed in a running buffer **(Appendix A – running buffer)** and 5µL of a molecular weight ladder (Precision Plus Protein Kaleidoscope, BioRad, 1610375) was placed in the first well.

Protein sample volume was calculated from the BCA quantification, to ensure an equal total amount of protein per sample (usually 30µg). Samples together with loading buffer (5x Laemmli buffer with bromophenol blue and 10% β-mercaptoethanol) were heated at 95°C for 5 minutes. Samples were then pipetted into the wells of the western blot cassette along with the molecular weight ladder. The gels were run for 1 hour and 30 minutes at 100V, using the bromophenol blue dye and the molecular ladder as a guide to ensure adequate distribution of protein by molecular weight.

On completion of electrophoresis the gels were carefully removed from the cassette and placed onto a pre-cut polyvinylidene difluoride (PVDF) membrane before being inserted into a transfer cassette immersed in a transfer buffer **(Appendix A – transfer buffer)**. Electrophoresis was again performed to transfer the protein from the gel to the PVDF membrane by running the transfer

cassette at 90V for 2 hours. On completion of the PVDF membranes were carefully removed from the gel, and the gel was discarded.

2.8.3 Antibody incubation

Freshly transferred PVDF membranes were immersed in 5% skimmed milk powder in TBS/T for 60 minutes at room temperature to block non-specific binding prior to incubation overnight in the primary antibody at 4°C. Primary antibodies were diluted in 5% milk in TBS/T at the concentrations shown **(Table 2)**, which were chosen either by manufacturer recommendation or previous experiments.

Table 2: Antibody dilutions for western blot

Primary antibody	Company (catalogue #)	Host	Dilution
β-actin, HRP conjugated	Fisher scientific (15527301)	Mouse	1:100,000
β-catenin (active)	Cell signalling (D13A1)	Rabbit	1:1000
β-tubulin	Sigma (T4026)	Mouse	1:1000
Ca9	Sigma (HPA055207)	Rabbit	1:500
HIF1α	BD Biosciences (610958)	Mouse	1:1000
HIF2α	Novus Bio (NB100-122)	Rabbit	1:1000
HIF3α	Abcam (Ab10134)	Rabbit	1:1000
LOXL2	R&D (AF2639)	Goat	1:1000
P-ERK1/2	Fisher scientific (36-8800)	Rabbit	1:1000
P-SMAD2/3	R&D (S465/S467)	Rabbit	1:1000
PLOD2	R&D (MAB4445)	Mouse	1:1000
Anti-goat IgG-HRP	Santa Cruz (Sc-2020)	Donkey	1:5000

Anti-mouse IgG-HRP	Dako (PO447)	Goat	1:5000
Anti-rabbit IgG-HRP	Dako (PO448)	Goat	1:5000

Following overnight incubation the membranes were washed in TBS/T three times for 5 minutes each before being incubated in a horseradish peroxidase (HRP)-conjugated secondary antibody (diluted in 5% milk in TBS/T) at room temperature for 60 minutes.

Following three additional 5 minute rinses in TBS/T the membrane was coated with 1ml of chemiluminescence reagent (Clarity Western Blotting ECL Substrate, BioRad 1705060) for 5 minutes. Excess solution was then removed before chemiluminescence was performed using an Amersham Imager 680. An automatic exposure was initially performed, followed by 4-8 incremental exposures to ensure optimal visualisation.

The membrane could be reused to blot for another primary antibody by incubating first in a stripping buffer with 0.7% β-mercaptoethanol **(Appendix A)** for 30 minutes at 50°C before washing for 10 minutes in TBS/T and re-blocking with 5% milk-TBS/T.

2.9 Immunofluorescent cytochemistry

Immunofluorescent cytochemistry was performed to identify patterns of LOXL2 expression within individual cells. Prior to the experiment, 2x2cm coverslips were cleaned by submerging in 100% isopropanol, dried and placed in the bottom of 6 well plates (all within a class II cabinet). The wells were rinsed with PBS and then the cells were seeded over the coverslips in the pre-prepared media.

On completion of the experiment and after removal of media and washing with PBS, the cell monolayer (including those adherent to the coverslips) was fixed with 4% paraformaldehyde (PFA, pre-prepared in a fume hood, 1mL per well in a 6-well plate) and incubated at room temperature for 15 minutes. 4% PFA was then removed and the cells washed again with PBS before storage at 4°C in 1mL per well of 0.05% sodium azide in PBS until use for staining.

For LOXL2 immunofluorescent staining the cell monolayer was washed 3 times with PBS and permeabilised with 0.1% Triton X-100 in PBS for 15 minutes followed by blocking buffer (1% BSA, 0.1% Tween 20 in PBS) for 30 minutes. The primary antibody, LOXL2 (R&D systems, raised in goat, 1:100), was then added (150µL for each coverslip) and the plate was incubated at 4°C overnight.

After four washes (5 minutes each with 0.1% tween in PBS (PBS/T) the secondary antibody was applied (FITC-conjugated anti-goat, Sigma 1:100, 150µL) and left to incubate at room temperature

in the dark for 1 hour. This was followed by incubation with 4',6-diamidino-2-phenylindole (DAPI, EMD Millipore, 1:1000, 150µL) for nuclear staining and phalloidin (Tetramethylrhodamine (TRITC)-conjugated phalloidin, EMD Millipore, 1:1000, 150µL) to stain for actin filaments (with four x 5 minute PBS/T washes in between). Following a final set of PBS/T washes the coverslips were gently removed from the well and placed face down onto glass adhesion slides with Mowiol (Sigma, 81381). The slides were left at room temperature for 10 minutes to dry and then stored at 4°C overnight in the dark.

Slides were analysed using confocal microscopy and Leica systems LAX software. LOXL2 immunofluorescent intensity was calibrated using the control slides, thereby allowing comparisons between conditions.

2.10 Tinctorial staining

2.10.1 Haematoxylin and eosin stain

H&E tinctorial staining enables identification of basic structures within lung tissue by delineating cellular nuclei (blue) from cellular cytoplasm and ECM (varying shades of pink). To perform an H&E stain, FFPE sections were deparaffinised and rehydrated through gradated alcohols to distilled water. They were subsequently incubated in Mayer's haematoxylin for 5 minutes followed by running water for 5 minutes. Then they were stained in eosin for 5 minutes before 3 dips in distilled water, 3 dips in 100% ethanol and dehydration through ethanol, clearene (Leica biosystems 3803600, two x 10 minutes incubation) and finally mounted with pertex.

2.10.2 Massons trichrome stain

Massons trichrome stain enables further differentiation of collagenous material against a cellular background, with ECM staining blue using aniline blue, cellular nuclei staining black using Weigert's haematoxylin (black) and other material including cellular cytoplasm staining various shades of pink-red using ponceau-acid fuchsin (pink) differentiated through phosphomolybdic acid.

Briefly, Weigert's haematoxylin stain was made fresh by preparing solution A (1000mg haematoxylin in 100mL of 100% ethanol) and solution B (30% ferric chloride in 1mL 37% HCl, diluted to 100mL in distilled H_2O). Solutions A and B were mixed equal parts for the final staining solution. Ponceau-acid fuchsin was prepared by adding equal parts 0.5% crystal ponceau in 1% acetic acid and 0.5% acid fuchsin in 1% acetic acid.

Histopathological sections were deparaffinised and rehydrated before being immersed in Weigert's haematoxylin stain for 5 minutes. They were then immersed in running water (to 'blue') for 5 minutes and subsequently immersed in ponceau-acid fuchsin solution for 3 minutes. Sections were subsequently differentiated by applying phosphomolybdic acid (150µL per slide) for 10 minutes. Sections were dipped in water and then counterstained using aniline blue stain for 5 minutes. After a final brief rinse, sections were dehydrated through gradated alcohol to clearene before mounting on coverslips with pertex.

2.10.3 Picrosirius stain

Collagen fibrils possess intrinsic birefringent characteristics due to their highly organised structure with co-alignment of the collagen molecules. This natural birefringence can be enhanced by staining with picrosirius red, a strong anionic dye which associates with the cationic collagen molecules[210]. Using cross-polarised light, fibrillar collagen appears in a range of red, yellow and green birefringence against the black background of non-fibrillar tissue. While the spectrum of colour has been proposed to represent different types of collagen, it has been demonstrated that the orientation of the collagen bundles is the key determinant of the colours absorbed and reflected by the collagen fibrils[211].

Picrosirius staining was performed using the Abcam Ab150681 Picrosirius Red Stain Kit according to the manufacturer instructions. Briefly, FFPE sections were deparaffinised and rehydrated through gradated alcohols to distilled water. They were subsequently incubated in picrosirius red solution for 60 minutes before 2 brief washes in the supplied acetic acid solution. The slides were then dipped in absolute alcohol before dehydration through alcohols to clearene (Leica biosystems 3803600, two x 10 minutes incubation) and mounting in pertex.

To image collagen fibrils an Olympus Polarised filter was applied to the Olympus Dotslide Microscope and the exposure adjusted to reduce background light before imaging was performed. Settings were calibrated to be identical between samples, ensuring comparison of fibrillar collagen content could be made. Specifically the polariser filter was set at 90° to the forward facing direction and camera exposure was set manually at 15 milliseconds.

2.11 Biomechanical analysis of the 3D fibroblastic foci model

2.11.1 Parallel plate compression testing

Stiffness in kilopascals (kPa) was estimated using parallel plate compression testing of samples followed by the application of Young's elastic modulus, which is the ratio of tensile stress (σ) to tensile strain (ε) within an elastic material **(Figure 2.6)**.

To measure matrix stiffness parallel plate compression testing was utilised on spheroids from the 3D fibroblastic focus model using a CellScale Microsquisher. The MicroSquisher possesses a motorised "actuator" to deliver force to the sample via a round tungsten beam and platen submerged in a fluid bath of PBS. The software program SquisherJoy V5.23 uses an imaging system to record sample compression live, determining the original height, cross-sectional area and subsequent displacement of the sample, and providing feedback to the actuator which enables cycling after a pre-determined level of displacement.

Choice of beam for use in the parallel plate compression was chosen both from pilot tests with surplus spheroids as well as experience from previous experiments based on the anticipated stiffness of the tissue[165]. The beams selected ranged between 0.2032mm and 0.5588mm in diameter. Where possible the same diameter beam was used within each experiment to measure samples from different test conditions. Specifically, the control (TGFβ-only) samples and IOX2-exposed samples were measured using a 0.5588mm beam, however the DMOG-exposed samples were much softer than this beam could measure, so were tested using a 0.2032mm beam.

Previously harvested and flash-frozen spheroids were removed from -80°C storage and transferred to sterile PBS to equilibrate. Using a 1.5mm skin punch biopsy the tissue sheet outgrowths which arose around the base of the spheroids were removed prior to testing.

The spheroids were subsequently tested with 5 cycles of compression (4 "pre-conditioning" cycles followed by the 5th "test" cycle). Each project was comprised of 2 identical experiments at different time points. Each experiment had 3 IPF donors, with duplicate samples per donor for parallel plate compression testing. This resulted in a total of 12 samples to be tested for each condition within a project. Maximal displacement of the spheroids from the 3D fibroblastic foci model experiment incorporating DMOG was set at 25%, which was standardised from previous experiments. However preliminary compression analysis of the IOX2 3D fibroblastic foci model suggested significantly increased stiffness in IOX2-exposed samples and incomplete recoil in the relaxation phase of compression when the spheroids were displaced to 25% (consistent with a possible loss of spheroid integrity).

This implied there may be irreversible changes due to shear stress within the samples as a result of the compression process. Subsequently pre-conditioning and testing was performed to a displacement of 21% on all samples within the 3D model experiments described in this study, which did not result in the same irreversible changes in structural integrity. Similarly to all previous experiments, tissue stiffness was still calculated on the 5th cycle using measurements of force (µN) taken from displacement of between 10-20%. All samples achieved adequate displacement and relaxation to calculate Young's modulus and thus the new methodology was considered valid.

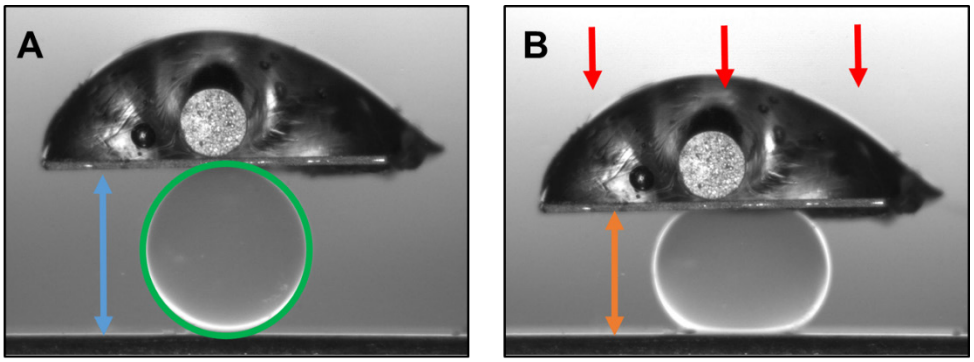

$$E = \frac{\sigma}{\varepsilon} = \frac{F/A}{\Delta L/L_0} = \frac{FL_0}{A\Delta L}$$

F – Force exerted on an object
L_0 – Original object length
A – Cross-sectional area perpendicular to the force
ΔL – Change in length of object

Figure 2.6: Parallel plate compression testing. Camera view of a control spheroid **(A)** at full relaxation and **(B)** undergoing parallel plate compression, with the beam and platen visible in cross-section view compressing the sample. Young's modulus states that elastance (*E*) can be estimated by dividing tensile stress (σ) by the strain (ε) in the initial linear portion of the stress-strain curve. Coloured markings indicate the measurements required to estimate elastance using Young's modulus in kilopascals (kPa).

2.11.2 Extraction, reduction and hydrolysis of collagen samples

In order to measure collagen content and pyridinoline cross-links within the 3D fibroblastic foci samples, samples were processed to extract and denature the collagen molecules before hydrolysis to form low molecular weight peptides. Both the spheroids and the surrounding outgrowths of ECM were used to measure collagen and pyridinoline cross-links in order to maximise sample quantity.

While not specifically measured in this study, immature collagen cross-links within the spheroids were first stabilised by reduction of each sample in 1mL of potassium borohydride (KBH_4, Sigma,

12mg/mL in 20mM NaOH, 30 minutes, room temperature) to produce hydroxylated equivalents (such as HLNL and DHLNL), which are capable of withstanding acid hydrolysis. After 30 minutes the reaction was stopped by adding acetic acid (CH_3CO_2H, Sigma, 3M, 750µL per 1ml of KBH_4) and the samples rinsed once in PBS and twice in dH_2O.

The sample collagen was then simultaneously extracted, denatured (to separate the triple helices into individual collagen molecules) and hydrolysed (to produce low molecular weight peptides) using thermal and acid treatment. Specifically, the reduced samples were immersed in hydrochloric acid (HCl, Sigma, 6M) and heated to 100°C for 18 hours before evaporation of the HCl using a Genevac EZ-2 Concentrator. Samples were then resolubilised in distilled water for use in the colorimetric assays.

2.11.3 Measuring collagen and cross-links

Hydroxyproline quantity and pyridinoline cross-link density were determined using a combination of colorimetric assays. Total protein was also measured to enable normalisation of collagen quantity. Each project had two identical experiments separated in time, and each experiment used fibroblasts cultured from 3 IPF donors, resulting in 6 samples per condition that underwent collagen and collagen cross-linking analysis.

Total protein in the samples (minus proline and hydroxyproline) was measured as per manufacturer instructions with the Total Protein Kit (QuickZyme Biosciences, QZBTOTPROT1), a specialised system capable of measuring protein in acid hydrolysates. It relies on a linear and concentration-dependent reaction between genipin, a hydrolysate product from gardenia fruits, and free amino acids to produce a blue pigment[212]. Briefly, the 15µL of kit standards (8 in total ranging from a concentration of 0.047 – 3mg/mL and including a negative control) and 10µL of experiment samples were added to a 96 well plate with 120µL of Assay buffer and 15µL of Colour reagent working solution before incubation at 85°C for 60 minutes. The plate was then cooled to room temperature before colorimetric analysis using a plate reader at 570nm. A standard curve was used to calculate the sample protein concentrations.

Collagen content of the samples was measured with the Hydroxyproline Assay Kit (Sigma, MAK008), using the manufacturer protocol. The kit is based on the production of colorimetric compounds in a concentration dependent manner when 4-(dimethylamino)benzaldehyde (DMAB) reacts with oxidised hydroxyproline[213]. In summary the hydroxyproline standards were prepared by dilution of the 1mg/mL Hydroxyproline Standard Solution supplied by the kit in sterile water, generating 5 standards ranging from 0.2 to 1.0µg plus a negative control. Test samples were prepared by adding 10µL of sample to a well. 100µL of Chloramine T/Oxidation Buffer Mixture

was added and incubated for 5 minutes at room temperature. For each sample 50µL of Diluted DMAB Reagent and 50µL of Perchloric Acid/Isopropanol Solution were pre-mixed and then applied, and the plate was incubated for 90 minutes at 60°C before colorimetric analysis using a plate reader at 560nm. Hydroxyproline content of the samples was calculated from the standard curve in the same manner as the BCA protein quantification previously detailed.

Mature pyridinium cross-links (pyridinoline – PYD, and deoxypyridinoline – DPD) were measured as per manufacturer instructions using a competitive enzyme immunoassay (Quidel MicroVue PYD/DPD, 8010). This kit utilises an anti-pyridinoline cross-link monoclonal antibody which binds to PYD and DPD present both in the test strips as well as in the samples[214]. A higher concentration of pyridinoline in the samples leads to less binding of pyridinoline in the test strips, which is detected using a colorimetric assay. 6 pyridinoline standards were supplied by the manufacturer as well as a high and low control. Samples, standards and controls were diluted 1:10 by combining 50µL each to 450µL of Assay Buffer before being added to wells coated with anti-PYD antibody. 100µL of the supplied Cold Conjugate was added and the plate incubated for 3 hours in the dark at 4°C. The wells were then washed with supplied Wash buffer, manually inverted and gently blotted on paper towel to empty the wells. 150µL of the supplied Working Substrate Solution was then applied and the plate incubated for 1 hour at room temperature. 100µL of Stop solution was then applied and colorimetric analysis performed with a plate reader at 405nm. A 4-parameter calibration curve fitting equation was used to calculate the sample measurements as per manufacturer instructions. Consistent with other groups, the pyridinoline cross-link density was expressed as the number of cross-links per collagen molecule assuming 300 hydroxyproline residues per triple helix[178].

Chapter 3 Expression and Regulation of Collagen Cross-linking Enzymes in Pulmonary Fibrosis

3.1 Introduction

Increased stiffness of interstitial ECM in the IPF lung not only impairs respiratory function but is thought to propagate and sustain the fibrogenic responses[64,165]. It is hypothesised that these pathologic changes to ECM stiffness involve aberrant expression of collagen cross-linking enzymes to form excess "bone-type" pyridinoline collagen cross-links. A variety of collagen cross-linking enzymes have been implicated in this process, including PLOD2 and the LOX(L) family (chiefly LOXL2)[165,177,194].

The cellular provenance of these collagen cross-linking enzymes remains unclear. Mesenchymal cells within IPF fibroblastic foci produce abundant ECM and could be considered the most likely source[122,123,128]. By contrast the alveolar epithelium is increasingly recognised for instrumental roles in early IPF pathogenesis, and is likely to promote fibrogenesis through multiple mechanisms of epithelial-mesenchymal cross-talk[111,126,215]. Both bronchial epithelial and lung fibroblast cell types are capable of producing collagen cross-linking enzymes upon exposure to pro-fibrotic conditions, with distinct patterns of expression[193]. Identifying the cellular origins of dysfunctional collagen cross-linking enzyme expression in the IPF lung would provide mechanistic insights into ECM remodelling and facilitate a targeted examination of upstream events.

The signalling pathways which drive dysregulated collagen modification in IPF are also poorly understood. TGFβ is considered the prototype of fibrosis-generating cytokines, capable of promoting epithelial cell apoptosis, recruitment and activation of mesenchymal cells as well as ECM production and modification[138,140,141,216,217]. However a variety of other pro-fibrotic signalling pathways are increasingly implicated in the fibrogenic cascade, including the MAPK/ERK, Wnt and HIF pathways[143,147,149,154,218]. The effects of these pathways on collagen cross-linking enzyme expression in key cell types pertinent to lung fibrosis, such as alveolar epithelial cells and lung fibroblasts, have not been robustly compared.

3.2 Objectives

The objectives of this study were to:

i) Analyse and compare expression patterns of collagen cross-linking enzymes within healthy and IPF tissue
ii) Identify cellular sources of collagen cross-linking enzyme expression in IPF tissue
iii) Explore the effects of key pro-fibrotic signalling pathways on collagen cross-linking enzyme expression in relevant cell types to lung fibrosis.

3.3 Results

3.3.1 Expression patterns of collagen cross-linking enzyme expression in lung fibrosis

To investigate the expression patterns, regional variation and cellular sources of collagen cross-linking enzymes in healthy and IPF lung tissue, two distinct methodologies of RNA analysis were employed – laser capture microdissection (LCMD) with RNA-sequencing, and in-situ mRNA hybridisation.

LCMD was performed on serial FFPE sections from 10 healthy and 10 IPF donors by Dr Mark Jones, sampling areas of alveolar septal tissue in healthy and IPF lung sections as well as fibroblastic foci in IPF sections. The selected samples were then processed for Ion Torrent RNA-sequencing at Yale School of Medicine, USA and the data processed and analysed for the expression levels of collagen cross-linking enzymes within these regionally isolated samples. Gene expression levels (expressed as Fragments Per Kilobase of transcript per Million mapped reads – FPKM) between the three different types of tissue were compared.

Substantially higher levels of collagen cross-linking expression were observed in IPF fibroblastic foci than alveolar septae from healthy or IPF tissue **(Figure 3.1)**. Specifically, IPF fibroblastic foci had substantially increased gene expression of *PLOD2* **(Figure 3.1 A)**, *LOX* **(Figure 3.1 B)**, *LOXL1* **(Figure 3.1 C)**, *LOXL2* **(Figure 3.1 D)** and *LOXL3* **(Figure 3.1 E)** compared to both healthy alveolar septal tissue and IPF alveolar septal tissue. A statistically significant difference in *LOXL4* was only observed between healthy alveolar epithelium and IPF fibroblastic foci **(Figure 3.1 F)**. Within IPF fibroblastic foci samples the expression of *PLOD2* and *LOXL2* was greatest, suggestive of key roles for these two enzymes, with comparatively moderate expression of *LOX* and *LOXL1* and low level expression of *LOXL3* and *LOXL4*.

No significant differences in expression of any collagen cross-linking enzymes were observed between healthy and IPF alveolar septae **(Figure 3.1 A-F)**, supporting the concept of discrete regions of fibrosis rather than a generalised dysregulation of cross-linking enzyme activity.

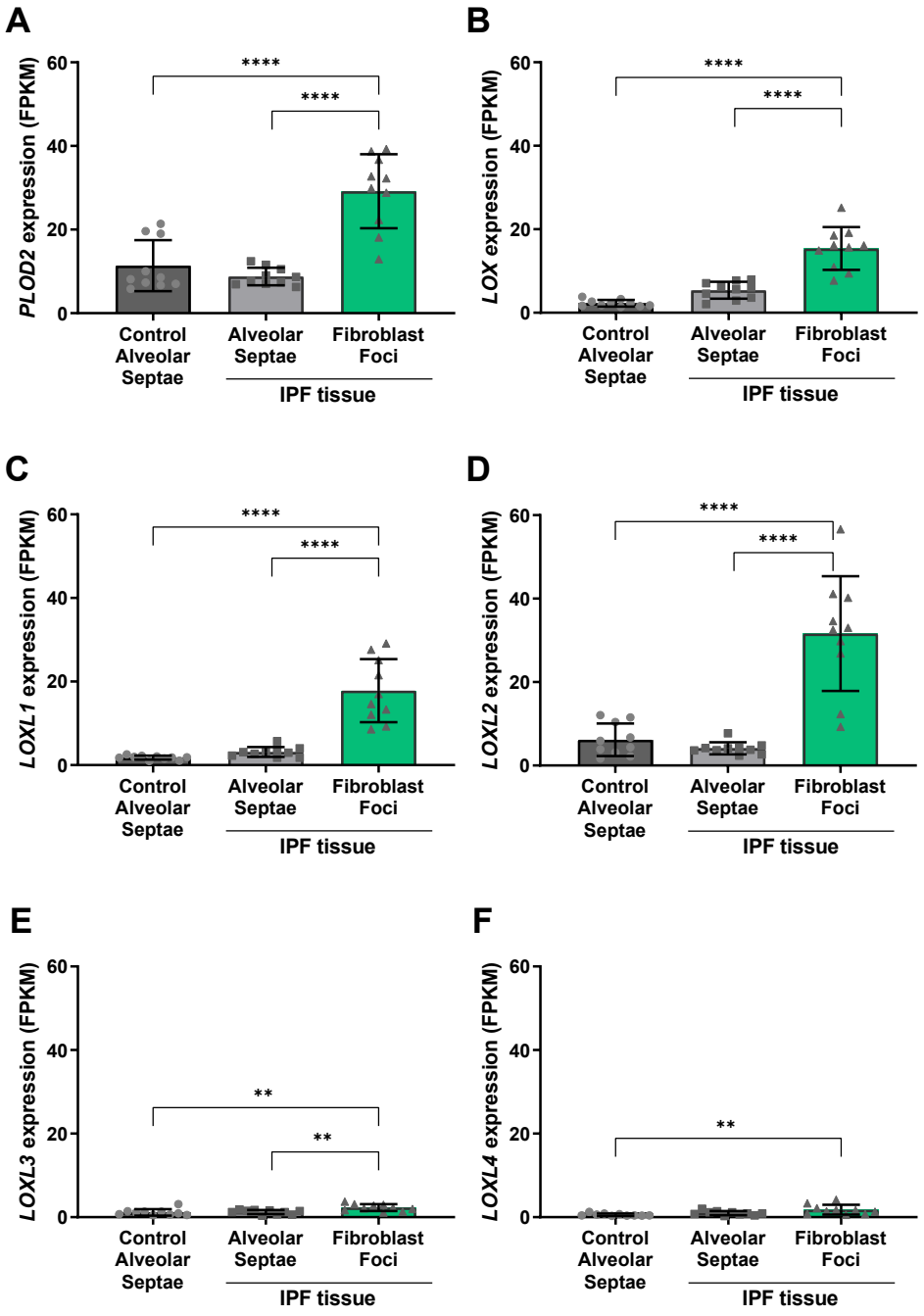

Figure 3.1 IPF fibroblastic foci are a key source of collagen cross-linking enzyme induction. RNA expression (FPKM) of **(A)** *PLOD2,* **(B)** *LOX* **(C)** *LOXL1*, **(D)** *LOXL2*, **(E)** *LOXL3,* and **(F)** *LOXL4* in healthy and IPF lung tissue, obtained using laser capture microdissection (LCMD) and analysed using RNA-sequencing. Data were analysed using grouped analysis and multiple comparisons (Dunnett's test). ** $p < 0.01$, **** $p < 0.0001$, error bars represent one standard deviation. N=10 healthy and 10 IPF donors.

By promoting hydroxylation of lysine residues on collagen telopeptides, increased PLOD2 activity provides the substrate for downstream extracellular modification by the LOX(L) family. This relationship was further explored by assessing for correlations between *PLOD2* and *LOX(L)* family expression in samples taken from the IPF fibroblastic foci. Scatter plots were compiled to illustrate this correlation **(Figure 3.2)**. Pearson's correlation coefficient was used to determine the strength of correlation (expressed as an r score with > 0.8 indicating a very strong correlation, 0.5 - 0.8 indicating a strong correlation, 0.2 – 0.5 indicating a fair correlation and < 0.2 indicating a poor correlation)[219]. A two-tailed P value was applied to determine the significance. Linear regression was performed to graphically illustrate strong or very strong correlations with a line of best fit.

Within IPF fibroblastic foci a strong and statistically significant positive correlation between *PLOD2* and *LOXL2* gene expression was observed (r=0.63, p=0.04) **(Figure 3.2 A)**, pointing towards common mechanisms for their dysregulation. Moderate positive but non-significant correlations were observed between *PLOD2* gene expression and that of *LOX* (r=0.43, p=0.21) (**Figure 3.2 B)** and *LOXL1* (r=0.40, p=0.25) **(Figure 3.2 C)**. Very weak positive, non-significant correlation was seen between *PLOD2* and *LOXL3* gene expression (r=0.06, p=0.83) **(Figure 3.2 D)**. Weak and non-significant correlation was observed between *PLOD2* and *LOXL4* gene expression (r=0.29, p=0.41) **(Figure 3.2 E)**.

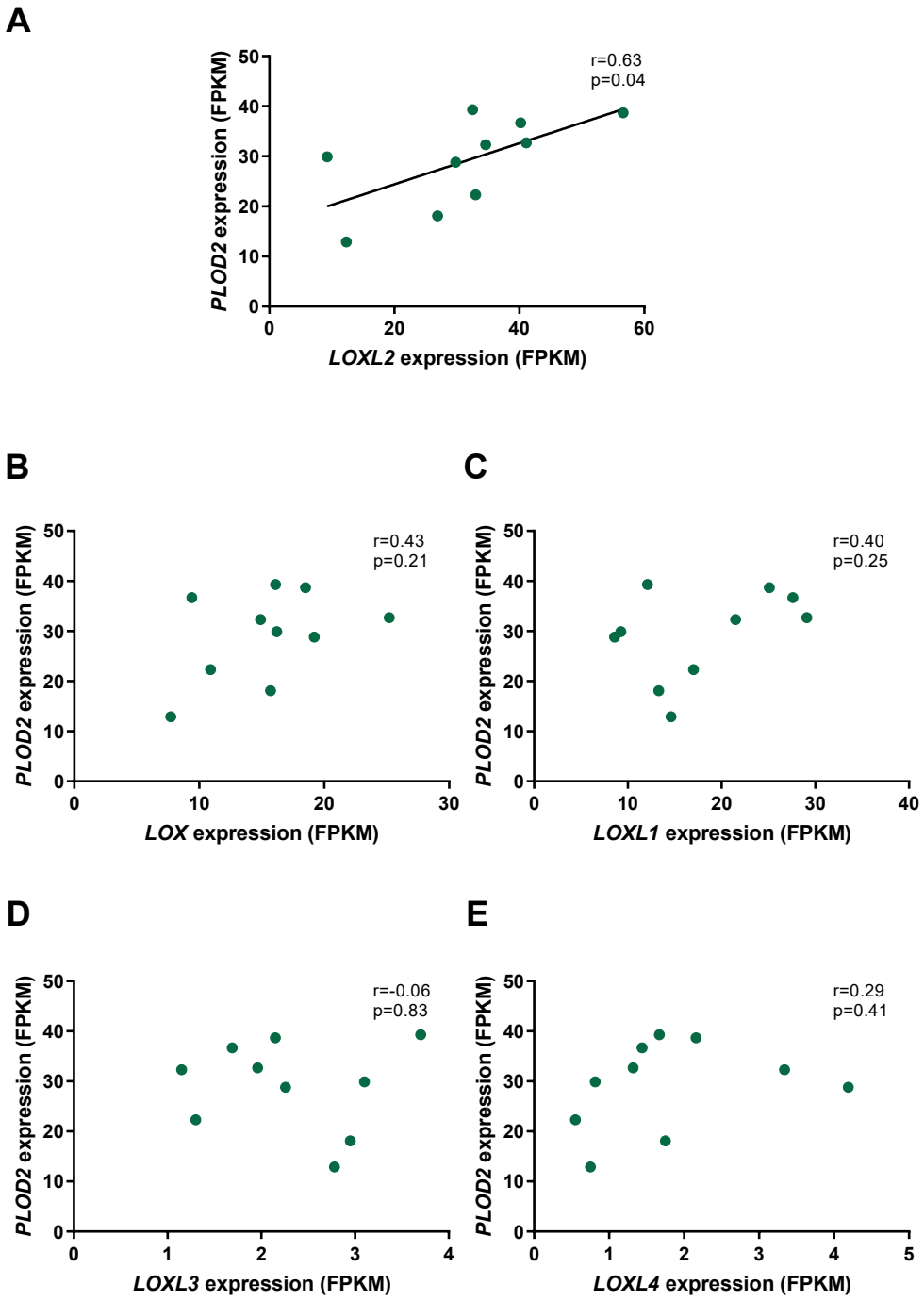

Figure 3.2 *PLOD2* and *LOXL2* expression in IPF fibroblastic foci is strongly correlated. Using Pearson correlation calculations to determine the correlation coefficient (r) and significant (two-tailed P value), the gene expression of *PLOD2* (y axis) within IPF fibroblastic foci tissue was compared to that of the *LOX(L)* family (x axis). **(A)** *LOXL2* gene expression was strongly, positively correlated with *PLOD2* gene expression (A, r=0.63, p=0.04). No significant correlations between *PLOD2* gene expression and **(B)** *LOX*, **(C)** *LOXL1*, **(D)** *LOXL3* or **(E)** *LOXL4* were observed. N=10 IPF donors.

Expression levels of the fibrillar collagen gene *COL1A1* were subsequently analysed, in order to confirm the presence of mesenchymal cells within the fibroblastic foci samples and compare this collagen expression to the alveolar septae samples **(Figure 3.3)**. Significantly increased levels of *COL1A1* expression (FPKM) were observed in IPF fibroblastic foci compared to control and IPF alveolar septae **(Figure 3.3 A)**, consistent with the gene expression profile of a mesenchymal cell population. Intriguingly, *PLOD2* **(Figure 3.3 B)** and *LOXL2* **(Figure 3.3 C)** expression correlated poorly with *COL1A1* expression, suggesting regulation of collagen cross-linking enzyme expression occurred independently of collagen fibrillogenesis.

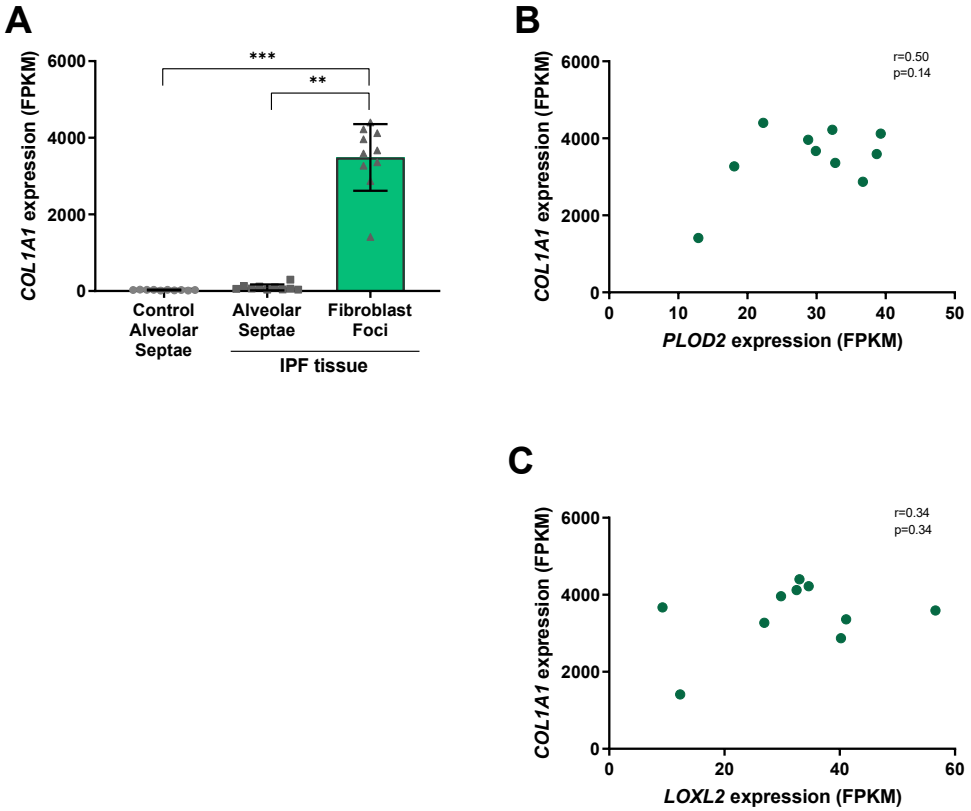

Figure 3.3: Induction of collagen I is significantly increased in the fibroblastic foci samples yet correlates poorly with expression of key cross-linking enzymes. RNA expression (FPKM) of **(A)** *COL1A1* in healthy alveolar and IPF alveolar or fibroblastic foci tissue. Data were analysed using grouped analysis and multiple comparisons (Dunnett's test). ** $p < 0.01$, *** $p < 0.001$, error bars representative of one standard deviation. Correlation between *COL1A1* expression and **(B)** *PLOD2* or **(C)** *LOXL2* using Pearson calculations to determine the correlation coefficient (r) and significance (two-tailed P value). N=10 healthy and 10 IPF donors.

In summary, RNA-sequencing of regionally distinct areas from healthy and IPF tissue revealed IPF fibroblastic foci to be a source of substantially upregulated collagen cross-linking enzyme expression compared to both healthy and IPF alveolar septae. The roles of *PLOD2* and *LOXL2* may

be particularly relevant, as they possessed the highest overall levels of expression and a strong correlation within fibroblastic foci. The expression of these enzymes poorly correlated to collagen I induction, suggesting independent regulatory pathways for production and modification of collagen within active areas of fibrosis.

3.3.2 Identifying the cellular sources of collagen cross-linking enzymes in IPF

To confirm the findings observed in the LCMD RNA-sequencing data and further investigate the cell-type specific sources of collagen cross-linking enzymes in IPF tissue, expression of key collagen cross-linking enzymes was further analysed using mRNA *in-situ* hybridisation (RNAscope) on healthy and IPF tissue sections.

Duplex probes for *LOX* or *LOXL2* (green) and *LOXL3* or *PLOD2* (red) were used in combination on FFPE tissue sections from seven IPF and three healthy lung donors. Manufacturer-produced positive and negative controls were used on adjacent tissue sections to confirm appropriate tissue staining **(Figure 2.3 A-B)**. Gills Haematoxylin was used to counterstain the tissue. The sections were reviewed and scored by an independent expert histopathologist (Prof. Aurelie Fabre, Dublin).

Overall IPF fibroblastic foci exhibited the highest levels of collagen cross-linking mRNA expression, in particular *LOX*, *LOXL2* and *PLOD2*, while low levels of expression of these enzymes were observed in IPF alveolar septae and negligible expression was seen in healthy alveolar septae **(Figure 3.4 A-C)**. *LOXL3* mRNA expression was very low and located predominantly in vessel walls **(Figure 3.5)**.

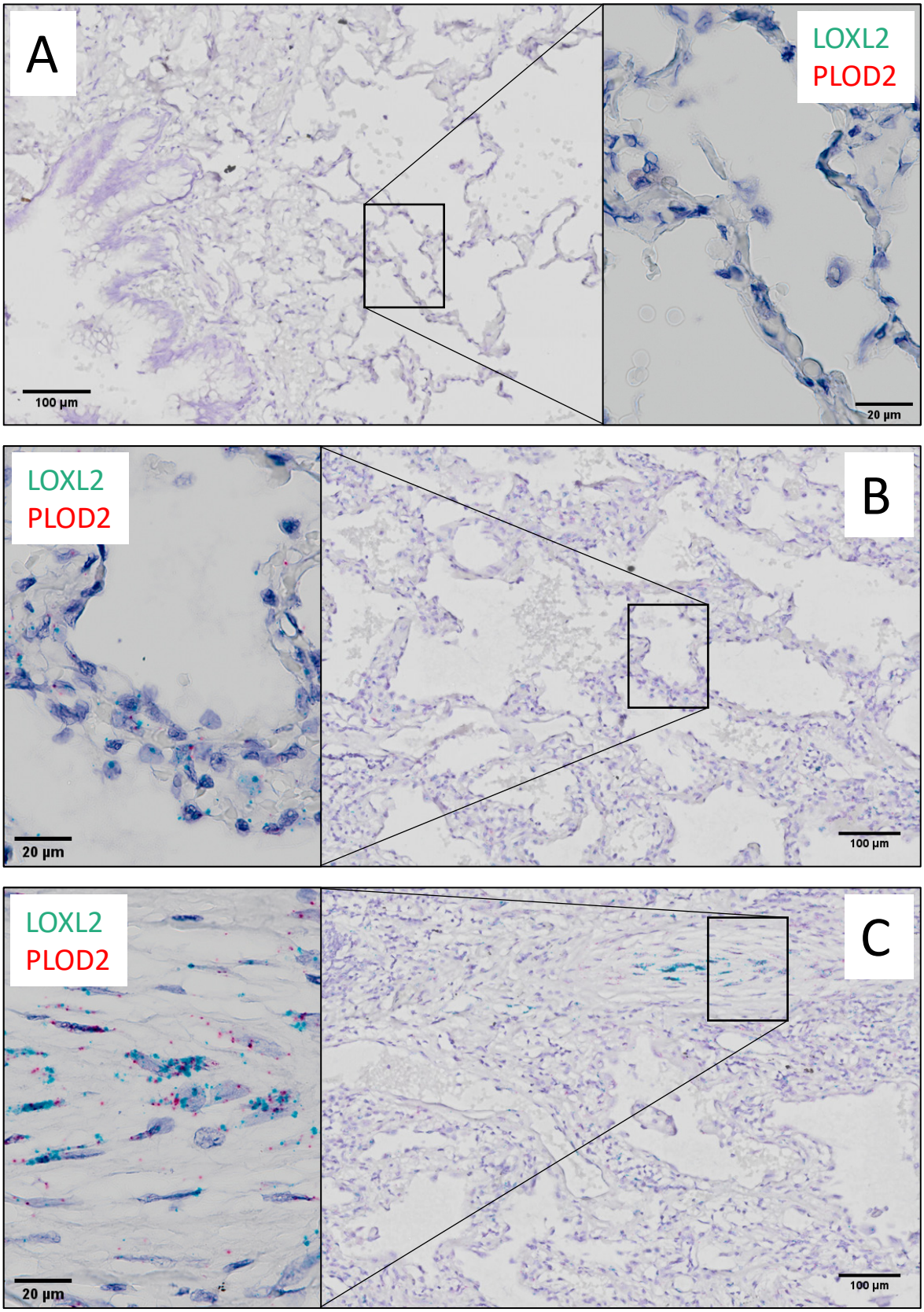

Figure 3.4: Expression of collagen cross-linking enzymes is low in healthy lung tissue. *In-situ* mRNA hybridisation demonstrating expression of LOXL2 (green) and PLOD2 (red) in **(A)** healthy alveolar tissue **(B)** IPF alveolar tissue and **(C)** an IPF fibroblastic focus. Images representative of sections from N=3 healthy and N=7 IPF donors.

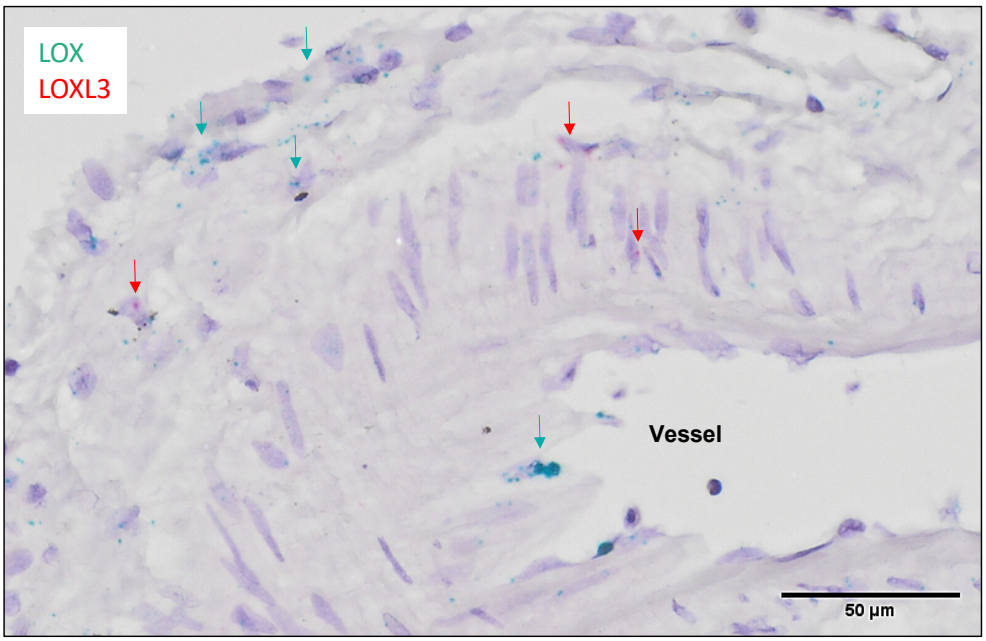

Figure 3.5 Healthy lung bronchiolar epithelium and vessel walls have very low expression of *LOXL3*. *In-situ* mRNA expression of *LOX* (green) and *LOXL3* (red) in healthy lung tissue. Images representative of sections from N=3 healthy donors. Staining identified by green arrows for *LOX* and red arrows for *LOXL3* respectively.

IPF lung tissue had highly variable, regionally dependent levels of collagen cross-linking enzyme expression. Consistent with the findings from the LCMD RNA-sequencing data, the most striking levels of expression were found within mesenchymal cells of the fibroblastic foci, with very high expression of *LOXL2*, moderate expression of *PLOD2* and *LOX*, and low expression of *LOXL3* **(Figure 3.6 A-B).** This was in sharp contrast to tissue surrounding areas of active fibrosis which had very low levels of collagen cross-linking enzyme activity, similar to healthy lung tissue. The findings confirmed discrete areas of intense dysreuglation of collagen cross-linking, interspersed with relatively unaffected areas. Notably, co-localisation of *PLOD2* and *LOXL2* was observed within individual mesenchymal cells **(Figure 3.6 B inset)**, consistent with the correlation seen within the LCMD RNA-sequencing data, and supporting the possibility for unifying mechanisms regulating their activity.

Alveolar epithelial tissue of IPF donors exhibited significant heterogeneity in collagen cross-linking activity, with many regions possessing low levels of expression similar to healthy control tissue, while a small number of regions demonstrated moderately elevated levels of *LOX*, *LOXL2* and *PLOD2* activity **(Figure 3.7 A-B)**. These regions of active collagen cross-linking expression were often located near areas of active fibrosis, with evidence of both early and established fibroblastic foci, and possibly represented sites of early fibrogenesis.

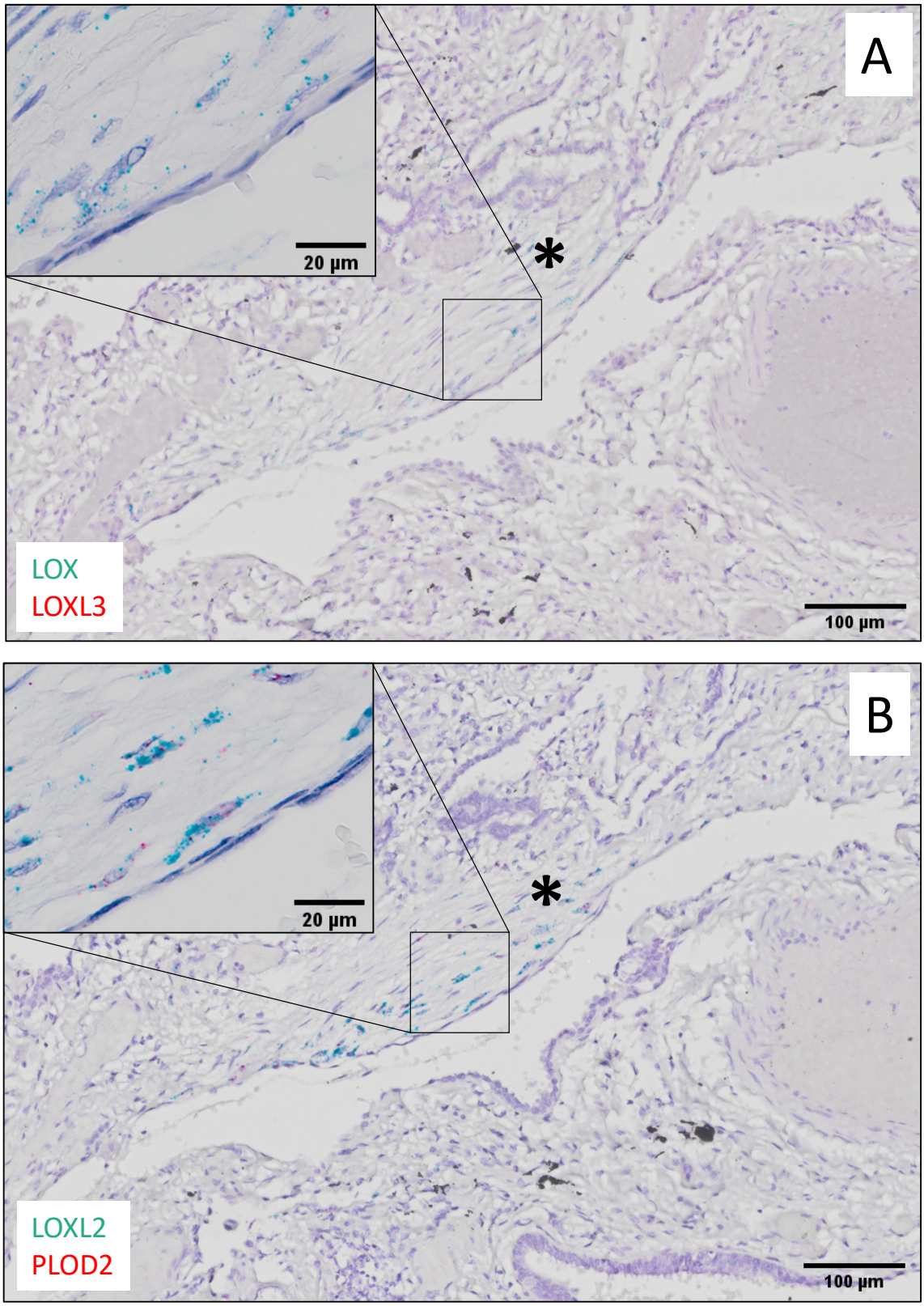

Figure 3.6 Fibroblastic foci are a key source of collagen cross-linking enzyme activity in IPF lung tissue. *In-situ* mRNA expression of **(A)** *LOX* (green) / *LOXL3* (red) and **(B)** *LOXL2* (green) / *PLOD2* (red) in IPF lung tissue with a magnified view of a fibroblastic focus (star and inset). Images representative of sections from N=7 IPF donors.

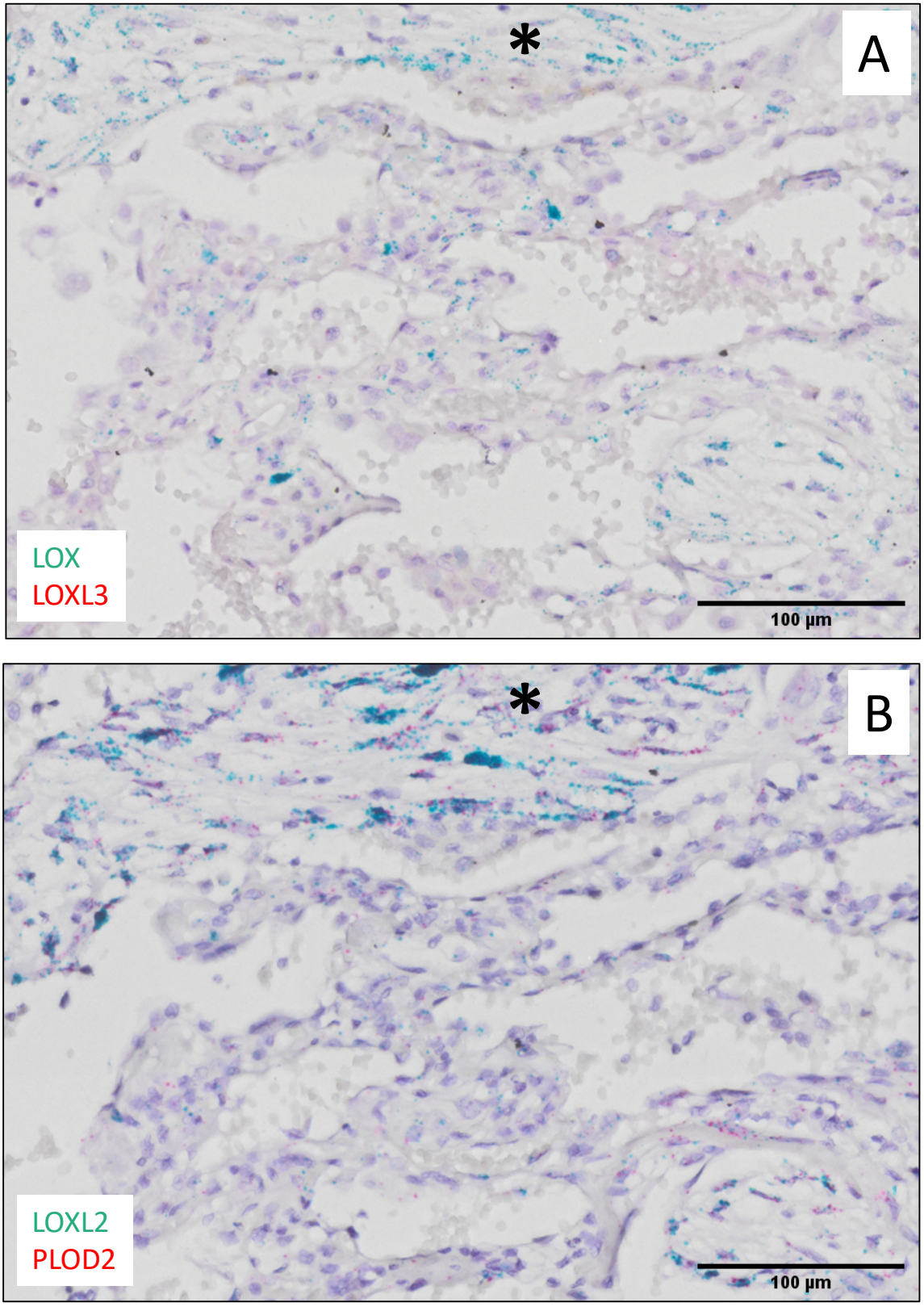

Figure 3.7 Discrete areas of increased collagen cross-linking activity within alveolar epithelium suggest sites of early fibrogenesis. *in-situ* mRNA expression of **(A)** *LOX* (green) / *LOXL3* (red) and **(B)** *LOXL2* (green) / *PLOD2* (red) in IPF lung tissue with areas of fibrogenesis (star). Images representative of sections from N=7 IPF donors.

The hyperplastic alveolar epithelium overlying fibroblastic foci exhibited relatively modest levels of *LOXL2* expression and low levels of *PLOD2* expression compared to the underlying mesenchymal cells **(Figure 3.8 A-B)**. However a striking degree of *LOXL2* activity was consistently observed at the epithelial border of the fibroblastic focus, in an area termed by other groups as the 'active fibrotic front'[170], with staining often diminishing as the distance from the alveolar surface increased. The patterns of staining suggest collagen cross-linking activity was being driven by stimuli at the alveolar surface, or within the alveolar epithelium.

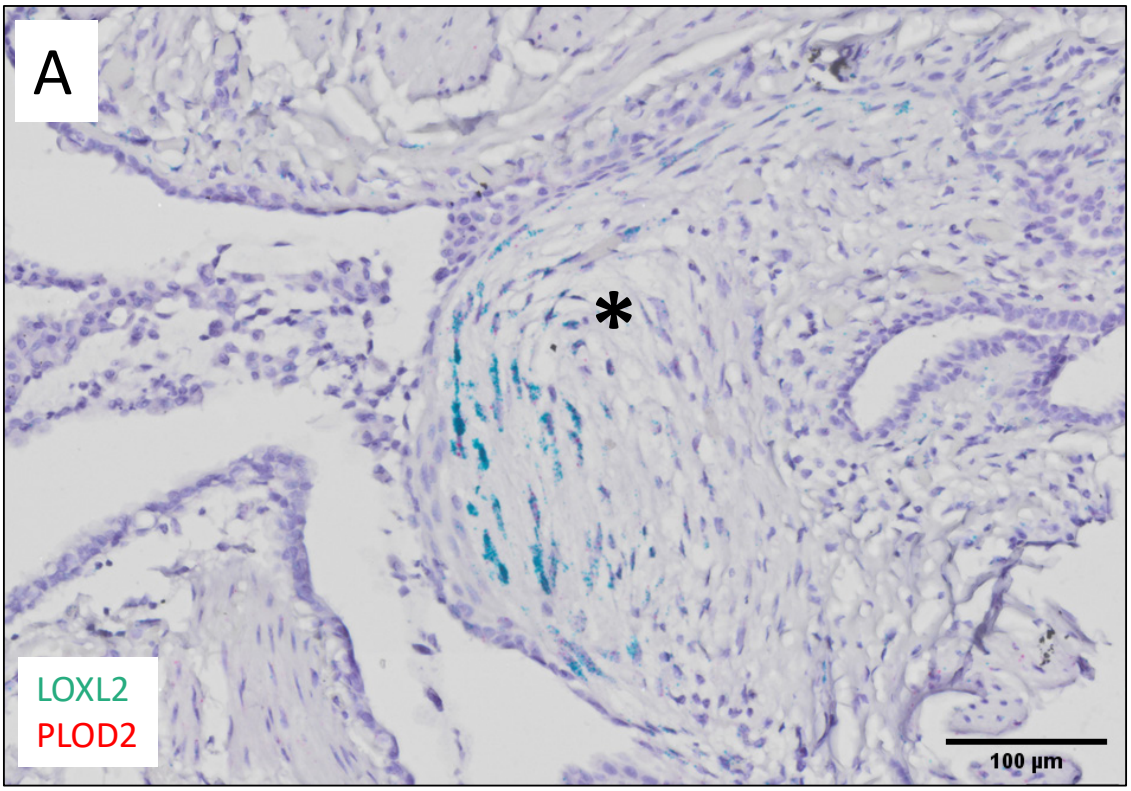

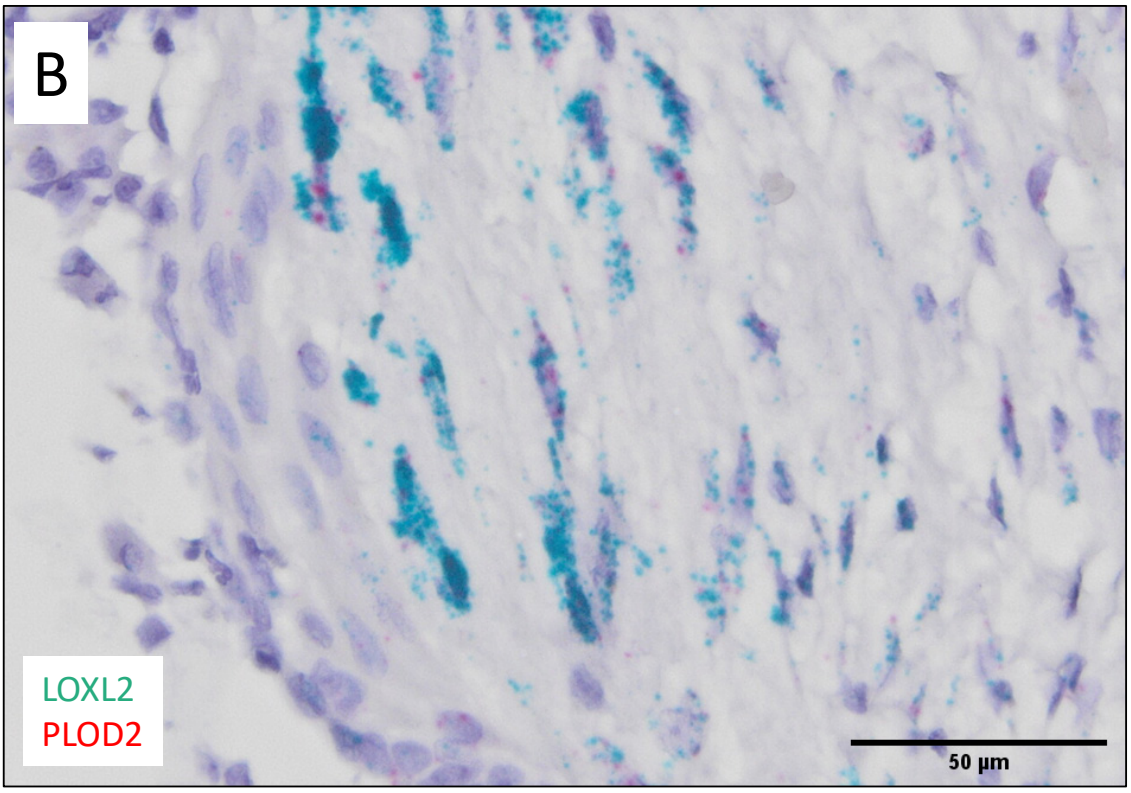

Figure 3.8: Collagen cross-linking activity is greatest within mesenchymal cells located near the alveolar epithelium. *In-situ* mRNA expression of *LOXL2* (green) and *PLOD2* (red) in **(A)** IPF lung tissue with a fibroblastic focus (star). **(B)** Magnified view of the fibroblastic focus. Images representative of staining performed on sections from N=7 IPF donors.

Taken together these results confirm fibroblastic foci, and in particular the mesenchymal cells within the foci, are the primary sources of the upregulated collagen cross-linking enzyme activity within the IPF lung. In particular PLOD2 and LOXL2, critical enzymes for the production of 'bone-type' pyridinoline cross-links, were highly expressed and co-localised within mesenchymal cells, pointing towards shared mechanisms for their dysregulation. Notably the greatest levels of expression were seen in mesenchymal cells closest to the overlying alveolar epithelium, implying the source of their dysregulation may arise from the alveolar surface or within the alveolar epithelial cells. While the origins of the collagen cross-linking enzyme dysregulation were identified, it remained unclear what signalling pathways were promoting their induction.

3.3.3 Comparative expression patterns of collagen cross-linking enzymes in lung fibroblasts under a range of pro-fibrotic signalling pathways

In order to identify and compare potential drivers of these collagen cross-linking enzymes, a series of *in vitro* timecourse experiments were performed using primary lung fibroblasts exposed to a series of candidate pro-fibrotic signalling pathways. Patterns of collagen cross-linking enzyme expression were assessed after exposure to these pathways over 24 – 72 hours, with particular attention to the previously identified key enzymes *PLOD2* and *LOXL2*.

The five pre-determined pro-fibrotic signalling pathways chosen were TGFβ1, EGF/RAS/MEK pathways, canonical Wnt and non-canonical Wnt signalling pathways, and HIF pathways. RAS/MEK activity was promoted in lung fibroblasts using Epidermal Growth Factor. Recombinant peptides for TGFβ1, the canonical Wnt3a and non-canonical Wnt5a were applied directly, while HIF pathways were stabilised through the hypoxia mimetic DMOG, which stabilises HIF1α and HIF2α through pan-PHD inhibition[220,221].

Downstream activation of each signalling pathway was confirmed by western blotting **(Figure 3.9)**. RAS/MEK pathway activation was confirmed by expression of phospho-ERK 1 and 2. TGFβ1 signalling was demonstrated with phosphorylated (P)-Smad 2 and 3. Exposure to DMOG promoted HIF1a stabilisation. Both canonical Wnt3a and non-canonical Wnt5a signalling promoted phospho-ERK signalling however only the canonical Wnt3a condition (along with TGFβ1) demonstrated significant levels of the active (non-phosphorylated) form of β-catenin.

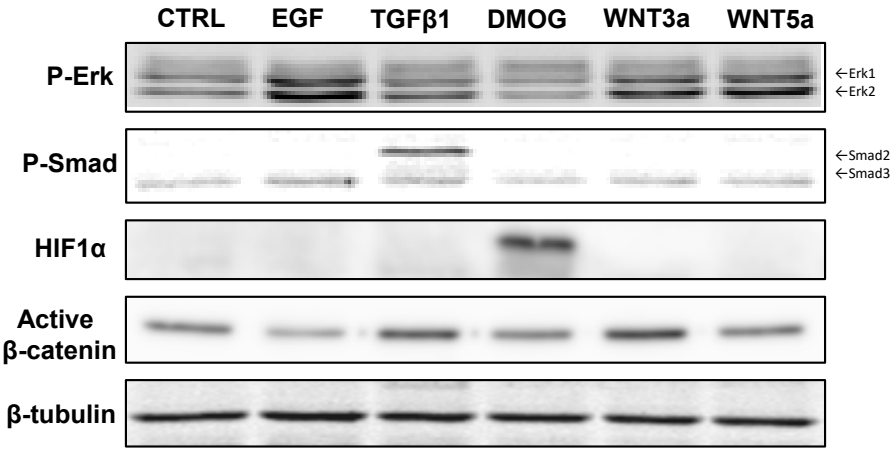

Figure 3.9: Confirmation of pro-fibrotic pathway activation through downstream markers in lung fibroblasts. Western blot of protein from healthy donor lung fibroblasts exposed to either control conditions or one of five different pro-fibrotic pathways – EGF 10ng/mL, TGFβ1 10ng/mL, HIF (through DMOG 1mM), Wnt3a 100ng/mL and Wnt5a 100ng/mL. Four primary antibodies were applied – P-ERK 1/2, SMAD2/3, HIF1α or active β-catenin – to 4 separate membranes. β-tubulin was used as a loading control (above is representative of one membrane only). Blots representative of N=3 experiments.

Following confirmation of pathway activation, collagen cross-linking enzyme mRNA expression patterns were analysed across the time-course **(Figure 3.10)**. *PLOD2* expression was significantly upregulated in lung fibroblasts exposed to DMOG, with relatively smaller changes seen with TGFβ1 and no changes seen with other pro-fibrotic pathways **(Figure 3.10 A)**. Induction of *PLOD2* with either DMOG or TGFβ1 was greatest at 24 hours however remained significantly elevated throughout the time course.

Within the *LOX(L)* family, HIF stabilisation through DMOG resulted in significant upregulation of *LOXL2* and (to a lesser extent) *LOX* at all time-points **(Figure 3.10 B, C)**. TGFβ1 also induced *LOX* and *LOXL2* expression however comparatively less than HIF stabilisation through DMOG, and only at the later time point of 72 hours. **(Figure 3.10 B, C)**. Intriguingly, *LOXL3* expression was significantly upregulated by both DMOG and TGFβ1 at 24 hours but then normalised over 48 and 72 hours **(Figure 3.10 D)**. Wnt signalling did not have any observed effect on *PLOD2*, *LOX*, *LOXL2* or *LOXL3* expression **(Figure 3.10 A-D)**.

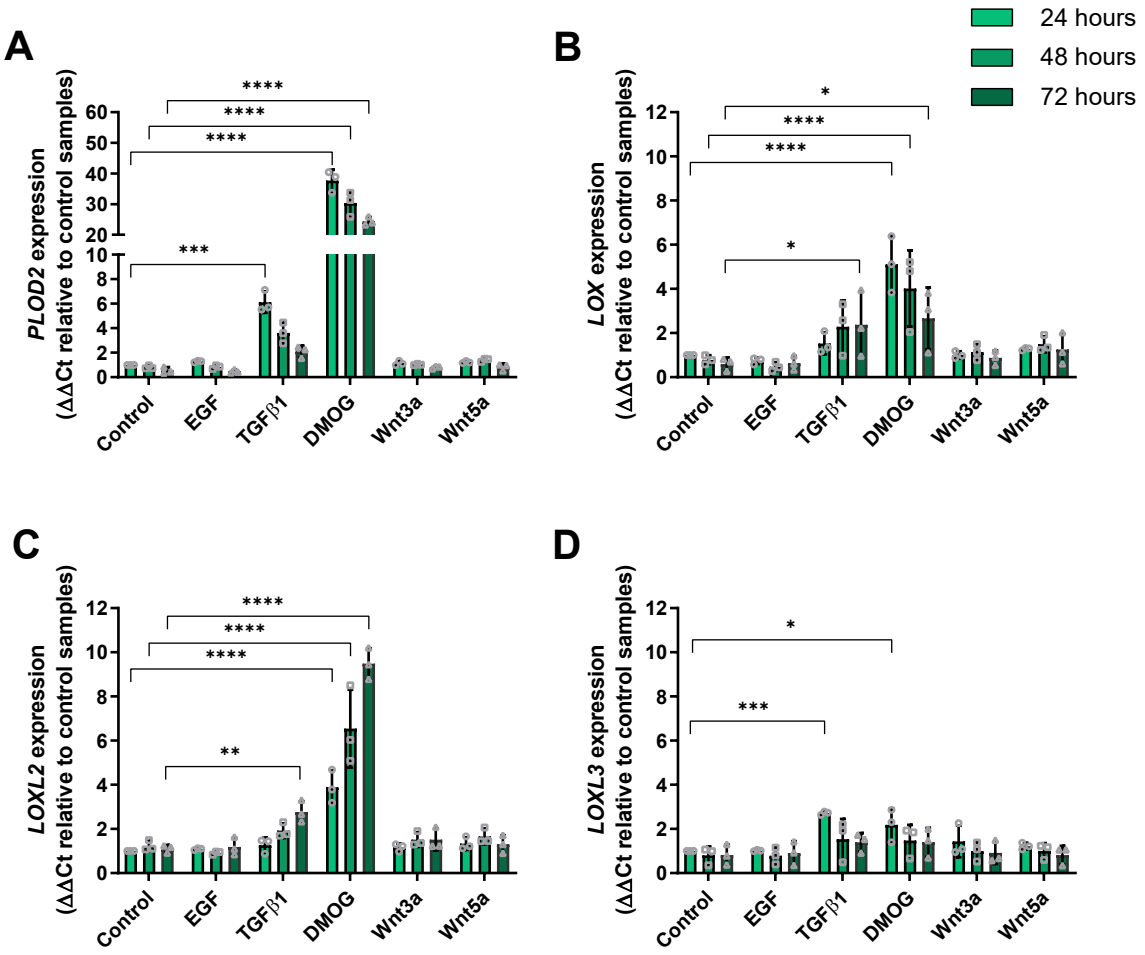

Figure 3.10: HIF stabilisation through pan-prolyl hydroxylase inhibition significantly upregulates the expression of *PLOD2*, *LOXL2* and *LOX* in lung fibroblasts. Time course of healthy donor lung fibroblasts exposed to either control, EGF 10ng/mL, TGFβ1 10ng/mL, DMOG 1mM, Wnt3a 100ng/mL or Wnt5a 100ng/mL for 24, 48 or 72 hours. mRNA expression levels for **(A)** PLOD2, **(B)** LOX, **(C)** LOXL2 and **(D)** LOXL3 were determined using the ΔΔ CT method, normalised to the sample control. Data were analysed using grouped analysis and multiple comparisons (Dunnett's test). * p<0.05, ** p<0.01, *** p<0.001, ****p<0.0001, error bars represent 1 standard deviation. N=3 independent experiments.

The effect of these pathways on the expression of key interstitial collagen genes – collagen I (*COL1A1*) and collagen III (*COL3A1*) were subsequently analysed[60]. Of the five pro-fibrotic conditions applied to the primary healthy lung fibroblasts across 24, 48 or 72 hours, only TGFβ1 had a significant effect on upregulation of *COL1A1* and *COL3A1* gene expression **(Figure 3.11 A-B)**. For both collagen genes this effect increased over time, with the greatest effect seen at 72 hours.

Notably despite the potent effect of the HIF pathway stabiliser DMOG to upregulate expression of *PLOD2* and *LOXL2*, the effect on collagen gene expression was negligible **(Figure 3.11 A-B)**.

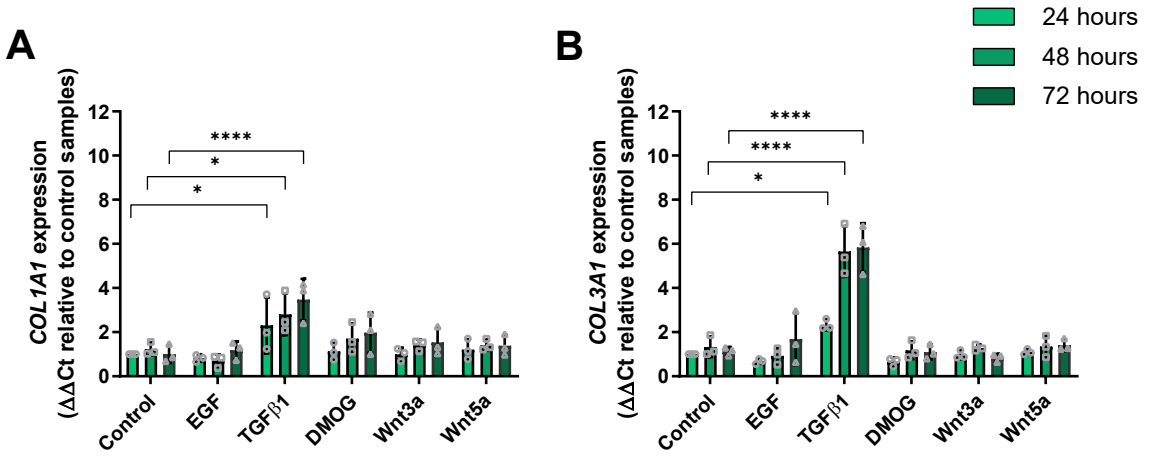

Figure 3.11: TGFβ1 but not HIF pathways promote expression of interstitial collagen genes *COL1A1* and *COL3A1*. mRNA expression of **(A)** COL1A1 and **(B)** COL3A1 expression in healthy donor lung fibroblasts exposed to 5 pro-fibrotic conditions for 24, 48 or 72 hours. mRNA expression levels were determined using the ΔΔ CT method. Data were analysed using grouped analysis and multiple comparisons (Dunnett's test). * p< 0.05, **** p < 0.0001, error bars represent 1 standard deviation. N=3 independent experiments.

PLOD2 and LOXL2 upregulation by DMOG, and to a lesser extent TGFβ1, was confirmed at 72 hours by western blot **(Figure 3.12)**. No change in PLOD2 or LOXL2 expression was seen for EGF, Wnt3a or Wnt5a.

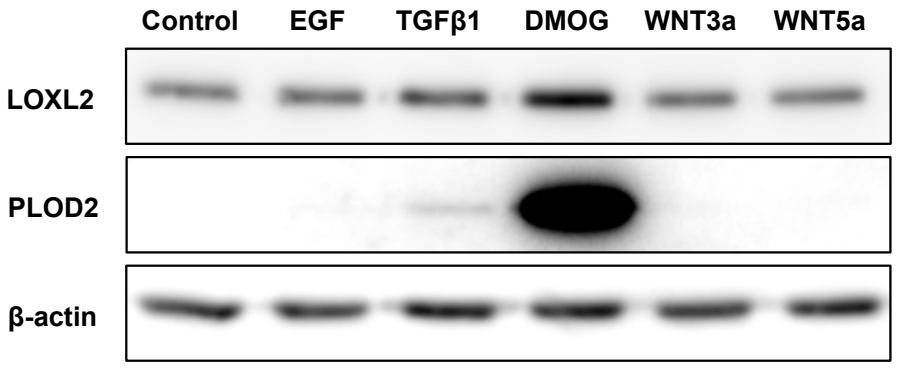

Figure 3.12: HIF stabilisation with pan-prolyl hydroxylase inhibition promotes collagen cross-linking enzymes PLOD2 and LOXL2 to a greater extent than TGFβ1. Western blotting for collagen cross-linking enzymes in lysates of healthy donor lung fibroblasts after exposure to 5 pro-fibrotic conditions – EGF, TGFβ1, HIF (through DMOG), Wnt3a and Wnt5a for 72 hours. Blot representative of N=3 experiments.

When observing the conditions of HIF stabilisation or TGFβ1 treatment over time, expression of PLOD2 increased over 72 hours in either condition **(Figure 3.13)**. LOXL2 expression appeared to peak at 48 hours, with no discernible increase at 72 hours, possibly due to its extracellular secretion.

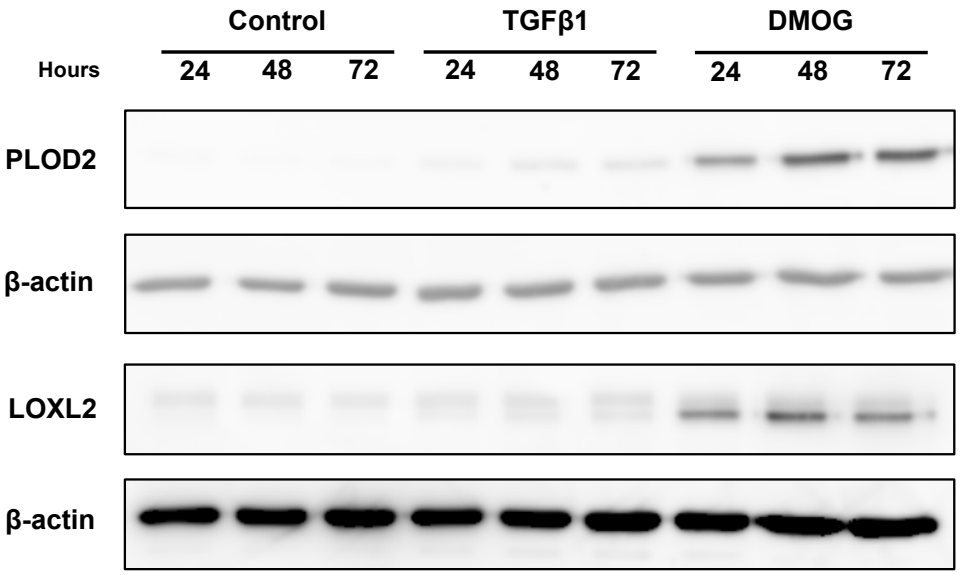

Figure 3.13: PLOD2 expression increases over time with both HIF pathway stabilisation and TGFβ1 signalling. Western blotting for PLOD2 and LOXL2 in healthy primary lung fibroblasts exposed to 5 pro-fibrotic conditions – EGF, TGFβ1, HIF (through DMOG), Wnt3a and Wnt5a. B-actin was used as a loading control. Blot representative of N=3 experiments.

Rather than simply facilitating collagen cross-linking, the LOXL2 enzyme has broad transcriptional functions that pertain to epithelial mesenchymal transition (EMT)[53-55,57-59]. Therefore the localisation of LOXL2 within the cell under certain pro-fibrotic conditions could provide important insights into specific roles under given conditions. Immunocytochemistry was thus performed not only to confirm the relative effects of HIF pathway stabilisation and TGFβ on fibroblast expression of LOXL2, but also to determine the cellular location of LOXL2 expression. Two HIF stabilising compounds were used – the selective prolyl 2-hydroxylase (PHD2) inhibitor, N-[[1,2-Dihydro-4-hydroxy-2-oxo-1-(phenylmethyl)-3-quinolinyl]carbonyl]-glycine (IOX2)[222], and the non-selective pan-PHD inhibitor DMOG.

To provide a comparable assessment between conditions, fluorescence was visualised by confocal microscopy and the gain intensity calibrated to the DMOG condition before being applied to the other conditions. Immunocytochemistry revealed HIF stabilisation through either IOX2 or DMOG as more potent inducers of LOXL2 expression than the prototypical TGFβ1 signalling **(Figure 3.14)**. The cellular pattern of LOXL2 staining in the DMOG condition was predominantly cytoplasmic with

some perinuclear staining also detected, suggesting LOXL2 was not specifically acting at the nucleus to exert transcriptional functions.

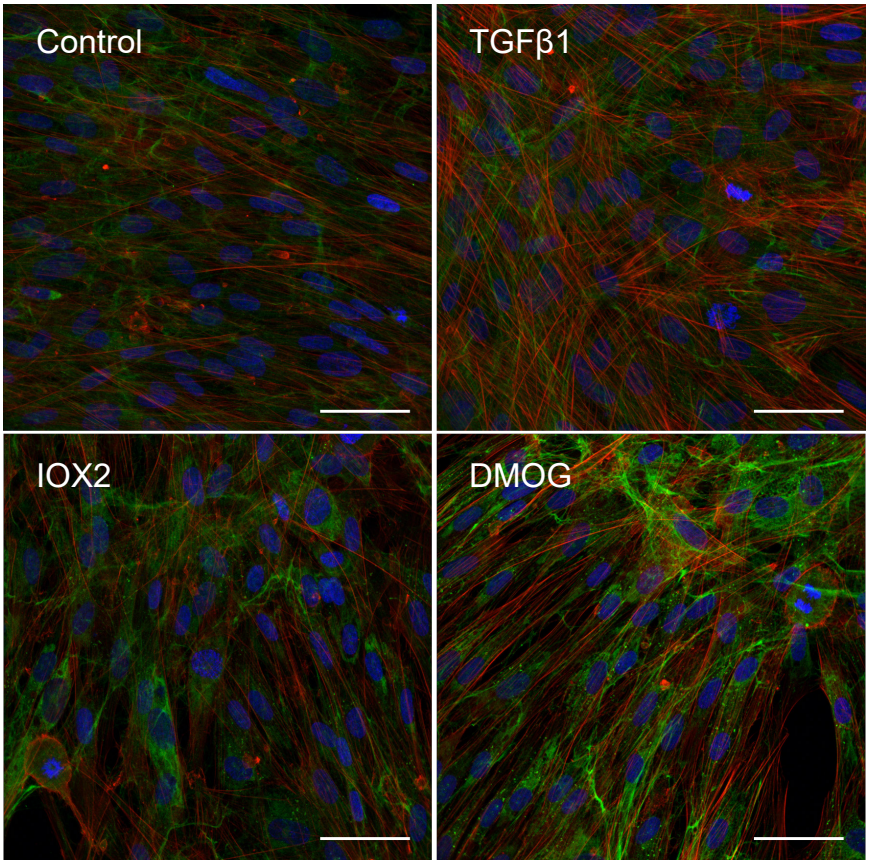

Figure 3.14: HIF stabilisation through either selective or pan-prolyl hydroxylase inhibition significantly increases LOXL2 *e*xpression in a cytoplasmic and perinuclear pattern. Confocal immunofluorescence of LOXL2 (green), DAPI (blue – nuclear staining) and Phalloidin (red – actin filament staining) expression in primary healthy lung fibroblasts exposed to pro-fibrotic conditions (TGFβ1 10ng/mL, IOX2 50μM or DMOG 0.5mM) for 48 hours. LOXL2 fluorescent intensity calibrated to control condition. Scale bar 50μm. Representative images from N=1 experiment.

The striking effects of DMOG on PLOD2 and LOXL2 expression required further examination to confirm they were HIF mediated and not simply 'off-target' effects of the compound. Functional silencing experiments were therefore performed on healthy donor lung fibroblasts by Liudi Yao (PhD student, School of Biomedical Sciences, University of Southampton). She silenced individual HIF genes (HIF1α, HIF2α and HIF1/2α) in primary human lung fibroblasts and then exposed them to DMOG. HIFβ, a ubiquitously expressed subunit which is essential for all HIF-mediated transcription, was also silenced as a positive control to effectively prevent all HIF pathway activation.

Western blotting by Liudi Yao from these experiments revealed the effects of DMOG on PLOD2 and LOXL2 upregulation were HIF-mediated **(Figure 3.15)**. Specifically, DMOG exposure increased PLOD2 and LOXL2 expression in fibroblasts with control siRNA, but not in siHIF1/2α or siHIF1β conditions.

Furthermore, in DMOG-treated conditions, silencing of HIF1α, but not HIF2α, suppressed PLOD2 expression, thereby demonstrating DMOG-mediated upregulation of PLOD2 is HIF1α dependent. Conversely LOXL2 expression was increased despite individual HIF1α or HIF2α silencing, but reduced following combined HIF1/2α silencing, implying both HIF1a and HIF2a are capable of promoting LOXL2 expression.

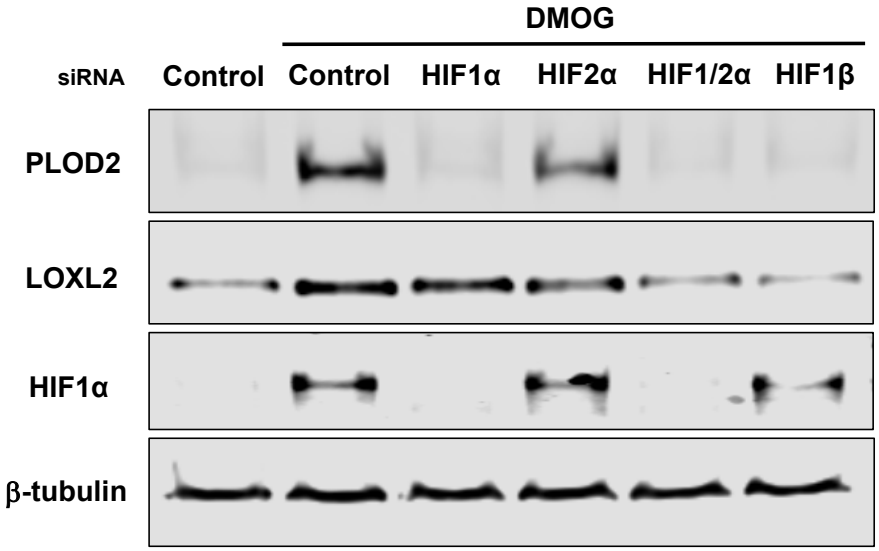

Figure 3.15: Upregulation of PLOD2 and LOXL2 by pan-prolyl hydroxylase inhibition is mediated through HIF pathways. Functional silencing of HIF activity in primary lung fibroblasts performed by Liudi Yao demonstrates PLOD2 expression is dependent on HIF1α and not HIF2α, while silencing of both HIF1α and HIF2α is required to prevent expression of LOXL2.

Taken together, HIF stabilisation was identified as a potent regulator of key 'bone-type' collagen cross-linking enzymes in lung fibroblasts, while the prototypical TGFβ also induced these enzymes, albeit less effectively. Notably, HIF pathway activation had no appreciable effect on *COL1A1* and *COL3A1* expression while TGFβ1 signalling was capable of significant upregulation of both fibrillogenesis genes. These divergent responses could have important downstream biomechanical implications within the ECM.

3.3.4 Comparative expression patterns of collagen cross-linking enzymes in a type two alveolar epithelial cell line under a range of pro-fibrotic conditions

A dysfunctional alveolar epithelial barrier characterised by basaloid and senescent AT2 cells is believed to be a significant component in the initiation and progression of pulmonary fibrosis[111,121,126,215]. A gradient of abnormal LOXL2 expression was observed, strongest at the epithelial edge and diminishing into the focus, suggesting the alveolar epithelium may be implicated in driving collagen cross-linking dysregulation within mesenchymal cells. It is increasingly recognised that the origins of the fibrogenic process in IPF are likely to occur at the alveolar epithelium, although the specific mechanisms are not clear. Epithelial-mesenchymal cross-talk could account for these effects through pro-fibrotic paracrine signalling. EMT is another method, although its relevance in IPF is controversial.

To investigate these possibilities, a stable AT2 cell line ($AT2^{KRAS:V12}$) was exposed to pro-fibrotic signalling pathways to explore morphological changes, markers of EMT and patterns of collagen cross-linking enzyme expression. The conditions were identical to those applied for the lung fibroblast experiments (TGFβ1, DMOG, Wnt3a, Wnt5a) with the exception of RAS activation. Rather than use EGF, an inbuilt RAS promoting pathway was instead activated through the 4-hydroxytamoxifen (4-OHT)-RAS chimeric protein (ER:KRAS:V12) stably expressed in the $AT2^{KRAS:V12}$ cell line[203,204].

Downstream effects of pro-fibrotic pathways on the AT2 cell line were observed using phase contrast microscopy. Compared with untreated control cells, morphological changes were noted in RAS (4-OHT), TGFβ1 and DMOG conditions, with no changes discernible in either the canonical Wnt3a or non-canonical Wnt5a treatments **(Figure 3.16)**. Both treatment with 4-OHT to activate RAS and DMOG to stabilise HIF activity induced morphological changes which suggested a transition to a more mesenchymal state, including loss of intercellular attachments and an increase in extracellular extensions to suggest enhanced motility. Morphological changes were also noted with TGFβ1, although more subtle. Namely, while the AT2 cells maintained their intercellular attachments they appeared more elongated in appearance. No change in morphology was observed with either canonical or non-canonical Wnt signalling.

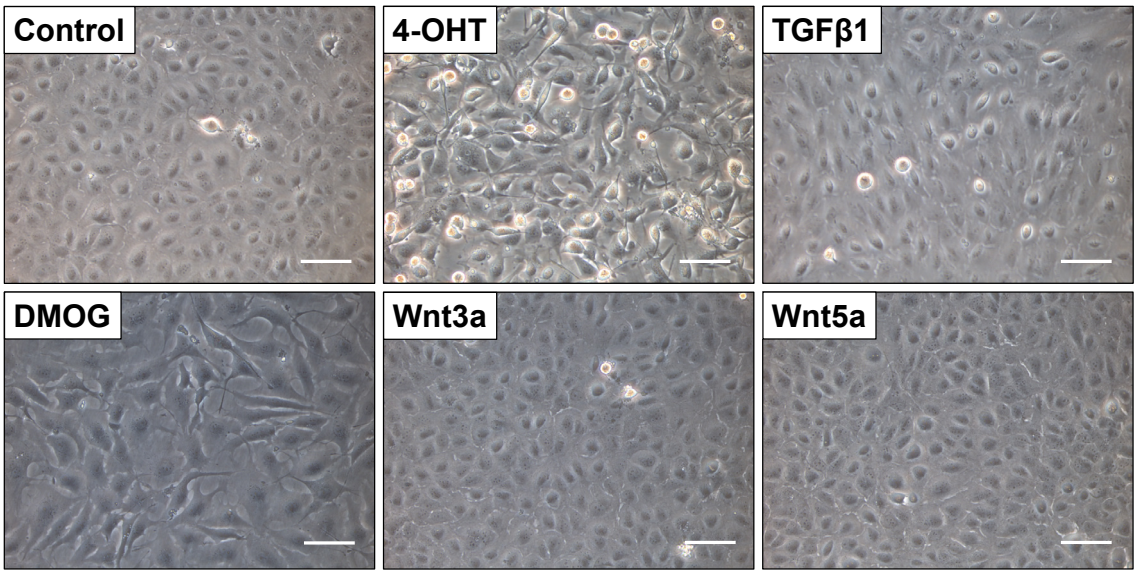

Figure 3.16: Morphological effects of pro-fibrotic signalling pathways on alveolar type 2 cells. Representative phase contrast images demonstrating the morphology of AT2$^{KRAS:V12}$ cells 72 hours after treatment with 4-OHT (250nM) to activate RAS, TGFβ1 (10ng/mL), DMOG (1mM) to stabilise HIF, Wnt3a (100ng/mL) or Wnt5a (100ng/mL). Scale bar 500um. Images representative of N=3 independent experiments.

The EMT-promoting effects of these pro-fibrotic pathways were subsequently compared in the AT2 cell line using RTqPCR to measure fold change in mRNA expression across the 72 hour time-course **(Figure 3.17)**. Downregulation of E-cadherin (*CDH1*), a key protein involved in intercellular attachment, and upregulation of the mesenchymal intermediate filament vimentin (*VIM*) are considered hallmarks of the EMT process, while *SNAIL1*, *SNAIL2*, *ZEB1* and *TWIST1* are all considered important transcription factors that can induce EMT traits within a cell[115].

Significant loss of *CDH1* expression was observed in the RAS (4-OHT) condition, while discernible but not statistically significant downregulation was also detected through HIF stabilisation with DMOG across the time-course **(Figure 3.17 A)**. Contrastingly, TGFβ1 increased *CDH1* expression significantly at 72 hours, however also increased *VIM* expression **(Figure 3.17 B)**. Significant upregulation of *VIM* was also seen with Wnt3a conditions at 24 hours, while DMOG has no significant effect.

Consistent with previous reports, TGFβ1 upregulated *SNAIL1* expression **(Figure 3.17 C)** while there was no effect from RAS, HIF or Wnt signalling. None of the 5 pro-fibrotic pathways influenced *SNAIL2* expression significantly **(Figure 3.17 D)**. Consistent with previously published reports, RAS induction through 4-OHT upregulated *ZEB1* expression throughout the time-course **(Figure 3.17 E).** None of the pro-fibrotic signalling pathways upregulated TWIST1 however HIF stabilisation through DMOG reduced its expression[143] **(Figure 3.17 F)**.

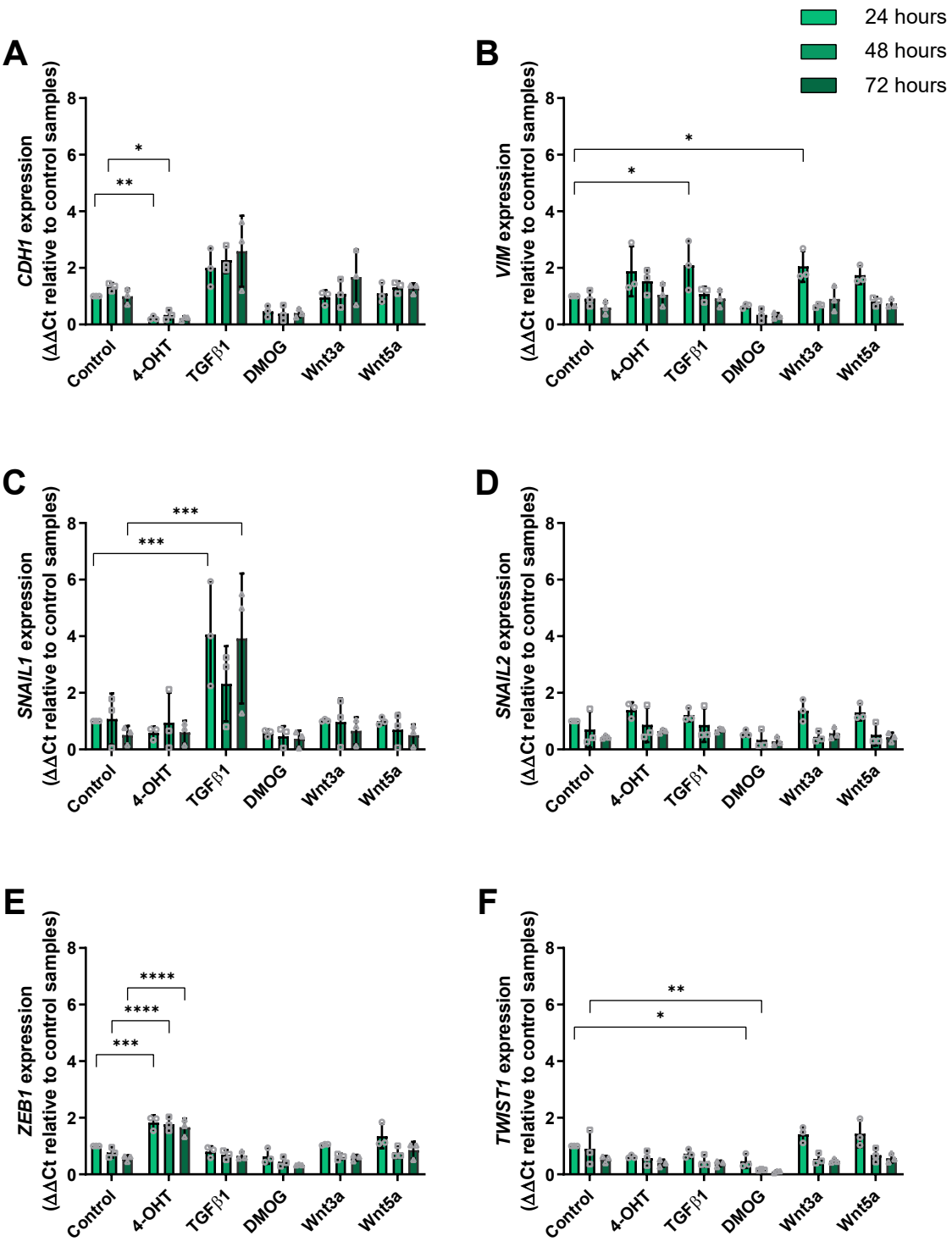

Figure 3.17: Pro-fibrotic signalling pathways induce mixed epithelial mesenchymal transition responses in alveolar type 2 cells. mRNA expression of EMT markers in the AT2 epithelial cell line exposed to different pro-fibrotic conditions for the times indicated. mRNA expression levels of **(A)** CDH1, **(B)** VIM, **(C)** SNAIL1, **(D)** SNAIL2, **(E)** ZEB1 and **(F)** TWIST1 were determined using the ΔΔ CT method with grouped analysis and multiple comparisons (Dunnett's test). * p< 0.05, ** p < 0.01, *** p < 0.001, ****p < 0.0001. N=3 experiments.

In summary no convincing effect was observed for any of the pro-fibrotic pathways to induce a complete EMT response in the AT2 cells, with significant heterogeneity in the expression of EMT markers and transcription factors. TGFβ1 promoted the prototypical EMT transcription factor *SNAIL1* yet increased CDH1 expression. Meanwhile both RAS activation through 4-OHT and HIF stabilisation through DMOG reduced CDH1 but only RAS was capable of promoting any of the EMT transcription factors (ZEB1). HIF pathway activation did not induce any of the EMT transcription factors. The mechanism by which HIF stabilisation was capable of reducing CDH1 could be through induction of LOXL2, which has previously been established to act directly on the CDH1 promoter to suppress its expression[52,223].

Mesenchymal cells were previously identified as the primary source of collagen cross-linking enzymes in IPF tissue. However a relative increase in the activity of core cross-linking enzymes was also observed in the alveolar epithelium overlying fibroblastic foci and in discrete regions of early fibrogenesis, suggesting alveolar epithelial cells may also be responsible for early collagen modification. Additionally, the aforementioned transcriptional roles of LOX(L) enzymes may be relevant to autocrine and paracrine signalling within the IPF lung. The relative expression of key collagen cross-linking enzymes were therefore examined within the AT2 cell line after exposure to pro-fibrotic signalling pathways **(Figure 3.18)**.

Notably, *PLOD2* expression was significantly elevated throughout the time-course by HIF stabilisation, while no other pro-fibrotic pathways had a significant effect on *PLOD2* expression **(Figure 3.18 A)**. *LOX* expression was also significantly upregulated through HIF activation at 48 and 72 hours, and to a lesser (non-significant) extent by TGFβ1 **(Figure 3.18 B)**. There were discernible but non-significant increases in mRNA expression of *LOXL2* through HIF stabilisation **(Figure 3.18 C)**, while TGFβ did not induce LOXL2 activity in the AT2 cells. No pro-fibrotic pathway induced LOXL3 expression in AT2 cells however HIF stabilisation appeared to suppress its activity **(Figure 3.18 D)**.

Taken together, stabilisation of HIF pathways through DMOG appeared to upregulate collagen cross-linking enzymes such as PLOD2 and LOX to a greater extent than TGFβ1 in this AT2 cell line. However the breadth and magnitude of HIF-mediated collagen cross-linking expression changes in AT2 cells was less marked than in lung fibroblasts, possibly indicating less relevance for their role in alveolar epithelial function.

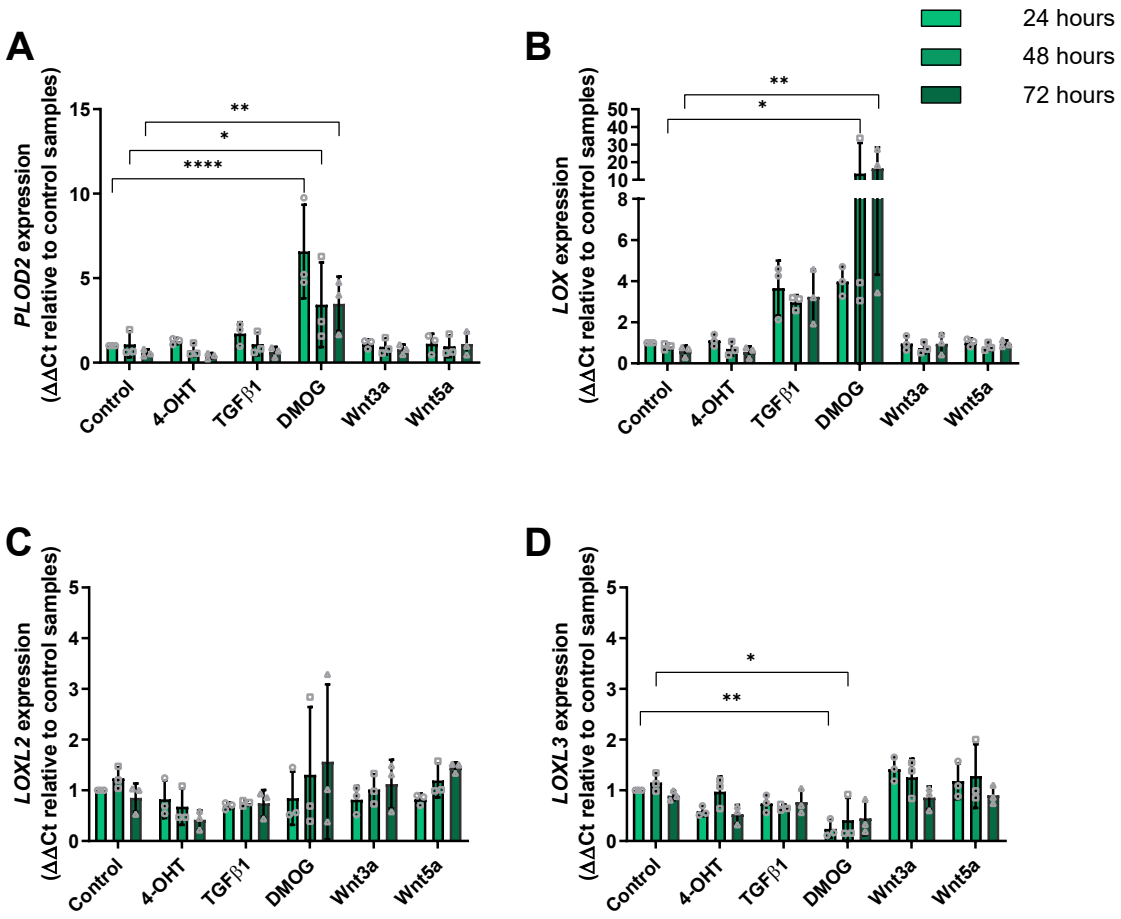

Figure 3.18: Induction of collagen cross-linking enzymes in alveolar type 2 cells through pro-fibrotic pathways is less marked than in lung fibroblasts. mRNA expression of collagen cross-linking enzymes in the AT2$^{KRAS:V12}$ epithelial cell line exposed to different pro-fibrotic conditions for 24, 48 or 72 hours. mRNA expression of **(A)** PLOD2, **(B)** LOX, **(C)** LOXL2, and **(D)** LOXL3 were determined using the ΔΔ CT method with grouped analysis and multiple comparisons (Dunnett's test). * p< 0.05, ** p < 0.01, *** p < 0.001, ****p < 0.0001. N=3 experiments.

As previously described above, *LOXL2*'s role as a transcription factor for EMT is increasingly recognised. With this in mind, the cellular pattern of *LOXL2* expression was assessed further in AT2 cells cultured on chamber slides under key pro-fibrotic conditions using confocal immunofluorescence **(Figure 3.19)**.

A higher intensity of *LOXL2* (green) fluorescence was observed in AT2 cells exposed to DMOG compared to TGFβ1 or control. The pattern of staining in all conditions was cytoplasmic, suggesting transcriptional activity for LOXL2 at the cell nucleus was not increased by these conditions. Staining for actin filaments with phalloidin also enabled a comparison of cytoskeletal reconstruction under the four conditional treatments. Compared to control cells, the TGFβ1-exposed cells appeared to possess longer and more organised actin filaments, while RAS

activation through 4-OHT and HIF stabilisation through DMOG resulted in less organised phalloidin staining, possibly due to the cells developing an EMT phenotype by becoming more motile and undergoing changes in polarisation.

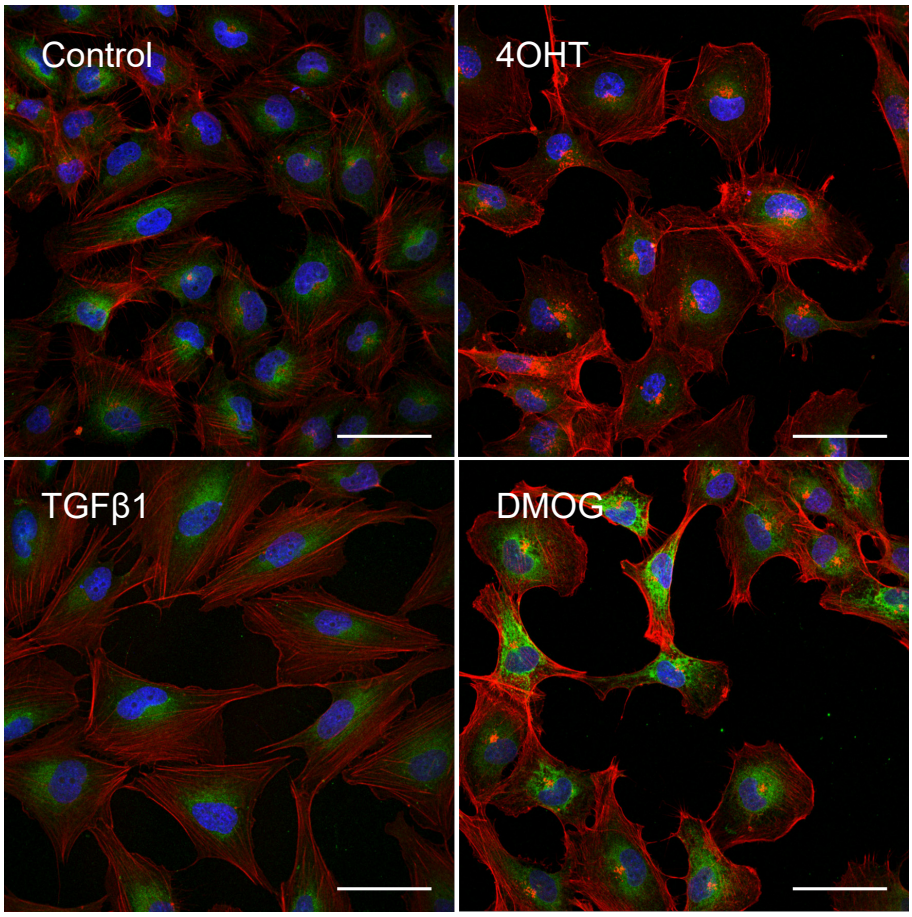

Figure 3.19: Cytoplasmic and perinuclear staining of LOXL2 is increased with HIF stabilisation. Confocal immunofluorescence of LOXL2 (green), DAPI (blue) and Phalloidin (red) in an AT2 cell line exposed to pro-fibrotic conditions (4-OHT 250nM, TGFβ1 10ng/mL or DMOG 1mM) for 48 hours. Signal gain calibrated in DMOG condition and fixed for other conditions to enable direct comparison. Scale bar 50µm.

3.4 Discussion

Abnormal matrix remodelling in IPF not only impairs respiration through limitations on compliance and diffusive capacity, but may even sustain a progressive fibrotic response through aberrant mechano-signalling pathways[165,168,169,224]. Pathological induction of 'bone-type' collagen cross-linking enzymes such as *PLOD2* and the *LOX(L)* family are likely to be critical mediators of this process through accumulation of dense and relatively insoluble pyridinoline cross-links[165].

Using two independent methods of RNA analysis, this study identified significant upregulation of bone-type collagen cross-linking enzymes within mesenchymal cells of the fibroblastic foci. The cellular source of these enzymes and the pathways which drive their dysregulation have not been comprehensively studied before. Historically, the analyses of collagen cross-linking enzymes in IPF have focused on serum or whole lung sampling, thereby failing to delineate regional differences in their expression[165,194]. Limitations in conventional *in situ* staining methodologies have also hindered an accurate analysis. In particular, immunohistochemical assays are impaired by the predominantly extracellular location of LOX(L) enzymes, leading to ubiquitous staining of matrix which lacks insight into the enzyme origins. This is compounded by poor specificity for many of the LOX(L) antibodies to their antigenic target, making assessments for specific LOX(L) family members difficult to perform[193].

A key finding within the RNA sequencing data was a strong correlation in the expression of *PLOD2* and *LOXL2* within the fibroblastic focus, supported by co-localisation of these enzymes within individual mesenchymal cells using mRNA in-situ hybridisation. Excessive hydroxylation of lysine residues at the collagen telopeptide by PLOD2 is considered a specific fibrotic phenomenon and a principal tipping point in pathological stiffening of ECM[177]. All LOX(L) members are capable of oxidising both lysine and hydroxylysine residues to facilitate cross-linking, yet difference in substrate selectivity within the individual LOX(L) enzymes is unknown[183]. The significant correlation and co-localisation observed could suggest a preference of LOXL2 for the PLOD2-induced hydroxylysine residues, over other LOX(L) members. This may also explain the increased levels of LOXL2 reported in serum and lung tissue of patients with IPF[131,194]. Alternatively, common regulatory pathways could be promoting both PLOD2 and LOXL2. For example TGFβ, the archetypal pro-fibrotic mediator, is capable of inducing the expression of both enzymes through SMAD signalling[197,225].

Intriguingly collagen cross-linking enzyme activity was greatest within mesenchymal cells adjacent to the alveolar surface of the fibroblastic foci compartment, suggesting this to be the "active front" of matrix remodelling. This finding is in line with a growing body of evidence suggesting the alveolar epithelium as the location for fibrogenesis in IPF[111,126,215]. Induction of collagen cross-linking enzymes at the leading edge could be due to direct stimulation of mesenchymal cells from exogenous exposures entering the interstitium through a maladaptive alveolar barrier. Perhaps more likely however is that paracrine signalling from the alveolar epithelium itself is inducing the collagen cross-linking activity within mesenchymal cells. For example, in vitro and in vivo studies revealed increased mechanical tension on AT2 cells generated a TGFβ-signalling loop which generated typical UIP-like patterns of ECM remodelling within mouse lungs[126]. In another study, disruption of telomere function in AT2 cells (but not mesenchymal cells) was capable of producing

a fibrotic response[119]. Yet the specific regulatory signalling pathways which were inducing collagen cross-linking expression at this location were unclear.

A comparative analysis of pro-fibrotic signalling pathways was subsequently performed on lung fibroblasts. Strikingly, HIF stabilisation through DMOG was a potent inducer of both PLOD2 and LOXL2, inducing expression fold changes of both enzymes that eclipsed prototypical TGFβ signalling.

HIF signalling has emerged as an important transcriptional mechanism for cellular responses to regional environmental changes, chiefly oxygen tension. Our understanding of cellular oxygen sensing began just 30 years ago with the identification of the hypoxia response element (HRE) in 1991 - initially on the erythropoietin gene and subsequently in a diverse range of different cell types[226,227]. A decade of research unveiled the mechanisms of HRE regulation, beginning with the identification of a HRE-binding transcription factor (HIF1α) in 1995[228], and then the control on HIF accumulation in 2001 through prolyl-hydroxylation and VHL degradation[229-232]. These discoveries led to the 2019 Nobel Prize for Physiology and Medicine, as well as innumerable developments of HIF pathway relevance in both health and disease.

HIF proteins are a group of heterodimeric transcription factors which mediate cellular responses, primarily to environmental oxygen tension, through the regulation of broad-ranging gene expression[152]. These effects are exerted from within the nuclear-located HRE when the unstable HIFα subunits bind to the stable HIFβ subunit, forming the stable HIF transcription factor[150].

There are three isoforms of the HIFα subunit (HIF1α, HIF2α, and HIF3α). HIF1α and HIF2α isoforms are highly conserved within areas such as the basic Helix-Loop-Helix (bHLH) and Per-Arnt-Sim (PAS) domains, responsible for DNA binding and dimerisation with HIFβ, thereby reflecting similar expression and HIFβ-binding capacity of these two isoforms[233]. However HIF1α and HIF2α have reduced homology in the transactivating domains at the N and C-termini (N-TAD and C-TAD respectively) which likely accounts for a divergence in their downstream transcriptional effects. HIF3α is even more unique, displaying the ability to dimerise with HIFβ but lacking the same transcriptional response, leading to its current perceived role as a negative regulator of HIF expression[151].

In normoxia, the HIFα subunit is rapidly degraded before it can dimerise with HIFβ to exert a transcriptional effect. This occurs through proline hydroxylation of at least one highly conserved HIFα proline residue at the oxygen dependent degradation domain (ODDD) by

prolyl hydroxylases (PHDs), which subsequently facilitate the proteosomal degradation of HIFα by the von Hippel-Lindau tumour-suppressor protein (VHL) before it can bind to HIFβ[234].

Another oxygen-dependent regulatory mechanism for HIF turnover exists in Factor Inhibiting HIF (FIH), an asparaginyl hydroxylase which targets the asparagine 803 residue within the HIFα COOH-terminal transactivation domain (CAD), thereby blocking its interaction with p300-CREB co-activating proteins in the nucleus[220,235]. Both PHDs and FIH function in normoxia to prevent dimerisation of HIFα with HIFβ at the cell nucleus, and are themselves inhibited with varying degrees of hypoxia.

The PHD family can broadly be differentiated by their function into collagen-PHDs and HIF-PHDs, which differ in both location and the proline substrates targeted[229]. HIF-PHDs possess catalytic activity which is highly dependent on oxygen tension in the surrounding cellular environment, with increased activity at higher oxygen partial pressures. There are 3 known HIF-PHDs (PHD1, 2 and 3) which are responsible for the oxygen-dependent HIF concentrations. The substrate selectivity and individual roles of each isoform are still a topic of ongoing research, although emerging evidence supports PHD2 as the principal regulator of hypoxia-mediated HIF-signalling in health and disease[236-238]. Inhibitors of PHDs, either pan-PHD inhibitors such as DMOG or selective HIF-PHD inhibitors such as IOX2 (which targets PHD2), therefore mimic hypoxia by facilitating the accumulation of HIFα and downstream pathway activation through the HIFα/β heterodimer[239].

HIFs are highly expressed in the developing lung, seen as early as 8 weeks into embryological development, and are critical to pulmonary organogenesis including neovascularisation and airway branching[240]. Reductions in HIF levels during development or during pre-term delivery may lead to significant impairment in respiratory development including alveolar, vascular and bronchopulmonary hypoplasia[241,242]. Following birth and commencement of respiration HIF pathway activation in the normal lung declines, and healthy adults have relatively low levels of pulmonary HIF expression[243].

HIF pathway dysregulation in adulthood has been implicated in a wide range of pulmonary diseases including acute lung injury, pulmonary hypertension, and lung cancer[244]. However the roles of HIF pathway activation in fibrotic interstitial lung diseases such as IPF are less well described. In this study it was apparent that the effects of HIF stabilisation on collagen cross-linking enzyme induction were more potent in lung fibroblasts than in an AT2 cell line.

Many HIF effects are pro-fibrotic in nature, including activation of fibroblasts and synergistic interaction with TGFβ1/SMAD3 signalling[245,246]. While immunohistochemical expression of

HIF1α and HIF2α expression has been identified within IPF lung tissue the cause or effect nature of these expression changes, and the drivers of this pathway activation (such as hypoxia) are unclear[153,247]. Studies examining the effects of HIF pathway activation on ECM modification and stiffness are conflicting, and have not been mechanistically explored in pulmonary fibrosis[248-250]. The results of this study therefore raise important questions surrounding a possible role for HIF pathways in driving the dysregulated bone-type collagen cross-linking enzyme expression in mesenchymal cells, and the downstream biomechanical consequences on the IPF ECM.

3.5 Conclusion

Using regionally-selective RNA sequencing, collagen cross-linking enzyme expression was found to be markedly upregulated within IPF fibroblastic foci compared to healthy and IPF alveolar septae. In particular the 'bone-type' pyridinoline cross-linking enzymes *PLOD2* and *LOXL2* were highly expressed and exhibited strong correlation, suggesting common mechanisms for their induction. *In situ* mRNA analysis confirmed areas of discrete cross-linking activity within IPF fibroblastic foci, identified mesenchymal cells as the source of this activity, and detected substantial co-localisation of *PLOD2* and *LOXL2* within individual mesenchymal cells. *In vitro* experiments identified HIF pathway activation to be a more potent inducer of both *PLOD2* and *LOXL2* expression in fibroblasts than prototypical TGFβ signalling. An understanding of the prevalence, location and mechanisms of HIF pathway activation within the IPF lung is required to aid in interpreting these findings, and will be reviewed in the next chapter.

Chapter 4 HIF Pathways as Key Regulators of Collagen Cross-linking Enzyme Expression

4.1 Introduction

HIF stabilisation through prolyl hydroxylase (PHD)-inhibiting compounds were previously identified as potent stimuli for upregulation of collagen cross-linking enzymes in similar patterns to that seen in IPF lung. In particular, PLOD2 and LOXL2 enzyme dysregulation by HIF pathway activation was greater than by the conventional pro-fibrotic TGFβ signalling pathways.

PHD inhibitors such as DMOG and IOX2 prevent the VHL-mediated ubiquitination and proteosomal degradation of HIFα, thereby mimicking hypoxia in enabling dimerisation of the HIFα subunit with HIFβ at the nucleus to promote transcription within the HRE **(Figure 4.1)**.

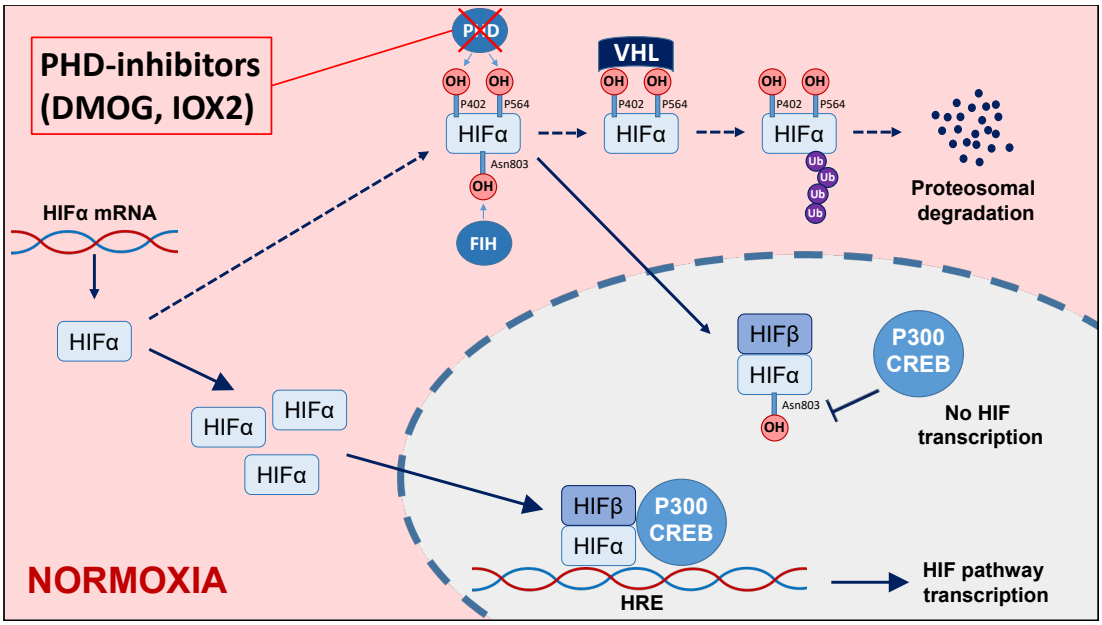

Figure 4.1: Prolyl hydroxylase inhibitors mimic hypoxia to activate HIF pathways through stabilisation and accumulation of HIFα. The pan-PHD inhibitor DMOG and selective PHD2 inhibitor IOX2 both stabilise HIFα by preventing proteosomal degradation, enabling accumulation and dimerisation with HIFβ in the cell nucleus, with subsequent HIF pathway transcription at the hypoxic response element (HRE).

Hypoxia is the conventional means for HIF pathway activation, and may be the mechanism of HIFα stabilisation in areas of active fibrosis within the IPF lung[153,246]. HIF pathways are increasingly implicated in IPF pathogenesis, particularly with regard to fibroblast proliferation

and activation, but also in association with alveolar epithelial cell apoptosis[153,154,156,218,246]. However a role for HIF pathways as key inducers of pathologic collagen post-translational modification has not been explored in IPF. This study therefore sought to confirm HIF pathway activation in IPF tissue and analyse the patterns of expression compared to those of key collagen cross-linking enzymes. Furthermore, to explore hypoxia as a possible source for HIF pathway-mediated collagen cross-linking enzyme activity in the IPF lung, the effects of hypoxia on primary lung fibroblasts and alveolar epithelial cells were analysed *in vitro*.

4.2 Objectives

The objectives of this study were to:

i) Observe patterns of HIF pathway expression in healthy and IPF lung tissue and compare this to collagen cross-linking enzyme expression.

ii) Examine the effects of hypoxia on HIF pathway activation and downstream collagen cross-linking enzyme expression in primary healthy and IPF lung fibroblasts, and primary alveolar epithelial cells.

4.3 Results

4.3.1 HIF pathway expression in IPF tissue

HIF pathway activation has been observed in IPF tissue, most prominently in areas of fibrogenesis surrounding hyperplastic alveolar epithelium and mesenchymal lung fibroblasts[153,247]. However difficulties with antibody selectivity and tissue preparation have left these findings difficult to reproduce, and the association between patterns of HIF pathway activation and collagen cross-linking enzyme expression such as *PLOD2* and *LOXL2* have not previously been demonstrated.

This study sought to confirm HIF pathway activation in IPF tissue by measuring key HIF pathway markers HIF1α and carbonic anhydrase IX (Ca9), a downstream transcriptional target of HIF which is widely used in immunohistochemical studies to reflect HIF stabilisation[153,251]. Serial sections of healthy and IPF lung tissue were examined for expression of HIF1α and Ca9 using an avidin-biotin-DAB-peroxidase system **(Figure 4.2)**. Adjacent sections were stained with H&E to provide architectural reference, and with mRNA *in situ* hybridisation for key 'bone type' collagen cross-linking enzymes to enable comparison of regional expression.

Increased expression of HIF1α was seen in IPF alveolar septae compared to healthy septae, with cytoplasmic and nuclear staining of alveolar epithelial cells as well as smooth muscle cells within

vessel walls. Membranous and nuclear staining for Ca9 was seen in both healthy and IPF alveolar epithelial cells, however there appeared to be a greater proportion of positively stained cells in IPF tissue, as well as a stronger intensity of staining within IPF blood vessels.

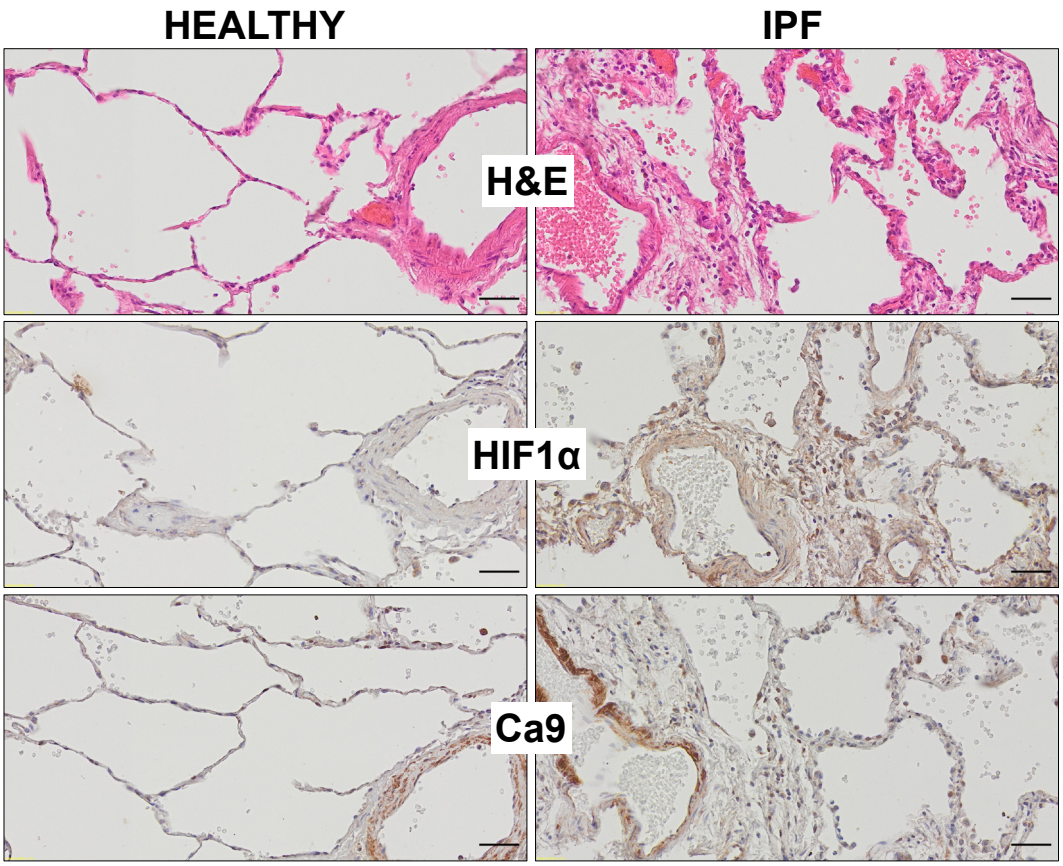

Figure 4.2: Markers of HIF pathway activation are increased within IPF alveolar septae. H&E staining (top row) and IHC staining for HIF1α (middle row) and Ca9 (bottom row) of serial sections of healthy and IPF human lung tissue. IHC staining was performed for each protein of interest using an avidin-biotin-DAB-peroxidase system (brown). Sections were counterstained with haematoxylin (blue). Staining representative of N=3 healthy and 5 IPF donors. Scale bar 50µm.

As previously described, bone-type collagen cross-linking enzymes were highly expressed within IPF fibroblastic foci compared to surrounding IPF tissue and healthy lung donor tissue. HIF1α and Ca9 expression was observed in mesenchymal cells within the IPF fibroblastic foci **(Figure 4.3).** Furthermore, individual mesenchymal cells within the foci which expressed markers of HIF pathway activation also co-expressed *PLOD2* and *LOXL2* **(Figure 4.3 insets)**.

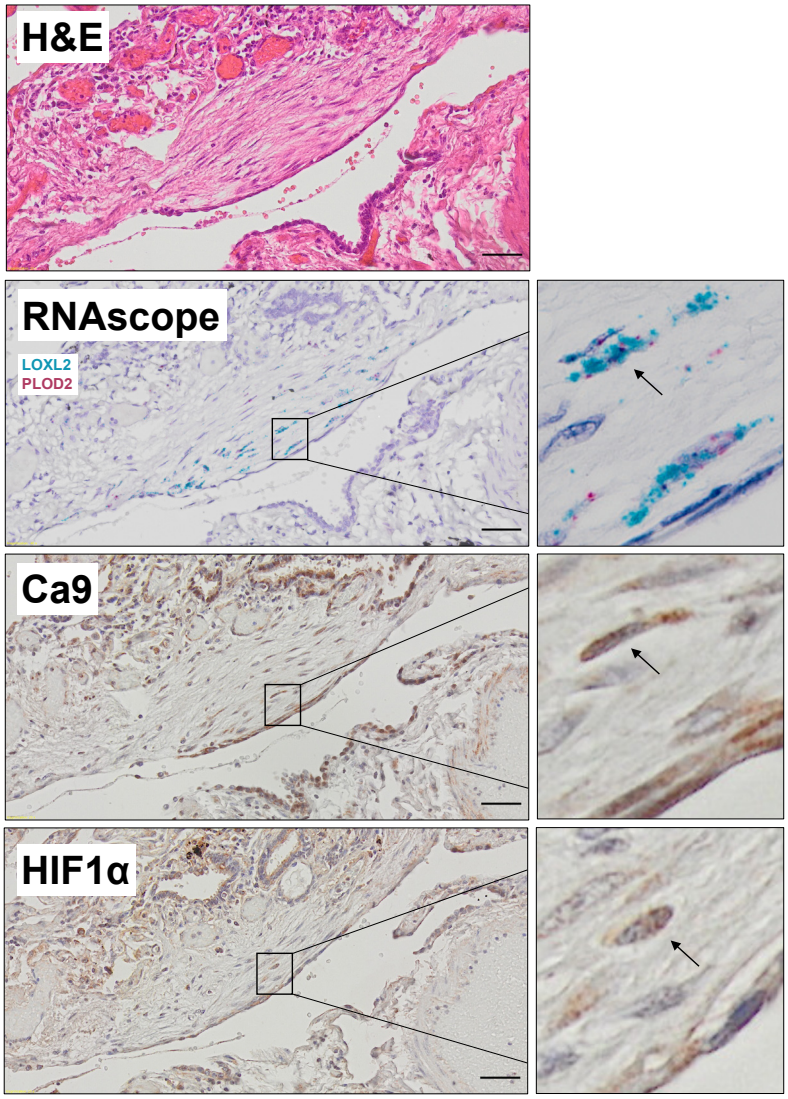

Figure 4.3: Mesenchymal cells within IPF fibroblastic foci co-express markers of HIF pathway activation and collagen cross-linking enzyme activity. Adjacent histopathological sections of IPF tissue were examined with H&E staining (top row), mRNA in-situ hybridisation for bone-type collagen cross-linking enzymes (*LOXL2* green channel, *PLOD2* red channel, second row) and IHC staining for markers of HIF pathway activation (Ca9, third row, and HIF1α, bottom row). IHC staining was performed using an avidin-biotin-DAB-peroxidase system for protein of interest (brown). Sections were counterstained with haematoxylin (blue). Staining representative of 5 IPF donors. Scale bar 50μm.

Markers of HIF pathway activation were also seen in the hyperplastic alveolar epithelium overlying fibroblastic foci **(Figure 4.4)**. As previously described, collagen cross-linking enzyme activity was most intense in mesenchymal cells within IPF fibroblastic foci that were in close proximity to this alveolar epithelium, and diminished with distance from the 'leading edge'.

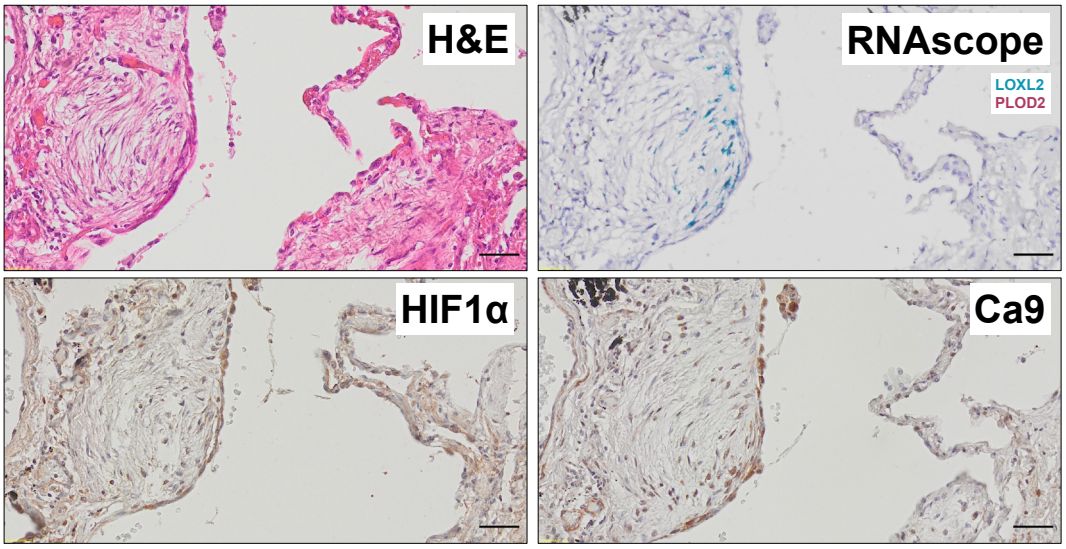

Figure 4.4: Markers of HIF pathway activation are expressed in hyperplastic alveolar epithelium overlying IPF fibroblastic foci. Adjacent histopathological sections of IPF tissue were examined with H&E staining (top left), mRNA in-situ hybridisation (*LOXL2* green channel, *PLOD2* red channel, top right) and markers of HIF pathway activation using IHC for HIF1α (bottom left) and Ca9 (bottom right). IHC staining was performed using an avidin-biotin-DAB-peroxidase system for protein of interest (brown). Sections were counterstained with haematoxylin (blue). Images representative of 3 healthy and 3 IPF donors. Scale bar 50μm.

4.3.2 Comparative effects of hypoxia on HIF pathway activation in healthy and IPF lung fibroblasts

Following the identification of HIF pathway activation within IPF tissue, both in mesenchymal cells within the fibroblastic foci and in the alveolar epithelium overlying the foci, further in vitro experiments were performed to establish the relevance of HIF accumulation to the collagen cross-linking activity of alveolar epithelial cells and lung fibroblasts. A comparison of fibroblasts from healthy and IPF donors was performed to determine if functional differences existed in HIF and collagen cross-linking responses.

To reflect the mechanisms by which HIF pathway activation occurs in the IPF lung, hypoxia was used to stabilise HIFα proteins (1% environmental O_2, equating to a PO_2 of 7.6mmHg at sea level). Lung fibroblasts from three healthy and three IPF donors each were plated and incubated in parallel (in a standard incubator with ambient O_2 levels), and exposed to 1% O_2 for either 0, 24 or 48 hours before immediate harvest while still in the hypoxic environment (if applicable). Cell confluence was carefully controlled by plating and harvesting cells at the same time, but

staggering the time of hypoxia exposure. Gene expression changes were identified at the mRNA level using RTqPCR and at the protein level using western blotting.

Following exposure to either 24 or 48 hours of 1% O_2, both healthy and IPF lung fibroblasts demonstrated marked increases in expression of the downstream HIF pathway marker Ca9 **(Figure 4.5 A).** Presumably in response to HIFα stabilisation and accumulation within the cell, hypoxic conditions for 24 or 48 hours resulted in a marked downregulation of *HIF1α* **(Figure 4.5 B)** and *HIF2α* **(Figure 4.5 C)** expression compared to healthy and IPF lung fibroblasts cultured in normoxia. In contrast, the mRNA expression of *HIF3α* **(Figure 4.5 D)** was increased in both healthy and IPF fibroblasts exposed to the hypoxic environment, likely explained by its regulatory role in negative feedback of HIF1α and HIF2α. Notably, IPF fibroblasts cultured in normoxia had greater expression of *HIF3α* than healthy fibroblasts, suggesting an enhanced role for negative feedback on HIF pathway activation **(Figure 4.5 D)**.

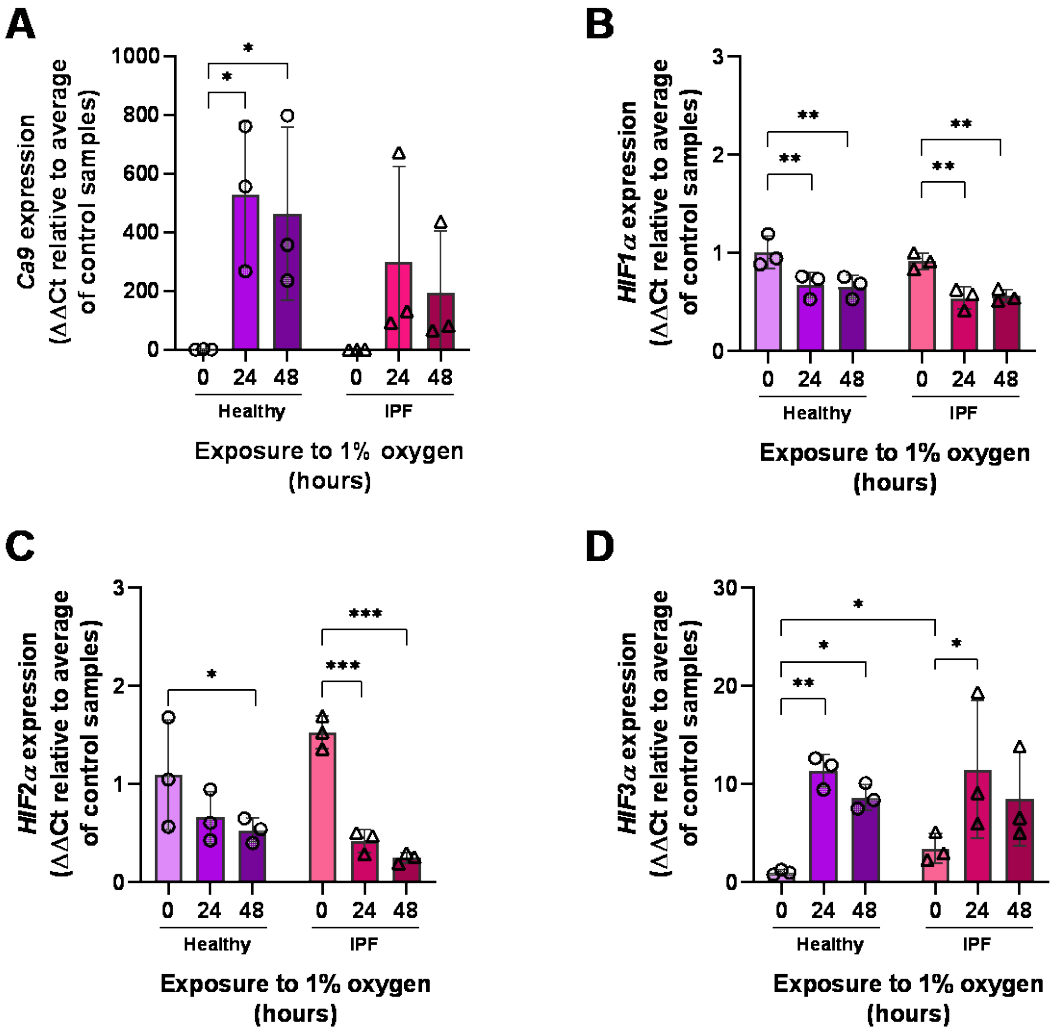

Figure 4.5: Responses in HIF pathway activation to hypoxia in healthy and IPF lung fibroblasts. mRNA expression of **(A)** *Ca9*, **(B)** *HIF1α,* **(C)** *HIF2α* and **(D)** *HIF3α* in healthy and IPF primary fibroblasts exposed to 1% O_2 for 0, 24 or 48 hours. mRNA expression levels were determined using the ΔΔ CT method with grouped analysis and multiple comparisons (Dunnett's test). * p< 0.05, ** p < 0.01, *** p < 0.001, N=3 healthy and 3 IPF donors, with experiments performed in duplicate.

HIFα proteins are in constant turnover, with production dependent on gene expression and translation while degradation is dependent on the activity of HIF-PHDs and FIH. Therefore while informative, HIF mRNA expression alone represents only part of the HIF response. To quantify protein expression of HIFα, western blotting was performed in an identical experiment on lung fibroblasts from 3 healthy and 3 IPF donors exposed to 1% O_2 for 0, 24 and 48 hours **(Figure 4.6)**.

Healthy lung fibroblasts exposed to hypoxia for 24 or 48 hours exhibited increased expression of HIF1α, HIF2α and HIF3α **(Figure 4.6 A)**. Densitometry analysis of blots from three separate healthy donors confirmed HIFα stabilisation and accumulation for all three subunits **(Figure 4.6 B-D)**.

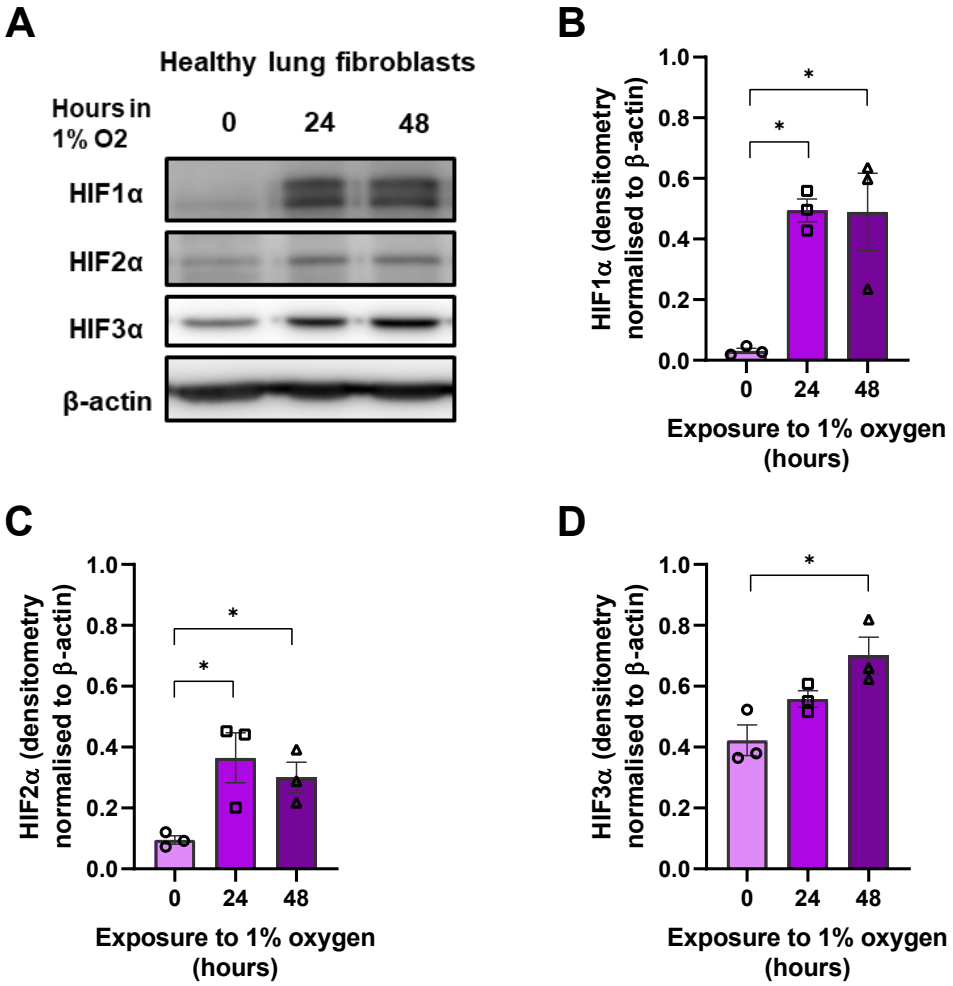

Figure 4.6: Hypoxia stabilises all three HIFα subunits in lung fibroblasts from healthy donors. (A) Western blotting for HIFα in early passage healthy primary lung fibroblasts exposed to 0, 24 or 48 hours of hypoxia. Blot representative of 3 separate healthy donors. β-actin was used as a loading control. Densitometry analysis demonstrating protein expression of **(B)** HIF1α, **(C)** HIF2α and **(D)** HIF3α normalised to β–actin. Grouped analysis and multiple comparisons (Dunnett's test). * p< 0.05. N=3 healthy donors, with experiments performed in duplicate.

Conversely, exposure of IPF fibroblasts to 1% O_2 for 24 or 48 hours was associated with an accumulation of HIF1α and HIF2α protein yet a reduction in the presence of HIF3α **(Figure 4.7 A)**. Densitometry analysis of fibroblasts from all three IPF donors confirmed a consistent increase in HIF1α **(Figure 4.7 B)** and HIF2α **(Figure 4.7 C)** expression after exposure to 1% O_2, with no difference observed between 24 and 48 hours. Contrary to healthy lung fibroblasts, IPF fibroblast HIF3α protein expression was consistently reduced after exposure to hypoxia for 24 or 48 hours in all three donors **(Figure 4.7 D)**.

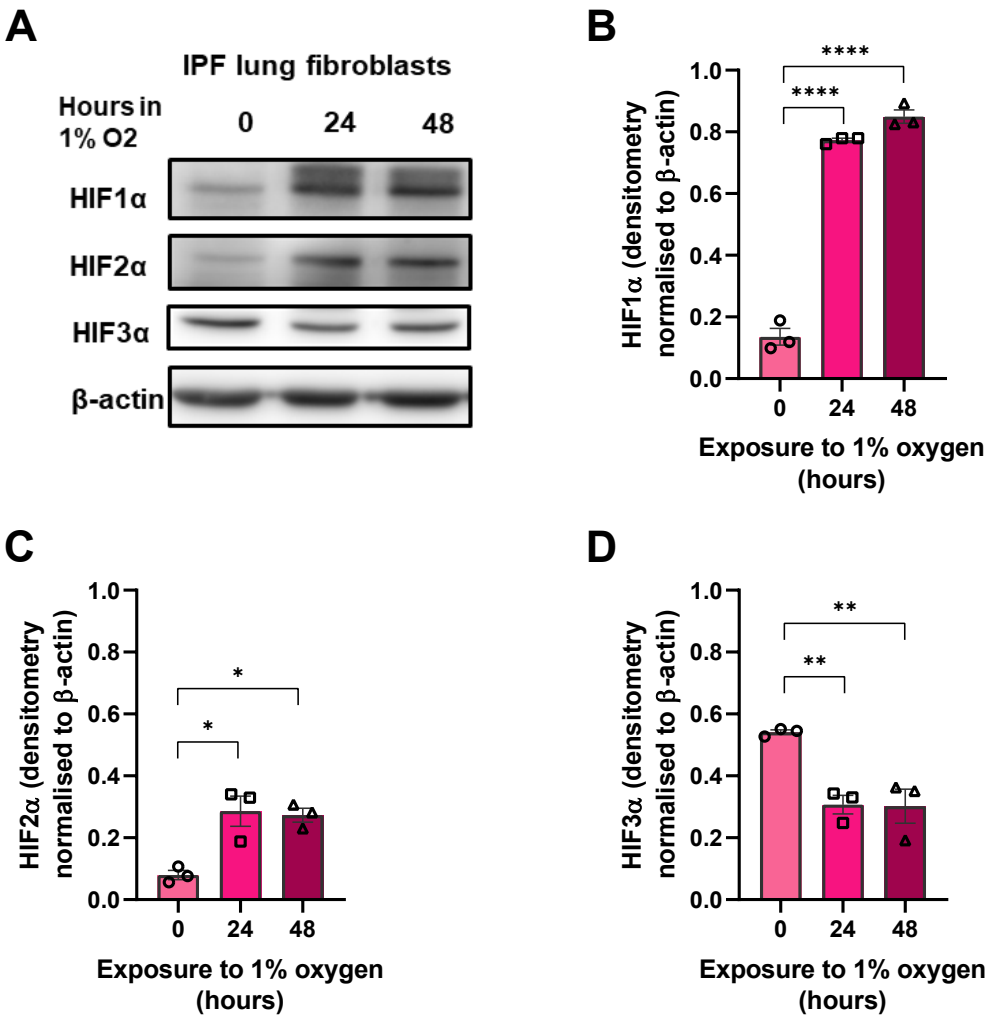

Figure 4.7: Hypoxia results in stabilisation of HIF1α and HIF2α but not HIF3α in IPF fibroblasts. **(A)** Western blotting for HIFα in early passage IPF primary lung fibroblasts exposed to 0, 24 or 48 hours of hypoxia. Blot representative of 3 separate IPF donors. β-actin was used as a loading control. Densitometry analysis demonstrating protein expression of **(B)** HIF1α, **(C)** HIF2α and **(D)** HIF3α normalised to β–actin. Grouped analysis and multiple comparisons (Dunnett's test). * $p < 0.05$, ** $p < 0.01$, **** $p < 0.0001$, N=3 IPF donors, with experiments performed in duplicate.

Taken together, hypoxia led to stabilisation of HIF1α and HIF2α in lung fibroblasts from both healthy and IPF donors, with an increase in cellular protein expression and decline in mRNA expression, possibly due to negative feedback. Of particular significance, HIF3α stabilisation was seen in fibroblasts from healthy donors only, with increases in both mRNA and protein expression indicative of a growing regulatory feedback mechanism in response to the prolonged hypoxic conditions. Contrastingly, there was an apparent loss of HIF3α protein in fibroblasts from IPF donors following exposure to hypoxia, and higher baseline *HIF3α* mRNA expression in normoxia

than in healthy fibroblasts. These results could suggest an increase in HIF3α turnover, possibly in response to excessive conditions of HIF pathway activation.

4.3.3 Effects of hypoxia on collagen cross-linking enzyme induction in lung fibroblasts from healthy and IPF donors

A comparative analysis of collagen I and collagen cross-linking enzyme induction was subsequently performed in lung fibroblasts from healthy and IPF donors exposed to hypoxia for 0, 24 or 48 hours.

Both healthy and IPF lung fibroblasts exhibited increased *PLOD2* expression after exposure to 1% O_2 **(Figure 4.8 A)**. Although there was some heterogeneity between donors, mean expression levels were similar between 24 hour and 48 hour hypoxia exposure. Surprisingly, *LOXL2* expression was increased in healthy lung fibroblasts exposed to hypoxia, but not in IPF fibroblasts **(Figure 4.8 B)**. Notably, levels of *LOXL2* expression appeared higher in IPF compared to healthy fibroblasts at baseline (ambient air), and the overall expression levels of LOXL2 in IPF fibroblasts were elevated to a similar threshold seen in healthy fibroblasts exposed to hypoxia, suggesting a blunted hypoxic response in *LOXL2* induction due to higher baseline expression levels. LOXL3 expression appeared unaffected by hypoxia in lung fibroblasts from either healthy or IPF donors **(Figure 4.8 C).** Notably, a small but significant increase in collagen I gene induction was seen with healthy fibroblasts to hypoxia for 24 or 48 hours, while no detectable change was observed in IPF fibroblasts **(Figure 4.8 D).**

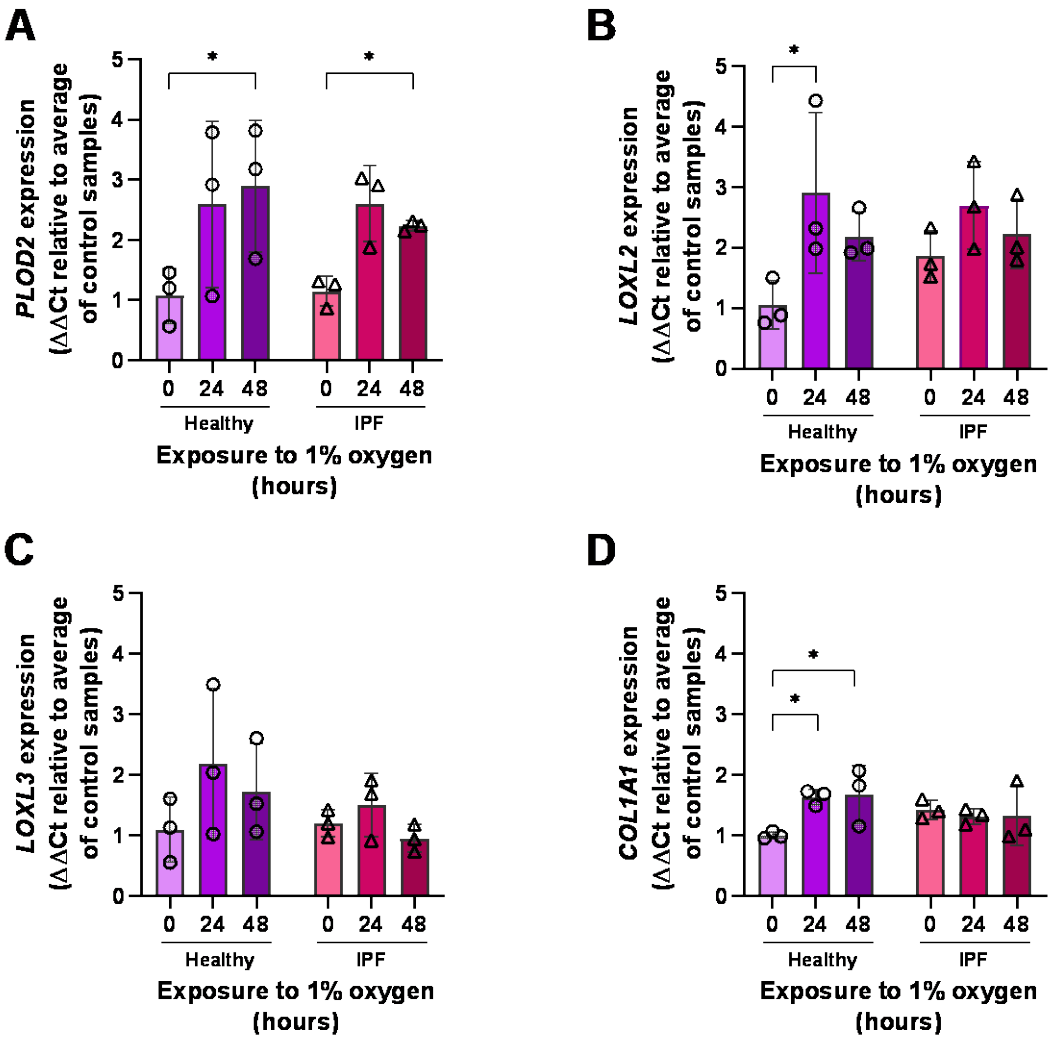

Figure 4.8: A blunted response to hypoxia is seen on collagen cross-linking enzyme induction in IPF fibroblasts. mRNA expression of **(A)** *PLOD2,* **(B)** *LOXL2,* **(C)** *LOXL3* and **(D)** *COL1A1* in healthy and IPF primary fibroblasts exposed to 1% O_2 for 0, 24 or 48 hours. mRNA expression levels were determined using the ΔΔ CT method with grouped analysis and multiple comparisons (Dunnett's test). * $p< 0.05$, ** $p < 0.01$, *** $p < 0.001$, N=3 healthy and 3 IPF donors, with experiments performed in duplicate.

Western blotting was performed to determine protein expression of the key 'bone-type' collagen cross-linking genes PLOD2 and LOXL2 **(Figure 4.9)**. PLOD2 expression gradually increased in fibroblasts from healthy donors exposed to hypoxia, however this effect was not seen in fibroblasts from IPF donors **(Figure 4.9 A, B)**. Similarly, increases in LOXL2 expression were demonstrated in both healthy and IPF lung fibroblasts exposed to hypoxia however the magnitude of increase from baseline was much lower in fibroblasts from IPF donors **(Figure 4.9 A, C)**. Of interest, both PLOD2 and LOXL2 expression were relatively increased in IPF fibroblasts compared to healthy fibroblasts in baseline normoxic conditions (although not statistically

significant), which could explain the reduced response to hypoxia compared to fibroblasts from healthy donors **(Figure 4.9 A-C)**.

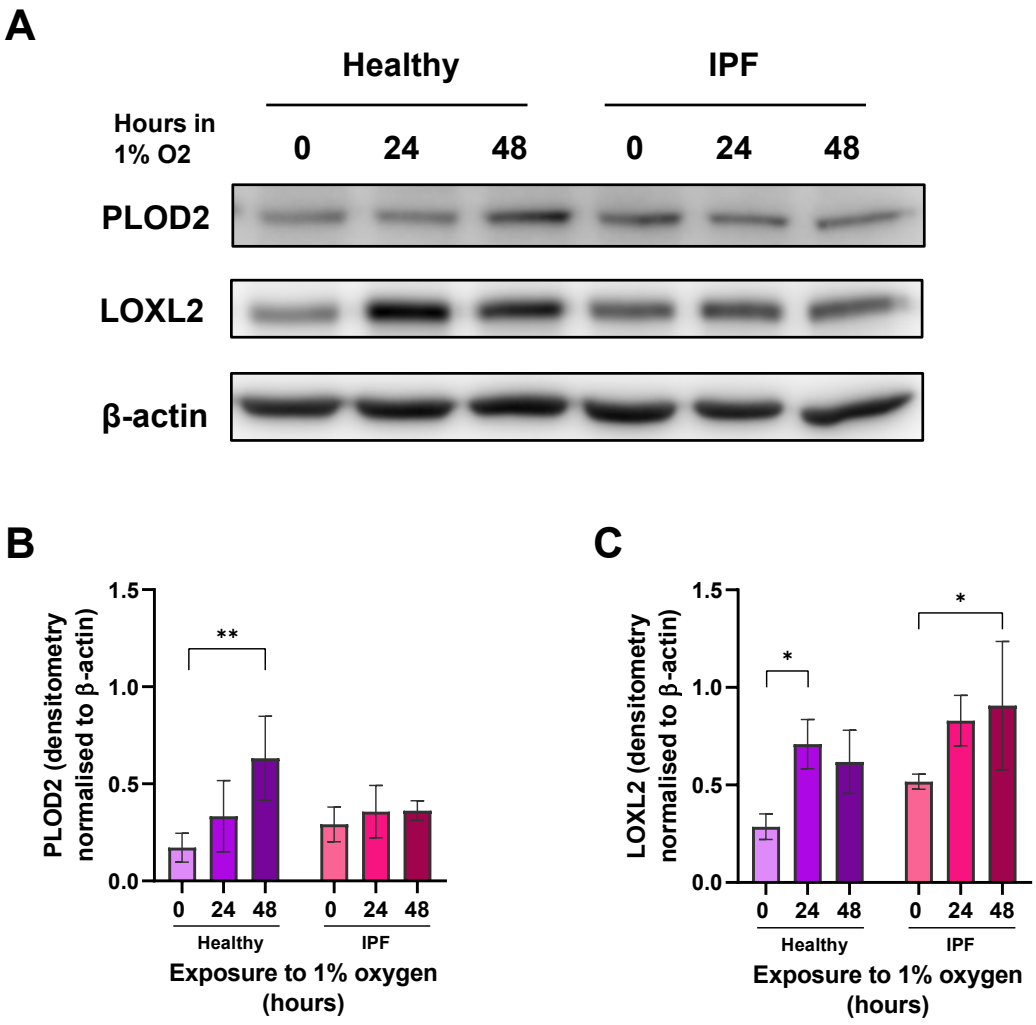

Figure 4.9: Blunted effects of hypoxia on collagen cross-linking enzymes in IPF fibroblasts could be due to higher baseline levels compared to healthy fibroblasts in normoxia.

Western blotting for PLOD2 and LOXL2 in early passage IPF primary lung fibroblasts exposed to 0, 24 or 48 hours of hypoxia. **(A)** Blot representative of 3 separate healthy and IPF donors. Densitometry analysis of western blots from 3 separate healthy and IPF donors exposed to hypoxia for 0, 24 or 48 hours demonstrating protein expression of **(B)** PLOD2 and **(C)** LOXL2 normalised to β–actin. Grouped analysis and multiple comparisons (Dunnett's test). * $p< 0.05$, ** $p < 0.01$, N=3 healthy and 3 IPF donors, with experiments performed in duplicate.

4.3.4 Effects of hypoxia on HIF pathway activation in primary alveolar epithelial cells

Results from this study have thus far established collagen cross-linking enzyme induction to be highest in mesenchymal cells near the alveolar epithelial edge of the IPF fibroblastic foci, and that markers of HIF pathway activation are present in both these mesenchymal cells and in the neighbouring alveolar epithelial cells. The HIF response within primary alveolar epithelial cells exposed to hypoxia is therefore of interest. Primary alveolar epithelial cells were thawed and cultured on collagen-coated wells prior to exposure to 1% O_2 for 0, 24 or 48 hours. Similarly to the previous experiment with fibroblasts, the plating and lysis of the alveolar epithelial cells in different conditional treatments was kept the same, while exposure to hypoxia was staggered depending on the length of treatment for each condition. Gene expression at the mRNA level was analysed using real time qPCR, and at the protein level with western blotting.

Primary alveolar epithelial cells exposed to hypoxia demonstrated marked increases in *Ca9* expression, with one donor line exhibiting much greater changes in expression than the 2 other donor samples **(Figure 4.10 A)**. The alveolar epithelial cells also exhibited significant reduction in *HIF1α* and *HIF2α* mRNA expression consistent with a negative feedback loop from stabilisation and accumulation of HIFα protein **(Figure 4.10 B-C)**. Concordant with the pattern seen in lung fibroblasts, expression of *HIF3α* was increased in alveolar epithelial cells exposed to hypoxia, although there was substantial variation in the degree of upregulation **(Figure 4.10 D)**.

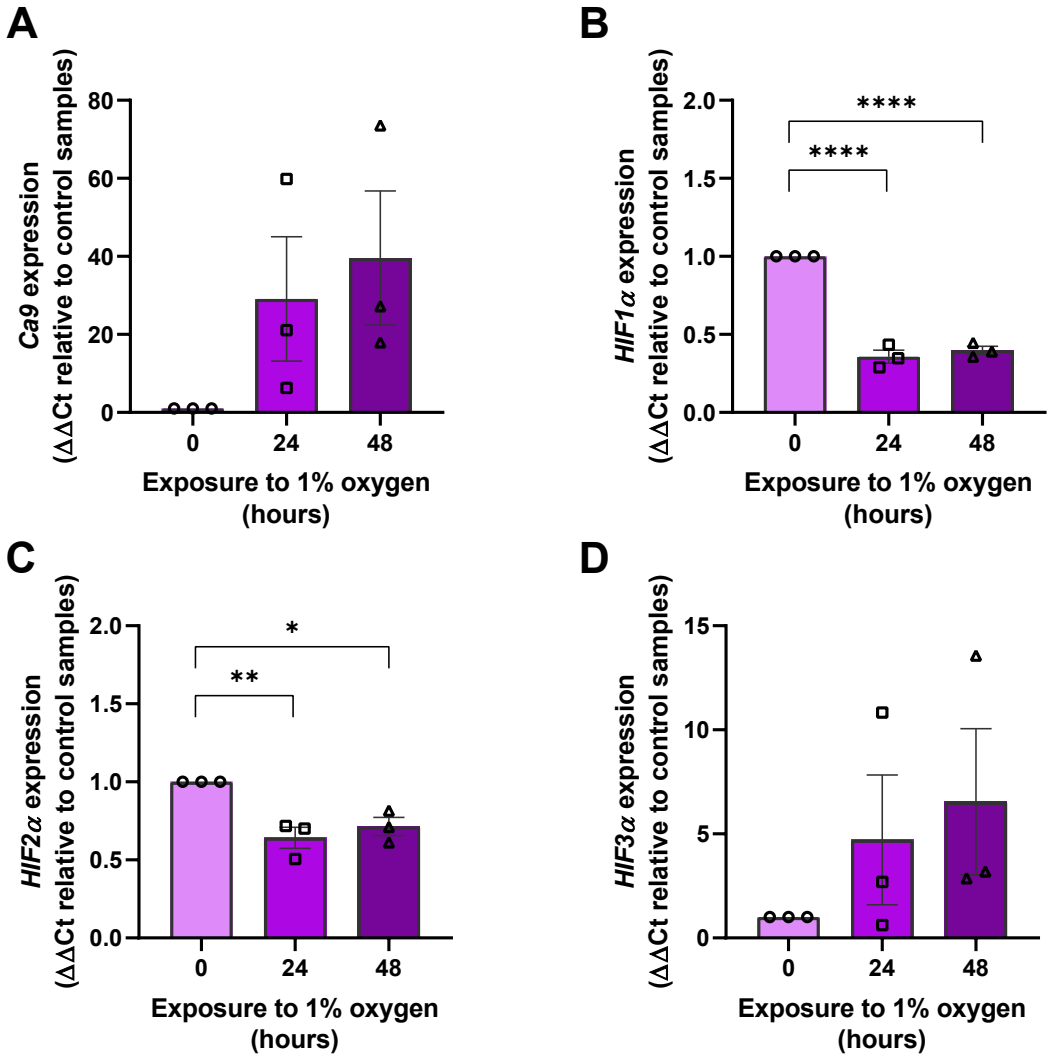

Figure 4.10: Primary alveolar epithelial cells demonstrate similar *HIFα* expression patterns to healthy lung fibroblasts. mRNA expression of **(A)** *Cα9*, **(B)** *HIF1α*, **(C)** *HIF2α*, and **(D)** *HIF3α* in healthy alveolar epithelial cells exposed to 1% O_2 for 0, 24 or 48 hours. mRNA expression levels were determined using the ΔΔ CT method with grouped analysis and multiple comparisons (Dunnett's test). * p< 0.05, ** p < 0.01, N=3 healthy donors, with experiments performed in duplicate.

4.3.5 Effects of hypoxia on collagen cross-linking enzymes in primary alveolar epithelial cells

The expression of collagen cross-linking enzymes in the primary alveolar epithelial cells were subsequently examined. Primary healthy alveolar epithelial cells exposed to hypoxia for 24 or 48 hours demonstrated increased mRNA expression of *PLOD2* **(Figure 4.11 A)**, with high concordance between individual donors. In contrast, the expression of *LOX* and *LOXL2* **(Figure 4.11 B-C)** was

generally increased in primary alveolar epithelial cells exposed to hypoxia however with significant heterogeneity in the magnitude of response between donors, leading to a statistically non-significant effect overall. Similar to patterns seen in both healthy and IPF fibroblasts, the expression of *LOXL3* in primary alveolar epithelial cells did not appear to be affected by hypoxia **(Figure 4.11 D)**.

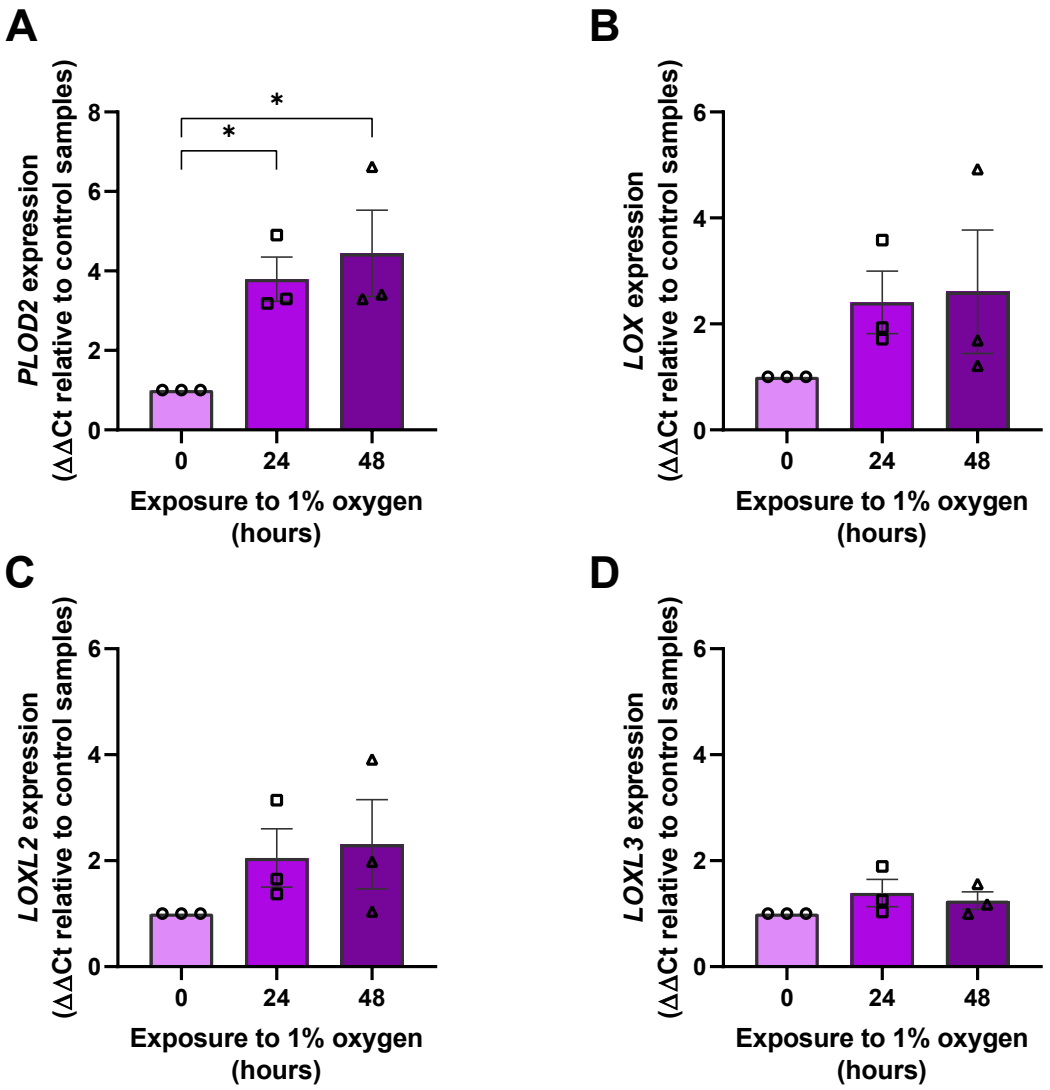

Figure 4.11: Hypoxic expression of PLOD2 and LOX(L) enzymes in primary alveolar epithelial cells. mRNA expression of **(A)** *PLOD2,* **(B)** *LOX,* **(C)** *LOXL2* and **(D)** *LOXL3* in healthy alveolar type 2 epithelial cells exposed to 1% O_2 for 0, 24 or 48 hours. mRNA expression levels were determined using the ΔΔ CT method with grouped analysis and multiple comparisons (Dunnett's test). ** p< 0.01, *** p < 0.001, N=3 healthy donors, with experiments performed in duplicate.

Western blotting was performed on protein lysate from the alveolar epithelial cells **(Figure 4.12)**. One of the three donors demonstrated increases in both LOXL2 and PLOD2 expression, while another demonstrated PLOD2 upregulation only. The final donor did not demonstrate any detectable PLOD2 or LOXL2 expression at 0, 24 or 48 hours despite the presence of β-actin in the cell lysate, suggesting the response to hypoxia of collagen cross-linking induction in alveolar epithelial cells is variable and donor dependent.

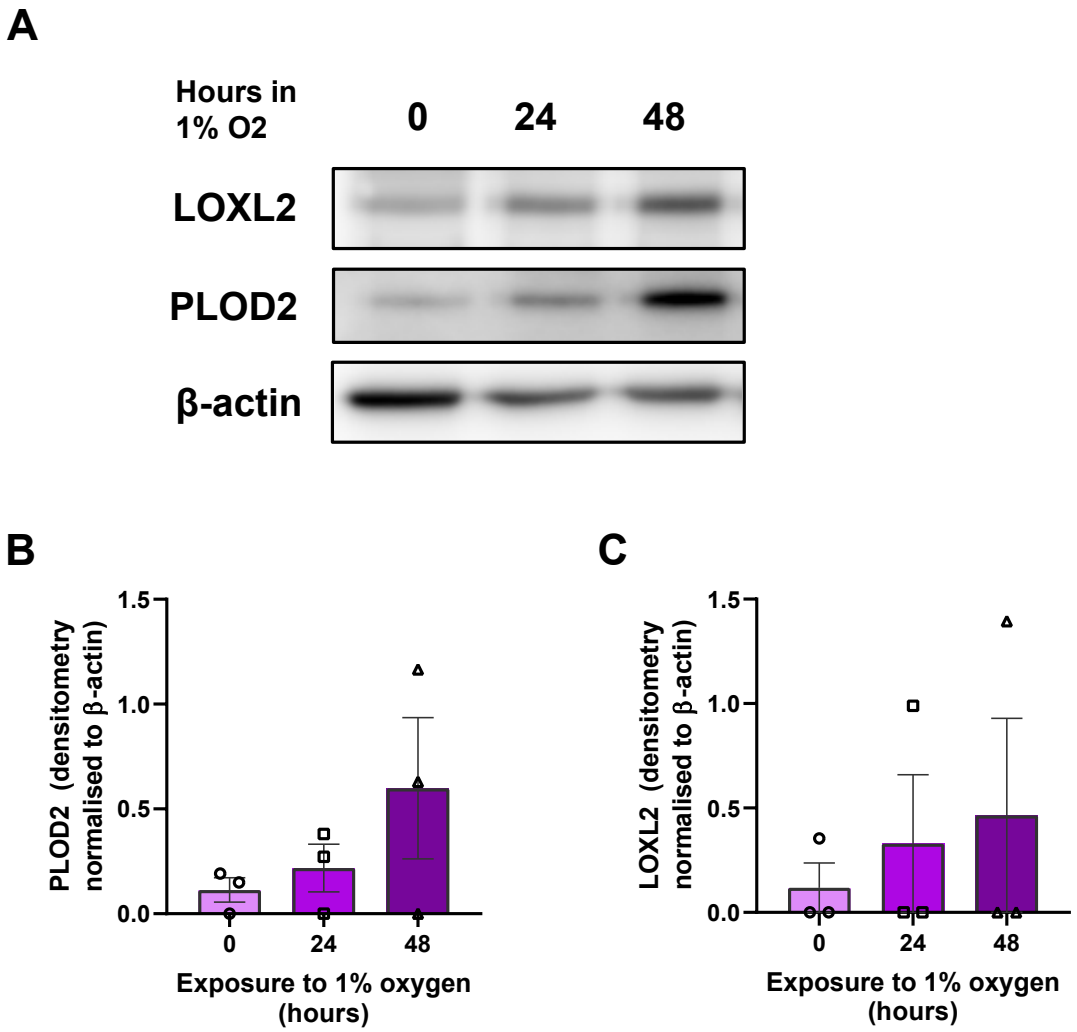

Figure 4.12: Collagen cross-linking induction in primary alveolar epithelial cells exposed to normoxia or hypoxia was highly variable between donors (A) Western blotting for LOXL2 and PLOD2 in healthy primary AT2 cells exposed to 0, 24 or 48 hours of hypoxia. Densitometry analysis demonstrates cellular expression for **(B)** PLOD2 in 2 out of 3 donors and for **(C)** LOXL2 in 1 out of 2 donors. β-actin was used as a loading control. N=3 healthy donors, with experiments performed in duplicate.

Similarly, the induction of collagen gene expression was variable between primary alveolar epithelial cell donors, with minimal changes in *COL1A1* and *COL3A1* expression in 2 donors and moderate induction in 1 donor **(Figure 4.13 A)**.

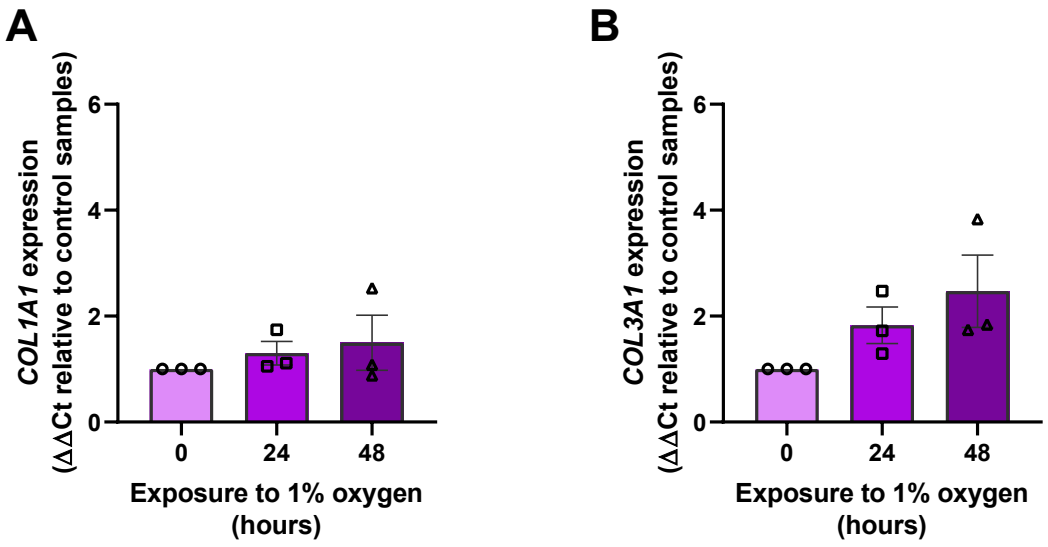

Figure 4.13: Primary alveolar epithelial cells exposed to hypoxia do not demonstrate significant changes in collagen expression. mRNA expression of **(A)** *COL1A1* and **(B)** *COL3A1* in healthy alveolar type 2 epithelial cells exposed to 1% O_2 for 0, 24 or 48 hours. mRNA expression levels were determined using the ΔΔ CT method with grouped analysis and multiple comparisons (Dunnett's test). N=3 healthy and 3 IPF donors.

Taken together, significant donor variability was observed in primary alveolar epithelial cell responses to hypoxia, although in general it appears that a low oxygen environment is capable of promoting HIF pathway activation within alveolar epithelial cells as well as collagen cross-linking enzyme induction.

4.4 Discussion

HIF pathway activation has previously been demonstrated in IPF tissue, most prominently in areas of active fibrosis within hyperplastic alveolar epithelium and myofibroblasts[153,247]. Here these findings were confirmed using immunohistochemical analysis, and the expression patterns of HIF pathway markers were compared to collagen cross-linking induction. Both the fibroblastic foci and the overlying hyperplastic alveolar epithelium strongly expressed HIF1α and Ca9, and this was associated with areas of increased *PLOD2* and *LOXL2* mRNA expression on adjacent sections.

On closer examination the individual cells which co-expressed *PLOD2* and *LOXL2* also stained positive for HIF1α, and the greatest expression of both HIF and collagen cross-linking enzymes were located within or adjacent to the alveolar epithelial barrier overlying IPF fibroblastic foci. While this association should not be mistaken for a correlation, it leads to an intriguing hypothesis that HIF pathway activation at the alveolar epithelium may be a key regulatory driver of the increased *PLOD2* and *LOXL2* activity observed in IPF fibroblastic foci. Consistent with our current understanding of IPF pathogenesis, it is possible that stimuli at the alveolar surface (recurrent alveolar micro-injuries) or predisposing traits within the alveolar cells themselves (pathogenetic abnormalities) promote the stabilisation of HIF in an immediate regional distribution. HIF pathway activation could be a key contributor to alveolar epithelial dysfunction and apoptosis in IPF[154]. Furthermore, HIF activation at the alveolar epithelium may be responsible for mesenchymal cell recruitment, proliferation and activity, leading to the conglomeration of matrix-producing cells and formation of a fibroblastic focus[153,218,246]. Finally, results from this study suggest HIF pathways could induce the activity of key collagen cross-linking enzymes within both AT2 and mesenchymal cells, although the biomechanical effects of this induction remain to be seen.

Hypoxia was chosen in this study as a physiologically-relevant mechanism to stabilise HIF, and other studies investigating HIF pathways in IPF have also used hypoxia[153,154,218,246]. While hypoxia and HIF pathways are sometimes (mistakenly) considered synonymous, hypoxia has a broader effect on cell behaviour, such as changes to alveolar epithelial metabolic and ion-transport functions[252]. The degree of hypoxia is also important, and while there is no accepted definition for a 'hypoxic threshold', a PO_2 of 8-10mmHg (1% O_2 at sea level) has been observed to cause maladaptive effects in tissue and tumours, and is commonly used for *in vitro* experiments[253]. Notably, cellular behaviour can change with different levels of hypoxia. For example lung fibroblast proliferation may be increased with 2% O_2 yet reduced with 0.1% O_2[254]. HIF stabilisation is also likely to be affected by the absolute O_2 concentration, with PHD inhibition more susceptible to relatively 'milder' hypoxic conditions while FIH suppression requiring more extreme

degrees of hypoxia[255]. It is thus imperative to recognise these limitations when working with hypoxia to investigate the effects of HIF pathway activation.

Markers of HIF pathway activation were found within mesenchymal cells of the IPF fibroblastic foci as well as the overlying alveolar epithelium. This pattern of expression could be considered unusual if hypoxia was the underlying trigger, with a hypoxic gradient expected to occur in regions distant to the alveolar surface. Furthermore, if hypoxia were to incite HIF-mediated collagen cross-linking enzyme induction, it might be anticipated that expression of enzymes such as PLOD2 and LOXL2 would be highest within the fibrotic foci core, rather than along the alveolar edge. These patterns point toward possible other sources of HIF stabilisation, which arise specifically from the alveolar epithelium. Indeed if HIF pathway activation is likely to have a role in the early IPF disease process then it would be counter-intuitive to assume this occurs through hypoxia alone, as cellular O_2 tension in epithelial cells and fibroblasts are unlikely to be significantly altered in early disease when remodelling of lung architecture and subsequent respiratory failure is yet to take place.

Hypoxia is not the only modulator of HIF-PHD activity (and thus HIF expression). While the precise mechanisms remain controversial, oxidative stress from mitochondrial reactive oxygen species (ROS) such as hydrogen peroxide, nitric oxide and glucose oxidase are capable of promoting HIF expression through inhibitory effects on HIF hydroxylases[256]. PHD activity is also affected by iron, ascorbate and metabolic intermediates of cellular adenosine triphosphate production such as fumarate, succinate, lactate and pyruvate[150,257-259]. Although this hypothesis remains to be explored oxidative stress is recognised to occur with recurrent epithelial micro-injury and could stabilise HIF1α under normoxic conditions, thereby accounting for HIF dysregulation in early disease[256]. Nonetheless, as a key environmental condition for which HIF pathway regulation exists, hypoxia serves as a useful tool for the analysis of cell-specific HIF responses.

Differences in the hypoxia-HIF response of lung fibroblasts from healthy and IPF donors were observed in this study. In particular, a divergence in HIF3α stability was seen, with accumulation in healthy fibroblasts but a decline in IPF fibroblasts. This was despite enhanced baseline levels of *HIF3α* mRNA expression in IPF fibroblasts, suggesting the difference was due to either impaired translation or increased turnover of HIF3α in IPF fibroblasts. The cause of these differences is unclear, however the effect is likely to be maladaptive, with HIF3α thought to regulate the transcriptional effects of HIF1α and HIF2α by competitively binding HIFβ[260]. The HIF3α/β complex has relatively few transcriptional effects compared to HIF1α and 2α-mediated pathways, yet it possesses a similar ODDD (albeit with only one proline residue as opposed to 2 residues in both

HIF1α and 2α)[261]. A loss of HIF3α stabilisation in hypoxia could conceivably leave cellular activities vulnerable to excessive HIF1α and HIF2α-mediated transcriptional effects.

These findings correlate with the results of another group that have recently identified HIF3α expression to be reduced in IPF fibroblasts compared to healthy lung fibroblasts in normoxia[218]. While they did not assess the response to hypoxia over time, they also found baseline HIF1α and HIF2α expression to be increased in IPF compared to healthy lung fibroblasts. That finding could not be reproduced in this study, possibly due to differences in sample size and cellular processing prior to culture, however their findings raise an important question regarding baseline levels of HIF expression in IPF lung cells (irrespective to hypoxic conditions). Intrinsically greater levels of HIF pathway activation, either through enhanced HIF1/2α stability or loss of HIF3α regulation (or both), could sustain excessive collagen cross-linking activity regardless of environmental oxygen levels. Such an effect may explain the blunted response of hypoxia on the *in vitro* IPF fibroblast induction of collagen cross-linking enzymes in this study.

The extension of *in vitro* hypoxia experiments to primary AT2 cells was intended to provide insights into the behaviour of an alveolar epithelial barrier under hypoxic stress, with particular attention to the HIF response on matrix remodelling through collagen cross-linking enzymes. Primary AT2 cells are extremely challenging to work with as they are highly sensitive to environmental stimuli and quickly undergo senescence[262]. These difficulties were compounded by the inability to monitor AT2 cell health and behaviour microscopically while in hypoxic culture. In each donor induction of CA9 was identified and so plausibly the variation in PLOD2 and LOXL2 expression identified between donors could reflect donor specific differences in the response of AT2 cells to hypoxia or the transition towards a mesenchymal cell phenotype during cell culture. The low number of donors in this experiment limits further interpretation and repeat experiments with an expanded donor cohort would provide further insight.

4.5 Conclusion

In summary, markers of HIF pathway activation within IPF tissue were identified, and co-localised with collagen cross-linking enzyme induction at the 'leading edge' of the fibroblastic focus. A mechanism for HIF-induced dysregulation of collagen cross-linking enzyme induction through hypoxia was confirmed *in vitro*, with key differences in both the HIF response and collagen cross-linking enzyme induction to hypoxia in lung fibroblasts from healthy and IPF donors. While these results support an emerging relationship between HIF pathway activation and dysregulated

activity of collagen cross-linking enzymes, the downstream biomechanical effects of these changes on collagen fibril structure and function remain unknown.

Chapter 5 Functional Effects of HIF Pathway Mediated Collagen Cross-linking Enzyme Dysregulation

5.1 Introduction

The premise for this study was based on the key finding that matrix stiffness in IPF lung correlates not with collagen quantity but with the density of mature trivalent pyridinoline cross-links, which are the product of *PLOD2*-mediated hydroxylation of lysine residues at the collagen telopeptide, followed by *LOX(L)*-mediated oxidative deamination of these precursors[165]. TGFβ1 signalling has conventionally been viewed as the critical driver of aberrant matrix changes in IPF, including upregulation of these 'bone-type' collagen cross-links[126,138,140,141,217].

However this study has identified HIF stabilisation as an alternative and potentially more potent mediator of these enzymes, and confirmed HIF pathway activation in IPF tissue at corresponding sites to active collagen cross-linking. Given both TGFβ and HIF pathways may have relevance to ECM remodelling in IPF, a closer analysis of their individual and combined effects on collagen gene induction and cross-linking enzyme activity in IPF lung fibroblasts is warranted.

While TGFβ-mediated biomechanical effects on ECM have been well documented, the downstream effects of HIF-mediated promotion of collagen cross-linking enzymes on tissue stiffness remain controversial, with some studies suggesting increases in stiffness while others demonstrating a reduction[248-250]. In addition to this, the effects of these HIF pathways on the mechanical properties of matrix have never been considered in the remit of pulmonary fibrosis, where such changes can have profound effects on both respiratory physiology and fibrotic progression.

It is therefore critical to determine the effects of HIF pathway-mediated dysregulation of collagen cross-linking enzymes on collagen nano-architecture and matrix compliance as might be seen within the IPF lung, to further our understanding on the biomechanical effects of these changes.

5.2 Objectives

The objectives of this study were to:

i) To investigate the effects of HIF pathway activation with and without TGFβ signalling on the expression of collagen cross-linking enzyme and collagen fibrillogenesis genes in primary IPF lung fibroblasts.

ii) To explore the downstream effects of HIF pathway activation on collagen fibrillogenesis, tissue stiffness and collagen nano-architecture using an *in vitro* 3D fibroblastic foci model.

5.3 Results

5.3.1 Effects of HIF stabilisation through pan-prolyl hydroxylase inhibition with and without TGFβ signalling on collagen cross-linking enzyme induction in IPF lung fibroblasts

Using the pan-prolyl hydroxylase inhibitor DMOG, the downstream effects of HIF pathway activation on the expression of collagen fibrillogenesis and collagen cross-linking enzyme expression in IPF fibroblasts were examined. Primary lung fibroblasts from 3 IPF donors were exposed to either vehicle control (DMSO 1%), DMOG 1mM, TGFβ1 10ng/mL or both DMOG 1mM + TGFβ1 10ng/mL for 48 hours before harvesting for mRNA and protein.

Expression of collagen cross-linking enzymes was examined using RTqPCR **(Figure 5.1)**. *PLOD2* was only modestly and non-significantly increased with TGFβ exposure yet markedly elevated with DMOG-mediated HIF stabilisation **(Figure 5.1 A)**. Furthermore the combination of TGFβ1 signalling and HIF stabilisation had a synergistic effect on *PLOD2* expression that was greater than the sum of individual signalling pathways.

Mean *LOX* expression was equally increased with exposure to TGFβ1 or DMOG while combination exposures demonstrated an additive effect **(Figure 5.1 B)**. *LOXL2* expression was more prominently expressed with DMOG exposure than with TGFβ1, and similarly to *LOX* expression the combination DMOG + TGFβ1 conditions had an additive effect on *LOXL2* upregulation **(Figure 5.1 C)**. By contrast *LOXL3* upregulation appeared greater with TGFβ1 exposure compared to HIF pathway induction through DMOG, yet the effect of combination treatment also appeared additive **(Figure 5.1 D)**.

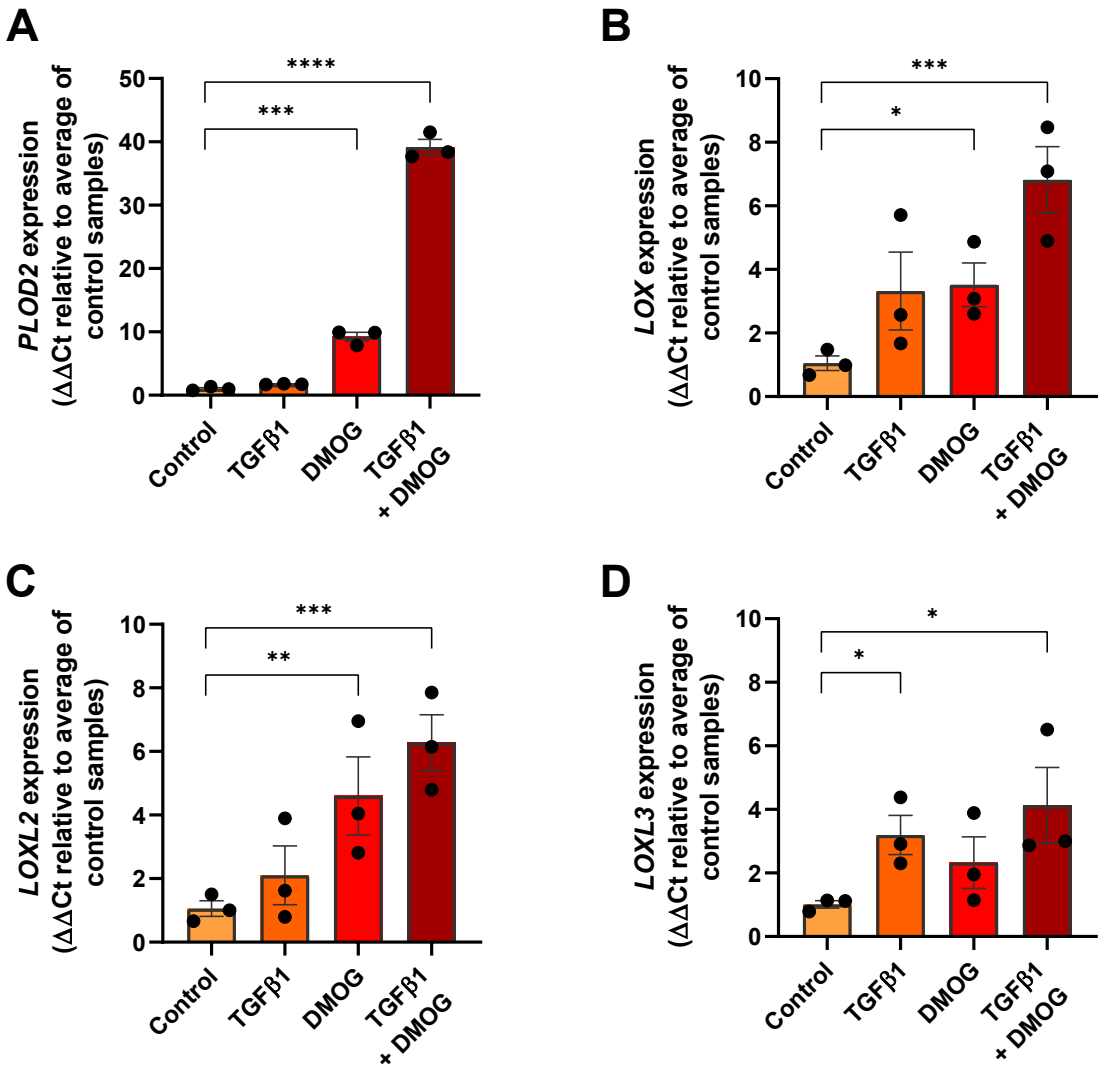

Figure 5.1: Combined TGFβ1 and HIF signalling have synergistic effects on *PLOD2* expression and additive effects on *LOX(L)* expression in IPF fibroblasts. mRNA expression of **(A)** *PLOD2,* **(B)** *LOX,* **(C)** *LOXL2* and **(D)** *LOXL3* in IPF fibroblasts exposed to TGFβ1 10ng/mL, DMOG 1mM or both for 48 hours. mRNA expression levels were determined using the ΔΔ CT method with grouped analysis and multiple comparisons (Dunnett's test). * p< 0.05, ** p < 0.01, *** p < 0.001, **** p < 0.0001. N=3 IPF donors, with experiments performed in duplicate.

To determine the individual and combined effects of TGFβ and HIF signalling on collagen fibrillogenesis, mRNA expression of *COL1A1* and *COL3A1* was also assessed **(Figure 5.2)**. Both *COL1A1* **(Figure 5.2 A)** and *COL3A1* **(Figure 5.2 B)** expression was significantly increased with TGFβ1 alone. HIF pathway activation through DMOG however appeared to have no effect on *COL1*A1 or *COL3A1* expression. Furthermore the addition of DMOG appeared to dampen the TGFβ1 effect on promoting collagen gene upregulation **(Figure 5.2 A-B)**.

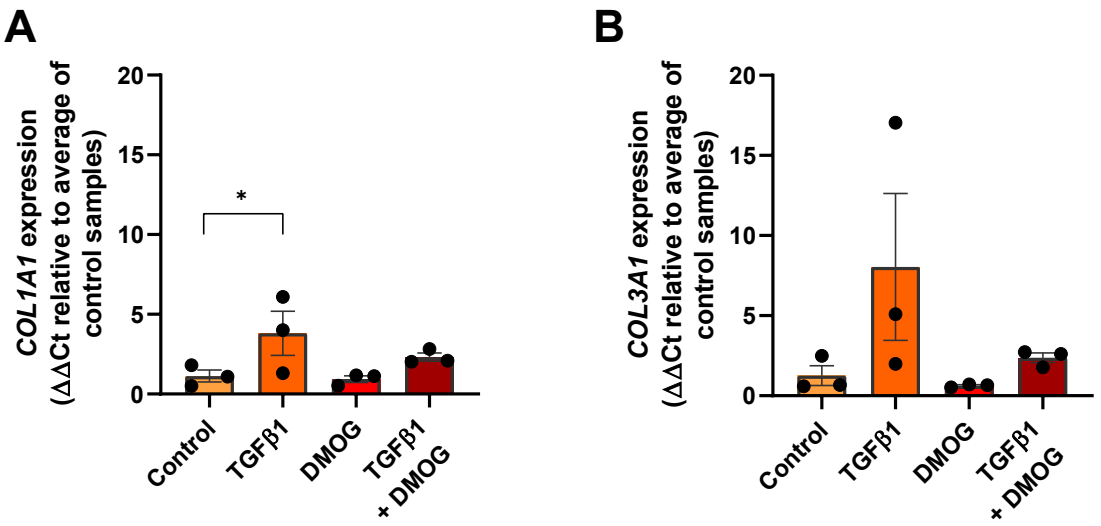

Figure 5.2: TGFβ1 signalling but not HIF stabilisation induces the expression of key interstitial collagen genes. mRNA expression of **(A)** *COL1A1* and **(B)** *COL3A1* in IPF fibroblasts exposed to exposed to TGFβ1 10ng/mL, DMOG 1mM or both for 48 hours. mRNA expression levels were determined using the ΔΔ CT method with grouped analysis and multiple comparisons (Dunnett's test). * $p < 0.05$. N=3 IPF donors, with experiments performed in duplicate.

Considering these findings together, the effects of HIF stabilisation on IPF fibroblasts were similar to that seen in healthy lung fibroblasts in earlier experiments, with a greater effect than TGFβ1 in promoting *PLOD2* and *LOXL2* mRNA expression. Additionally synergism between HIF stabilisation and TGFβ1 signalling was observed to augment *PLOD2* expression to greater levels than the additive effects of either pathway alone. By comparison the effect of combined HIF and TGFβ1 signalling on LOX(L) enzyme expression was no greater than the sum of each individual pathway alone.

Notably TGFβ1 signalling but not HIF pathway activation upregulated expression of key interstitial collagen genes *COL1A1* and *COL3A1*, implying that HIF pathways and TGFβ1 pathways may have different influences on collagen biosynthesis within lung fibroblast ECM.

To better understand the differences in effects on collagen fibrillogenesis of HIF and TGFβ1 the normalised Cycle threshold (Ct) values were analysed from key collagen cross-linking enzymes *PLOD2* and *LOXL2*, and divided them by the normalised Ct values of the *COL1A1* and *COL3A1* expression, giving an indication of the proportion of collagen cross-linking enzyme expression relative to collagen fibrillogenesis expression for each treatment condition **(Figure 5.3)**.

Using this ratio, TGFβ1 signalling did not appear to influence the proportionate expression of collagen cross-linking enzymes to collagen fibrillogenesis genes. Specifically, *PLOD2* to *COL1A1* **(Figure 5.3 A)**, *PLOD2* to *COL3A1* **(Figure 5.3 B)**, *LOXL2* to *COL1A1* **(Figure 5.3 C)** and *LOXL2* to *COL3A1* **(Figure 5.3 D)** ratios in TGFβ1 conditions were unchanged compared to control.

By comparison HIF stabilisation with DMOG was identified to significantly disrupt proportionate expression of collagen cross-linking enzymes relative to interstitial collagen genes. Mean ratios of *PLOD2* expression to collagen fibrillogenesis were elevated to 10 times that of control **(Figure 5.3 A-B)**, while ratios of *LOXL2* to collagen gene was elevated to greater than 5 times control ratios **(Figure 5.3 C-D)**. The combined HIF and TGFβ1 treatment produced different effects on the *PLOD2-COL1A1/3A1* ratios compared to the *LOXL2-COL1A1/3A1* ratios. Combined TGFβ1 and HIF signalling elicited an enhanced disruption of PLOD2 to collagen expression ratios compared to HIF stabilisation alone **(Figure 5.3 A-B)**. Contrastingly, the addition of TGFβ1 signalling to HIF pathway activation reduced the disruption of the *LOXL2-COL1A1* and *LOXL2-COL3A1* ratios compared to HIF stabilisation alone **(Figure 5.3 C-D)**.

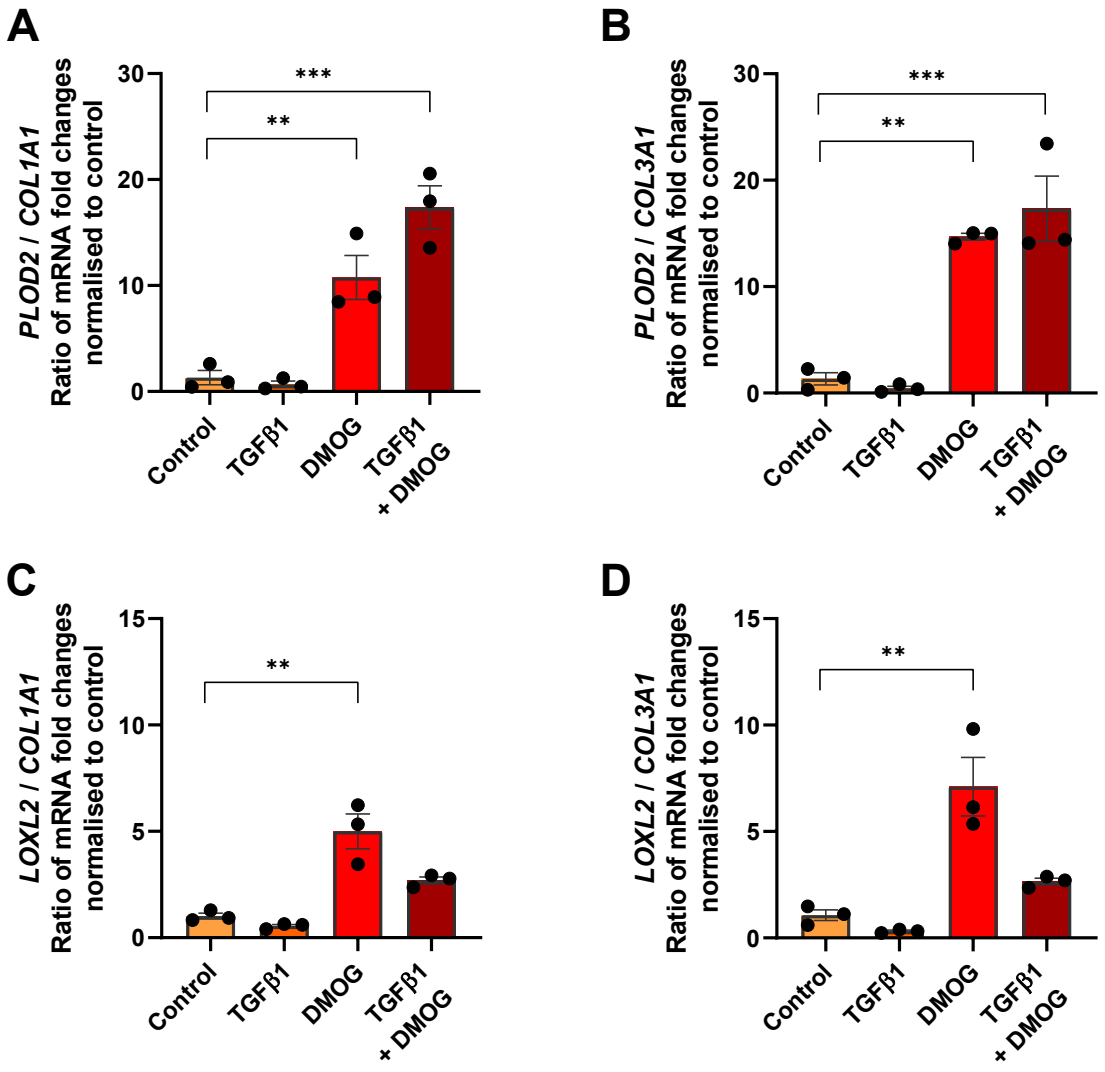

Figure 5.3: Proportionate expression of cross-linking enzymes to interstitial collagen genes is significantly disrupted by HIF pathways. Ratios of normalised mRNA expression of **(A-B)** *PLOD2* and **(C-D)** *LOXL2* divided by *COL1A1* and *COL3A1* in IPF fibroblasts exposed to DMOG 1mM, TGFβ1 10ng/mL or both. mRNA expression levels were determined using the ΔΔ CT method with grouped analysis and multiple comparisons (Dunnett's test). ** $p < 0.01$, *** $p < 0.001$. N=3 IPF donors, with experiments performed in duplicate.

While the gene expression patterns are not the most accurate method for assessing the degree of collagen fibrillogenesis and cross-linking activity occurring in lung fibroblast ECM, these results suggest HIF stabilisation through DMOG promotes collagen cross-linking enzymes without necessarily increasing collagen fibrillogenesis, which may lead to excessive modification of pre-existing collagen molecules with a higher density of mature pyridinoline cross-links. Contrastingly TGFβ1 appears to upregulate expression of collagen fibrillogenesis genes in a proportionate manner to the level of collagen cross-linking enzymes induction. Of particular interest, the

combined TGFβ1 and HIF signalling treatment profoundly increased the proportion of *PLOD2* expression to collagen fibrillogenesis, but was less effective at disrupting the ratios of LOX(L) enzymes to collagen genes than HIF pathways alone.

5.3.2 Testing HIF stabilisation through pan-prolyl hydroxylase inhibition in a 3D fibroblastic focus model

These results provided sufficient evidence to proceed with a long-term culture 3D fibroblastic focus model in order to investigate the functional effects of HIF pathways on lung fibroblast ECM. This model uses fibroblasts from IPF donors grown on transwells in optimised culture media. Media is replaced 3 times per week and contains necessary components for ECM production including freshly prepared ascorbic acid. After a week of culture, TGFβ1 is added to induce homogenous contraction of the fibroblast sheet, forming spheroids of lung fibroblasts within ECM that mimics fibroblastic foci. To promote maturation of collagen fibrils the fibroblastic foci models are cultured for 5 weeks in conditions (6 weeks total).

Initial pilot studies were performed over 2 weeks in order to optimise the dose and investigate the influence of DMOG on the 3D model. After 1 week of culture in 3D model media, the lung fibroblast sheets were treated with vehicle alone, with 3 different doses of DMOG alone or with TGFβ1 added to each of these 4 conditions (8 conditions in total) and samples were harvested after 1 week under these conditions.

Transwells were observed for macroscopic changes during this time **(Figure 5.4)**. Conditions without TGFβ1 did not contract and simply grew as opalescent sheets at the base of the transwell, whereas TGFβ1-containing conditions contracted into spheroids. DMOG had no appreciable effect on the appearance of the sheets in the absence of TGFβ1 or the shape or size of the spheroids in the presence of TGFβ1.

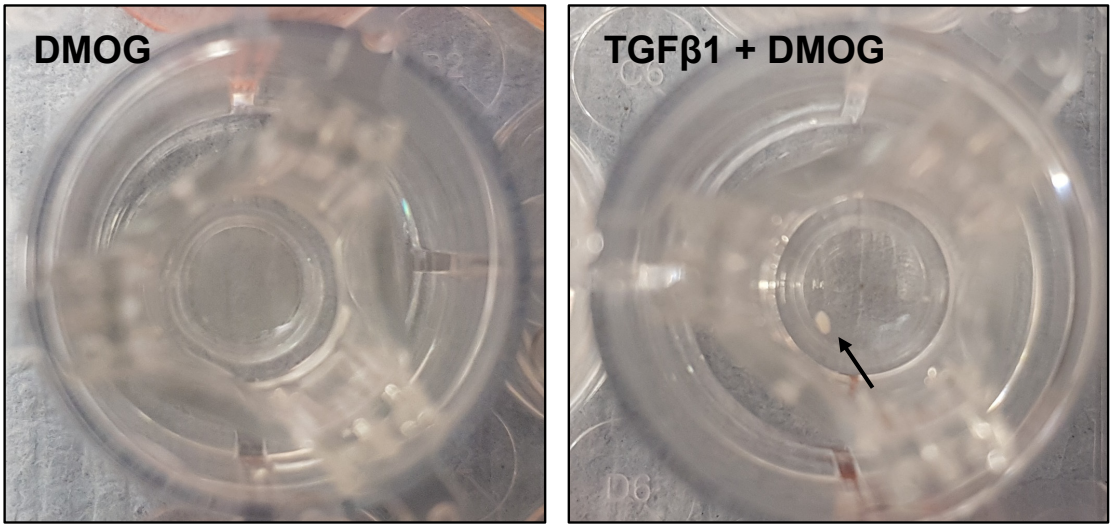

Figure 5.4: TGFβ1 is still required to stimulate fibroblast ECM clumping to form spheroids in samples exposed to pan-prolyl hydroxylase inhibition. 24-well transwells with IPF fibroblasts in apical compartment cultured for 7 days before being exposed to DMOG alone or DMOG plus TGFβ1 for 72 hours. Black arrow indicates fibroblast spheroid formed from ECM clumping.

After 2 weeks of culture, the cell sheets or spheroids were harvested for protein using a combination of mechanical and enzymatic lysis. Protein was quantified and western blot performed using 10ug of cell lysate per condition **(Figure 5.5)**. In treatment conditions without TGFβ1 a dose-dependent stabilisation of HIF1α protein was observed with DMOG. Similarly, in treatment conditions containing TGFβ1 there was a dose-dependent effect although only the higher doses of DMOG (0.5mM and 1mM) were capable of inducing appreciable levels of HIF stabilisation. LOXL2 expression was increased by TGFβ1 except in the presence of the highest dose of DMOG (1mM) while PLOD2 expression was increased by DMOG at 0.5mM or 1mM, regardless of TGFβ1 presence.

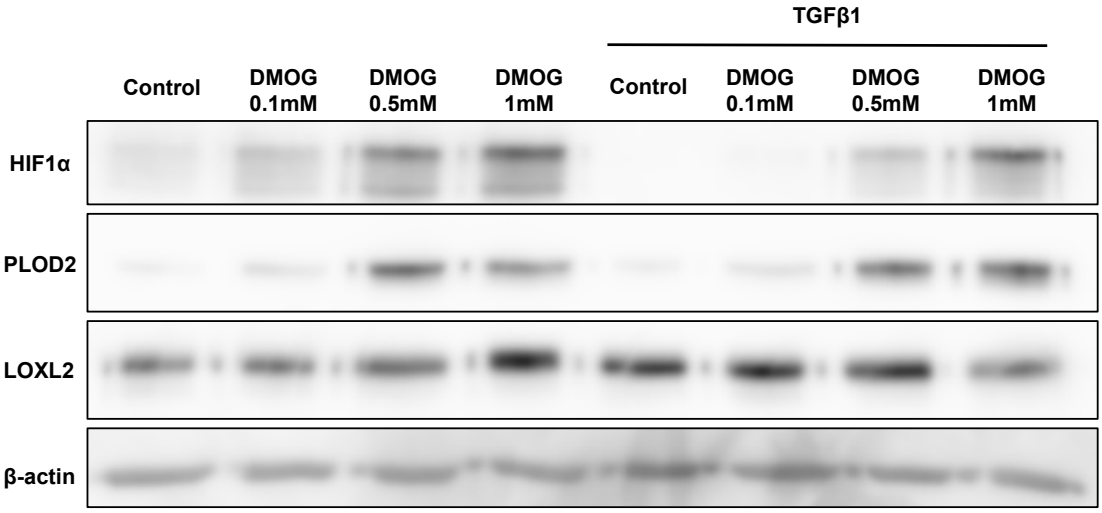

Figure 5.5: Pan-prolyl hydroxylase inhibition stabilises HIF and promotes PLOD2 and LOXL2 expression in a 3D fibroblastic foci model. Western blotting for HIF1α, LOXL2 and PLOD2 in the 3D fibroblastic foci model exposed to incremental doses of DMOG with or without TGFβ1 3ng/mL for 1 week. β-actin was used as a loading control. Blot representative of 3 individual donor experiments.

In summary, TGFβ1 was required to produce the spheroid within a long-term 3D model culture, with no apparent effect from DMOG on this sheet contraction. Furthermore DMOG did not appear to interfere with this process, with appropriate formation of spheroids in all DMOG-containing TGFβ1 treated condition. A DMOG dose of 0.5mM was capable of upregulating HIF expression, resulting in appreciable induction of PLOD2 and LOXL2 in the 3D fibroblast spheroids (i.e. TGFβ1 conditions).

5.3.3 Biomechanical effects of HIF pathway activation through pan-prolyl hydroxylase inhibition in a long-term 3D fibroblastic foci model

To determine the effects of HIF pathway activation through DMOG on mature collagen cross-linking a 6 week 3D fibroblastic focus model experiment was performed with 1 week in media alone to allow fibroblast sheet formation followed by 5 weeks of treatment using DMOG at 0.5mM. Early passage lung fibroblasts were selected from 3 IPF donors and cultured for 1 week in media alone before treatments were added (control - TGFβ1 3ng/mL, or DMOG 0.5mM plus TGFβ1 3ng/mL). As anticipated the conditions containing TGFβ1 contracted to form spheroids while the conditions without TGFβ1 grew as sheets on the base of the transwell. Following 5 weeks of culture in conditioned media the sheets and spheroids were harvested for FFPE blocks,

parallel plate compression analysis and collagen analysis. The entire experiment was repeated once more (24 samples per condition in total).

FFPE blocks were sectioned and a Masson's trichrome stain performed to examine the cellular (pink) and ECM (blue) composition of the samples **(Figure 5.6)**. This demonstrated profound differences in ECM production between spheroids cultured with TGFβ1 alone and with combined TGFβ1 and DMOG. Samples cultured in TGFβ1 alone formed spheroids of lung fibroblasts with significant quantities of surrounding ECM **(Figure 5.6 A)**. Samples cultured in TGFβ1 plus DMOG 0.5mM also formed spheroids however massons staining confirmed a paucity of ECM surrounding the lung fibroblasts **(Figure 5.6 B)**.

Spheroids from the control treatment (TGFβ1 alone) and combined treatment (TGFβ1 + DMOG) were further analysed to investigate effects on collagen fibrillogenesis. Visualisation of collagen fibrils was performed using picrosirius red staining. Under polarised light the control spheroids (TGFβ1 alone) demonstrated pronounced accumulation of fibrillar collagen **(Figure 5.7 A)** while a striking paucity of collagen fibrils was seen in samples exposed to combined DMOG 0.5mM plus TGFβ1 **(Figure 5.7 B)**.

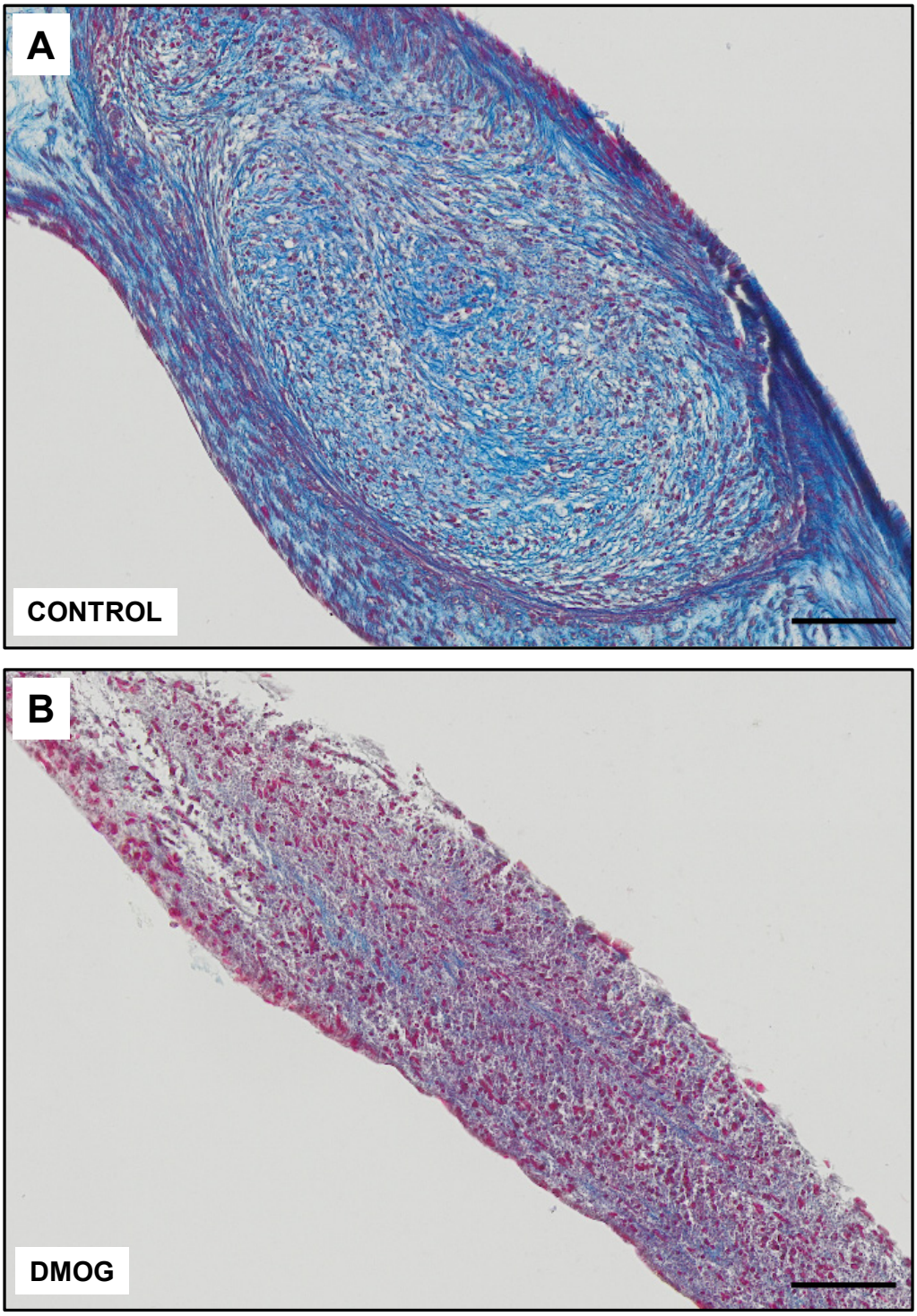

Figure 5.6: Pan-prolyl hydroxylase inhibition substantially reduces extracellular matrix production in a 3D fibroblastic foci model. Massons trichrome stain of 3D fibroblastic foci samples exposed to **(A)** control media (TGFβ1 3ng/mL alone) or **(B)** combined (DMOG 0.5mM and TGFβ1 3ng/mL) for 5 weeks. Fibroblast cytoplasm stained with acid fuchsin (pink) and ECM with aniline blue (blue). N = 3 IPF donors stained. Scale bar 100µM.

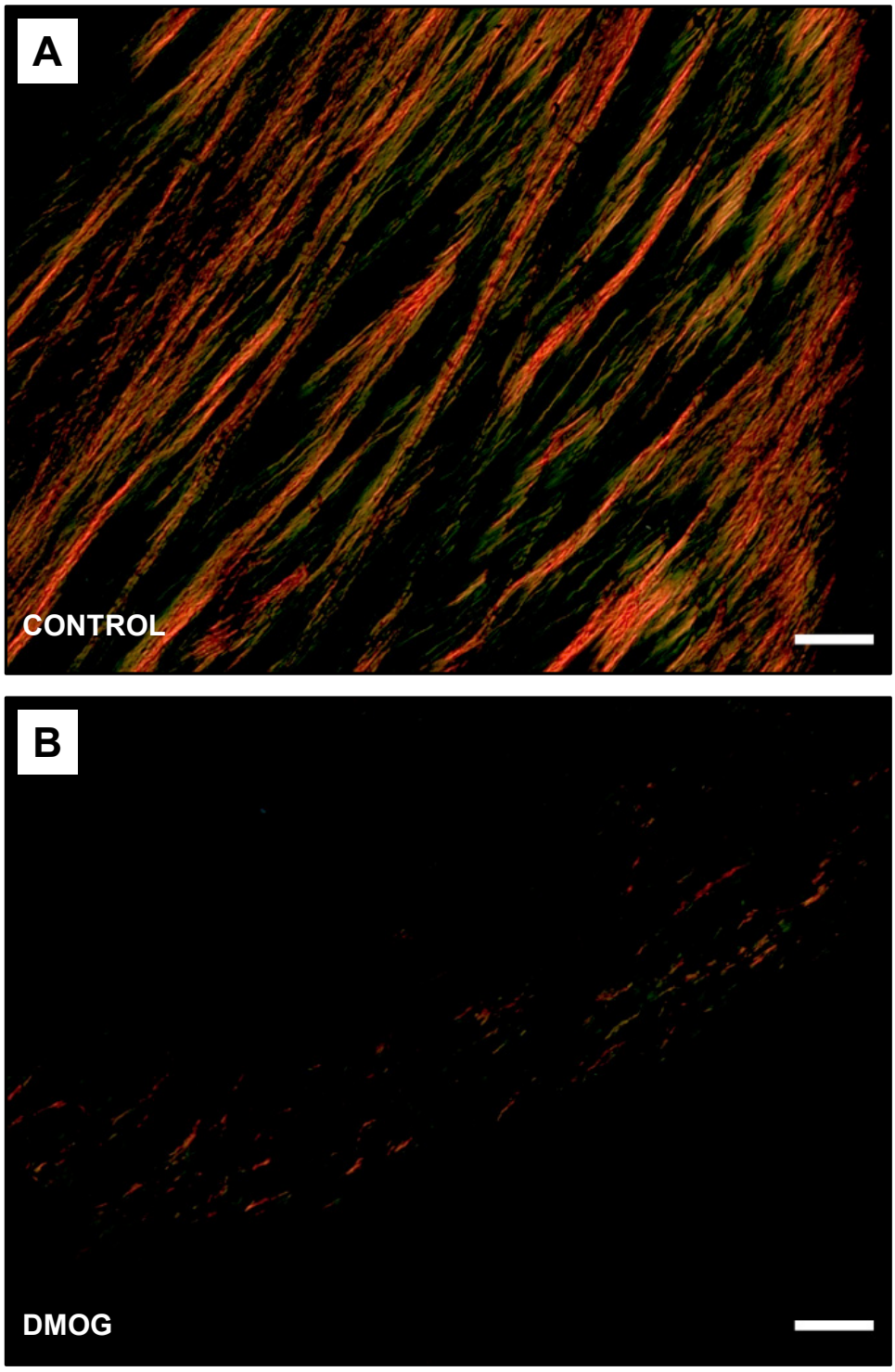

Figure 5.7: Pan-prolyl hydroxylase inhibition results in near absence of collagen fibrillogenesis in a 3D fibroblastic foci model. Representative examples of picrosirius red staining of collagen fibrils from 3D fibroblastic foci viewed under polarised light, after exposure to treatments with **(A)** control (TGFβ 3ng/mL alone) or **(B)** combined DMOG 0.5mM plus TGFβ 3ng/mL for 5 weeks. N = 3 IPF donors stained. Scale bar 20µm.

Collagen structure-function was further assessed through mechanical testing of ECM compliance followed by analysis of collagen quantity and cross-linking density in individual samples **(Figure 5.8)**. Tissue stiffness was assessed using parallel plate compression testing, followed by sample hydrolysis before measuring protein, hydroxyproline and pyridinoline cross-links using colorimetric assays, to enable comparison for overall collagen content (normalised to protein) and pyridinoline cross-links (normalised to collagen molecules).

On testing with parallel plate compression, spheroids from control and DMOG samples were observed to be of similar shape and size **(Figure 5.8 A)**. Despite this however, substantially reduced compliance in the DMOG condition was observed (mean tissue stiffness 0.283kPa +/- 0.03kPa) compared to the control (TGFβ alone) condition (mean 22.88 +/- 2.72 kPa) **(Figure 5.8 B)**. Described another way, DMOG-exposed samples produced spheroids which were on average 98.5% less stiff than the control samples (mean stiffness DMOG 1.48 +/- 0.27%) **(Figure 5.8 C)**.

Collagen content in the control samples measured approximately 0.4mg per mg of total protein, which was generally consistent with measurements from controls in previous work **(Figure 5.8 D)**[165]. Contrastingly however the additional treatment of samples with DMOG resulted in an undetectable level of collagen (measured as hydroxyproline) within the limits of the assay, even following extended sample analysis with larger sample volumes.

Pyridinoline (PYD/DPD) cross-links were also measured in the control and DMOG conditions, and density of cross-links calculated per collagen molecule using the measured quantity of collagen. In the control condition PYD/DPD cross-link density was again similar to the controls in previous work, with a mean cross link density of just over 0.1 cross-links per collagen molecule **(Figure 5.8 E)**. In the DMOG treatment conditions however PYD/DPD concentrations were undetectable to the limits of the assay.

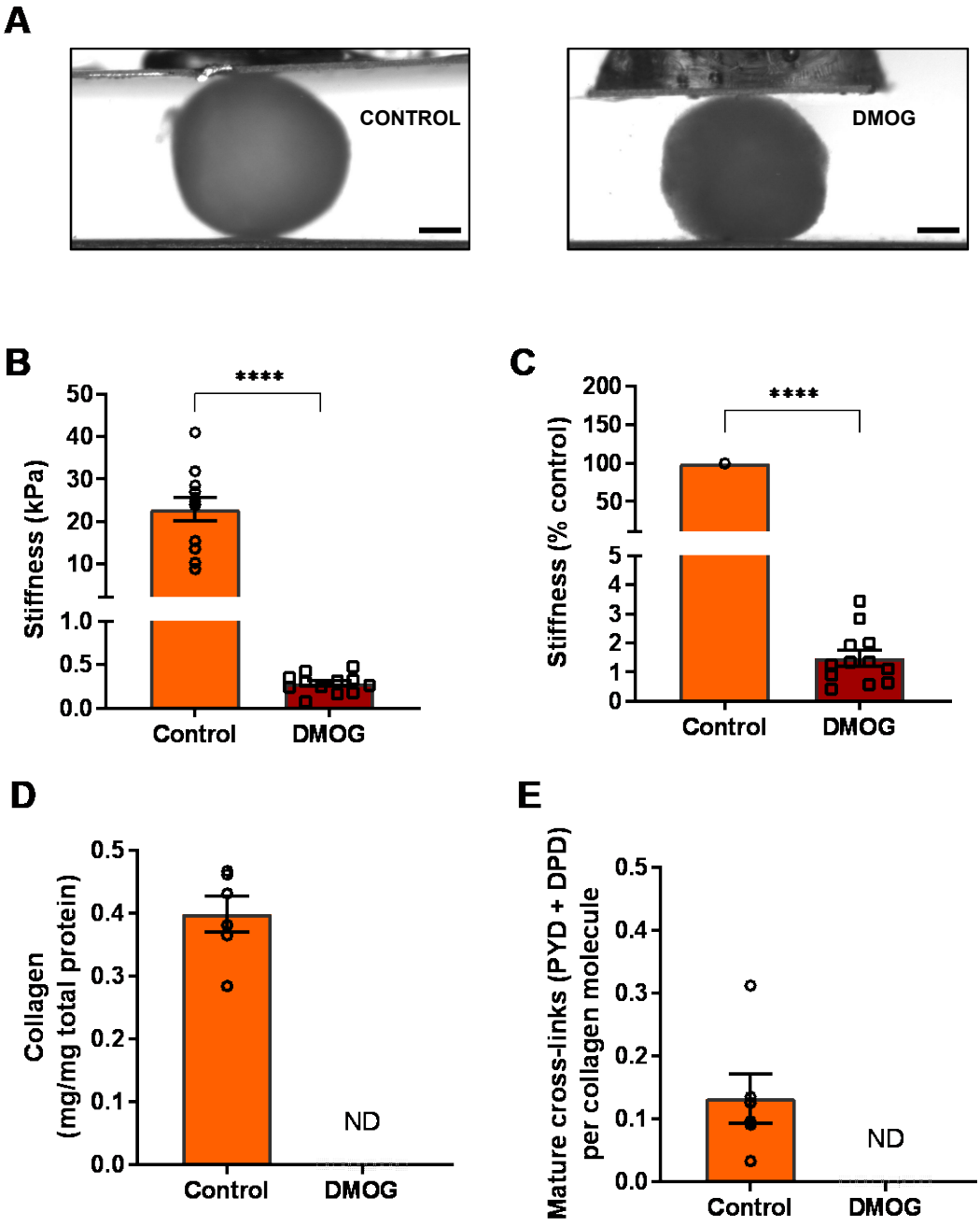

Figure 5.8: Pan-prolyl hydroxylase inhibition greatly reduces extracellular matrix stiffness, with undetectable collagen or collagen cross-links, in a 3D fibroblastic foci model. IPF fibroblasts grown in the 3D in vitro model of fibrosis with control or DMOG 0.5mM. **(A)** Side view of samples undergoing parallel plate compression testing. Scale bar 200Mm. Tissue stiffness in **(B)** kilopascals and **(C)** as a proportion of control expressed in percentage, measured by parallel plate compression testing. Samples were subsequently hydrolysed before measurement of **(D)** collagen (hydroxyproline) content normalised to protein and **(E)** mature pyridinoline cross-links normalised to collagen. Data from N=2 experiments using 3 IPF donors each (in quadruplicate), with stiffness measurements from N=12 samples and collagen and cross-link analysis from N=6 samples.

Taken together these findings suggest that while DMOG is capable of inducing HIF pathway activation to promote *PLOD2* and *LOXL2* upregulation, it exerts potent downstream effects to inhibit collagen synthesis and fibrillogenesis.

These results may seem incongruous with earlier findings, however in the long-term 3D culture system they are likely to be 'off-target' effects of DMOG, rather than a key feature of HIF pathway activation. As a pan-prolyl hydroxylase inhibitor DMOG has the potential to inhibit not just HIF-PHDs but also collagen-PHDs integral to intracellular procollagen formation[263]. This was clearly evident by the complete absence of hydroxyproline in the DMOG-exposed samples, and therefore the modulation of collagen cross-linking enzyme expression were irrelevant to downstream matrix stiffness. This would account for previous findings reporting reduced stiffness with HIF pathway activation in DMOG samples, and is consistent with a growing body of evidence where DMOG-related suppression of collagen synthesis has been observed[248,264-266].

5.3.4 Effects of HIF stabilisation through selective prolyl hydroxylase 2 inhibition with and without TGFβ signalling on collagen cross-linking enzyme induction in IPF lung fibroblasts

HIF pathway activation is possible without interfering with collagen PHD activity. Selective PHD2 inhibitors such as IOX2 are capable of promoting HIF pathway activation, and it was hypothesised that their selective nature would not interfere with collagen biosynthesis.

To investigate the effect of HIF pathway activation through selective PHD2 inhibition on matrix remodelling a time-course experiment was first performed to observe the effect of the PHD2-inhibitor IOX2 at 50µM concentration over 24 – 72 hours **(Figure 5.9)**. Increased expression of HIF1α, LOXL2 and PLOD2 expression was observed in IPF fibroblasts exposed to IOX2 50µM at each time point compared to the control condition.

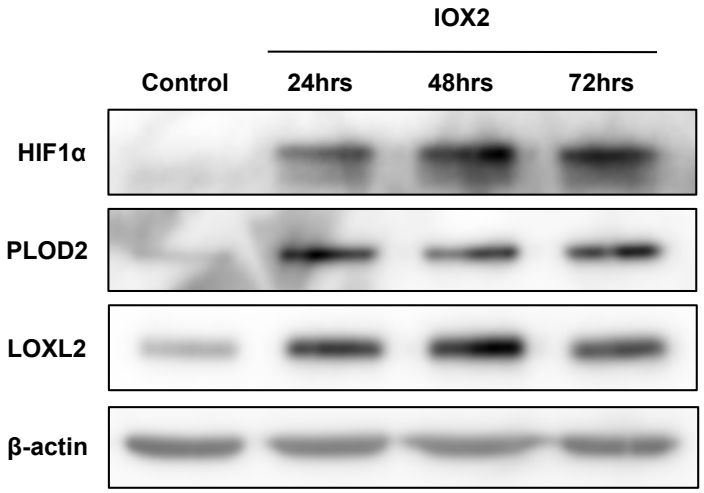

Figure 5.9: Selective prolyl hydroxylase 2 inhibition promotes HIF pathway activation and increased expression of LOXL2 and PLOD2 in IPF fibroblasts. Western blotting for HIF1α, LOXL2 and PLOD2 in the primary IPF fibroblasts exposed to IOX2 50uM for 0, 24, 48 or 72 hours. β-actin was used as a loading control.

Having confirmed that selective PHD2 inhibition with IOX2 was capable of upregulating HIF pathways as well as dysregulation of the key collagen cross-linking enzymes PLOD2 and LOXL2, the effects of HIF stabilisation through IOX2 50μM were subsequently tested in parallel and combination with TGFβ1 10ng/mL on IPF lung fibroblasts. Gene expression was analysed at 48 hours of treatment using RTqPCR **(Figure 5.10)**.

PLOD2 was observed to be equally increased with TGFβ1 10ng/mL or IOX2 50μM **(Figure 5.10 A)**. Notably, combination exposure to TGFβ1 plus HIF stabilisation through IOX2 resulted in markedly greater expression of *PLOD2* than either condition alone. *LOXL2* expression was only slightly increased with either TGFβ1 or IOX2 alone, but the combined condition TGFβ1 + IOX2 had an additive effect to promote significant induction of *LOXL2* **(Figure 5.10 B)**.

Similarly to previous results using DMOG to promote HIF pathway activation, *COL1A1* and *COL3A1* expression were increased with TGFβ1-only while HIF stabilisation through IOX2 did not appear to influence *COL1A1* or *COL3A1* expression **(Figure 5.10 C-D)**. The combined condition TGFβ1 + IOX2 had similar levels of *COL1A1* and *COL3A1* expression to the TGFβ1-only condition.

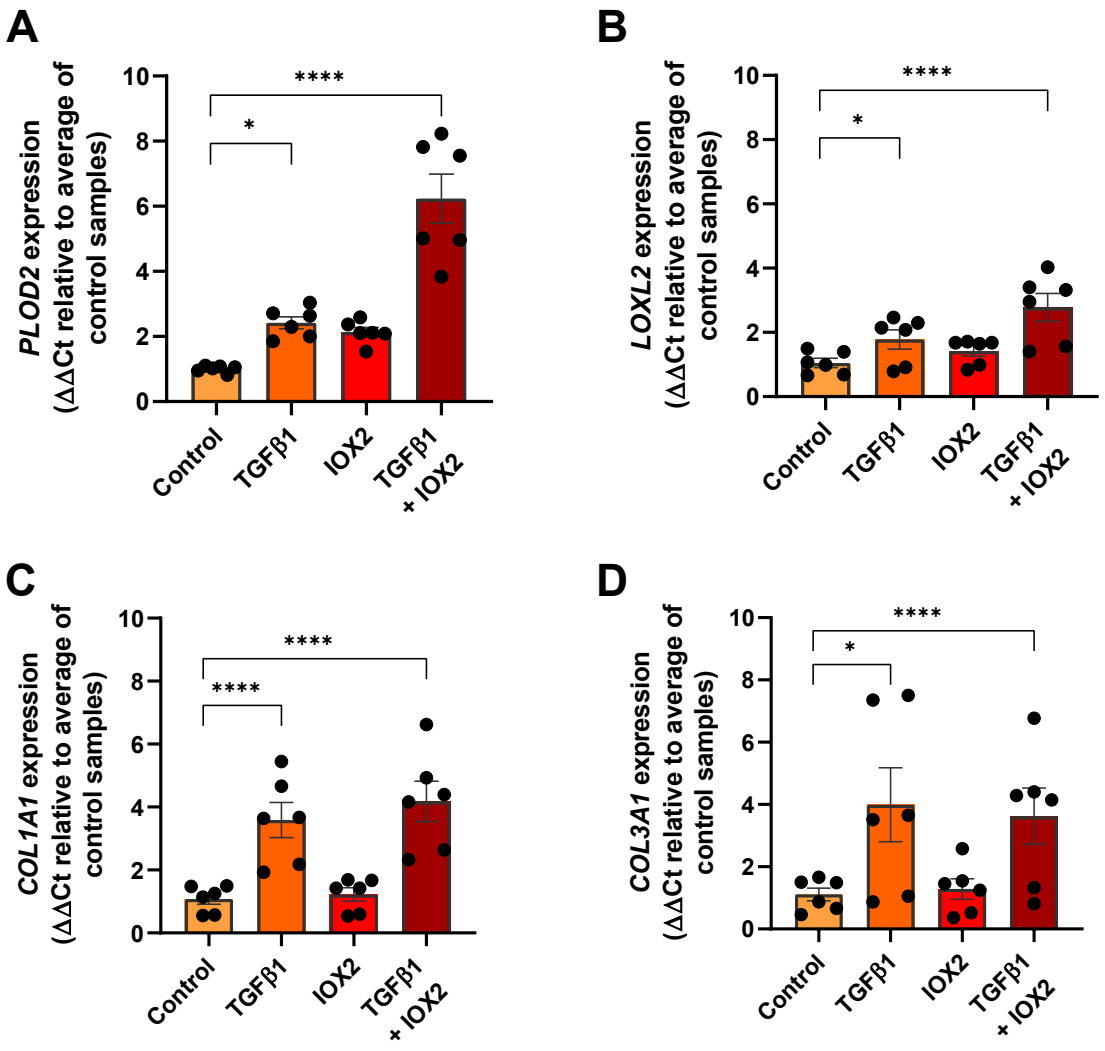

Figure 5.10: Combined HIF and TGFβ1 signalling augment collagen cross-linking enzyme expression but only TGFβ1 promotes interstitial collagen gene induction. mRNA expression of **(A)** *PLOD2,* **(B)** *LOXL2,* **(C)** *COL1A1* and **(D)** *COL3A1* in IPF fibroblasts exposed to IOX2 50μM, TGFβ1 10ng/mL or both for 48 hours. mRNA expression levels were determined using the ΔΔ CT method with grouped analysis and multiple comparisons (Dunnett's test). * $p < 0.05$, **** $p < 0.0001$. N=6 IPF donors in duplicate from 2 individual experiments.

In summary these results reveal that selective PHD2 inhibition using IOX2 at 50μM concentration is effective in promoting HIF pathway activation and upregulating expression of the cross-linking enzymes *PLOD2* and *LOXL2*. Furthermore the patterns of expression were similar to earlier DMOG experiments, with no discernible effects on collagen fibrillogenesis gene expression.

5.3.5 Biomechanical effects of HIF pathway activation through selective prolyl-hydroxylase 2 inhibition in a long term 3D fibroblastic foci model

With confirmation of IOX2's effects on HIF pathway induction and key collagen cross-linking enzyme expression, functional effects of HIF pathway activation through selective PHD2 inhibition were subsequently tested in the 3D fibroblastic foci model.

Similarly to the DMOG experiment, a 2 week pilot study was conducted with fibroblasts from 3 IPF donors cultured for 1 week in the 3D fibroblastic foci model, before being exposed to conditions for a second week. Conditions included a vehicle control (DMSO), TGFβ1, and 2 different doses of IOX2 alone or with TGFβ1 (6 conditions in total, IOX2 50μM or 250μM) and samples were harvested after 1 week of exposure to conditions.

Samples from each of the 6 conditions were harvested for protein using a combination of mechanical and enzymatic lysis. Protein was quantified and western blot performed using 10ug of cell lysate per condition **(Figure 5.11)**. HIF1α was upregulated with both doses of IOX2 compared to control **(Figure 5.11 A)**. Consistent with earlier experiments, the combination of TGFβ1 and HIF induction through IOX2 resulted in the greatest expression of HIF1α. Both PLOD2 and LOXL2 were upregulated by IOX2 treatment with or without TGFβ1 **(Figure 5.11 A-B)**.

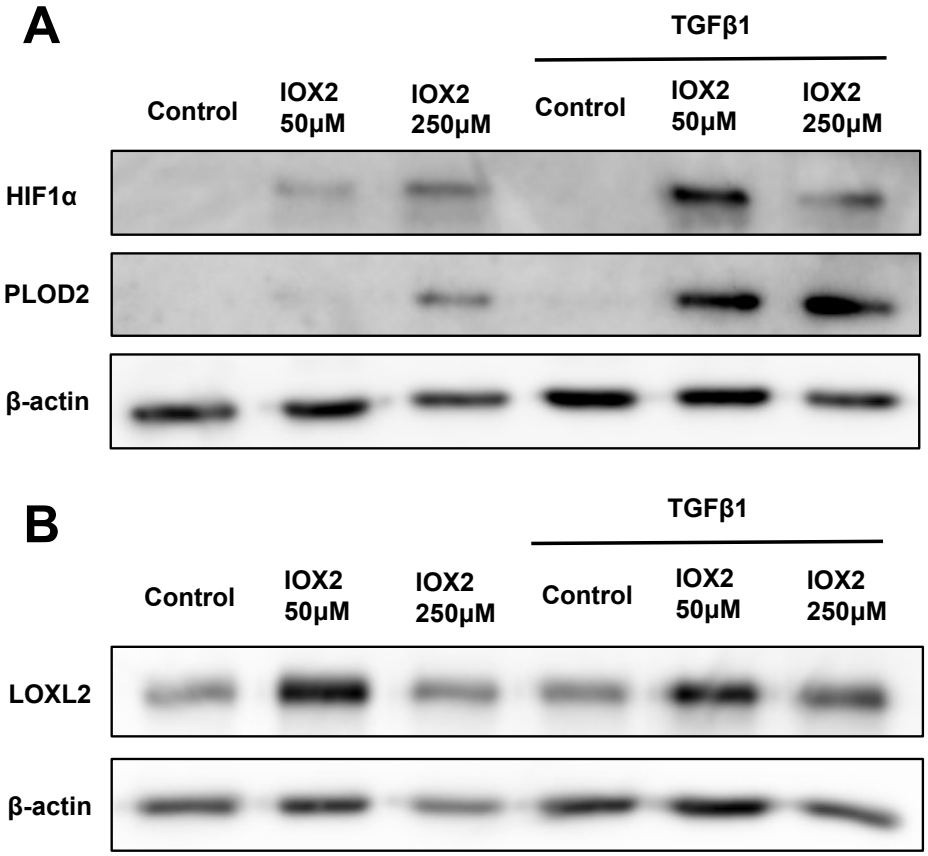

Figure 5.11: Selective prolyl hydroxylase 2 inhibition stabilises HIF and promotes PLOD2 and LOXL2 expression in a 3D fibroblastic foci model. Western blotting for **(A)** HIF1α and PLOD2 and **(B)** LOXL2 in the 3D fibroblastic foci model exposed to low (50μM) or high (250μM) dose IOX2 with or without TGFβ1 for 1 week. β-actin was used as a loading control. Blot representative of 3 individual IPF donor experiments.

Taken together IOX2 at a concentration of 50μM appeared sufficient to generate HIF1α expression and facilitate upregulation of PLOD2 and LOXL2 in the 3D fibroblastic foci model over 1 week of exposure. Furthermore the addition of TGFβ1 to IOX2 treatment increased the expression of both HIF1α and PLOD2 compared to IOX2 alone, suggesting the combined pathways could greatly enhance the production of collagen telopeptide hydroxylysine and subsequent pyridinoline cross-links.

The biomechanical effects of HIF stabilisation by IOX2 on lung fibroblast ECM were subsequently determined using a long term culture 3D fibroblastic focus model. Treatments included a vehicle control containing TGFβ1 3ng/mL alone and a combined treatment condition with HIF pathway stabilisation through IOX2 50μM and TGFβ1 3ng/mL. On completion of the 6 week experiment, spheroids were harvested and processed for histochemical staining, parallel plate compression and collagen analysis.

The effects of IOX2 versus control on cell proliferation, ECM production and collagen fibrillogenesis were examined microscopically using sections from FFPE samples for H&E and picrosirius red staining **(Figure 5.12)**. Control and IOX2 conditions produced 3D fibroblastic foci spheroids with a similar abundance of fibroblasts and ECM **(Figure 5.12 A-B)**. Collagen fibrillogenesis was identified using picrosirius red staining with polarised light, and demonstrated an abundance of collagen fibrils in both control and IOX2 samples, with no discernible difference in fibrillar quantity or density **(Figure 5.12 C-D)**.

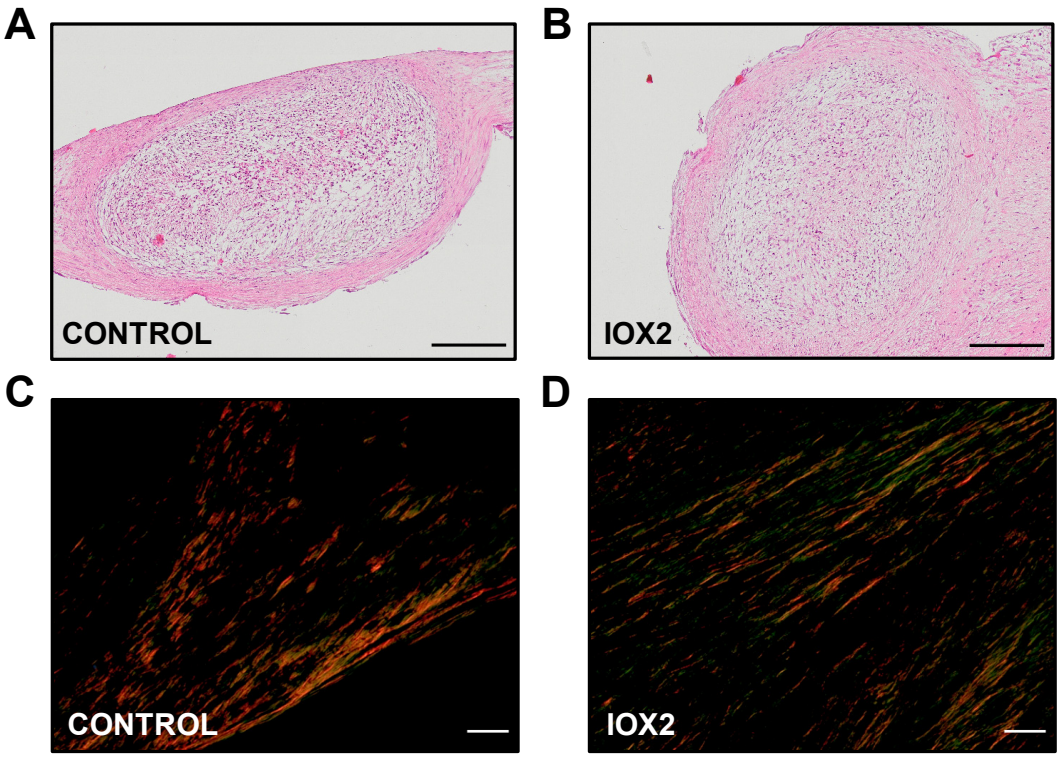

Figure 5.12: Selective prolyl hydroxylase 2 inhibition does not impair collagen fibrillogenesis in the fibroblastic foci 3D model. IPF fibroblasts grown in the 3D in vitro model of fibrosis with control or IOX2 50µM. H&E of **(A)** Control or **(B)** IOX2. Scale bar 200uM. Picrosirius red staining imaged under polarised light of **(C)** control or **(D)** IOX2 samples. Scale bar 20µm. Representative images from N = 3 IPF donors per experiment, from 2 individual experiments.

Together these findings suggest that unlike earlier findings with DMOG, HIF pathway induction through IOX2 did not suppress ECM matrix production and collagen fibrillogenesis.

After confirming that selective PHD2 inhibition with IOX2 was capable of inducing HIF pathway activation but did not impair collagen biosynthesis, the effects of HIF stabilisation through IOX2 on collagen structure-function were then examined **(Figure 5.13)**.

Parallel plate compression testing was performed to test ECM compliance **(Figure 5.13 A).** A profound increase in stiffness was observed in the IOX2 condition compared to control, with a mean stiffness (+/- SEM) of 107.1kPa (+/- 10.68) with HIF stabilisation through IOX2 compared to 35.83kPa (+/- 4.019) in the control condition (TGFβ alone) **(Figure 5.13 B)**. When measuring proportional changes in compliance, IOX2 increased the stiffness of fibroblast ECM by a mean of 346% (SEM +/- 56%) compared to control spheroids.

The effects of IOX2-mediated HIF induction on collagen and collagen cross-links were subsequently analysed. Collagen content (hydroxyproline) normalised to milligrams of total protein was significantly reduced with HIF pathway induction in IOX2 samples (mean 0.26mg, SEM +/- 0.01) compared to control samples (mean 0.33mg, SEM +/- 0.01) **(Figure 5.13 C)**. Furthermore the density of mature pyridinoline cross-links per collagen molecule (mean 0.31 cross-links, SEM +/- 0.02) was substantially increased in IOX2 samples compared to control (mean 0.18 cross-links, SEM +/- 0.01) **(Figure 5.13 D)**.

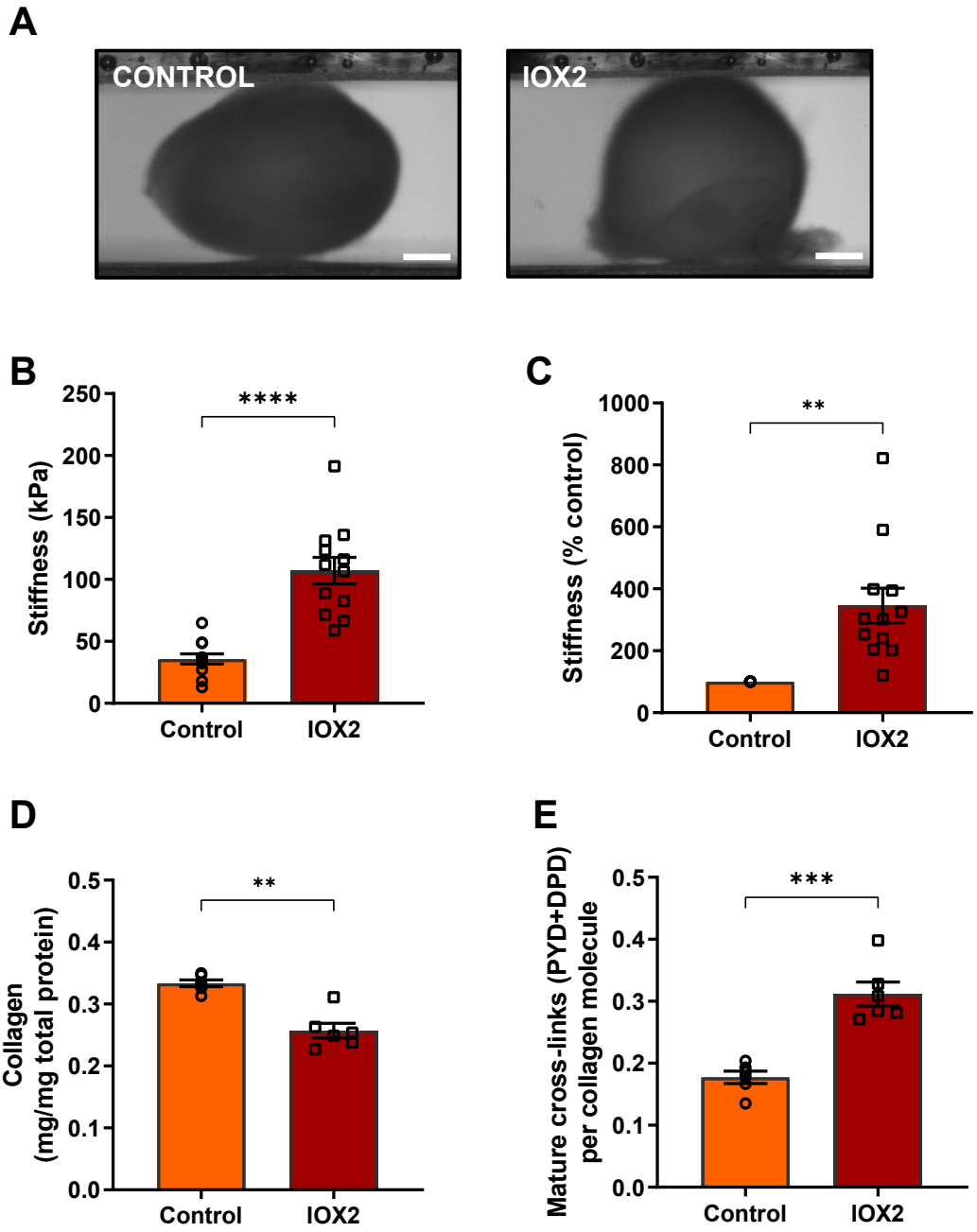

Figure 5.13: HIF stabilisation through selective prolyl hydroxylase 2 inhibition significantly increases tissue stiffness, reduces collagen content and increases pyridinoline cross-link density in a 3D fibroblastic foci model. IPF fibroblasts grown in the 3D in vitro model of fibrosis with control or IOX2 50µM. **(A)** Side view of samples undergoing parallel plate compression testing. Scale bar 200µM. Tissue stiffness in **(B)** kPa and **(C)** % control, measured by parallel plate compression testing. Samples were subsequently hydrolysed before measurement of **(D)** Collagen (hydroxyproline) content normalised to protein and **(E)** Mature pyridinoline cross-links normalised to collagen. Data from N=2 experiments using 3 IPF donors each (in quadruplicate), with stiffness measurements from N=12 samples and collagen and cross-link analysis from N=6 samples.

In summary, stabilisation of HIF through IOX2-mediated selective PHD2 inhibition produced significantly stiffer lung fibroblast ECM than control conditions containing TGFβ1 alone. This IOX2-mediated increase in matrix stiffness was associated with a detectable reduction in collagen content and an increase in pyridinoline cross-link density. It could therefore be postulated that the increases in pyridinoline were the effect of reduced collagen substrate, culminating in excessive cross-linking of available collagen molecules. However pyridinoline density was normalised to collagen molecules, thereby accounting for this reduction. Furthermore the reduction in collagen with IOX2 was around 20% of control samples, while the increase in pyridinoline cross-links per collagen molecule was 40% of control. Finally, the observed induction in collagen cross-linking expression suggests increased activity rather than a similar degree of activity on a smaller quantity of substrate. Notably while pyridinoline cross-link density in control samples was similar to earlier work with the 3D fibroblastic foci model performed by our group, the density in IOX2 conditions approached levels seen in IPF tissue[165].

To further examine changes to collagen nano-architecture, control and IOX2 samples from 2 donors were subsequently processed and imaged under electron microscopy, and compared to earlier results from Dr Mark Jones using healthy and IPF lung tissue **(Figure 5.14)**. The cross-sectional diameters of 300 individual collagen fibrils were measured for each of the 3D fibroblastic foci samples by a blinded investigator (Dr Elizabeth Davies) and tabulated. Collagen fibrils in samples exposed to HIF pathway activation through IOX2 50μM were significantly smaller (median 31.51nm, IQR 26.84 – 36.50) than fibrils from control samples (33.86nm, 29.60 – 38.60) with a median difference of -2.35nm **(Figure 5.14 A-B)**. This was comparable to the difference observed by Dr Mark Jones in an analysis of dry weight collagen fibril diameters from “healthy” (non-fibrotic) and IPF lung tissue (median fibril diameter for non-fibrotic lung 29.87nm and for IPF lung 26.69nm, median difference -3.18nm) **(Figure 5.14 C)**.

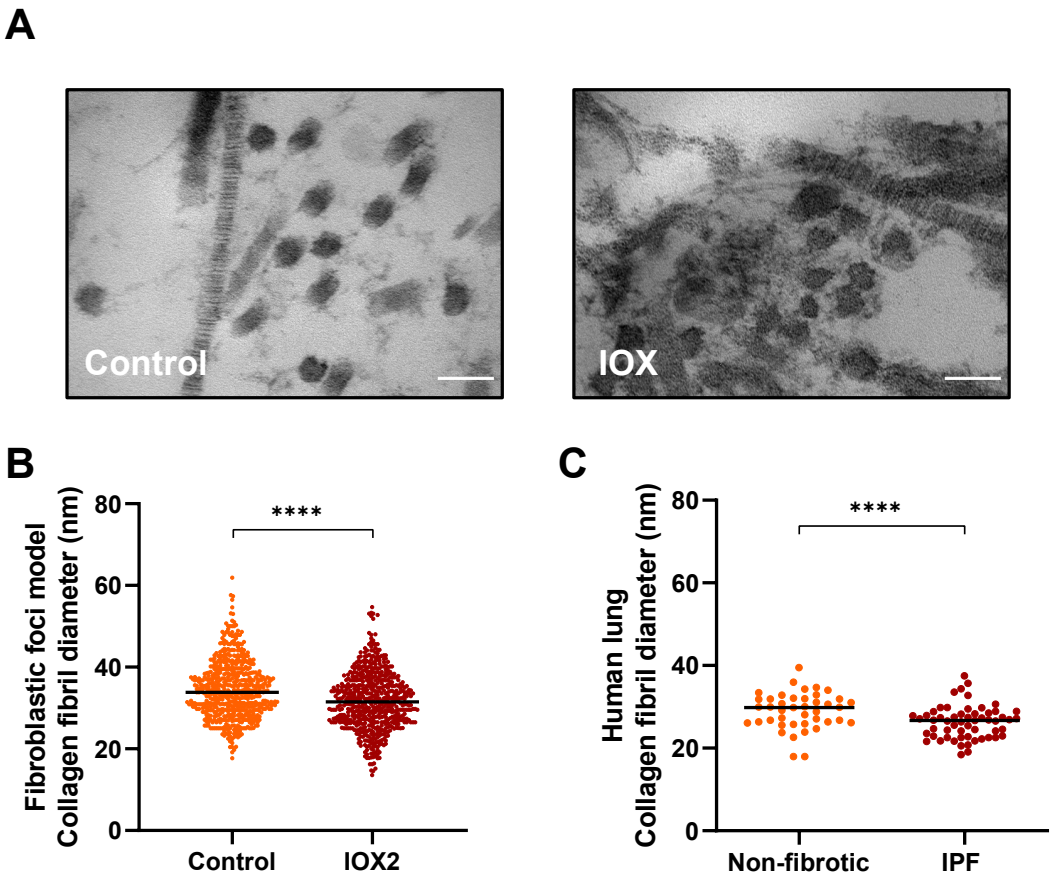

Figure 5.14: HIF stabilisation in the 3D fibroblastic foci model reduces collagen fibril diameter, similarly to changes seen in IPF lung. (A) Representative images of cross-sectional and longitudinal collagen fibrils. **(B)** Mean collagen fibril diameters in 3D model fibroblastic focus tissue exposed to control of IOX2 (collagen fibril diameter measured by short axis of 300 transverse fibres per condition, in each of 2 IPF donors). Scale bar 50nm. **(C)** Data from Dr Mark Jones demonstrating non-hydrated collagen fibril diameters in non-fibrotic and IPF lung tissue determined by atomic force microscopy. **** $p<0.0001$ (unpaired t-test). Data from 2 individual donor experiments.

In summary selective PHD2 inhibition through IOX2 is capable of promoting HIF pathway activation and downstream dysregulation of collagen cross-linking enzyme expression, with changes to the mRNA expression proportion of these enzymes compares to collagen fibrillogenesis genes. The biomechanical consequences of HIF stabilisation through IOX2 in the 3D fibroblastic focus model were striking changes to both matrix compliance and collagen nano-structure, with a marked increase in pyridinoline cross-link density as well as a reduction in collagen concentration and fibril diameter. The changes between control and IOX2-exposed matrix were observed to be similar in pattern and scope to the changes observed between healthy and IPF lung tissue.

5.4 Discussion

IPF is characterised by progressive deposition of abnormal ECM leading to impairments in pulmonary compliance and gas exchange which are ultimately fatal[14]. Conventionally TGFβ is considered the core regulatory pathway within the milieu of pro-fibrotic signals that orchestrate abnormal matrix remodelling, largely due to wide-ranging effects to promote fibroblast proliferation, activation and ECM production[126,137,138,141,216,217].

HIF pathways are also capable of modulating the expression of ECM-related genes, have synergistic mechanisms with TGFβ and have been implicated in IPF pathogenesis[153,154,156,218,246,250,267-270]. HIF pathways may represent an alternative or "second-hit" stimulus for abnormal matrix remodelling in IPF. Consistent with observations in this study of changes to collagen cross-linking enzyme expression, HIF pathway activation appears to operate synergistically with TGFβ1/SMAD3 signalling to enhance the pro-fibrotic response in a variety of cancer and fibrosis models[245,268,270]. In particular, specific sites on the PLOD2-promoter have been identified for both TGFβ1-mediated SMAD proteins and HIF1α to bind and induce expression[271]. Independently of TGFβ signalling, HIF pathways appear to have direct effects on matrix remodelling in cancer *in vitro* studies through upregulation of ECM genes including *LOX(L)* family members[198,250,267].

Significantly in this study, HIF pathway induction but not TGFβ1 signalling was found to disrupt proportional expression changes of collagen cross-linking enzymes to collagen fibrillogenesis genes. This led to an intriguing concept that HIF pathways, rather than TGFβ signalling, might be core disruptors of the homeostasis between matrix collagen biogenesis and enzymatic modification to produce densely cross-linked fibrillar collagen and propagate abnormal matrix stiffness.

Previous studies are conflicted regarding the effects of HIF pathway induction on changes to matrix stiffness. Madsen et al found cancer associated fibroblasts embedded in 3D collagen I matrices and incubated in 1% oxygen had reduced contraction and this was associated with lower matrix stiffness over 72 hours, while silencing of PHD2 also reduced α-SMA expression and fibroblast contractility to reduce the overall stiffness of the model[248]. Due to the short term nature of these experiments (72 – 96 hours) it can be assumed that the stiffness changes observed here are likely related to cellular re-organisation rather than modification to ECM matrix. They also reviewed modifications to the matrix itself using a breast cancer mouse model to demonstrate that 3 weeks of treatment with the pan-PHD inhibitor DMOG significantly reduced tumour stiffness but not size. While they observed a reduction in α-SMA

expression in the DMOG exposed samples, the mechanisms underlying the reduction in matrix stiffness were not explored.

Other studies suggest ECM modification by HIF pathways leads to increases in matrix stiffness. Gilkes and colleagues used atomic force spectroscopy on cell-free ECM derived from human foreskin fibroblasts cultured in normoxic or hypoxic (1% O2) conditions for 72 hours to demonstrate a 3-fold increase in stiffness for matrix exposed to hypoxia[250]. Silencing of *HIF1α* or *PLOD2* but not *HIF2α* in the foreskin fibroblasts prior to culture was sufficient to normalise ECM stiffness in their experiments. Again these experiments were limited by their short term nature, preventing analysis of HIF effects on mature collagen cross-linking. Independently of these results Stegen et al demonstrated that postnatal mice (day 2.5) possessing a PHD2 conditional deletion in chondrocytes experienced significant qualitative changes to bony matrix with reduced solubility and a marked increase in pyridinoline cross-links, mediated through HIF1α[249].

Notably none of these experiments used a long-term model to examine the effects of HIF pathways on mature collagen cross-linking over time. HIF pathway stabilisation was incorporated into the *in vitro* 3D fibroblastic focus model to investigate these questions and analyse downstream effects on collagen structure-function within lung fibroblast ECM.

Advantages of this model not only include the production of endogenous ECM by IPF fibroblasts and sufficient time in culture to facilitate maturation of this ECM, but also homogeneity in size and shape between samples that enables direct comparison of biomechanical properties under different conditions. Incorporation of TGFβ into this model aids in homogenous spheroid formation and also reflects the conditions seen in lung fibrosis, although importantly it limits the ability of the model to replicate what might be considered "healthy" control ECM. Rather, the strength of this model lies in the downstream analysis of additional pro-fibrotic pathways, such as HIF signalling, as well as mechanisms of interfering with these pathways.

Two HIF pathway-promoting compounds were used to stabilise HIFα in the 3D fibroblastic focus model with strikingly divergent end-results between the pan-PHD inhibitor DMOG and the selective PHD2 inhibitor IOX2. In 2 week pilot studies both HIF activating compounds were confirmed to accumulate HIF1α within the model and promote downstream activation of the bone-type collagen cross-linking enzymes PLOD2 and LOXL2. However following 5 week exposure to DMOG 0.5mM, ECM from IPF lung fibroblasts was 98.5% less stiff than control matrix, with an almost complete absence of collagen fibrillogenesis seen on picrosirius staining and undetectable levels of hydroxyproline in hydrolysed samples. By

comparison exposure to IOX2 50μM for 5 weeks resulted in IPF fibroblast ECM which was on average 346% stiffer than control matrix, with a corresponding loss of in collagen content, increase in pyridinoline cross-link density, and reduction in collagen fibril diameter.

The explanation for these contrasting results is likely to lie in the PHD selectivity of the HIF-stabilising compounds. Both PHD inhibitors prevent HIFα degradation by impeding the hydroxylation of proline residues on the HIFα protein (for example Pro402 and Pro564 in HIF1α), thereby preventing HIFα ubiquitination by VHL protein which would otherwise lead to its rapid proteosomal degradation[152]. Due to the broad effects on all PHDs, DMOG has been shown to better simulate the cell's transcriptional hypoxic response than other hypoxia-mimicking agents, thus making it a popular first choice for HIF mechanistic studies[239].

However DMOG's potent effects on PHDs can extend beyond the HIF pathways, with the earliest report by Baader and colleagues in 1994 demonstrating dose-dependent suppression of hydroxyproline synthesis in 15 day old chick embryos treated with DMOG for 2.5 hours[264]. More recently these effects have also been observed in studies of articular cartilage, with DMOG interfering with normal collagen metabolism and reducing matrix stiffness[265,266].

Collagen PHDs (C-PHDs) modify proline to 4-hydroxyproline on pro-collagen α-chains, an essential step to ensure appropriate folding for triple helix formation[272]. Inadequately hydroxylated and folded proteins are proteolytically degraded, leading to a reduction in collagen formation and deposition. C-PHDs are functionally and geographically distinct from HIF-PHDs, residing in the endoplasmic reticulum (rather than the cellular cytoplasm for HIF-PHDs) and targeting different proline substrates[229]. As a cell-permeable oxoglutarate analogue, DMOG is capable of inhibiting all members of the oxoglutarate-requiring dioxygenase family, including C-PHDs, HIF-PHDs and FIH[273]. DMOG's inhibition of collagen-PHDs therefore fundamentally alters normal collagen biosynthesis, as evidenced by the lack of detectable hydroxyproline or fibrillar collagen on picrosirius staining in the 3D fibroblastic focus samples exposed to DMOG. This distinction is important, as the overlap of inhibition between HIF-PHDs and C-PHDs by DMOG is likely to lead to false conclusions about hypoxia and HIF pathway effects on matrix remodelling as seen in the results of Madsen et al using the breast cancer mouse model[248].

Furthermore within the specific HIF-PHD family, the 3 isoforms (PHD1, 2, and 3) possess non-redundant functional roles, with PHD2 having been previously identified as the most abundant and critical regulator of HIF1α in response to cellular oxygen tension[237,274]. HIF activation through selective inhibition of PHD2 has previously been observed to increase matrix synthesis in human chondrocytes, while conditional deletion of PHD2 in the chondrocytes of mice stimulated increased bone formation and mass[275,276]. Yet research on

PHD2 inhibition in the lung is limited and focused predominantly on pulmonary hypertension. PHD2 knockdown in mice results in embryonic lethality while mice with genetic mutations resulting in up to 90% less PHD2 expression develop severe pulmonary arterial hypertension and vascular remodelling[277]. The effects of HIF pathway activation on matrix mechano-biology were therefore examined through selective PHD2 inhibition to avoid off-target effects on C-PHDs.

In the 3D fibroblastic focus model, HIF pathway activation through the IOX2-mediated selective inhibition of PHD2 promoted substantially increased matrix stiffness, with a mean stiffness greater than 3 times that of control matrix. Furthermore the dramatic changes in compliance were associated with a small but significant reduction in collagen content normalised for protein (likely counterbalanced by the strong effect of TGFβ on collagen accumulation), increased bone-type pyridinoline collagen cross-link density per collagen molecule and a reduction in mean collagen fibril diameter. The reduction in collagen content could be due to inhibitory effects on collagen PHDs similar to those observed by DMOG, however the selectivity of IOX2 for HIF-PHD2 makes this less likely[278].

In the fibrotic lung these results would have a number of consequences. Firstly, matrix stiffening is likely to impede normal physiological function, including critical changes to lung compliance culminating in ventilatory restriction[64,159]. Secondly increases in matrix stiffness are likely to generate positive feedback loops through release of growth factors and mechano-signalling to recruit and activate lung fibroblasts, generating a population of active mesenchymal cells in regional areas of increased stiffness which sustain and propagate matrix remodelling[163,169-172,174,224]. The summary of these effects is a sustained and progressive fibrotic response with physiological impairments detrimental to ongoing normal function.

These results draw a number of parallels to the changes seen between healthy and IPF tissue. The level of matrix stiffness generated with HIF pathway activation through IOX2 in the 3D fibroblastic foci model approached levels seen in IPF tissue using atomic force microscopy by our group[165]. Booth and colleagues have also observed increases in IPF matrix stiffness upwards of 200kPa, while mouse models involving bleomycin have observed changes in matrix stiffness of over 300%[172,279]. Modification in collagen nano-architecture within the HIF-exposed model also correlated with changes seen between human non-fibrotic and IPF lung, with increases in pyridinoline collagen cross-link density and reductions in collagen fibril diameter[165]. While it is impossible to perfectly replicate the conditions of IPF within an *in vitro* model these findings

represent a significant step forward in simulating the matrix remodelling of this disease, and support further research into HIF pathways as a modifiable target for matrix normalisation.

5.5 Conclusion

HIF pathway activation either alone or in synergy with TGFβ signalling disrupts collagen cross-linking homeostasis leading to a substantially higher density of pyridinoline cross-links in lung fibroblast ECM. This is associated with marked changes to collagen nano-architecture and increases in tissue stiffness of greater than 300%. Importantly, the changes observed between control and HIF-exposed samples in pyridinoline density, collagen fibril diameter and matrix stiffness parallel the changes observed between non-fibrotic and IPF lung tissue.

HIF stabilisation could represent an important fibrotic catalyst or, in lieu with other pro-fibrotic mediators such as TGFβ signalling, an amplifying “second-hit” event, disrupting normal ECM homeostasis and profoundly altering structure-function through excessive collagen post-translational modification.

In such an environment, targeting the excessive HIF pathway activation could normalise matrix stiffness, and may have important therapeutic ramifications such as the improvement in tissue function and amelioration of fibrogenic forward-feeding loops. Thus both mechanistically and therapeutically, the interference with HIF-mediated collagen cross-linking represents an important avenue for further investigation.

Chapter 6 Modulating the Effects of HIF Pathways on Matrix Remodelling

6.1 Introduction

This study has identified HIF pathway-mediated upregulation of collagen cross-linking enzymes as a critical process in promoting pyridinoline cross-linking, thereby fundamentally altering matrix compliance and collagen nano-architecture. The degree of these HIF-promoting changes in the 3D fibroblastic focus model were substantially greater than in samples exposed to TGFβ alone, recapitulating the pattern and degree of changes seen in the IPF lung.

Modulation of these pathways may facilitate the normalisation of ECM compliance, with both upstream HIF pathway stabilisation and downstream collagen cross-linking activity representing potential targets. A comparison of these two strategies would provide further mechanistic insights and demonstrate novel pathways for therapeutic application.

Methods to target these pathways include silencing of gene expression and inhibition of catalytic or transcriptional activity. SiRNAs are synthetically produced double-stranded RNA molecules which inhibit specific gene expression through activation of the RISC to promote target mRNA cleavage and degradation[206]. Application of siRNA to silence individual components of the HIF/collagen cross-linking pathway has never been attempted using the *in vitro* 3D fibroblastic focus model, but provides a promising avenue to interrogate and dissect mechanisms of pathological ECM modification. Effective silencing of *LOXL2* and combined *HIF1/2α* have previously been demonstrated, allowing an established platform to build on and also enabling a clear comparison between upstream and downstream targets.

By contrast clinical experience with HIF and LOX(L) inhibiting compounds is limited, however they offer broader scope for therapeutic development. Due to the importance of HIF signalling in malignant processes a variety of HIF inhibitors have been identified and investigated in clinical trials, yet none have translated into clinical practice[233]. Furthermore pre-clinical studies are yet to address the role HIF inhibition may play on the effects of pathologic ECM remodelling[250]. Selective LOXL2/3 catalytic inhibition through PXS-S2A has already been applied to the 3D fibroblastic focus model and has demonstrated efficacy in reducing pyridinoline cross-linking to normalise matrix stiffness in TGFβ-exposed conditions. Furthermore an orally bioavailable form (PXS-S3B) has been shown to attenuate lung fibrosis

in vivo using a rat model with TGFβ overexpression, with an improvement in Ashcroft scores and lung function compared to vehicle control. Yet it remains to be seen if PXS-S2A is capable of ameliorating the substantially greater pathological changes seen in the HIF-stabilised 3D fibroblastic foci model, which possess ECM properties more consistent with the IPF lung.

6.2 Objectives

The objectives for this study were to:

i) Confirm siRNA efficacy in lung fibroblasts and investigate the downstream effects of siRNA targeting *HIF1/2α* and *LOXL2* in a 3D fibroblastic focus model exposed to HIF pathway activation

ii) Identify suitable candidates of HIF inhibition in lung fibroblasts for incorporation into a 3D fibroblastic focus model exposed to HIF pathway activation

iii) Investigate the downstream effects of PXS-S2A, a LOX(L) catalytic inhibiting compound, in a 3D fibroblastic focus model exposed to HIF pathway activation

6.3 Results

6.3.1 Evaluating the efficacy of short interfering RNA in short-term 2D cultures

To explore the potential of siRNA for modulating HIF pathways, the efficacy of silencing target genes was first confirmed through 2D experiments in lung fibroblasts. A successful protocol for silencing *HIF1α* and *HIF2α* had already been established by Liudi Yao in earlier mechanistic studies using control and HIF pathway-promoting conditions **(Figure 3.15)**, however it was not known if siLOXL2 would have the same efficacy. SiLOXL2 was therefore evaluated in healthy lung fibroblasts exposed to TGFβ or HIF pathway activation through either IOX2 or DMOG for 48 hours. Despite the off-target effects of DMOG on collagen production, its potent LOXL2 upregulation provided an extreme condition for testing siLOXL2 efficiency. A scrambled siControl probe was used to account for potential expression changes due to non-specific effects of the transfection/silencing process.

Western blotting of protein samples harvested from cell lysate demonstrated increased LOXL2 expression with HIF promotion via IOX2 and DMOG **(Figure 6.1)**. Furthermore there was a complete absence of LOXL2 expression in siLOXL2 fibroblasts within all treatment samples, even with the highly potent LOXL2-promoting DMOG. As anticipated PLOD2 expression increased with

both IOX2 and DMOG, and importantly no significant difference in PLOD2 expression was seen between siControl and siLOXL2 treatment.

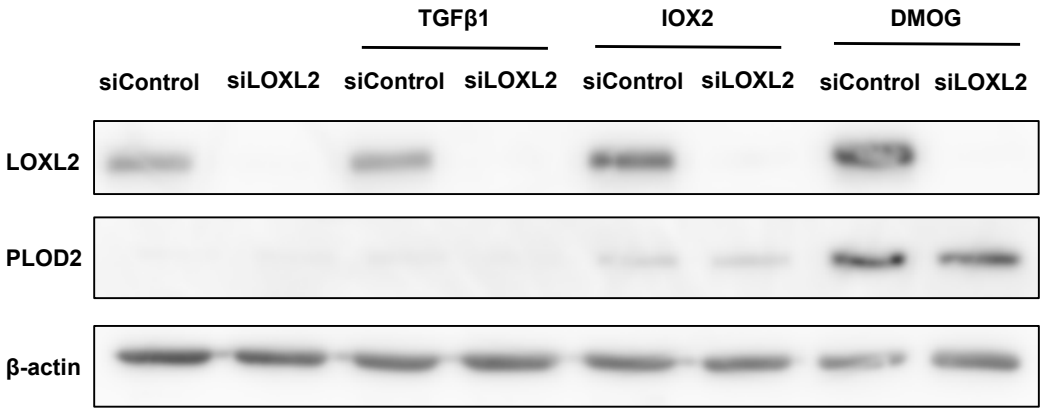

Figure 6.1: Short-interfering RNA effectively silences LOXL2 expression in lung fibroblasts exposed to a range of pro-fibrotic conditions. Western blotting for PLOD2 and LOXL2 in primary healthy lung fibroblasts exposed to IOX2 250μM or DMOG 0.5mM for 48 hours. β-actin was used as a loading control. Blot representative of experiments from N=3 IPF donors.

The efficacy of siLOXL2 was further evaluated using immunocytochemistry **(Figure 6.2)**. Primary healthy lung fibroblasts were transfected with siRNA targeting either *LOXL2* or a scrambled control, and cultured for 48 hours in the presence of IOX2 or DMOG before fixation and immunofluorescence staining for LOXL2 (green). Slides were counterstained for nuclear (DAPI – blue) and actin filament (phalloidin – red) fluorescence. In the siControl conditions an increase in LOXL2 fluorescence was observed with IOX2 and DMOG compared to vehicle control. LOXL2 fluorescence was predominantly seen in in a cytoplasmic and perinuclear distribution. In the siLOXL2 conditions only traces of LOXL2 fluorescence were seen (predominantly nuclear) in all treatment conditions, with marked loss of LOXL2 expression compared to siControl conditions.

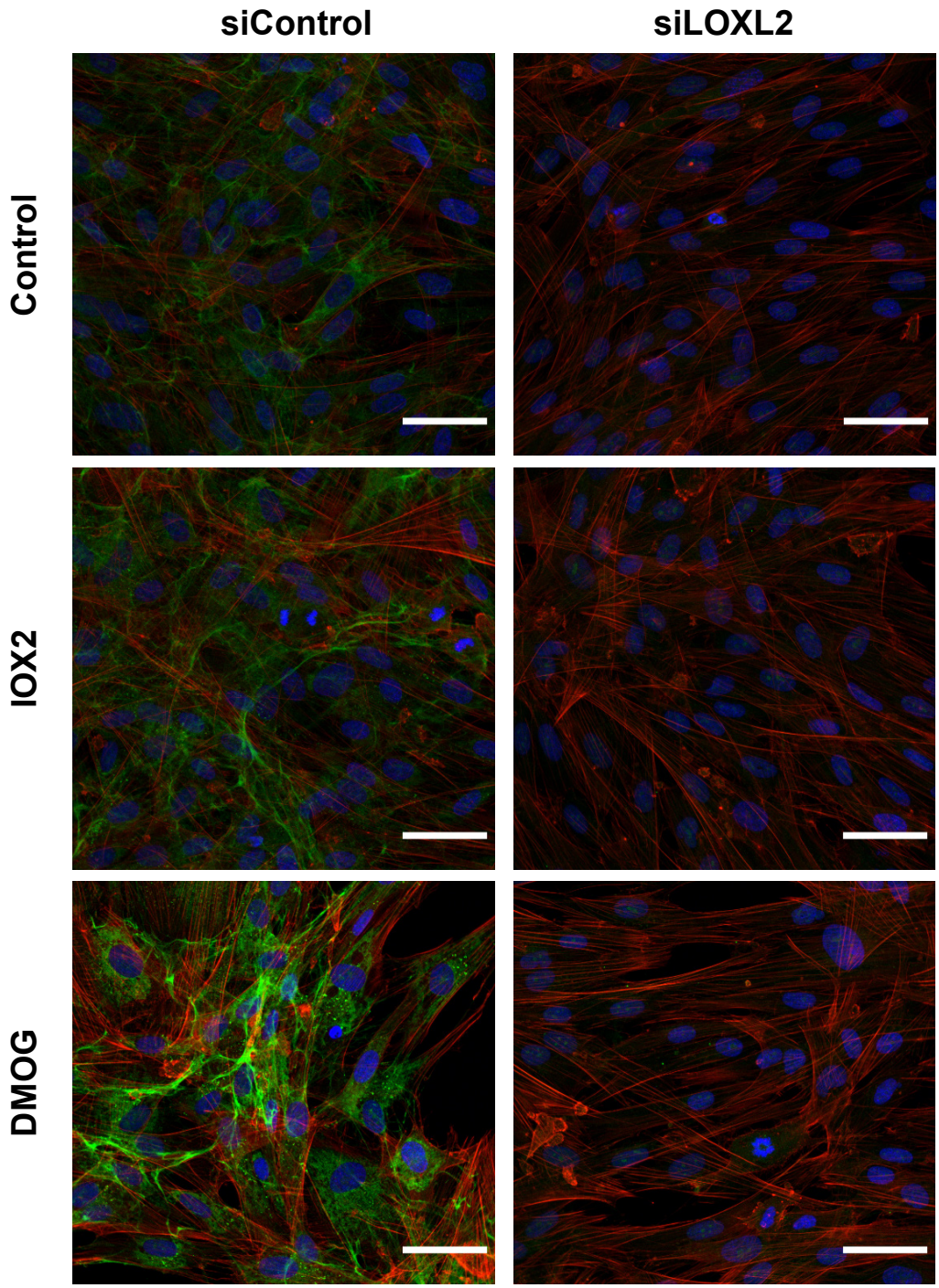

Figure 6.2: Suppression of LOXL2 expression using short-interfering RNA is effective despite HIF stabilising conditions. Confocal immunofluorescence of *LOXL2* (green), DAPI (blue – nuclear staining) and Phalloidin (red – actin filament staining) expression in primary healthy lung fibroblasts exposed to IOX2 250µM or DMOG 0.5mM for 48 hours. LOXL2 fluorescent intensity calibrated to DMOG condition. Scale bar 50µm. Representative images from N=1 experiment.

Both the western blotting and immunofluorescence analysis demonstrated highly efficient silencing of LOXL2 gene expression in primary lung fibroblasts. However it remained unclear how long this silencing efficacy would last in the long-term culture of the 3D fibroblastic focus model.

6.3.2 Incorporating short interfering RNA into a HIF-stabilised 3D fibroblastic focus model

A series of pilot experiments were performed, transfecting IPF lung fibroblasts with siRNA to silence the expression of either *HIF1α/HIF2α* or *LOXL2* in the 3D fibroblastic foci model. At 2 weeks post-transfection the samples were harvested for RNA and the mRNA expression fold change was analysed to determine the efficacy of the siRNA at this time point **(Figure 6.3)**.

At 2 weeks post-transfection of siRNA in the 3D fibroblastic focus model, the mRNA expression of *HIF1α* substantially was reduced with siHIF1/2α compared to siControl and siLOXL2 **(Figure 6.3 A)**. Similarly, compared to siControl and siLOXL2, samples transfected with siHIF1/2α demonstrated substantial reduction in *HIF2α* expression at 2 weeks **(Figure 6.3 B)**. The expression of *HIF3α* appeared to increase with siHIF1/2α compared to siControl, possibly as part of a regulatory feedback loop, although the changes were not statistically significant **(Figure 6.3 C)**. *LOXL2* mRNA expression was persistently reduced in 2 of the 3 donors exposed to siLOXL2 transfection after 2 weeks of culture in the 3D model, although the mean change of all 3 donors was not statistically significant **(Figure 6.3 D)**. No changes in *PLOD2* expression were evident in either siHIF1/2α or siLOXL2 conditions **(Figure 6.3 E)**, however siLOXL2 appeared to increase *COL1A1* expression in the 3D model at 2 weeks, with the difference between means being close to reaching statistical significance ($p = 0.0546$) **(Figure 6.3 F)**.

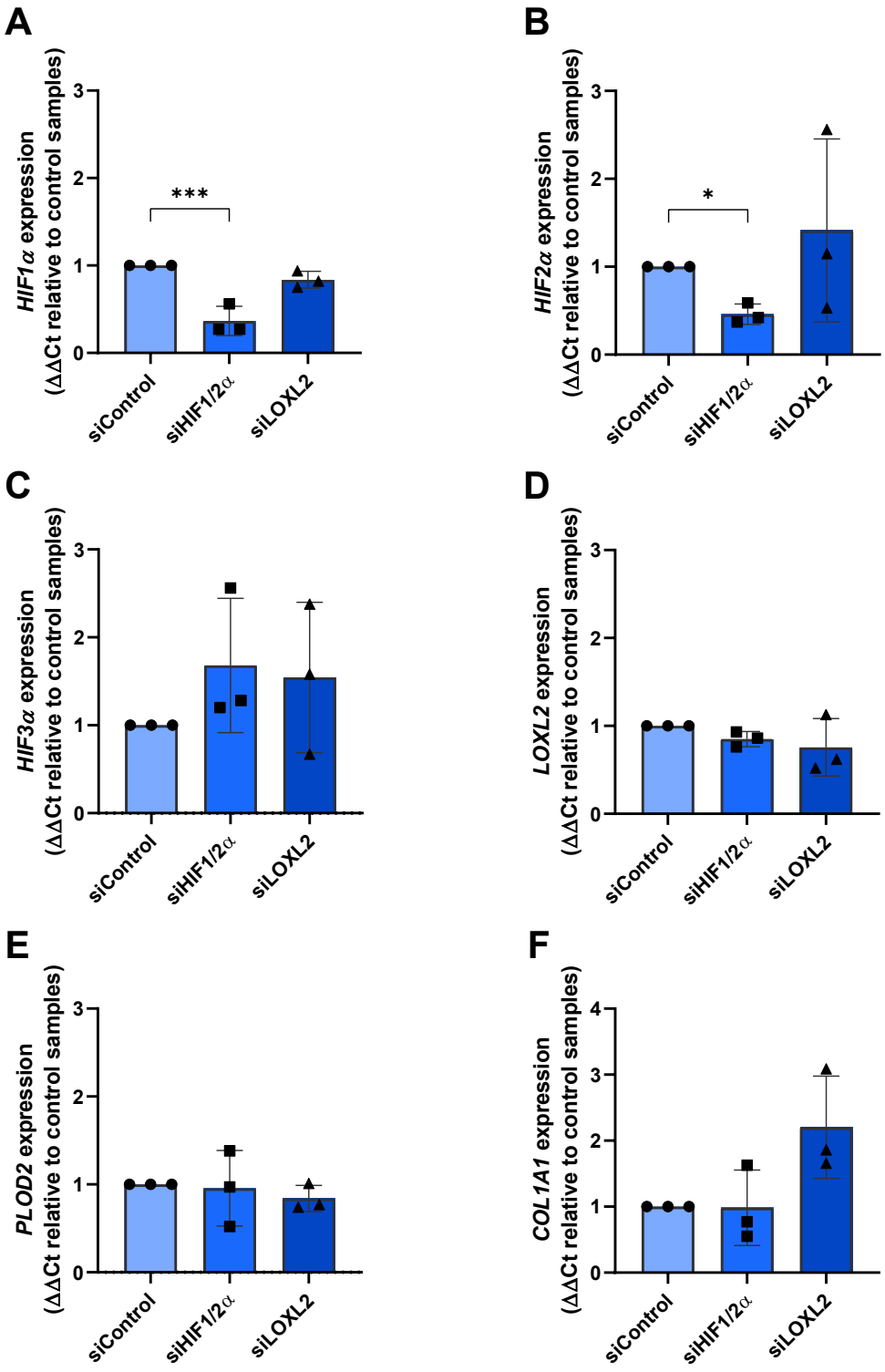

Figure 6.3: Efficacy of short-interfering RNA in the 3D fibroblastic focus model after 2 weeks. mRNA expression of **(A)** *HIF1α*, **(B)** *HIF2α*, **(C)** *HIF3α,* **(D)** *LOXL2*, **(E)** *PLOD2,* and **(F)** *COL1A1* in the 3D fibroblastic foci model following 2 weeks culture in 3D model media without additional treatment conditions. mRNA expression levels were determined using the ΔΔ CT method with grouped analysis and multiple comparisons (Dunnett's test). * $p < 0.05$, **** $p < 0.0001$. N=3 IPF donors in a single experiment.

As an extracellularly secreted protein, LOXL2 can be detected in cellular media, and the media from 3D model samples exposed to siRNA treatment was subsequently analysed to determine if there was any change in LOXL2 secretion. Media was also blotted for carbonic anhydrase 9 (Ca9), a downstream transmembrane marker of HIF activation, which has also been detected in cell media previously[280]. Equal volumes of media from each condition was collected at 72 hours and blotted for LOXL2 and Ca9 **(Figure 6.4 A)**. No extracellularly secreted LOXL2 was observed in the siLOXL2 conditioned media compared to siControl and siHIF1/2α at 72 hours **(Figure 6.4 A-B)**. Notably, despite regulation of *LOXL2* expression through HIF1/2α pathways, the efficacy of HIF1/2α silencing in our 3D model was not sufficient to modulate secretion of LOXL2 into siHIF1/2α cellular media at 72 hours (**Figure 6.4 A-B)**. However in one donor, a reduced level of Ca9 was observed in the siHIF1/2α conditioned media at 72 hours post transfection compared to siControl and siLOXL2, suggesting some impact of siHIF1/2α on downstream hypoxia pathways **(Figure 6.4 A)**.

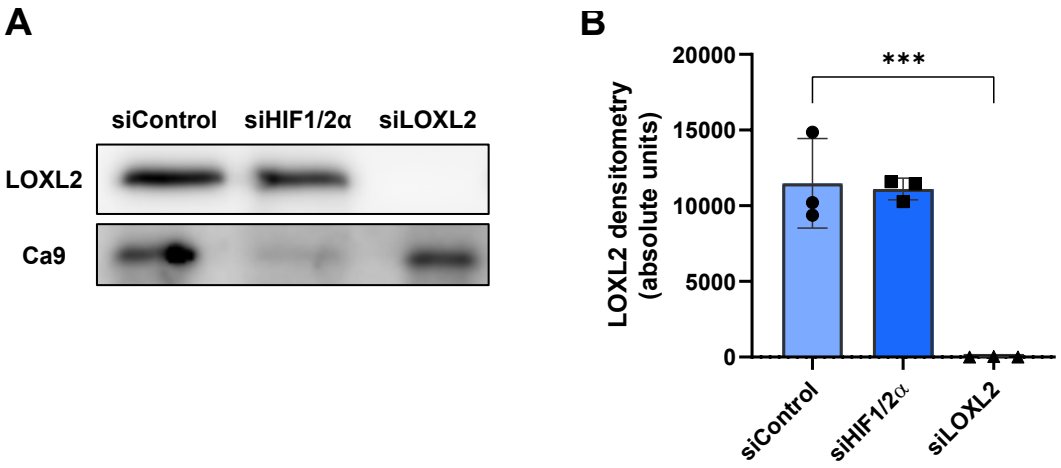

Figure 6.4: Short-interfering RNA targeting LOXL2 substantially reduce LOXL2 enzyme in cell media at 72 hours. (A) Cell media analysed for expression of LOXL2 or Ca9 using western blot of equal volumes (40µL) media from each siRNA condition. Media from 3 IPF donors blotted for LOXL2 and 1 donor blotted for Ca9. **(B)** Densitometry analysis of western blots for LOXL2 in cell media at 72 hours following transfection of 3 IPF donors with LOXL2 siRNA. N=3 IPF donors in two experiments.

These results established the viability of incorporating siRNA into the 3D fibroblastic focus model, with gene silencing observed from 72 hours and up to 2 weeks post-transfection. It remained unclear however if the transfected state would last until the full 3D model culture termination at 6 weeks. Therefore the efficacy of siRNA in the 3D fibroblastic focus model was subsequently analysed at 6 weeks using mRNA expression analysis **(Figure 6.5)**.

6 weeks after initial transfection the expression of *HIF1α*, *HIF2α* and *HIF3α* was similar across the silencing conditions, with the effects of siHIF1/2α in particular on *HIF1α* and *HIF2α* expression appearing to have fully reversed **(Figure 6.5 A-C)**. *LOXL2* expression was also similar across the siRNA conditions, with no discernible effects remaining in the siLOXL2 condition at 6 weeks **(Figure 6.5 D).** *PLOD2* expression was broadly similar across conditions **(Figure 6.5 E)** however *COL1A1* expression was slightly reduced in siHIF1/2α at 6 weeks and significantly reduced in the siLOXL2 condition **(Figure 6.5 F)**. The reason for this result is unclear, however given the increase in *COL1A1* expression at 2 weeks post-transfection of siLOXL2, this change could represent a negative feedback as the gene silencing effects subsided.

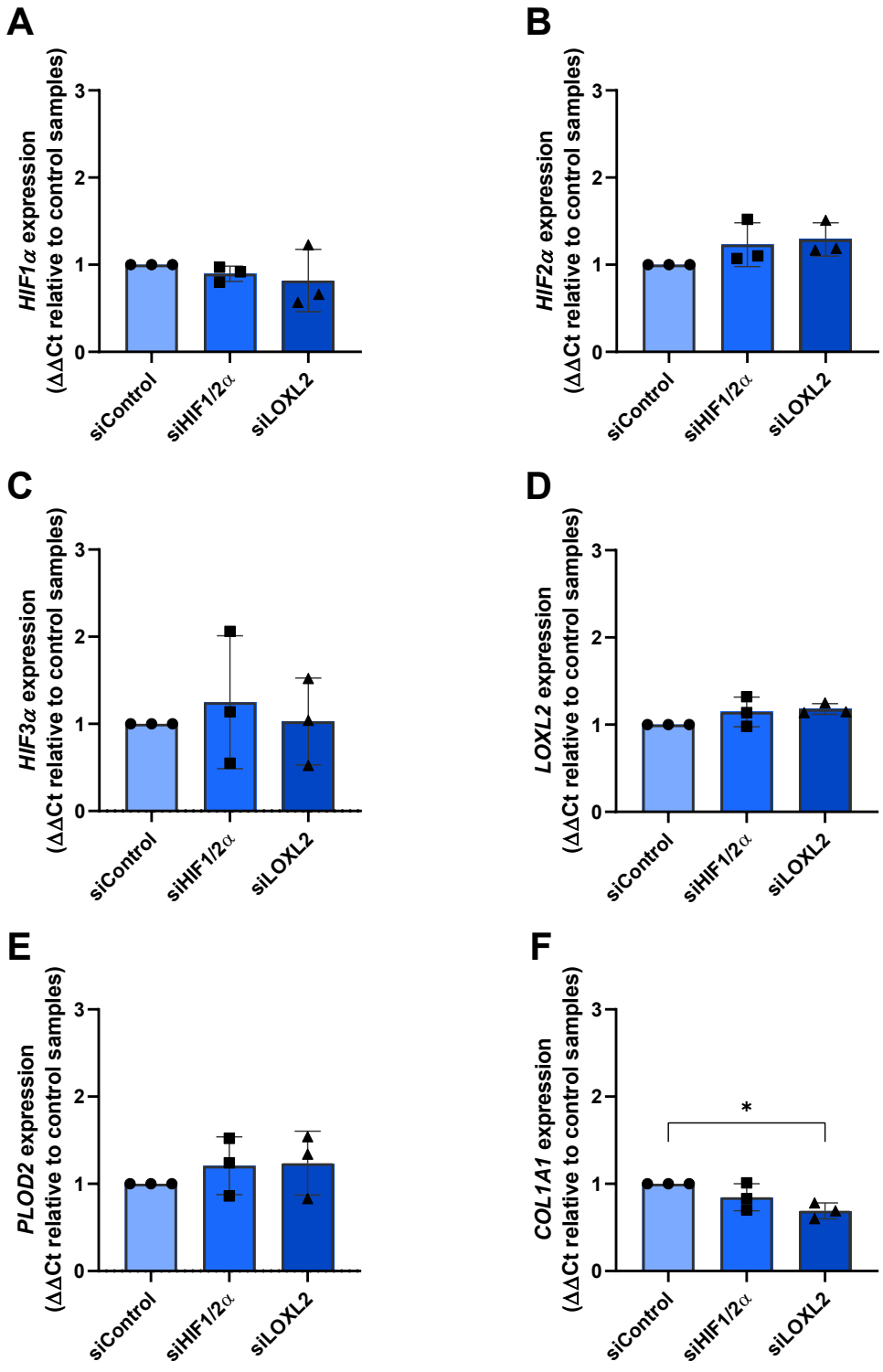

Figure 6.5: Short-interfering RNA targeting HIF1/2α and LOXL2 have no lasting effect on mRNA expression in 3D fibroblastic foci model at 6 weeks post-transfection. mRNA expression of **(A)** *HIF1α*, **(B)** *HIF2α*, **(C)** *HIF3α,* **(D)** *LOXL2*, **(E)** *PLOD2,* and **(F)** *COL1A1* in the 3D fibroblastic foci model cultured for 6 weeks. mRNA expression levels were determined using the ΔΔ CT method with grouped analysis and multiple comparisons (Dunnett's test). * $p < 0.05$. N=3 IPF donors in two experiments.

To investigate the silencing efficacy in this 6 week model further, LOXL2 was blotted from cellular media taken at weeks 1, 2, 4 and 6 after transfection with siRNA **(Figure 6.6)**. Minimal LOXL2 secretion was seen in all treatment conditions at week 1 post-transfection. At 2 weeks post transfection media taken from the siLOXL2 condition still had undetectable LOXL2 expression, while siControl and siHIF1/2α had detectable LOXL2 expression. However between 4 and 6 weeks the level of LOXL2 expression normalised in siLOXL2-treated conditions, suggesting a loss of gene silencing between this period post transfection. Again, the efficacy of HIF1/2α silencing was insufficient at all time periods to alter the secretion of LOXL2 into siHIF1/2α cellular media, possibly due to a lack of sufficient HIF pathway activation to detect any changes.

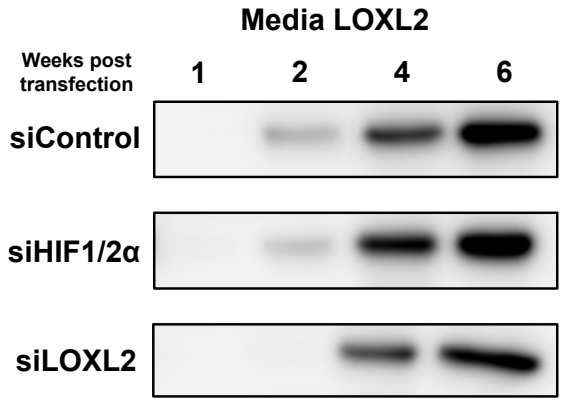

Figure 6.6: Extracellular LOXL2 secretion is reduced 2 weeks following LOXL2 short-interfering RNA transfection, but efficacy wanes between 4 and 6 weeks post transfection. Western blotting of LOXL2 in 40uL of conditioned media from the apical well of the 3D fibroblast model at 1, 2, 4 and 6 weeks post-transfection with LOXL2 siRNA. Blot representative of N=3 IPF donors in 2 separate experiments.

From these results it was determined that siRNA could be incorporated into the 3D model however the efficacy of gene silencing was variable and subsided between 2 and 6 weeks of culture. It remained unclear if the early period of gene silencing had any downstream effects on matrix stiffness or collagen modification at the 6 week time point. It was hypothesised that the initial silencing period may have residual effects out to 6 weeks on collagen structure and tissue stiffness.

Tissue stiffness was therefore measured in spheroids harvested at 6 weeks following exposure to either control (n=6 samples per condition) or 5 weeks of IOX2 (n=12 samples per condition) using parallel plate compression testing, followed by hydrolysis and quantification of protein, collagen and pyridinoline cross-links **(Figure 6.7)**.

Consistent with previous findings, siControl spheroids exposed to HIF stabilisation through IOX2 were twice as stiff as spheroids unexposed to IOX2 **(Figure 6.7 A-B)**. Furthermore, siHIF1/2α and siLOXL2 spheroids exposed to 6 weeks of control media were no less compliant than siControl spheroids, however on exposure to IOX2, gene silencing of *HIF1α/2α* or *LOXL2* conferred a reduction in tissue stiffness to an almost equivalent level seen in control conditions, suggesting efficacy for early HIF1/2α and LOXL2 gene silencing to alter IOX2-mediated changes to matrix compliance.

No differences in collagen quantity normalised to protein was observed for any of the siRNA conditions **(Figure 6.7 C)**. Pyridinoline cross-link density per collagen molecule was increased in the IOX2 exposed spheroids compared to control spheroids, however no significant difference was detected between either siHIF1/2α or siLOXL2 and control despite reduced tissue stiffness **(Figure 6.7 D)**. While this might suggest the reduction in tissue stiffness by both siHIF1/2α and siLOXL2 was not related to pyridinoline cross-linking, an alternative explanation is that methodological limitations in the measurement of pyridinoline may have prevented any detection in effect size. Specifically, outgrowths of daughter cells from the fibroblastic focus which grow from the 6 weeks culture, while not having any material impact on the tissue stiffness, are likely to influence the results of collagen cross-linking sampling **(Figure 6.7 E)**. These cells develop in the latter part of the culture period and are likely to have the least amount of siRNA effect, thereby possibly explaining the discrepancy in results.

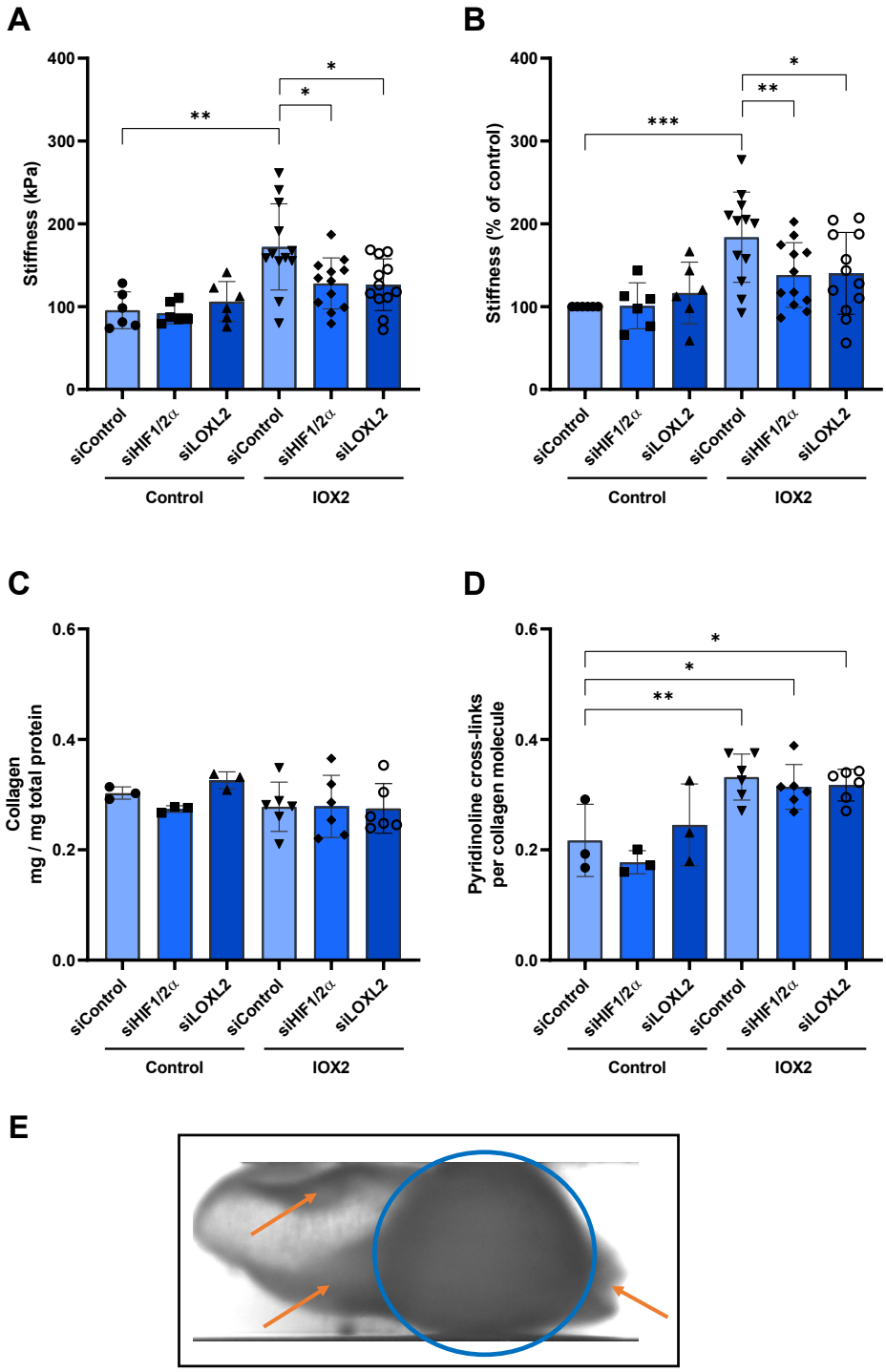

Figure 6.7: Short-interfering RNA targeting HIF1/2α and LOXL2 is capable of reducing tissue stiffness in a HIF-stabilised 3D fibroblastic model, but a change in collagen or pyridinoline cross-links is not observed. Tissue stiffness of siRNA spheroids exposed to either control or IOX2, measured by parallel plate compression testing and illustrated both in **(A)** absolute levels of stiffness (kPa) of control and IOX2 samples and **(B)** percent of paired control samples. Samples were subsequently hydrolysed before measurement of **(C)** Collagen (hydroxyproline) content normalised to protein and **(D)** mature pyridinoline cross-links normalised to collagen. **(E)** Representative

image of spheroid (blue circle) undergoing parallel plate compression with sheets of outgrowth tissue (orange arrows) visible. Significance determined with grouped analysis and multiple comparisons (Dunnett's test). * p< 0.05, ** p< 0.01, *** p< 0.001. Data from N=2 experiments using 3 IPF donors each (in quadruplicate), with stiffness measurements from N=12 samples and collagen and cross-link analysis from N=6 samples.

These results reveal the potential for both upstream inhibition of HIF pathways and downstream inhibition of LOXL2 expression to interfere with ECM changes as a result of HIF stabilisation.

6.3.3 Applying HIF inhibitors to primary IPF fibroblasts in conditions of HIF stabilisation

HIFα subunits represent potential targets for preventing downstream HIF pathway activation. HIF inhibitors are an expanding and heterogeneous group of compounds with a range of mechanistic effects and mixed selectivity for specific HIFα subunits. Three candidate inhibitors were identified which have previously been tested on human cells and demonstrate established HIFα inhibition *in vitro*. Digoxin, a commonly prescribed medication for its effects in prolonging the cardiac action potential but which also inhibits HIF1α mRNA expression, was selected due to previous work exploring effects on reducing HIF-mediated LOX(L) family expression, as well as its established presence in clinical use[281,282]. Echinomycin, an antibiotic originally isolated from Streptomyces bacteria, prevents binding of HIFα/β complex to the HRE to exert downstream effects of HIF pathways, and is increasingly used as a HIF inhibitor with anti-neoplastic effects[283-285]. The final selection was NSC134754, a novel inhibitor of HIFα translation with previous studies of *in vitro* and *in vivo* efficacy in cancer models[286-288]. These three compounds were selected for their different mechanisms of HIF inhibition and, to the best of our knowledge, appeared to be well tolerated at HIF-inhibiting doses in malignant cell lines. However it remained unclear how these HIF inhibiting compounds would be tolerated in human primary lung fibroblasts. A series of dose-finding pilot experiments was therefore performed using these 3 HIF inhibitors with primary IPF lung fibroblasts over 48 hours.

IPF lung fibroblasts were exposed to both IOX2 and digoxin at a dose range from 10nM to 100nM for 48 hours **(Figure 6.8)**. Cellular morphology was observed at 48 hours prior to harvest of cell lysate for protein and western blotting for HIF1α and LOXL2 after a BCA protein quantification to ensure equal loading. Western blot revealed a potent dose-dependent inhibitory effect of digoxin on both HIF1α and LOXL2 expression, with almost complete suppression of HIF1α and LOXL2 at 100nM **(Figure 6.8 A)**. However increasing doses of digoxin also resulted in a decline in cell lysate

protein concentration **(Figure 6.8 B)** and clear reductions in cell density, suggesting cellular toxicity even at lower doses of 25 – 50nM **(Figure 6.8 C)**.

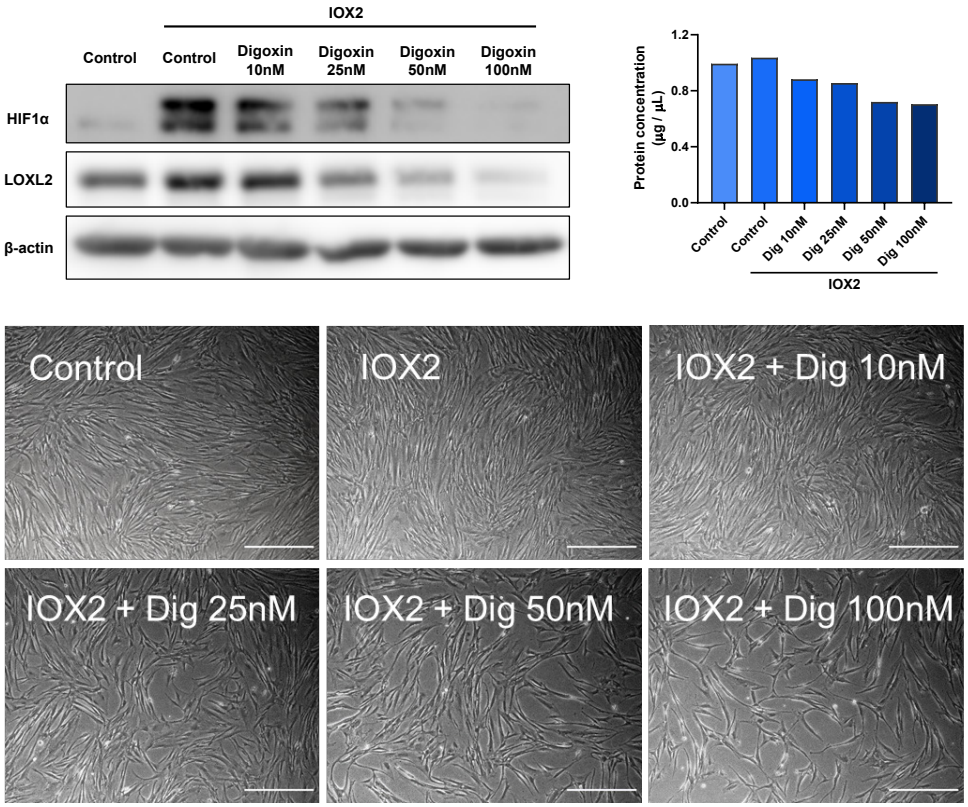

Figure 6.8: Digoxin inhibits HIF1α and LOXL2 expression in HIF-stabilised lung fibroblasts however appears to exert a dose-dependent toxic effect. Primary IPF lung fibroblasts were exposed to control media or IOX2 250µM with increasing doses of digoxin (10nM – 100nM). **(A)** Western blotting of cell lysate for HIF1α and LOXL2 using β-actin as a loading control. **(B)** BCA protein quantification of cell lysate in µg/µL. **(C)** Cellular morphology at 48 hours just prior to harvest. Scale bar 500µm. N=2 IPF donors in a single experiment.

The second HIF inhibitor, echinomycin, was subsequently applied to IPF lung fibroblasts in an identical experiment at concentrations of 1 – 20nM before morphological analysis, cell lysis for protein and western blotting for PLOD2 and LOXL2 **(Figure 6.9)**. While the lowest dose of Echinomycin (1nM) appeared to counterintuitively increase PLOD2 expression there was a clear reduction in LOXL2 expression compared to the IOX2-only condition, and increasing doses of 5-20nM appeared to suppress both PLOD2 and LOXL2 expression **(Figure 6.9 A)**. However increasing doses of echinomycin also appeared to have a toxic effect on lung fibroblasts, with a decrease in protein concentrations of cell lysate **(Figure 6.9 B)** and a reduction in cell density on morphological analysis even at the lowest dose of 10nM **(Figure 6.9 C)**.

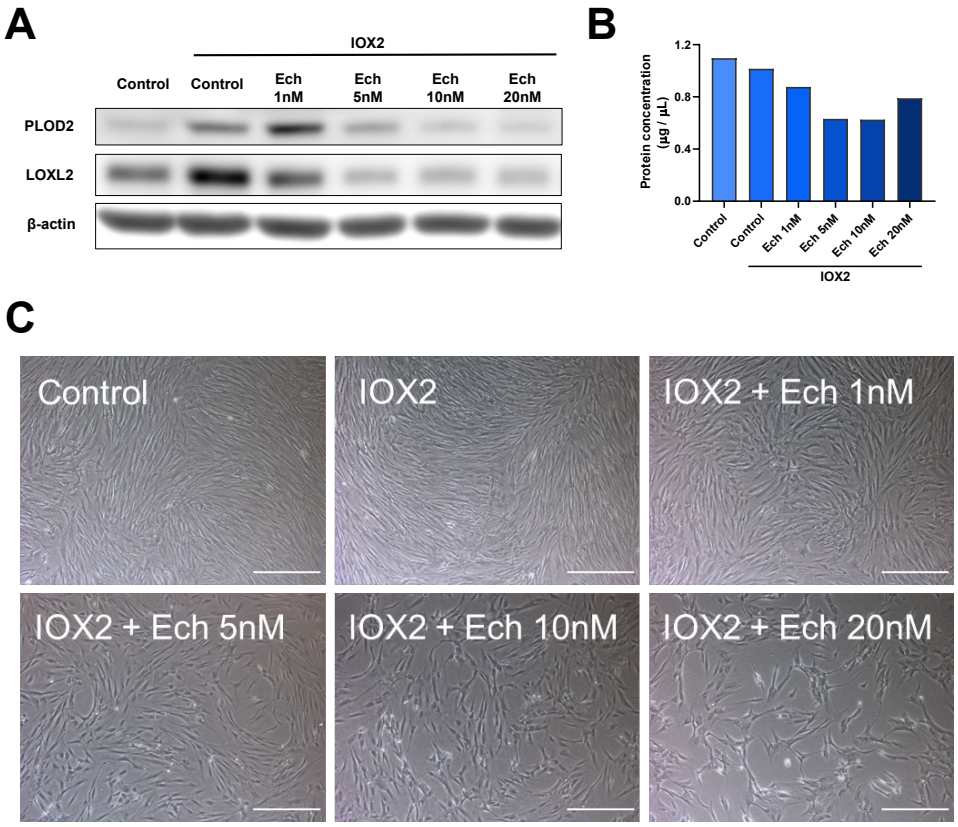

Figure 6.9: Echinomycin suppresses HIF-mediated PLOD2 and LOXL2 expression in lung fibroblasts however also confers dose-dependent cellular toxicity. Primary IPF lung fibroblasts were exposed to control media or IOX2 250µM with increasing doses of echinomycin (1nM – 20nM). **(A)** Western blotting of cell lysate for PLOD2 and LOXL2 using β-actin as a loading control. **(B)** BCA protein quantification of cell lysate in µg/µL. **(C)** Cellular morphology at 48 hours just prior to harvest. Scale bar 500µm. N=2 IPF donors in a single experiment.

Finally, the HIF inhibitor NSC134754 was tested in identical conditions on IPF lung fibroblasts, using a range of doses from 100nM through to 20µM, followed by morphological assessment, protein analysis and western blot **(Figure 6.10)**. Between doses of 100nM and 1µM, NSC134754 did not appear to have any demonstrable effect on PLOD2 expression, however exerted a dose-dependent inhibition on LOXL2 expression **(Figure 6.10 A)**. At doses above 1µM there was suppression of both PLOD2 and LOXL2 expression. Similarly to the other two HIF inhibitors however a dose-dependent effect on cellular viability was observed at doses greater than 500nM in both protein concentration **(Figure 6.10 B)** and cell density **(Figure 6.10 C)**.

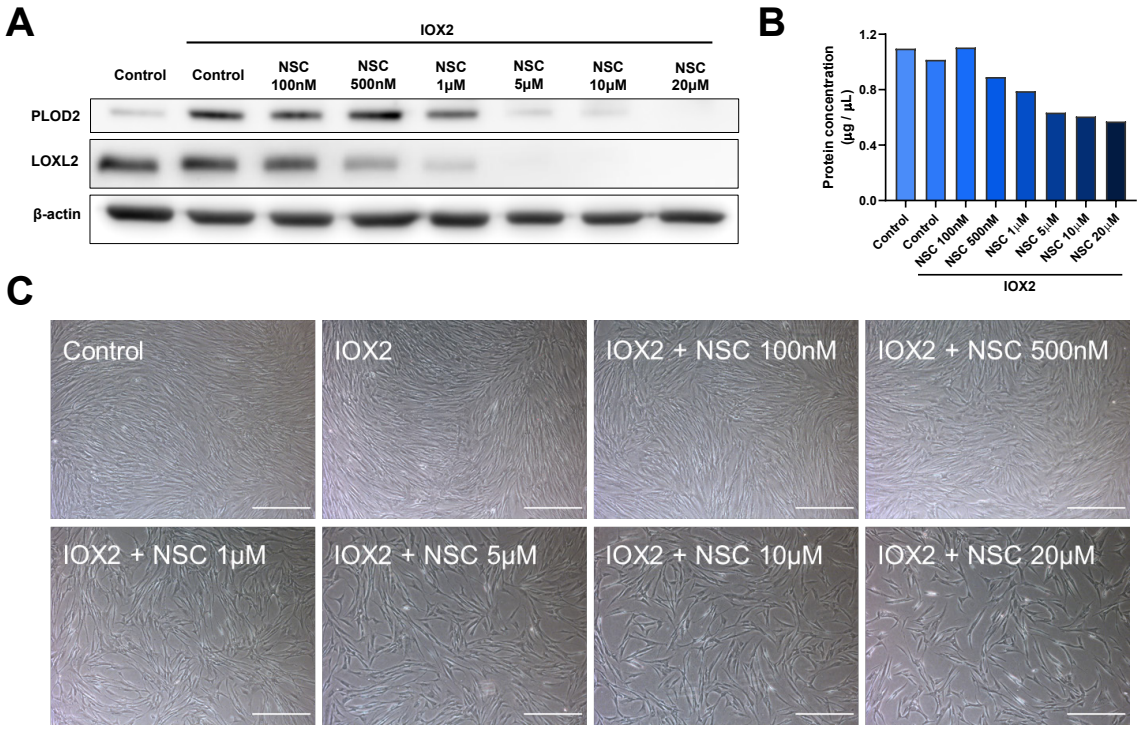

Figure 6.10: The HIF inhibitor NSC134754 suppresses HIF-mediated PLOD2 and LOXL2 however has dose-dependent effects on cellular viability. Primary IPF lung fibroblasts were exposed to control media or IOX2 250μM with increasing doses of NSC134754 (100nM – 20μM). **(A)** Western blotting of cell lysate for PLOD2 and LOXL2 using β-actin as a loading control. **(B)** BCA protein quantification of cell lysate in μg/μL. **(C)** Cellular morphology at 48 hours just prior to harvest. Scale bar 500μm. N=2 IPF donors in a single experiment.

In summary these pilot studies using established HIF inhibitors to modulate the HIF-mediated effects on collagen cross-linking expression had mixed results. While all three compounds demonstrated the ability to suppress collagen cross-linking expression in a dose-dependent fashion they also exhibited significant toxic effects with reductions in cell density and lysate protein concentrations at 48 hours of culture. These effects were visible even at lower doses of the inhibitors. It was unclear from these experiments if the toxic effects were secondary to their HIF-inhibitory actions or off-target effects of the individual compounds. However none of these compounds were deemed suitable to pursue further in the form a 3D fibroblastic focus model experiment, where the longer culture periods (6 weeks) would require a compound with minimal cytotoxicity. While HIF inhibitors remain a promising avenue for future exploration, further analysis was beyond the scope of this study.

6.3.4 Selective and pan-inhibition of LOX(L) activity in a HIF-stabilised 3D fibroblastic foci model

PXS-S2A is a haloallylamine-derived amine oxidase inhibitor capable of selective LOXL2/3 inhibition at lower doses (0.1µM) and pan-LOX(L) inhibition at higher doses (10µM) **(Figure 6.11)**[165]. The novel compound was previously used for selective LOXL2/3 inhibition in a TGFβ-only 3D fibroblastic focus model to demonstrate a reduction in tissue stiffness and normalisation of collagen fibril assembly at both lower doses selective for LOXL2/3 and higher doses which inhibit all LOX(L) members, yet it is unclear if this catalytic inhibitor is capable of abrogating the more extreme matrix changes from HIF pathway activation which mirror IPF disease.

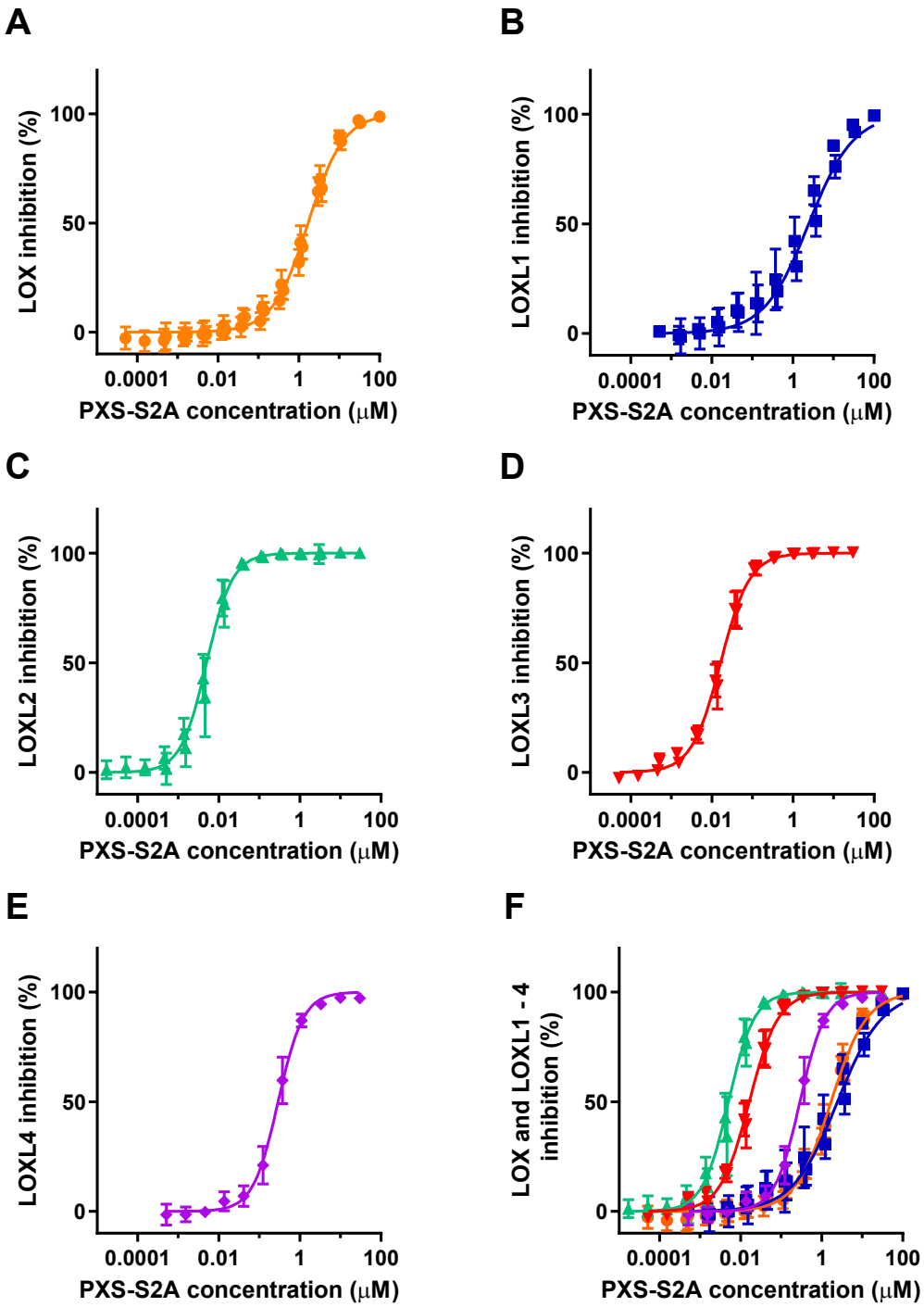

Figure 6.11: The LOX(L) catalytic inhibitor PXS-S2A exerts variable selectivity for LOX(L) enzymes which is dose dependent. Data from James Roberts, Synairgen Research Ltd demonstrating the inhibitory effect of PXS-S2A on **(A)** LOX, **(B)** LOXL1, **(C)** LOXL2, **(D)** LOXL3, **(E)** LOXL4 and **(F)** combined LOX(L) enzymes using bovine LOX and recombinant LOXL enzymes with an Amplex Red assay as per manufacturer instructions and putrescine as the substrate[131].

To determine the effect of LOX(L) inhibition on HIF pathway-mediated ECM remodelling PXS-S2A was tested in a 6 week 3D fibroblastic focus model. IPF lung fibroblasts were cultured for 1 week in the model before exposure for 5 weeks to control or low dose PXS-S2A without IOX2, or control, low dose or high dose PXS-S2A with IOX2. At 6 weeks samples were harvested and RNA isolated for RTqPCR to measure HIF pathway activation **(Figure 6.12)**. No differences in the downstream HIF pathway marker *Ca9* or in *HIF1α, HIF2α* or *HIF3α* mRNA expression were observed between samples exposed to vehicle control and PXS-S2A at either the low or high dose **(Figure 6.12 A-D)**. Consistent with previous results, IOX2 resulted in a substantial increase in expression of the downstream HIF-pathway marker Ca9 **(Figure 6.12 A)**, and a reduction in *HIF1α* expression compared to control conditions **(Figure 6.12 B)**. Smaller, non-significant reductions in *HIF2α* expression were observed **(Figure 6.12 C)** while no significant changes in *HIF3α* expression were observed between control and IOX2 samples **(Figure 6.12 D)**.

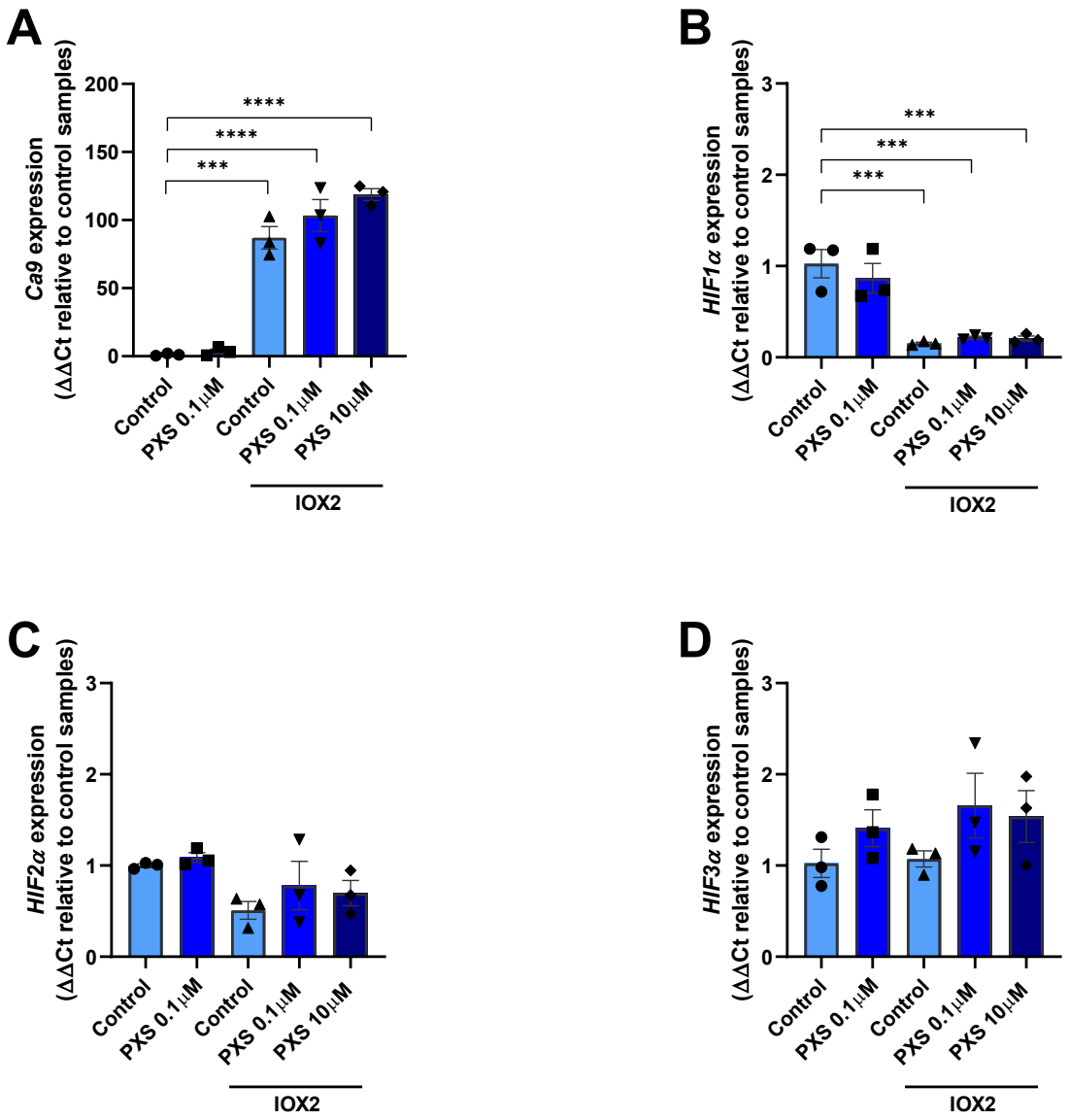

Figure 6.12: PXS-S2A has no effect on HIFα expression in a HIF-stabilised 3D fibroblastic foci model. mRNA expression of **(A)** *Ca9* **(B)** *HIF1α,* **(C)** *HIF2α* and **(D)** *HIF3α* in the 3D fibroblastic foci model exposed to conditioned media with control or IOX2 50μM and PXS inhibitor. mRNA expression levels were determined using the ΔΔ CT method with grouped analysis and multiple comparisons (Dunnett's test). *** $p < 0.001$. N=3 IPF donors.

Collagen cross-linking enzyme expression was also measured at 6 weeks **(Figure 6.13)**. PXS-S2A had no significant effect on the expression of *PLOD2* or *LOX(L)* enzymes within the samples **(Figure 6.13)**. Increases in *PLOD2*, *LOXL2* and *LOXL3* expression were observed in samples exposed to IOX2 **(Figure 6.13 A, C, D)**.

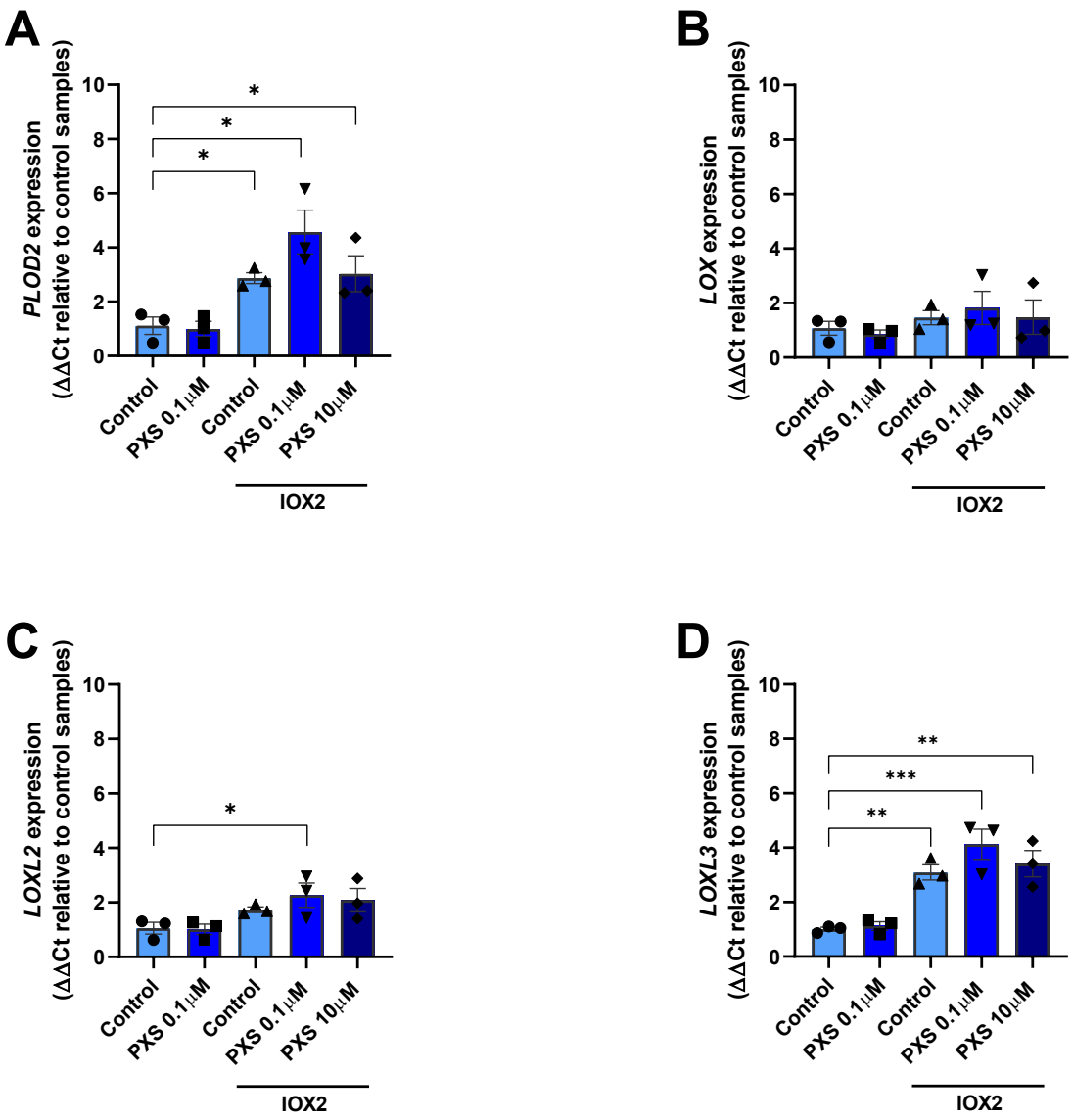

Figure 6.13: PXS-S2A does not significantly affect collagen cross-linking mRNA expression in a 3D fibroblastic foci model at 6 weeks. mRNA expression of *PLOD2, LOX, LOXL2* and *PLOD2* in the 3D fibroblastic foci model exposed to conditioned media with control or IOX2 50μM with or without PXS inhibitor. mRNA expression levels were determined using the ΔΔ CT method with grouped analysis and multiple comparisons (Dunnett's test). * $p < 0.05$, ** $p < 0.01$, *** $p < 0.001$. N=3 IPF donors.

Finally, mRNA expression of collagen fibrillogenesis genes *COL1A1* and *COL3A1* were tested in spheroids following 6 weeks in the 3D fibroblastic focus model **(Figure 6.14)**. No significant changes in *COL1A1* expression or *COL3A1* expression were observed in control of IOX2 conditions containing variable doses of PXS-S2A.

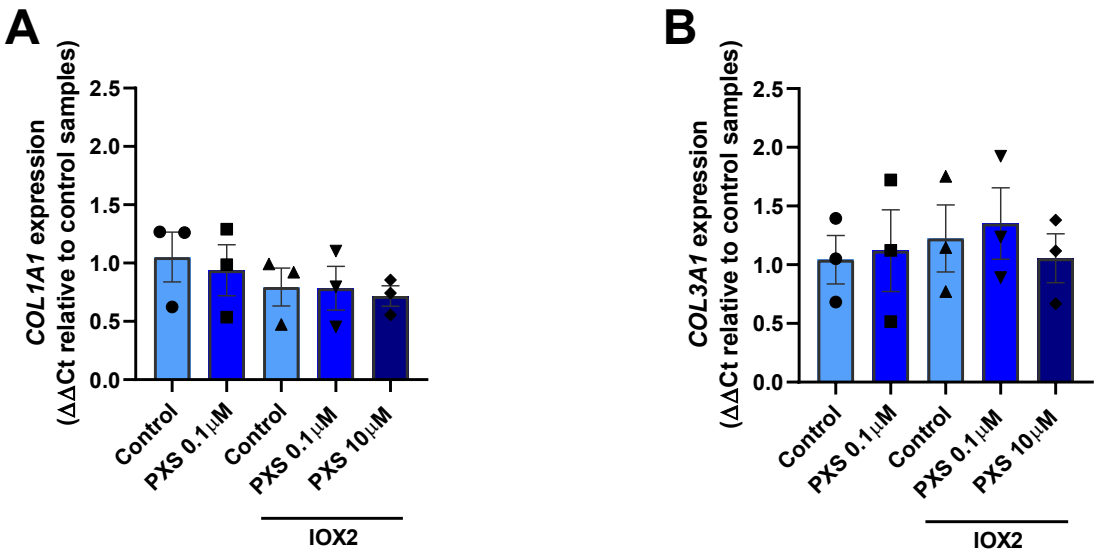

Figure 6.14: PXS-S2A has no effect on collagen mRNA expression in a HIF-stabilised 3D fibroblastic foci model. mRNA expression of *PLOD2, LOX, LOXL2* and *PLOD2* in the 3D fibroblastic foci model exposed to conditioned media with control or IOX2 50μM with or without PXS inhibitor. mRNA expression levels were determined using the ΔΔ CT method with grouped analysis and multiple comparisons (Dunnett's test). N=3 IPF donors.

These results suggested the 6 week fibroblastic focus model experiments incorporating the catalytic LOXL inhibitor PXS-S2A had adequate exposure to IOX2 to induce changes in HIF pathway and collagen cross-linking expression as previously established, while PXS-S2A itself did not appear to have any effect on collagen or collagen cross-linking gene expression.

To determine the effect of PXS-S2A on spheroid morphology and collagen fibrillogenesis samples were formalin fixed and paraffin embedded, sectioned and stained for H&E and picrosirius red while *PLOD2* and *LOXL2* mRNA expression was also examined *in-situ* using RNAscope mRNA hybridisation. **(Figure 6.15)**. On H&E staining low dose PXS-S2A did not appear to change spheroid morphology, including cellular density or ECM abundance, either with or without the presence of IOX2. In the IOX2 conditions, H&E staining revealed high dose PXS-S2A to reduce spheroid stromal structure, although the amount of ECM was unchanged. Analysis of sections stained for picrosirius red and viewed under polarised light however revealed no significant differences in collagen fibrillogenesis between the control and IOX2 samples with and without PXS-S2A at low or high doses. Additionally mRNA co-expression of *PLOD2* (red chromagen) and *LOXL2* (green chromagen) appeared uniformly distributed within all conditions.

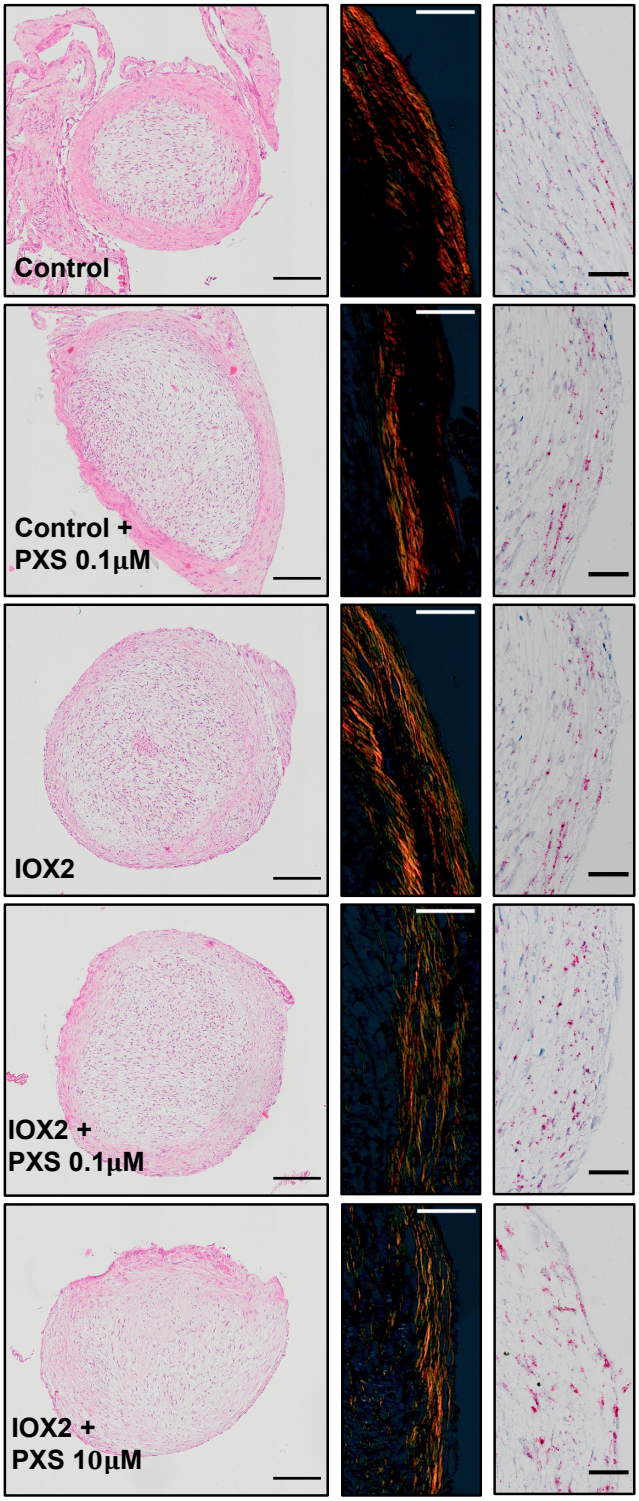

Figure 6.15: PXS-S2A does not alter extracellular matrix production, collagen fibrillogenesis or distribution of collagen-crosslinking enzyme expression in a HIF-stabilised 3D fibroblastic focus model. 3D fibroblastic foci model exposed to conditioned media with control or IOX2 with or without PXS inhibitor. H&E stains of spheroids (left column, scale bar 200µM), picrosirius staining under polarised light (middle column, scale bar 50µM) and duplex RNAscope for PLOD2 (red) and LOXL2 (green) mRNA expression (right column, scale bar 50µM). Images representative of N = 3 IPF donors.

To determine the effect of PXS-S2A on matrix compliance and collagen nano-architecture in HIF-pathway exposed samples parallel plate compression testing was performed, followed by spheroid hydrolysis and quantification of protein, collagen and pyridinoline cross-links **(Figure 6.16)**. HIF-pathway activation through IOX2 again resulted in substantially increased tissue stiffness compared samples that were not exposed to IOX2 **(Figure 6.16 A-B).** Notably selective LOXL2/3 catalytic inhibition with PXS-S2A at a concentration of 0.1µM reduced matrix stiffness in samples both exposed and unexposed to IOX2, compared to vehicle control. Pan-LOX(L) inhibition using PXS-S2A 10µM substantially reduced tissue stiffness in IOX2-conditioned media. Similarly to earlier experiments, samples exposed to IOX2 had a moderate reduction in collagen content **(Figure 6.16 C)**. Intriguingly PXS-S2A at the higher, pan-LOX(L)-inhibiting concentration appeared to increase collagen content of the samples, possibly due to positive feedback on collagen production from the highly compliant tissue, although as noted earlier no significant changes in *COL1A1* or *COL3A1* expression were observed at 6 weeks.

Pyridinoline cross-links were again increased with HIF pathway activation through IOX2, while selective LOXL2/3 inhibition with PXS-S2A 0.1µM resulted in a non-significant reduction in cross-link density in both non-conditioned and IOX2-conditioned media **(Figure 6.16 D)**. This may represent an effect size too small to be statistically significant with n=6 samples, or could reflect additional factors contributing to matrix stiffness outside of trivalent collagen cross-links. By contrast the higher, pan-LOXL(L)-inhibiting dose of PXS-S2A substantially inhibited pyridinoline cross-link density compared to vehicle controls. The dramatic reduction in pyridinoline density at the higher concentration also correlated with an increase in collagen content, suggesting a positive feedback loop driving collagen production to account for the reduction in compliance.

The large differences in both stiffness and pyridinoline cross-links between selective and pan-LOX(L) doses of PXS-S2A suggests shared cross-linking activity within the LOXL family upon HIF exposure that required broad catalytic inhibition in order to modulate successfully. More detailed dose-ranging experiments are required to explore this observation.

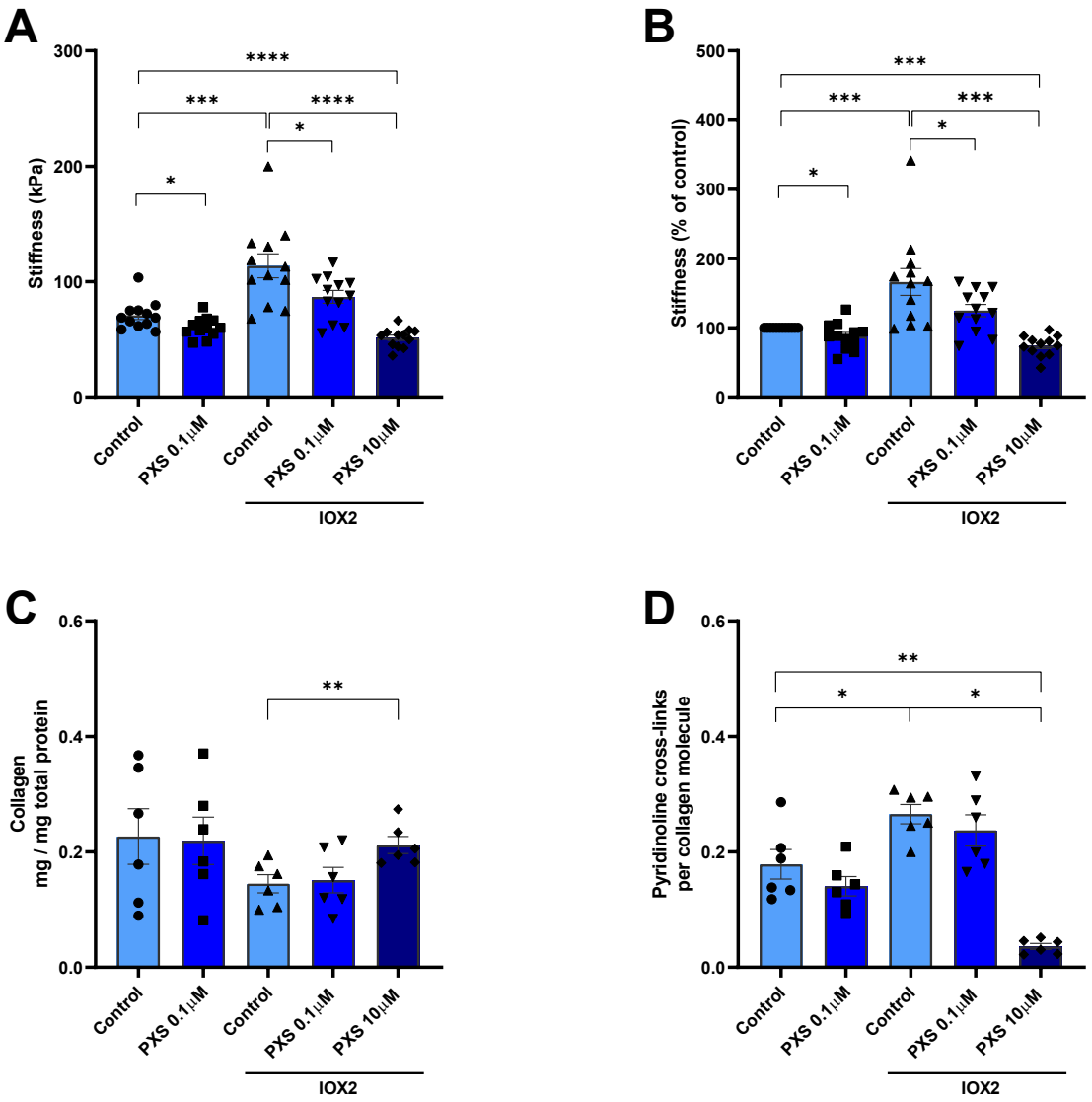

Figure 6.16: PXS-S2A reduces tissue stiffness and pyridinoline cross-links in a HIF-stabilised 3D fibroblastic model. (A) Tissue stiffness (kPa) of control and IOX2 samples and **(B)** Tissue stiffness (% control) of IOX2 samples only) measured by parallel plate compression testing. Samples were subsequently hydrolysed before measurement of **(C)** Collagen (hydroxyproline) content normalised to protein and **(D)** Mature pyridinoline cross-links normalised to collagen. Significance determined with grouped analysis and multiple comparisons (Dunnett's test). * $p< 0.05$, ** $p< 0.01$, *** $p< 0.001$, **** $p < 0.0001$. Data from N=2 experiments using 3 IPF donors each (in quadruplicate), with stiffness measurements from N=12 samples and collagen and cross-link analysis from N=6 samples.

6.4 Discussion

HIF stabilisation within the 3D fibroblastic focus model recapitulates the ECM changes seen in the IPF lung, representing an important advancement for *in vitro* models with which novel antifibrotic compounds can be tested. In particular, compounds which target pathological collagen cross-linking activity or their upstream promoters could normalise matrix compliance and prevent the mechanosensitive feed-forward loops which are postulated to sustain progressive fibrosis. The aim for this study was to examine HIF signalling and downstream LOX(L) dysregulation as modifiable targets of matrix reorganisation in the HIF-stabilised 3D fibroblastic focus model, initially with gene silencing and then subsequently through application of therapeutic compounds which inhibited upstream HIF or downstream collagen cross-linking activity.

Treatment with siHIF1/2α and siLOXL2 in the 3D fibroblastic focus model demonstrated gene silencing efficacy for at least 2 weeks, although was insufficient to substantially suppress gene expression at 4 or 6 weeks. Importantly, matrix changes were seen with both siHIF1/2α and siLOXL2 in IOX exposed conditions, suggesting a treatment effect with the inhibition of these pathways that may translate to the IPF lung. Discrepancies between matrix compliance and pyridinoline cross-linking within samples require could represent technical limitations of the study or alternatively extra-pyridinoline mechanisms, and require further validation.

Several problems were foreseen which could reduce the efficacy of siRNA in this format. Firstly sufficient maturation of trivalent pyridinoline collagen cross-links required a 6 week culture process, and the longevity of the siRNA transfection had not been tested over this time period before. Secondly after application of the 3D media to form fibroblast spheroids the surface area would be greatly reduced compared to a cell sheet, and therefore penetration of the siRNA to the spheroid core could be greatly reduced. To enhance the longevity of gene silencing and avoid difficulties with penetration two transfections of siRNA were applied, one on cell seeding and a second transfection at day 7 (just prior to spheroid formation). Despite this however, loss of gene silencing was observed between 2 and 4 weeks after initial transfection, which is likely to have impacted downstream matrix readouts such as collagen cross-linking at the 6 week time point.

Additionally there were unforeseen problems with incorporating siRNA into the 3D model. The non-specific effects of the siRNA process (separate to specific gene silencing), on collagen synthesis and modification were unknown prior to this investigation. While a siRNA control (scrambled) was included to account for off-target effects of gene silencing, the increases in matrix stiffness seen across all samples was not anticipated. While the effect was consistent across two independent experiments, a non-siRNA control would have been useful to confirm this to be an effect of the transfection process. It remains unclear how siRNA transfection may

increase matrix stiffness however off-target effects are well recognised and it is possible that cellular toxicity from the transfection process created a stress response which involves downstream fibroblast activation and matrix reorganisation[289,290]. Measurements of collagen content and pyridinoline cross-linking density in both control and HIF pathway-exposed samples were similar to previous non-siRNA experiments, suggesting the alterations in stiffness are independent of collagen cross-linking. Further research in this area is necessary to confirm this effect and identify underlying mechanisms.

As previously discussed, another unanticipated issue was the incorporation of spheroid outgrowths into the collagen and pyridinoline cross-link analysis. Discrepancy between pyridinoline density and matrix compliance in siHIF1/2α and siLOXL2 samples could be due to the dilution effect of these outgrowths, which were more likely to contain daughter cells with less siRNA-affected collagen. Future experiments excluding these outgrowths from sample hydrolysis will hopefully provide more accurate data.

As an exploratory arm of the study, this experiment was limited to just two treatment conditions – siHIF1/2α and siLOXL2 – however a number of other pathways are worth interrogating both in combination and individually. Gene silencing of other LOX(L) enzymes would enable a comparison of the relative effect of each family member on matrix remodelling, and also answer a key question on the redundancy of individual members. PLOD2 has been identified as a critical enzyme for telopeptide lysine hydroxylation, thereby creating the substrate for LOX(L) enzyme activity. Pyridinoline cross-links are present in healthy tissue (albeit at a lower level) and it is unclear if silencing PLOD2 would simply normalise pathological collagen cross-linking or instead produce an abnormally compliant ECM devoid of all cross-linking.

Future experiments may benefit from alternative methods of gene silencing. Gene editing techniques incorporating Clustered Regularly Interspaced Short Palindromic Repeats (CRISPR) and the CRISPR-associated (CAS)9 enzyme are increasingly available and capable of generating robust genetically-modified cell lines[291]. More importantly the durability of gene silencing with such techniques are better suited to the long-term culture requirements of our 3D fibroblastic focus model. These new methodologies could be applied to dissect the relevance and functional differences of individual HIF and LOX(L) isoforms on ECM biomechanics.

HIFs are increasingly implicated at multiple stages in IPF pathogenesis and HIF inhibition could be a novel therapeutic target to suppress aberrant mesenchymal activity and pathological ECM modifications. However no suitable candidates were identified in this study for long term culture, with all three selected inhibitors demonstrating a narrow therapeutic window with dose dependent cellular toxicity at incremental doses. The cause for this cellular toxicity is unknown,

although the parallel findings using three alternative agents with different mechanisms of inhibition suggests HIF inhibition is poorly tolerated by lung fibroblasts exposed to IOX2. The anti- or pro-apoptotic effects of HIF pathway expression appear to depend on cellular context, and excessive HIF inhibition may indeed be detrimental to normal cellular responses[292]. Intra-tumoral hypoxia-mediated upregulation of HIF pathways in a variety of malignancies has driven research in HIF inhibition. Yet to date no HIF inhibiting agents have been approved for treatment, with a large proportion failing to move beyond *in vitro* testing and others unable to demonstrate therapeutic efficacy[293]. Furthermore the results from cancer research do not necessarily translate to pulmonary fibrosis, where the aim of HIF pathway inhibition is to normalise cellular function rather than trigger cell death.

This study has consistently identified PLOD2 and LOXL2 as collagen cross-linking enzymes of significance for therapeutic targeting, however there remains no commercially available selective inhibitor of PLOD2. Minoxidil has been identified as a non-selective inhibitor of PLOD1, 2 and 3, with a particular preference for PLOD1, yet previous reports have not demonstrated an effect of this agent on pyridinoline cross-links in collagen matrix[294]. The novel selective LOXL2/3 catalytic inhibitor, PXS-S2A, has previously been demonstrated to reduce pyridinoline collagen cross-links and matrix stiffness in the 3D fibroblastic focus model[165]. Here, these experiments were extended to incorporate the more IPF-relevant model involving HIF stabilisation within the 3D fibroblastic focus model. PXS-S2A at the selective LOXL2/3 concentration was capable of normalising tissue stiffness in HIF-modified matrix, while at the pan-LOX(L) dose PXS-S2A substantially reduced stiffness beyond the HIF-unexposed control, with pyridinoline cross-link densities mirroring this effect.

Intriguingly the relative drop in pyridinoline cross-linking was greater than the decline in matrix stiffness. One possible explanation could be the activation of other cross-linking enzymes which are unaffected by LOX(L) inhibition. In particular, tissue transglutaminase 2 creates calcium-dependent protein-to-protein cross-links and is activated by both TGFβ and HIF pathways, and takes an active role in the early phases of matrix remodelling, providing another potential mechanism for stiffness changes which is unaccounted for in our model[295-297].

The magnitude of difference between the selective and pan-LOX(L) concentrations suggests an element of redundancy in LOXL2/3 activity, with the inhibition of the other LOX(L) family members being required for further effect. Yet an 'optimal' level of matrix compliance for pulmonary interstitial function has not been defined and therefore it remains unclear if reducing collagen cross-linking and matrix compliance beyond control tissue levels is necessarily of benefit. Future experiments should explore a wider range of PXS-inhibitor concentrations to better

understand the relationship between pyridinoline cross-linking and matrix stiffness in this HIF-affected model.

6.5 Conclusion

Upstream HIF1/2α and downstream LOXL2 were successfully, but only transiently, silenced in a HIF-stabilised 3D fibroblastic focus model, with reductions in matrix stiffness observed suggesting efficacy of gene silencing of these pathways to interfere with pathologic collagen cross-linking. HIF-mediated changes in the 3D fibroblastic focus were also normalised through selective catalytic inhibition of LOXL2/3, and at pan-LOX(L) doses matrix compliance was restored to levels seen in control conditions with associated profound reductions in pyridinoline cross-linking. The similarities in ECM compliance and collagen nanostructure between the HIF-stabilised fibroblastic foci model and the IPF condition render these findings even more important, with the potential for therapeutic development that may alter the extreme changes seen in the IPF lung. Furthermore these interventions have the potential to reduce the aberrant mechano-signalling which is increasingly recognised as a pathological driver of progressive fibrosis, enabling a resetting of ECM homeostasis and normalisation of collagen structure-function.

Chapter 7 Final Discussion and Future Work

7.1 Final discussion

7.1.1 Key findings

Building on the platform that excessive, mature 'bone-type' pyridinoline cross-links are a key determinant of ECM stiffness within IPF and a potential driver of sustained fibrogenesis, the aims of this study were to investigate the cellular sources of pyridinoline cross-linking enzyme expression in IPF, identify upstream signalling pathways, and examine downstream biomechanical effects of their dysregulation[165].

Through regionally selective RNA sequencing, substantially greater expression of *LOX(L)* family and *PLOD2* expression was seen within IPF fibroblastic foci compared to alveolar septae from either healthy or IPF donors. *LOXL2* exhibited the highest levels of expression within foci, and was the only LOX(L) member to demonstrate strong correlation to *PLOD2* expression. Using mRNA *in-situ* hybridisation, mesenchymal cell populations within IPF fibroblastic foci displayed high levels of collagen cross-linking expression, with co-expression of *PLOD2* and *LOXL2* seen within individual cells. Expression of collagen cross-linking enzymes was highest at the leading edge of the fibroblastic focus, with a gradual decline in activity toward the focus core, suggesting the catalyst for collagen cross-linking dysregulation was located at the alveolar barrier.

HIF pathway stabilisation was identified as a potent inducer of PLOD2 and LOXL2 expression through *in vitro* 2D fibroblast culture studies, and disproportionately induced these enzymes compared to collagen fibrillogenesis genes. In comparison, the effects of prototypical TGFβ signalling on these 'bone-type' cross-link enzymes was less marked, and induction was proportional to collagen gene expression. A differential HIF response to hypoxia was observed between fibroblasts from healthy and IPF donors, with a reduction in the expression of HIF3α. This isoform is thought to be responsible for negative feedback in the HIF pathway, competitively binding with HIFβ without exerting the same downstream transcriptional effects as HIF1α and HIF2α. Loss of HIF3α within mesenchymal cells could therefore leave the IPF lung vulnerable to excessive HIF pathway activation. HIF stabilisation was confirmed in IPF tissue through immunohistochemical studies. Increased expression of HIF1α and Ca9 was particularly seen within fibroblastic foci and co-localised to mesenchymal cells that co-expressed *PLOD2* and *LOXL2* mRNA.

Using an *in vitro* 3D fibroblastic focus model which enabled biomechanical testing, HIF pathway stabilisation exerted striking changes on collagen structure-function, with a mean increase in ECM

stiffness of over 300%, corresponding to a significant increase in 'bone-type' pyridinoline cross-link density and a reduction in collagen fibril diameter. These changes in collagen nanostructure paralleled differences seen in collagen between healthy and IPF lung tissue, with the results not only supporting the relevance of HIF pathway activation to pathogenetic ECM remodelling in IPF but also highlighting the utility of the 3D fibroblastic focus model with HIF stabilisation for further experimentation on fibrotic mechanisms and therapeutic development. Through selective gene silencing and inhibition of LOX(L) catalytic activity, the HIF-mediated changes to matrix stiffness were reduced within the 3D fibroblastic focus model. Significant reductions in pyridinoline cross-linking were also seen with pan-inhibition of LOX(L) enzyme activity.

7.1.2 Potential mechanisms for HIF stabilisation in IPF

This study identified HIF pathway stabilisation as an important promoter of pathologically excessive collagen cross-linking as seen in the ECM of the IPF lung. HIF pathway activation has previously been observed within the IPF alveolar epithelium and fibroblastic foci, and is implicated in other aspects of IPF pathogenesis such as fibroblast proliferation and activation[153,218,246,247]. Yet the mechanisms by which HIF pathways are stabilised within the IPF lung remain unclear.

Hypoxia is the canonical and perhaps most physiologically relevant trigger for HIF pathway activation, but its role as a driver of fibrotic progression in IPF remains to be confirmed. Several observations make hypoxia an unlikely candidate for HIF-mediated collagen cross-linking dysregulation in IPF. Firstly, the gradient of collagen cross-linking expression observed in this study is inconsistent with a hypoxic tissue gradient. Intuitively, the fibroblastic core is the region of greatest tissue hypoxia due to the spatial distance from sources of oxygen while the alveolar surface by contrast would be a region of relative normoxia. If HIF pathway activation of cross-linking enzymes was facilitated by hypoxia then the gradient of collagen cross-linking expression should be highest at the focus core and negligible at the alveolar surface.

Secondly, tissue hypoxia and hypoxaemia are seen in advanced disease, reflecting pre-existing fibrotic changes and the effects of these changes on increasing physiological dead space ventilation, ventilation/perfusion mismatch and oxygen diffusion limitation[64]. It is therefore implausible that a hypoxic environment would be an inciting trigger in early (subclinical) disease to catalyse fibrogenesis, although hypoxia may contribute to acceleration of HIF-mediated matrix changes as the disease advances.

A rational explanation for this conundrum is that HIF pathway stabilisation occurs through a variety of other "pseudohypoxic" mechanisms, independent of arterial or tissue PO_2. In keeping

with this concept, baseline levels of HIF1α and HIF2α were observed to be higher in early passage IPF fibroblasts compared to control lung fibroblasts despite culture in a normoxic environment[218].

A reduction in PHD co-factors such as Fe^{2+} and ascorbic acid can promote HIFα accumulation, while upstream signalling pathways such as ERK/MAPK and PI3K/Akt/mTOR have been demonstrated to stabilise HIFα in a normoxic environment as well[298]. A range of metabolites such as pyruvate and lactate inhibit HIF-PHD activity to increase HIF1α expression in normoxia[258,259]. Enhanced metabolic pathways have already been implicated in IPF disease, and both TGFβ and HIF signalling are likely to play important roles in those process[299-301]. Succinate, an intermediate of the Krebs cycle, has been observed in increased levels in fibrotic lungs and is also capable of inhibiting HIF1α hydroxylation to stabilise HIF pathways[301]. The authors who observed these findings proposed enhanced glycolytic pathways under aerobic conditions (known as the Warburg effect) as the source of increased succinate levels in lung fibrosis, which were capable of stabilising HIF1α (independent of hypoxia) to promote TGFβ-induced mesenchymal cell activation. Their argument was supported by both the prevention of TGFβ-induced fibroblast activation *in vitro* and the mitigation of bleomycin and TGFβ-mediated pulmonary fibrosis *in vivo* through inhibition of the glycolytic enzyme 6-phosphofructo-2-kinase/fructose-2,6-biphosphatase 3 (PFKB3).

Another important candidate source for 'pseudohypoxic' HIF stabilisation in the IPF lung is oxidative stress. This process involves an imbalance between reactive oxygen species (ROS) and anti-oxidant defences, with accumulation of ROS that are toxic to cellular structures[302,303]. The generation of ROS such as hydrogen peroxide, nitric oxide and glucose oxidase are established promoters of HIFα expression in normoxic conditions[256]. HIF-PHDs are relatively impervious to the effects of ROS however FIH (the other major regulator of HIF stabilisation) is more sensitive to peroxide and an oxidative stress-mediated reduction in FIH activity is thought to be the mechanism by which HIF pathway activation may occur[304]. A wealth of studies have previously linked oxidative stress to IPF disease, with markers of an increased oxidant burden localised primarily to the injured alveolar epithelium, along with a reduction in protective anti-oxidants such as glutathione[305-308]. Oxidative stress is linked to environmental exposures commonly associated with IPF, such as tobacco smoke and air pollution[309,310]. Endogenous processes can also enhance oxidative stress such as inflammation, metabolic changes within mitochondria and exhaustion of protective antioxidant sytems[302]. For example the reverse Warburg effect, a concept usually confined to cancer biology but which has previously been applied theoretically to pulmonary fibrosis, describes the generation of metabolic components such as pyruvate and lactate by stromal fibroblasts, which are utilised by adjacent tumour cells to increase oxidative phosphorylation and ROS production[300]. In this way, augmented metabolic pathways within IPF

cells may promote oxidative stress, with both events generating compounds that are capable of HIF stabilisation.

Taken together, HIF pathway activation in IPF is likely to be a critical event in the sustained fibrogenic response and pathological matrix remodelling however the mechanisms of induction are not clear. Tissue hypoxia occurs late in IPF and is unlikely to drive early pathogenesis, although development of hypoxaemia in advanced disease could accelerate HIF-mediated matrix changes. Pseudo-hypoxic HIF stabilisation through enhanced metabolic pathways and oxidative stress are already implicated in pulmonary fibrosis and can occur through a range of endogenous and exogenous insults at the alveolar surface. In the setting of this pseudo-hypoxic HIF stabilisation, the lack of inherent mechanisms for HIF pathway regulation such as HIF3α stabilisation could facilitate excessive downstream HIF pathway activation through HIF1/2α, initiating a series of HIF-mediated events to fundamentally alter mesenchymal activity and ECM structure-function in the lung.

7.1.3 The effects of HIF pathway activation on extracellular matrix remodelling

The IPF lung exhibits discrete areas of fibrosis with substantially increased matrix stiffness, correlating strongly with changes to collagen fibril diameter and density of pyridinoline cross-links[131,168]. TGFβ signalling alone was incapable of recapitulating changes of an equivalent magnitude within an *in vitro* 3D fibroblastic focus model, yet the addition of HIF stabilisation as a 'second hit' mechanism resulted in profound disruption of collagen cross-linking with significant consequences on both matrix compliance and collagen nanostructure that better reflected previous observations within IPF lung tissue.

While this is the first study to examine the biomechanical consequences in pulmonary fibrosis, synergy between TGFβ and HIF pathways has previously been implicated in fibrotic disease. Enhanced recruitment and activity of lung mesenchymal cells was observed *in vitro* with combined TGFβ/HIF activation through an augmented response on mRNA and long non-coding RNA expression[156]. Both TGFβ and HIF signalling have been identified as key regulatory pathways within *in vitro* experiments of nickel oxide nanoparticle-mediated pulmonary fibrosis, with synergistic effects on α-SMA and collagen 1 expression[269]. In the same study, inhibition of either HIF1α or TGFβ1 resulted in reduced expression of the other pathway.

Although not demonstrated in this study, mechanisms for enhanced HIF pathway stabilisation through TGFβ signalling may exist. *In vitro* studies in renal fibrosis have observed inter-dependent expression of the two pathways, with TGFβ signalling capable of stabilising HIF1α expression in a normoxic environment[267]. As previously discussed, augmentation of metabolic pathways such as

glycolysis under aerobic conditions (the Warburg effect) in IPF cells is capable of facilitating TGFβ1-induced HIF stabilisation[301]. In other work, a mechanism by which TGFβ could stabilise HIF pathways has been demonstrated through SMAD-mediated inhibition of PHD2[311,312]. Finally, TGFβ-mediated stabilisation of HIF in the findings of some groups may lie in technical limitations due to a lack of controlling for cellular confluence, which can have an impact on micro-environmental oxygen tension. The effect of TGFβ on cell proliferation may inadvertently influence HIF stabilisation, with a reduction in pericellular oxygen concentrations observed as cell density increases within *in vitro* experiments[313,314]. Yet the results of this study and the magnitude of changes in the IPF lung suggest the level of HIF stabilisation required exceeds that which can be delivered by TGFβ effects alone, supporting the concept of HIF pathway activation as a separate entity which has a synergistic relationship with TGFβ signalling.

Overall this and previous studies have demonstrated strong correlations between lung fibroblast ECM compliance and pyridinoline cross-linking[165]. However discrepancies between stiffness and pyridinoline density were seen with HIF and LOX(L) pathway interference using both gene silencing and catalytic inhibition. These differences may represent technical limitations within individual experiments, but could also suggest an interplay between HIF pathways and other ECM components independent of pyridinoline cross-linking. Other types of cross-linking are involved in the regulation of matrix compliance, for which HIF may play a role. For example transglutaminases, namely TG2, are important inter- and intra-molecular cross-linking enzymes of collagen and other proteins in normal tissue repair[186]. Dysregulated expression of TG2 is seen in human fibrotic lung tissue and IPF fibroblasts while TG2-knockout mice had less collagen deposition following exposure to bleomycin[295,315]. TG2 is capable of stabilising HIF in mammary epithelial cells under normoxic conditions through constitutive activation of nuclear factor κ-light-chain-enhancer of activated B cells (NF-κB), while HIF pathway activation in pulmonary artery smooth muscle cells has been identified to increase TG2 expression[316,317].

HIF pathways may also be important to non-enzymatic cross-linking which occurs in ECM. For example advanced glycation end products (AGEs), which arise from glycation of lysine residues with carbonyl groups of a sugar moiety, are elevated in IPF lung compared to tissue from both control and other ILD donors[318,319]. Hypoxia has been implicated in the accumulation of AGEs such as long wave (LW)1, although the relevance of HIF pathways to this process and scope of activity remain unexplored[320]. Traction exerted by cells on the surrounding ECM can have a significant effect on ECM compliance within lung tissue[168]. RhoA/ROCK pathways, key transcriptional targets of HIF signalling, are critical regulators of cell contractility through the phosphorylation of myosin II[321].

As well as in matrix production and modification, HIF may have important effects on matrix degradation. It is already recognised that increased pyridinoline cross-linking renders ECM less susceptible to MMP1 collagenase activity, although this observation has not been translated to models of pulmonary fibrosis[162]. Complicating this picture, MMPs are recognised to be activated by reactive oxidative species and HIFs, while increased levels of MMP1 in the alveolar epithelium are capable of suppressing mitochondrial activity and inducing HIF1α [322,323]. It is plausible that both TGFβ and HIF-mediated MMP activity contribute to a loss of more compliant (and soluble) matrix, with progressive accumulation of the less digestible collagens composed of dense pyridinoline cross-links. This could explain the increased MMP activity within the IPF lung, as well as why absolute collagen quantity is increased in end-stage fibrosis but not in early disease[167,188-190].

Taken together, abnormal matrix remodelling in IPF could represent a 'second-hit' phenomenon whereby TGFβ and HIF pathway activation at sites of lung injury impede the normal wound healing response, firstly by augmenting the proliferation and activity of lung mesenchymal cells, and secondly by inducing pathogenetic changes within these cells, shifting the balance in ECM production toward excessive collagen post-translational modification **(Figure 7.1)**. Plausibly HIF could modulate multiple cross-linking components of the ECM in addition to LOX(L)-mediated pathways and upregulate cellular contractility to further compound changes to matrix stiffness. On a speculative level other mechanisms of ECM homeostasis such as increased MMP production may be insufficient to normalise matrix compliance, or could instead worsen compliance by removing softer, more soluble, collagen fibrils, leaving the remaining ECM vulnerable to further TGFβ and HIF-mediated pathological changes. This could account for the reduction in collagen content observed in HIF-stabilised treatments within the 3D fibroblastic focus model.

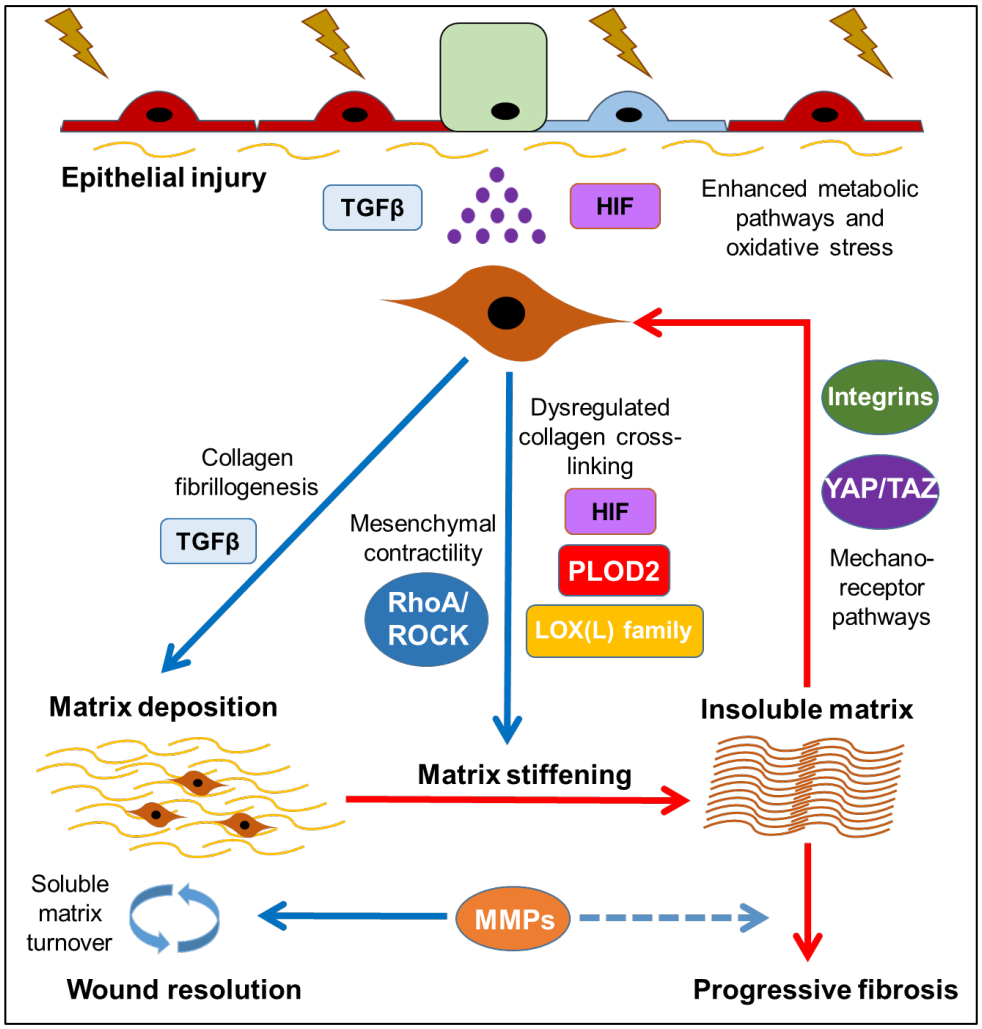

Figure 7.1: Proposed 'two hit' mechanism for pathologic matrix remodelling through the combined effects of HIF and TGFβ signalling. HIFs and TGFβ are both capable of mesenchymal recruitment and activation, while TGFβ is the core driver of collagen fibrillogenesis. HIF stabilisation is proposed to be a critical mediator of matrix stiffening through dysregulation of collagen cross-linking enzymes, generating dense pyridinoline cross-links which render collagen insoluble. The end-product is poorly compliant matrix which cannot be degraded, and generates a feed-forward loop to drive further ECM changes.

7.1.4 Targeting HIF pathways to normalise extracellular matrix homeostasis in IPF

Accurate and reproducible models are lacking in IPF research, thereby hindering the mechanistic evaluation of fibrotic pathways as well as pre-clinical assessment of potential pharmacological compounds. *In vitro* 3D models of IPF have historically relied upon pre-existing lung matrices for cellular seeding[168]. While useful in the analysis of cell behaviour and matrix interactions, the models are limited in the analysis of endogenous ECM production and modification. Others, such as the 'scar-in-a-jar' model, use endogenously produced ECM however do not accurately reflect

the mature cross-link density due to the relatively short-term culture conditions[324,325]. *In vivo* models of IPF most commonly involve an inhalation-introduced lung injury with compounds such as bleomycin, leading initially to inflammation, followed by fibrosis, and then often resolution (if inhalational exposure is ceased)[326]. IPF does not follow the same disease course and thus inherent limitations of these models are likely to have contributed to the lack of translation of novel compounds to clinical studies[49,51,327,328]. The HIF-stabilised 3D fibroblastic focus model faithfully recapitulates important parameters of post-translational collagen modification in IPF and represents an important advancement for pre-clinical *in vitro* analysis of ECM-modifying effects of novel antifibrotic compounds.

This study used the HIF-stabilised 3D fibroblastic focus model to examine HIF1/2α and LOXL2 expression as modifiable targets in HIF-mediated ECM changes, with detectable improvements in ECM compliance following gene silencing with siRNA. Furthermore the catalytic inhibition of LOX(L) enzymes was also capable of normalising matrix changes in HIF-stabilised 3D fibroblastic foci models through the reduction in density of pyridinoline collagen cross-links. Both studies require optimisation to ensure sufficient targeting of dysregulated cross-linking activity (or the upstream signals which promote the activity), however represent important steps forward in the application of matrix modifying therapies to normalise matrix homeostasis.

Progress in the development and application of compounds which modify collagen cross-linking in IPF have stalled since a phase 2 clinical trial using Simtuzumab, a monoclonal antibody directed against LOXL2 (previously known as AB0023), failed to prolong progression-free survival of patients with IPF[51]. Yet serious questions remain over the efficacy of this therapeutic compound to perform the desired function. The mechanism of anti-LOXL2 effect for Simtuzumab has been proposed to be allosteric, with the binding epitope located at the non-catalytic SRCR4 domain[329]. The LOXL2, LOXL3 and LOXL4 SRCRs are postulated to be involved in protein trafficking and immune regulation, and inhibition of these regions may account for many of the pre-clinical effects of Simtuzumab such as reductions in neovascularisation, tumour size and metastases[179,195]. Specific pre-clinical work examining the effects of Simtuzumab on collagen modification were limited, with modest (less than 30%) inhibitory action on LOXL2 enzymatic activity using collagen 1 as a substrate[329]. To date no analysis of Simtuzumab's effect on pyridinoline cross-linking has been performed, with erroneous suggestions of cross-linking inhibition based on picrosirius staining experiments that were incapable of measuring this effect[195]. It is therefore unclear if Simtuzumab is capable of modifying the catalytic activities of LOXL2 on collagen cross-linking in IPF.

In contrast, selective catalytic inhibition of LOXL2/3 activity through PXS-S2A has been observed to be efficacious at reducing pyridinoline cross-linking and ECM compliance *in vitro* and *in vivo*[165]. Additional properties which favour this method of inhibition include the capability for interference with both intra- and extracellular LOXL2/3 activity, as well as the potential for broader anti-LOX(L) effects at higher concentrations in the event of redundancy between family members. It remains unclear if inhibition of LOXL2 alone would result in effective inhibition of pathological cross-linking, or if the activity of other LOX(L) members increases in a compensatory response.

A key question which remains is the level of cross-linking inhibition that is sufficient to break the mechanosensitive pathway feedback loop but does not impair normal tissue function. The effects of excessive cross-linking inhibition on human lung are unknown but could be maladaptive on normal cellular and organ function. Furthermore collagen cross-linking is a ubiquitous process within the body, and the systemic effects of impairing catalytic LOX(L) activity are likely to limit the extent at which these therapeutics can be applied.

This and other studies have highlighted the importance of excessive PLOD2-mediated hydroxylation of collagen telopeptide lysine residues to alterations in ECM stiffness, which is promoted by both TGFβ and HIF signalling[192,271]. Inhibition of this excessive LH2 activity could reduce the substrate available for LOX(L)-mediated pyridinoline cross-linking and subsequently normalise ECM compliance. Minoxidil is capable of reducing PLOD2/LH2 expression as well as pyridinoline formation, yet its activity against other lysyl hydroxylases such as LH1 make it unsuitable for anti-fibrotic application[294]. The need for selective LH2 inhibitors has led to the development of a high throughput LH assay which reported the identification of a number of selective and potent candidates for LH2 inhibition[330]. Further advances in this field are likely to be highly applicable to IPF research.

7.2 Future work

A critical step for understanding the influence of HIF pathway activation within IPF is to identify the mechanism of HIF stabilisation. Conventionally (and incorrectly), hypoxia is often considered synonymous with HIF and yet a role for hypoxaemia and tissue hypoxia to incite and propagate a fibrogenic response has not been established. 'Pseudohypoxic' mechanisms of HIF stabilisation such as oxidative stress could play important roles at the epithelial-interstitial interface, mediated through FIH-dependent pathways. Future work will aim to understand pathways by which HIF is stabilised in IPF. In particular, a role for the dysregulation of FIH through both oxidative stress and other mechanisms will be explored using both in vitro and in vivo methods. The interplay between

oxidative stress and HIF stabilisation will also be extended to the realm of pulmonary fibrosis. This will include an analysis of HIF and oxidative stress signatures in IPF populations, as well as 2D and 3D *in vitro* studies to simulate oxidative stress-mediated HIF stabilisation and its effects on ECM modification.

The HIF-stabilised 3D fibroblastic focus model is an important advancement in the development of a system which can replicate the complex ECM changes that occur in IPF. While it remains to be tested, the 3D fibroblastic focus model with HIF pathway activation is likely to produce ECM that is resistant to degradation, as opposed to other models such as the bleomycin mouse that exhibit reversible changes. With matrix properties that recapitulate fibrotic lung to a greater extent than earlier TGFβ-only *in vitro* models, the HIF-stabilised model will be utilised to interrogate a range of candidate compounds which may modulate the abnormal collagen cross-linking responses which occur in IPF. Future work will re-examine the effects of selective LOXL2/3 inhibition through PXS-S2A on matrix stiffness and clarify the discrepancy between compliance changes and pyridinoline cross-link density. A wider range of concentrations will be incorporated to better understand the redundancy of LOXL2/3 activity in normalising HIF-mediated changes. Finally the effects of catalytic inhibition through PXS-S2A will be compared to the allosteric inhibition of Simtuzumab in order to answer a key question regarding the efficacy of Simtuzumab in modifying collage cross-linking.

Gene silencing through siRNA was performed to mechanistically dissect the roles of HIFα and downstream LOXL2 in the development of pyridinoline cross-links and loss of matrix compliance. A limitation of this study was the loss of siRNA efficacy over time, leading to inconclusive results. Advances in techniques for gene silencing may enable significant mechanistic insights. Gene editing systems incorporating CRISPR/Cas9 represent one such advancement, producing cell lines with stable silencing of select genes through CAS9 cleavage of specific DNA sequences[291]. Unlike siRNA methods, gene silencing with CRISPR is permanent and not associated with the off-target effects of the transfection process. Incorporating this technology into the 3D fibroblastic focus model would enable a more detailed comparison of HIFs and collagen cross-linking enzyme effects on downstream matrix changes in conditions of HIF stabilisation. Future studies will focus on the relevance of individual HIFα subunits, including the poorly understood HIF3α which was found to be downregulated in IPF fibroblasts. Furthermore, a broader range of collagen cross-linking enzymes can be targeted, such as PLOD2, LOX and LOXL3, enabling a comprehensive analysis of relevant pathways to ECM remodelling.

Multiple determinants of ECM compliance exist which were beyond the scope of this study, such as transglutaminase-mediated and non-enzymatic cross-linking, cellular contractility, and matrix

resorption. The relative contribution of HIF-facilitated changes to these pathways in the overall compliance of ECM is unclear, and has not been explored in pulmonary fibrosis. Future studies will therefore investigate mechanisms by which HIF pathways alter matrix structure-function independent of pyridinoline cross-linking, such as through upregulation of TG2, changes to fibroblast contractility or increased MMP activity to remove softer collagen fibrils.

7.3 Final conclusion

This study sought to investigate the dysregulation of collagen cross-linking enzymes which drive pathological matrix modification in IPF. Mesenchymal cells within fibroblastic foci were identified as the primary cellular source of core collagen cross-linking enzymes, and HIF pathways observed to be potent inducers of their expression. HIF and collagen cross-linking enzyme activity was greatest at the alveolar surface, and could represent a “second hit” phenomenon at the site of fibrogenesis. The source of HIF pathway stabilisation is postulated to occur through ‘pseudo-hypoxic’ mechanisms such as oxidative stress, with loss of normal negative feedback mechanisms such as HIF3α.

HIF pathway activation is essential to disrupt the balance between collagen fibrillogenesis and collagen cross-linking, facilitating excessive pyridinoline cross-link accumulation to pathologically alter tissue compliance, collagen nano-structure and function at magnitudes comparable to IPF lung tissue. Pathological collagen cross-linking activity and upstream HIF pathway dysregulation represent important modifiable targets, which may disrupt the feed-forward loop of fibrotic progression to normalise matrix homeostasis.

Appendix A Media and Buffers

A.1 Media for cell culture

A.1.1 Complete DMEM fibroblast media

- 86% DMEM
- 10% FBS
- 1% penicillin-streptomycin 100x
- 1% Non-essential amino acids (NEAA) 100x
- 1% L-glutamine 200mM
- 1% sodium pyruvate

A.1.2 Complete DCCM-1 media

- 89% DCCM-1
- 10% FBS
- 1% penicillin-streptomycin-L-glutamine

A.1.3 3D fibroblastic focus model media

- Phenol-free DMEM (Gibco, 31053-044) 180mL
- Ham's F-12 Nutrient Mix (Gibco 21765) 60mL
- 5% FBS
- 1% penicillin-streptomycin
- 1% L-glutamine 100x
- 1% NEAA 1mM
- 1% NaP 1mM
- EGF 10ng/mL
- Amphotericin B (Gibco, 15290-026) 2.5µg/mL
- Adenine 0.18mM (Sigma, A2786-5G)
- 4-(2-hydroxyethyl)-1-piperazineethanesulfonic acid (HEPES) 8mM (Sigma, 83264-100ML)
- Insulin 5µg/mL (Sigma, I9278-5ML)
- Hydrocortisone 0.5µg/mL (Sigma, H0888-1G)
- L-Ascorbic acid 2-phosphate sesquimagnesium salt hydrate (Sigma, A8960-5G) 1µL/mL added to media fresh 3 times per week. Stock solutions prepared from dry powder at least every 20 days.

A.2 Polyacrylamide gels and western blot buffers

A.2.1 Separation gel

7.5% Acrylamide

- 2.5mL 30% acrylamide
- 2.5mL 1.5M trisaminomethane (Tris)-HCL pH 8.8
- 4.9mL dH_2O
- 100µL 10% SDS
- 50µL 10% ammonium persulfate (APS)
- 5µL tetramethylethylenediamine (TEMED)

10% Acrylamide

- 3.3mL 30% acrylamide
- 2.5mL 1.5M Tris-HCL pH 8.8
- 4.1mL dH_2O
- 100µL 10% SDS
- 50µL 10% APS
- 5µL TEMED

A.2.2 4% Stacking gel

- 0.5mL 30% acrylamide
- 1.25mL 0.5M Tris-HCl pH 6.8
- 3.05mL dH_2O
- 50µL 10% (w/v) SDS
- 25µL 10% APS
- 10µL TEMED

A.2.3 10x Running buffer

- 15.5g 0.025M Tris
- 720g 0.192M glycine
- 250mls 20% SDS
- dH_2O to make up to 5 litres
- Dilute 1:10 for working concentration

A.2.4 10x Transfer buffer

- 151.5g 0.025M Tris
- 720g 0.192M glycine
- dH_2O to make up to 5 litres
- Dilute 1:10 for working concentration – for every 100mL 10x transfer buffer add 200mL methanol and 700mL dH2O

A.2.5 Stripping buffer

- 62.5mL 0.5M Tris HCL pH 6.8
- 50mL 20% SDS
- Make up to 500mL with dH_2O
- Add 70µL β-mercaptoethanol for every 10mL stripping buffer before use

Appendix B Publications, Posters and Presentations

Christopher J Brereton, Liudi Yao, Joseph Bell, Franco Conforti, Aiman Alzetani, Aurelie Fabre, Ben G Marshall, Luca Richeldi, Donna E Davies, Yihua Wang, Mark G Jones. *Hypoxia-inducible factor pathway activation promotes bone-type collagen cross-linking in Idiopathic Pulmonary Fibrosis.* European Respiratory Journal Sep 2019, 54 (suppl 63) PA2424; DOI: 10.1183/13993003.congress-2019.PA2424. Thematic poster

Christopher J Brereton, Robert Ridley, Franco Conforti, Liudi Yao, Aiman Alzetani, Ben Marshall, Sophie V Fletcher, Luca Richeldi, Yihua Wang, Donna E Davies, Mark G Jones. *HIF pathway activation is a core regulator of collagen structure-function in lung fibrosis.* European Respiratory Journal Sep 2020, 56 (suppl 64) 4323; DOI: 10.1183/13993003.congress-2020.4323. Presentation and thematic poster.

Christopher J Brereton, Liudi Yao, Yilu Zhou, Joseph Bell, R.A. Ridley, E.R. Davies, O.G. Andriotis, Franco Conforti, Soran Mohammed, Tim Wallis, Ali Tavassoli, R. Ewing, Aiman Alzetani, Ben G. Marshall, Sophie V. Fletcher, P.J. Thurner, Luca Richeldi, Donna E. Davies, Yihua Wang, Mark G. Jones. *Pseudohypoxic HIF pathway activation dysregulates collagen structure-function in human lung fibrosis.* Elife, Manuscript Under Review, July 2021.

List of References

1. Rosas IO, Dellaripa PF, Lederer DJ, et al. Interstitial lung disease: NHLBI Workshop on the Primary Prevention of Chronic Lung Diseases. *Ann Am Thorac Soc* 2014;11 Suppl 3:S169-77.

2. Society AT, Society ER. American Thoracic Society/European Respiratory Society International Multidisciplinary Consensus Classification of the Idiopathic Interstitial Pneumonias. This joint statement of the American Thoracic Society (ATS), and the European Respiratory Society (ERS) was adopted by the ATS board of directors, June 2001 and by the ERS Executive Committee, June 2001. *Am J Respir Crit Care Med* 2002;165(2):277-304.

3. Travis WD, Costabel U, Hansell DM, et al. An official American Thoracic Society/European Respiratory Society statement: Update of the international multidisciplinary classification of the idiopathic interstitial pneumonias. *Am J Respir Crit Care Med* 2013;188(6):733-48.

4. Raghu G, Remy-Jardin M, Myers JL, et al. Diagnosis of Idiopathic Pulmonary Fibrosis. An Official ATS/ERS/JRS/ALAT Clinical Practice Guideline. *Am J Respir Crit Care Med* 2018;198(5):e44-e68.

5. Snell N, Strachan D, Hubbard R, et al. P272 Epidemiology of idiopathic pulmonary fibrosis in the uk: findings from the british lung foundation's 'respiratory health of the nation' project. *Thorax* 2016;71(Suppl 3):A236-A36.

6. Hutchinson J, Fogarty A, Hubbard R, et al. Global incidence and mortality of idiopathic pulmonary fibrosis: a systematic review. *Eur Respir J* 2015;46(3):795-806.

7. Navaratnam V, Fleming KM, West J, et al. The rising incidence of idiopathic pulmonary fibrosis in the U.K. *Thorax* 2011;66(6):462-7.

8. Cordier JF, Cottin V. Neglected evidence in idiopathic pulmonary fibrosis: from history to earlier diagnosis. *Eur Respir J* 2013;42(4):916-23.

9. Lynch DA, Sverzellati N, Travis WD, et al. Diagnostic criteria for idiopathic pulmonary fibrosis: a Fleischner Society White Paper. *Lancet Respir Med* 2018;6(2):138-53.

10. Wells AU, Brown KK, Flaherty KR, et al. What's in a name? That which we call IPF, by any other name would act the same. *Eur Respir J* 2018;51(5).

11. Brereton CJ, Wallis T, Casey M, et al. Time taken from primary care referral to a specialist centre diagnosis of idiopathic pulmonary fibrosis: an opportunity to improve patient outcomes? *ERJ Open Res* 2020;6(2).

12. Sgalla G, Walsh SLF, Sverzellati N, et al. "Velcro-type" crackles predict specific radiologic features of fibrotic interstitial lung disease. *BMC Pulm Med* 2018;18(1):103.

13. Katzenstein AL, Myers JL. Idiopathic pulmonary fibrosis: clinical relevance of pathologic classification. *Am J Respir Crit Care Med* 1998;157(4 Pt 1):1301-15.

14. Richeldi L, Collard HR, Jones MG. Idiopathic pulmonary fibrosis. *Lancet* 2017;389(10082):1941-52.

15. Lancaster L, Crestani B, Hernandez P, et al. Safety and survival data in patients with idiopathic pulmonary fibrosis treated with nintedanib: pooled data from six clinical trials. *BMJ Open Respir Res* 2019;6(1):e000397.

16. Behr J, Prasse A, Wirtz H, et al. Survival and course of lung function in the presence or absence of antifibrotic treatment in patients with idiopathic pulmonary fibrosis: long-term results of the INSIGHTS-IPF registry. *Eur Respir J* 2020;56(2).

17. Brereton CJ, Jo HE. Acute exacerbations of idiopathic pulmonary fibrosis and the role of corticosteroids. *Breathe (Sheff)* 2020;16(3):200086.

18. Demedts M, Behr J, Buhl R, et al. High-dose acetylcysteine in idiopathic pulmonary fibrosis. *N Engl J Med* 2005;353(21):2229-42.

19. Raghu G, Anstrom KJ, King TE, et al. Prednisone, azathioprine, and N-acetylcysteine for pulmonary fibrosis. *N Engl J Med* 2012;366(21):1968-77.

20. Martinez FJ, de Andrade JA, Anstrom KJ, et al. Randomized trial of acetylcysteine in idiopathic pulmonary fibrosis. *N Engl J Med* 2014;370(22):2093-101.

21. Sakamoto S, Kataoka K, Kondo Y, et al. Pirfenidone plus inhaled N-acetylcysteine for idiopathic pulmonary fibrosis: a randomised trial. *Eur Respir J* 2020.

22. King TE, Bradford WZ, Castro-Bernardini S, et al. A phase 3 trial of pirfenidone in patients with idiopathic pulmonary fibrosis. *N Engl J Med* 2014;370(22):2083-92.

23. Noble PW, Albera C, Bradford WZ, et al. Pirfenidone in patients with idiopathic pulmonary fibrosis (CAPACITY): two randomised trials. *Lancet* 2011;377(9779):1760-9.

24. Richeldi L, du Bois RM, Raghu G, et al. Efficacy and safety of nintedanib in idiopathic pulmonary fibrosis. *N Engl J Med* 2014;370(22):2071-82.

25. Hilberg F, Roth GJ, Krssak M, et al. BIBF 1120: triple angiokinase inhibitor with sustained receptor blockade and good antitumor efficacy. *Cancer Res* 2008;68(12):4774-82.

26. Ellis PM, Kaiser R, Zhao Y, et al. Phase I open-label study of continuous treatment with BIBF 1120, a triple angiokinase inhibitor, and pemetrexed in pretreated non-small cell lung cancer patients. *Clin Cancer Res* 2010;16(10):2881-9.

27. Chaudhary NI, Roth GJ, Hilberg F, et al. Inhibition of PDGF, VEGF and FGF signalling attenuates fibrosis. *Eur Respir J* 2007;29(5):976-85.

28. Richeldi L, Costabel U, Selman M, et al. Efficacy of a tyrosine kinase inhibitor in idiopathic pulmonary fibrosis. *N Engl J Med* 2011;365(12):1079-87.

29. Crestani B, Quaresma M, Kaye M, et al. Long-term treatment with nintedanib in patients with IPF: An update from INPULSIS®-ON. *European Respiratory Journal* 2016;48(suppl 60):OA4960.

30. Crestani B, Huggins JT, Kaye M, et al. Long-term safety and tolerability of nintedanib in patients with idiopathic pulmonary fibrosis: results from the open-label extension study, INPULSIS-ON. *Lancet Respir Med* 2018.

31. Flaherty KR, Wells AU, Cottin V, et al. Nintedanib in Progressive Fibrosing Interstitial Lung Diseases. *N Engl J Med* 2019;381(18):1718-27.

32. Distler O, Highland KB, Gahlemann M, et al. Nintedanib for Systemic Sclerosis-Associated Interstitial Lung Disease. *N Engl J Med* 2019;380(26):2518-28.

33. Jin J, Togo S, Kadoya K, et al. Pirfenidone attenuates lung fibrotic fibroblast responses to transforming growth factor-β1. *Respir Res* 2019;20(1):119.

34. Kwapiszewska G, Gungl A, Wilhelm J, et al. Transcriptome profiling reveals the complexity of pirfenidone effects in idiopathic pulmonary fibrosis. *Eur Respir J* 2018;52(5).

35. Azuma A, Nukiwa T, Tsuboi E, et al. Double-blind, placebo-controlled trial of pirfenidone in patients with idiopathic pulmonary fibrosis. *Am J Respir Crit Care Med* 2005;171(9):1040-7.

36. Taniguchi H, Ebina M, Kondoh Y, et al. Pirfenidone in idiopathic pulmonary fibrosis. *Eur Respir J* 2010;35(4):821-9.

37. Karimi-Shah BA, Chowdhury BA. Forced vital capacity in idiopathic pulmonary fibrosis--FDA review of pirfenidone and nintedanib. *N Engl J Med* 2015;372(13):1189-91.

38. Noble PW, Albera C, Bradford WZ, et al. Pirfenidone for idiopathic pulmonary fibrosis: analysis of pooled data from three multinational phase 3 trials. *Eur Respir J* 2016;47(1):243-53.

39. Maher TM, Corte TJ, Fischer A, et al. Pirfenidone in patients with unclassifiable progressive fibrosing interstitial lung disease: a double-blind, randomised, placebo-controlled, phase 2 trial. *Lancet Respir Med* 2020;8(2):147-57.

40. Solomon JJ, Danoff SK, Goldberg HJ, et al. The Design and Rationale of the Trail1 Trial: A Randomized Double-Blind Phase 2 Clinical Trial of Pirfenidone in Rheumatoid Arthritis-Associated Interstitial Lung Disease. *Adv Ther* 2019;36(11):3279-87.

41. Cottin V, Koschel D, Günther A, et al. Long-term safety of pirfenidone: results of the prospective, observational PASSPORT study. *ERJ Open Res* 2018;4(4).

42. Costabel U, Albera C, Lancaster LH, et al. An Open-Label Study of the Long-Term Safety of Pirfenidone in Patients with Idiopathic Pulmonary Fibrosis (RECAP). *Respiration* 2017;94(5):408-15.

43. Sprunger DB, Olson AL, Huie TJ, et al. Pulmonary fibrosis is associated with an elevated risk of thromboembolic disease. *Eur Respir J* 2012;39(1):125-32.

44. Noth I, Anstrom KJ, Calvert SB, et al. A placebo-controlled randomized trial of warfarin in idiopathic pulmonary fibrosis. *Am J Respir Crit Care Med* 2012;186(1):88-95.

45. King TE, Brown KK, Raghu G, et al. BUILD-3: a randomized, controlled trial of bosentan in idiopathic pulmonary fibrosis. *Am J Respir Crit Care Med* 2011;184(1):92-9.

46. Zisman DA, Schwarz M, Anstrom KJ, et al. A controlled trial of sildenafil in advanced idiopathic pulmonary fibrosis. *N Engl J Med* 2010;363(7):620-8.

47. Raghu G, Brown KK, Bradford WZ, et al. A placebo-controlled trial of interferon gamma-1b in patients with idiopathic pulmonary fibrosis. *N Engl J Med* 2004;350(2):125-33.

48. King TE, Albera C, Bradford WZ, et al. Effect of interferon gamma-1b on survival in patients with idiopathic pulmonary fibrosis (INSPIRE): a multicentre, randomised, placebo-controlled trial. *Lancet* 2009;374(9685):222-8.

49. Daniels CE, Lasky JA, Limper AH, et al. Imatinib treatment for idiopathic pulmonary fibrosis: Randomized placebo-controlled trial results. *Am J Respir Crit Care Med* 2010;181(6):604-10.

50. Raghu G, Brown KK, Costabel U, et al. Treatment of idiopathic pulmonary fibrosis with etanercept: an exploratory, placebo-controlled trial. *Am J Respir Crit Care Med* 2008;178(9):948-55.

51. Raghu G, Brown KK, Collard HR, et al. Efficacy of simtuzumab versus placebo in patients with idiopathic pulmonary fibrosis: a randomised, double-blind, controlled, phase 2 trial. *Lancet Respir Med* 2017;5(1):22-32.

52. Canesin G, Cuevas EP, Santos V, et al. Lysyl oxidase-like 2 (LOXL2) and E47 EMT factor: novel partners in E-cadherin repression and early metastasis colonization. *Oncogene* 2015;34(8):951-64.

53. Cuevas EP, Moreno-Bueno G, Canesin G, et al. LOXL2 catalytically inactive mutants mediate epithelial-to-mesenchymal transition. *Biol Open* 2014;3(2):129-37.

54. Cuevas EP, Eraso P, Mazón MJ, et al. LOXL2 drives epithelial-mesenchymal transition via activation of IRE1-XBP1 signalling pathway. *Sci Rep* 2017;7:44988.

55. Iturbide A, García de Herreros A, Peiró S. A new role for LOX and LOXL2 proteins in transcription regulation. *FEBS J* 2015;282(9):1768-73.

56. Lugassy J, Zaffryar-Eilot S, Soueid S, et al. The enzymatic activity of lysyl oxidas-like-2 (LOXL2) is not required for LOXL2-induced inhibition of keratinocyte differentiation. *J Biol Chem* 2012;287(5):3541-9.

57. Millanes-Romero A, Herranz N, Perrera V, et al. Regulation of heterochromatin transcription by Snail1/LOXL2 during epithelial-to-mesenchymal transition. *Mol Cell* 2013;52(5):746-57.

58. Moreno-Bueno G, Salvador F, Martín A, et al. Lysyl oxidase-like 2 (LOXL2), a new regulator of cell polarity required for metastatic dissemination of basal-like breast carcinomas. *EMBO Mol Med* 2011;3(9):528-44.

59. Peinado H, Del Carmen Iglesias-de la Cruz M, Olmeda D, et al. A molecular role for lysyl oxidase-like 2 enzyme in snail regulation and tumor progression. *EMBO J* 2005;24(19):3446-58.

60. Laurent GJ. Lung collagen: more than scaffolding. *Thorax* 1986;41(6):418-28.

61. Agustí AG, Roca J, Gea J, et al. Mechanisms of gas-exchange impairment in idiopathic pulmonary fibrosis. *Am Rev Respir Dis* 1991;143(2):219-25.

62. Barisione G, Brusasco C, Garlaschi A, et al. Lung diffusing capacity for nitric oxide as a marker of fibrotic changes in idiopathic interstitial pneumonias. *J Appl Physiol (1985)* 2016;120(9):1029-38.

63. Fitting JW, Frascarolo P, Jéquier E, et al. Resting energy expenditure in interstitial lung disease. *Am Rev Respir Dis* 1990;142(3):631-5.

64. Plantier L, Cazes A, Dinh-Xuan AT, et al. Physiology of the lung in idiopathic pulmonary fibrosis. *Eur Respir Rev* 2018;27(147).

65. Selman M, Pardo A. Idiopathic pulmonary fibrosis: an epithelial/fibroblastic cross-talk disorder. *Respir Res* 2002;3:3.

66. Albert RK, Schwartz DA. Revealing the Secrets of Idiopathic Pulmonary Fibrosis. *N Engl J Med* 2019;380(1):94-96.

67. Barros A, Oldham J, Noth I. Genetics of Idiopathic Pulmonary Fibrosis. *Am J Med Sci* 2019;357(5):379-83.

68. Fingerlin TE, Murphy E, Zhang W, et al. Genome-wide association study identifies multiple susceptibility loci for pulmonary fibrosis. *Nat Genet* 2013;45(6):613-20.

69. Noth I, Zhang Y, Ma SF, et al. Genetic variants associated with idiopathic pulmonary fibrosis susceptibility and mortality: a genome-wide association study. *Lancet Respir Med* 2013;1(4):309-17.

70. Allen RJ, Porte J, Braybrooke R, et al. Genetic variants associated with susceptibility to idiopathic pulmonary fibrosis in people of European ancestry: a genome-wide association study. *Lancet Respir Med* 2017;5(11):869-80.

71. Sanders YY, Ambalavanan N, Halloran B, et al. Altered DNA methylation profile in idiopathic pulmonary fibrosis. *Am J Respir Crit Care Med* 2012;186(6):525-35.

72. Yang IV, Pedersen BS, Rabinovich E, et al. Relationship of DNA methylation and gene expression in idiopathic pulmonary fibrosis. *Am J Respir Crit Care Med* 2014;190(11):1263-72.

73. Selman M, Pardo A, Barrera L, et al. Gene expression profiles distinguish idiopathic pulmonary fibrosis from hypersensitivity pneumonitis. *Am J Respir Crit Care Med* 2006;173(2):188-98.

74. Yang IV, Burch LH, Steele MP, et al. Gene expression profiling of familial and sporadic interstitial pneumonia. *Am J Respir Crit Care Med* 2007;175(1):45-54.

75. Seibold MA, Wise AL, Speer MC, et al. A common MUC5B promoter polymorphism and pulmonary fibrosis. *N Engl J Med* 2011;364(16):1503-12.

76. Hunninghake GM, Hatabu H, Okajima Y, et al. MUC5B promoter polymorphism and interstitial lung abnormalities. *N Engl J Med* 2013;368(23):2192-200.

77. Juge PA, Lee JS, Ebstein E, et al. MUC5B Promoter Variant and Rheumatoid Arthritis with Interstitial Lung Disease. *N Engl J Med* 2018;379(23):2209-19.

78. Schwartz DA. Idiopathic Pulmonary Fibrosis Is a Genetic Disease Involving Mucus and the Peripheral Airways. *Ann Am Thorac Soc* 2018;15(Suppl 3):S192-S97.

79. Thomas AQ, Lane K, Phillips J, et al. Heterozygosity for a surfactant protein C gene mutation associated with usual interstitial pneumonitis and cellular nonspecific interstitial pneumonitis in one kindred. *Am J Respir Crit Care Med* 2002;165(9):1322-8.

80. Armanios M, Blackburn EH. The telomere syndromes. *Nat Rev Genet* 2012;13(10):693-704.

81. Cronkhite JT, Xing C, Raghu G, et al. Telomere shortening in familial and sporadic pulmonary fibrosis. *Am J Respir Crit Care Med* 2008;178(7):729-37.

82. Duckworth A, Gibbons MA, Allen RJ, et al. Telomere length and risk of idiopathic pulmonary fibrosis and chronic obstructive pulmonary disease: a mendelian randomisation study. *Lancet Respir Med* 2020.

83. Dressen A, Abbas AR, Cabanski C, et al. Analysis of protein-altering variants in telomerase genes and their association with MUC5B common variant status in patients with idiopathic pulmonary fibrosis: a candidate gene sequencing study. *Lancet Respir Med* 2018;6(8):603-14.

84. Baumgartner KB, Samet JM, Stidley CA, et al. Cigarette smoking: a risk factor for idiopathic pulmonary fibrosis. *Am J Respir Crit Care Med* 1997;155(1):242-8.

85. Bellou V, Belbasis L, Konstantinidis A, et al. Tobacco smoking and risk for idiopathic pulmonary fibrosis: a prospective cohort study in UK Biobank. *European Respiratory Journal* 2017;50(suppl 61):PA4887.

86. Antoniou KM, Hansell DM, Rubens MB, et al. Idiopathic pulmonary fibrosis: outcome in relation to smoking status. *Am J Respir Crit Care Med* 2008;177(2):190-4.

87. Taskar VS, Coultas DB. Is idiopathic pulmonary fibrosis an environmental disease? *Proc Am Thorac Soc* 2006;3(4):293-8.

88. Blanc PD, Annesi-Maesano I, Balmes JR, et al. The Occupational Burden of Nonmalignant Respiratory Diseases. An Official American Thoracic Society and European Respiratory Society Statement. *Am J Respir Crit Care Med* 2019;199(11):1312-34.

89. Raghu G, Amatto VC, Behr J, et al. Comorbidities in idiopathic pulmonary fibrosis patients: a systematic literature review. *Eur Respir J* 2015;46(4):1113-30.

90. Bédard Méthot D, Leblanc É, Lacasse Y. Meta-analysis of Gastroesophageal Reflux Disease and Idiopathic Pulmonary Fibrosis. *Chest* 2019;155(1):33-43.

91. Raghu G, Collard HR, Egan JJ, et al. An official ATS/ERS/JRS/ALAT statement: idiopathic pulmonary fibrosis: evidence-based guidelines for diagnosis and management. *Am J Respir Crit Care Med* 2011;183(6):788-824.

92. Tran T, Suissa S. The effect of anti-acid therapy on survival in idiopathic pulmonary fibrosis: a methodological review of observational studies. *Eur Respir J* 2018;51(6).

93. Tran T, Assayag D, Ernst P, et al. Effectiveness of proton pump inhibitors in idiopathic pulmonary fibrosis: a population-based cohort study. *Chest* 2020.

94. Sack C, Vedal S, Sheppard L, et al. Air pollution and subclinical interstitial lung disease: the Multi-Ethnic Study of Atherosclerosis (MESA) air-lung study. *Eur Respir J* 2017;50(6).

95. Johannson KA, Vittinghoff E, Lee K, et al. Acute exacerbation of idiopathic pulmonary fibrosis associated with air pollution exposure. *Eur Respir J* 2014;43(4):1124-31.

96. Yoon HY, Kim SY, Kim OJ, et al. Nitrogen Dioxide Increases the Risk of Mortality in Idiopathic Pulmonary Fibrosis. *Eur Respir J* 2020.

97. Sesé L, Nunes H, Cottin V, et al. Role of atmospheric pollution on the natural history of idiopathic pulmonary fibrosis. *Thorax* 2018;73(2):145-50.

98. Winterbottom CJ, Shah RJ, Patterson KC, et al. Exposure to Ambient Particulate Matter Is Associated With Accelerated Functional Decline in Idiopathic Pulmonary Fibrosis. *Chest* 2018;153(5):1221-28.

99. Ueda T, Ohta K, Suzuki N, et al. Idiopathic pulmonary fibrosis and high prevalence of serum antibodies to hepatitis C virus. *Am Rev Respir Dis* 1992;146(1):266-8.

100. Vergnon JM, Vincent M, de Thé G, et al. Cryptogenic fibrosing alveolitis and Epstein-Barr virus: an association? *Lancet* 1984;2(8406):768-71.

101. Stewart JP, Egan JJ, Ross AJ, et al. The detection of Epstein-Barr virus DNA in lung tissue from patients with idiopathic pulmonary fibrosis. *Am J Respir Crit Care Med* 1999;159(4 Pt 1):1336-41.

102. Garzoni C, Brugger SD, Qi W, et al. Microbial communities in the respiratory tract of patients with interstitial lung disease. *Thorax* 2013;68(12):1150-6.

103. Han MK, Zhou Y, Murray S, et al. Lung microbiome and disease progression in idiopathic pulmonary fibrosis: an analysis of the COMET study. *Lancet Respir Med* 2014;2(7):548-56.

104. Molyneaux PL, Cox MJ, Willis-Owen SA, et al. The role of bacteria in the pathogenesis and progression of idiopathic pulmonary fibrosis. *Am J Respir Crit Care Med* 2014;190(8):906-13.

105. Invernizzi R, Barnett J, Rawal B, et al. Bacterial burden in the lower airways predicts disease progression in idiopathic pulmonary fibrosis and is independent of radiological disease extent. *Eur Respir J* 2020;55(4).

106. Molyneaux PL, Willis-Owen SAG, Cox MJ, et al. Host-Microbial Interactions in Idiopathic Pulmonary Fibrosis. *Am J Respir Crit Care Med* 2017;195(12):1640-50.

107. O'Dwyer DN, Ashley SL, Gurczynski SJ, et al. Lung Microbiota Contribute to Pulmonary Inflammation and Disease Progression in Pulmonary Fibrosis. *Am J Respir Crit Care Med* 2019;199(9):1127-38.

108. Shulgina L, Cahn AP, Chilvers ER, et al. Treating idiopathic pulmonary fibrosis with the addition of co-trimoxazole: a randomised controlled trial. *Thorax* 2013;68(2):155-62.

109. A. W, Hammond M, Clark A, et al. The Efficacy and Mechanism Evaluation of Treating Idiopathic Pulmonary Fibrosis with the Addition of Co-Trimoxazole - A Randomised Controlled Trial *B16. ILD THERAPY II*; 2020 pA2753-A53.

110. Selman M, King TE, Pardo A, et al. Idiopathic pulmonary fibrosis: prevailing and evolving hypotheses about its pathogenesis and implications for therapy. *Ann Intern Med* 2001;134(2):136-51.

111. Parimon T, Yao C, Stripp BR, et al. Alveolar Epithelial Type II Cells as Drivers of Lung Fibrosis in Idiopathic Pulmonary Fibrosis. *Int J Mol Sci* 2020;21(7).

112. Guillot L, Nathan N, Tabary O, et al. Alveolar epithelial cells: master regulators of lung homeostasis. *Int J Biochem Cell Biol* 2013;45(11):2568-73.

113. Mason RJ. Biology of alveolar type II cells. *Respirology* 2006;11 Suppl:S12-5.

114. Barkauskas CE, Cronce MJ, Rackley CR, et al. Type 2 alveolar cells are stem cells in adult lung. *J Clin Invest* 2013;123(7):3025-36.

115. Lamouille S, Xu J, Derynck R. Molecular mechanisms of epithelial-mesenchymal transition. *Nat Rev Mol Cell Biol* 2014;15(3):178-96.

116. Liang J, Zhang Y, Xie T, et al. Hyaluronan and TLR4 promote surfactant-protein-C-positive alveolar progenitor cell renewal and prevent severe pulmonary fibrosis in mice. *Nat Med* 2016;22(11):1285-93.

117. Kropski JA, Blackwell TS. Endoplasmic reticulum stress in the pathogenesis of fibrotic disease. *J Clin Invest* 2018;128(1):64-73.

118. Mora AL, Bueno M, Rojas M. Mitochondria in the spotlight of aging and idiopathic pulmonary fibrosis. *J Clin Invest* 2017;127(2):405-14.

119. Naikawadi RP, Disayabutr S, Mallavia B, et al. Telomere dysfunction in alveolar epithelial cells causes lung remodeling and fibrosis. *JCI Insight* 2016;1(14):e86704.

120. Liu T, Gonzalez De Los Santos F, Zhao Y, et al. Telomerase reverse transcriptase ameliorates lung fibrosis by protecting alveolar epithelial cells against senescence. *J Biol Chem* 2019;294(22):8861-71.

121. Xu Y, Mizuno T, Sridharan A, et al. Single-cell RNA sequencing identifies diverse roles of epithelial cells in idiopathic pulmonary fibrosis. *JCI Insight* 2016;1(20):e90558.

122. Adams TS, Schupp JC, Poli S, et al. Single-cell RNA-seq reveals ectopic and aberrant lung-resident cell populations in idiopathic pulmonary fibrosis. *Sci Adv* 2020;6(28):eaba1983.

123. Habermann AC, Gutierrez AJ, Bui LT, et al. Single-cell RNA sequencing reveals profibrotic roles of distinct epithelial and mesenchymal lineages in pulmonary fibrosis. *Sci Adv* 2020;6(28):eaba1972.

124. Kage H, Borok Z. EMT and interstitial lung disease: a mysterious relationship. *Curr Opin Pulm Med* 2012;18(5):517-23.

125. Hill C, Jones MG, Davies DE, et al. Epithelial-mesenchymal transition contributes to pulmonary fibrosis via aberrant epithelial/fibroblastic cross-talk. *J Lung Health Dis* 2019;3(2):31-35.

126. Wu H, Yu Y, Huang H, et al. Progressive Pulmonary Fibrosis Is Caused by Elevated Mechanical Tension on Alveolar Stem Cells. *Cell* 2020;180(1):107-21.e17.

127. Savla U, Waters CM. Mechanical strain inhibits repair of airway epithelium in vitro. *Am J Physiol* 1998;274(6):L883-92.

128. Muhl L, Genové G, Leptidis S, et al. Single-cell analysis uncovers fibroblast heterogeneity and criteria for fibroblast and mural cell identification and discrimination. *Nat Commun* 2020;11(1):3953.

129. Willis BC, duBois RM, Borok Z. Epithelial origin of myofibroblasts during fibrosis in the lung. *Proc Am Thorac Soc* 2006;3(4):377-82.

130. Beisang DJ, Smith K, Yang L, et al. Single-cell RNA sequencing reveals that lung mesenchymal progenitor cells in IPF exhibit pathological features early in their differentiation trajectory. *Sci Rep* 2020;10(1):11162.

131. Jones MG, Fabre A, Schneider P, et al. Three-dimensional characterization of fibroblast foci in idiopathic pulmonary fibrosis. *JCI Insight* 2016;1(5).

132. Kuhn C, Boldt J, King TE, et al. An immunohistochemical study of architectural remodeling and connective tissue synthesis in pulmonary fibrosis. *Am Rev Respir Dis* 1989;140(6):1693-703.

133. El Agha E, Moiseenko A, Kheirollahi V, et al. Two-Way Conversion between Lipogenic and Myogenic Fibroblastic Phenotypes Marks the Progression and Resolution of Lung Fibrosis. *Cell Stem Cell* 2017;20(4):571.

134. Chambers RC, Mercer PF. Mechanisms of alveolar epithelial injury, repair, and fibrosis. *Ann Am Thorac Soc* 2015;12 Suppl 1:S16-20.

135. Phillips RJ, Burdick MD, Hong K, et al. Circulating fibrocytes traffic to the lungs in response to CXCL12 and mediate fibrosis. *J Clin Invest* 2004;114(3):438-46.

136. Aono Y, Kishi M, Yokota Y, et al. Role of platelet-derived growth factor/platelet-derived growth factor receptor axis in the trafficking of circulating fibrocytes in pulmonary fibrosis. *Am J Respir Cell Mol Biol* 2014;51(6):793-801.

137. Roberts AB, Sporn MB, Assoian RK, et al. Transforming growth factor type beta: rapid induction of fibrosis and angiogenesis in vivo and stimulation of collagen formation in vitro. *Proc Natl Acad Sci U S A* 1986;83(12):4167-71.

138. Yue X, Shan B, Lasky JA. TGF-β: Titan of Lung Fibrogenesis. *Curr Enzym Inhib* 2010;6(2).

139. Coker RK, Laurent GJ, Jeffery PK, et al. Localisation of transforming growth factor beta1 and beta3 mRNA transcripts in normal and fibrotic human lung. *Thorax* 2001;56(7):549-56.

140. Sime PJ, Xing Z, Graham FL, et al. Adenovector-mediated gene transfer of active transforming growth factor-beta1 induces prolonged severe fibrosis in rat lung. *J Clin Invest* 1997;100(4):768-76.

141. Aschner Y, Downey GP. Transforming Growth Factor-β: Master Regulator of the Respiratory System in Health and Disease. *Am J Respir Cell Mol Biol* 2016;54(5):647-55.

142. Grimminger F, Günther A, Vancheri C. The role of tyrosine kinases in the pathogenesis of idiopathic pulmonary fibrosis. *Eur Respir J* 2015;45(5):1426-33.

143. Yao L, Conforti F, Hill C, et al. Paracrine signalling during ZEB1-mediated epithelial-mesenchymal transition augments local myofibroblast differentiation in lung fibrosis. *Cell Death Differ* 2018.

144. Woodcock HV, Eley JD, Guillotin D, et al. The mTORC1/4E-BP1 axis represents a critical signaling node during fibrogenesis. *Nat Commun* 2019;10(1):6.

145. Ando M, Miyazaki E, Ito T, et al. Significance of serum vascular endothelial growth factor level in patients with idiopathic pulmonary fibrosis. *Lung* 2010;188(3):247-52.

146. Vuga LJ, Ben-Yehudah A, Kovkarova-Naumovski E, et al. WNT5A is a regulator of fibroblast proliferation and resistance to apoptosis. *Am J Respir Cell Mol Biol* 2009;41(5):583-9.

147. Königshoff M, Balsara N, Pfaff EM, et al. Functional Wnt signaling is increased in idiopathic pulmonary fibrosis. *PLoS One* 2008;3(5):e2142.

148. Baarsma HA, Königshoff M. : WNT signalling in chronic lung diseases. *Thorax* 2017;72(8):746-59.

149. Henderson WR, Chi EY, Ye X, et al. Inhibition of Wnt/beta-catenin/CREB binding protein (CBP) signaling reverses pulmonary fibrosis. *Proc Natl Acad Sci U S A* 2010;107(32):14309-14.

150. Kaelin WG, Ratcliffe PJ. Oxygen sensing by metazoans: the central role of the HIF hydroxylase pathway. *Mol Cell* 2008;30(4):393-402.

151. Hara S, Hamada J, Kobayashi C, et al. Expression and characterization of hypoxia-inducible factor (HIF)-3alpha in human kidney: suppression of HIF-mediated gene expression by HIF-3alpha. *Biochem Biophys Res Commun* 2001;287(4):808-13.

152. Pugh CW, Ratcliffe PJ. Regulation of angiogenesis by hypoxia: role of the HIF system. *Nat Med* 2003;9(6):677-84.

153. Bodempudi V, Hergert P, Smith K, et al. miR-210 promotes IPF fibroblast proliferation in response to hypoxia. *Am J Physiol Lung Cell Mol Physiol* 2014;307(4):L283-94.

154. Delbrel E, Soumare A, Naguez A, et al. HIF-1α triggers ER stress and CHOP-mediated apoptosis in alveolar epithelial cells, a key event in pulmonary fibrosis. *Sci Rep* 2018;8(1):17939.

155. Higgins DF, Kimura K, Bernhardt WM, et al. Hypoxia promotes fibrogenesis in vivo via HIF-1 stimulation of epithelial-to-mesenchymal transition. *J Clin Invest* 2007;117(12):3810-20.

156. Senavirathna LK, Huang C, Pushparaj S, et al. Hypoxia and transforming growth factor β1 regulation of long non-coding RNA transcriptomes in human pulmonary fibroblasts. *Physiol Rep* 2020;8(1):e14343.

157. Hynes RO, Naba A. Overview of the matrisome--an inventory of extracellular matrix constituents and functions. *Cold Spring Harb Perspect Biol* 2012;4(1):a004903.

158. Burgstaller G, Oehrle B, Gerckens M, et al. The instructive extracellular matrix of the lung: basic composition and alterations in chronic lung disease. *Eur Respir J* 2017;50(1).

159. Faffe DS, Zin WA. Lung parenchymal mechanics in health and disease. *Physiol Rev* 2009;89(3):759-75.

160. Laurent GJ. Rates of collagen synthesis in lung, skin and muscle obtained in vivo by a simplified method using [3H]proline. *Biochem J* 1982;206(3):535-44.

161. Page-McCaw A, Ewald AJ, Werb Z. Matrix metalloproteinases and the regulation of tissue remodelling. *Nat Rev Mol Cell Biol* 2007;8(3):221-33.

162. van der Slot-Verhoeven AJ, van Dura EA, Attema J, et al. The type of collagen cross-link determines the reversibility of experimental skin fibrosis. *Biochim Biophys Acta* 2005;1740(1):60-7.

163. Hynes RO. The extracellular matrix: not just pretty fibrils. *Science* 2009;326(5957):1216-9.

164. Hynes RO. Integrins: bidirectional, allosteric signaling machines. *Cell* 2002;110(6):673-87.

165. Jones MG, Andriotis OG, Roberts JJ, et al. Nanoscale dysregulation of collagen structure-function disrupts mechano-homeostasis and mediates pulmonary fibrosis. *Elife* 2018;7.

166. Pardo A, Cabrera S, Maldonado M, et al. Role of matrix metalloproteinases in the pathogenesis of idiopathic pulmonary fibrosis. *Respir Res* 2016;17:23.

167. Jenkins RG, Simpson JK, Saini G, et al. Longitudinal change in collagen degradation biomarkers in idiopathic pulmonary fibrosis: an analysis from the prospective, multicentre PROFILE study. *Lancet Respir Med* 2015;3(6):462-72.

168. Booth AJ, Hadley R, Cornett AM, et al. Acellular normal and fibrotic human lung matrices as a culture system for in vitro investigation. *Am J Respir Crit Care Med* 2012;186(9):866-76.

169. Huang X, Yang N, Fiore VF, et al. Matrix stiffness-induced myofibroblast differentiation is mediated by intrinsic mechanotransduction. *Am J Respir Cell Mol Biol* 2012;47(3):340-8.

170. Herrera J, Henke CA, Bitterman PB. Extracellular matrix as a driver of progressive fibrosis. *J Clin Invest* 2018;128(1):45-53.

171. Parker MW, Rossi D, Peterson M, et al. Fibrotic extracellular matrix activates a profibrotic positive feedback loop. *J Clin Invest* 2014;124(4):1622-35.

172. Liu F, Mih JD, Shea BS, et al. Feedback amplification of fibrosis through matrix stiffening and COX-2 suppression. *J Cell Biol* 2010;190(4):693-706.

173. Schiller HB, Fässler R. Mechanosensitivity and compositional dynamics of cell-matrix adhesions. *EMBO Rep* 2013;14(6):509-19.

174. Hinz B. Mechanical aspects of lung fibrosis: a spotlight on the myofibroblast. *Proc Am Thorac Soc* 2012;9(3):137-47.

175. Marchioni A, Tonelli R, Rossi G, et al. Ventilatory support and mechanical properties of the fibrotic lung acting as a "squishy ball". *Ann Intensive Care* 2020;10(1):13.

176. Yamauchi M, Sricholpech M. Lysine post-translational modifications of collagen. *Essays Biochem* 2012;52:113-33.

177. Chen Y, Terajima M, Yang Y, et al. Lysyl hydroxylase 2 induces a collagen cross-link switch in tumor stroma. *J Clin Invest* 2015;125(3):1147-62.

178. van der Slot AJ, van Dura EA, de Wit EC, et al. Elevated formation of pyridinoline cross-links by profibrotic cytokines is associated with enhanced lysyl hydroxylase 2b levels. *Biochim Biophys Acta* 2005;1741(1-2):95-102.

179. Umana-Diaz C, Pichol-Thievend C, Marchand MF, et al. Scavenger Receptor Cysteine-Rich domains of Lysyl Oxidase-Like2 regulate endothelial ECM and angiogenesis through non-catalytic scaffolding mechanisms. *Matrix Biol* 2020;88:33-52.

180. Trackman PC. Functional importance of lysyl oxidase family propeptide regions. *J Cell Commun Signal* 2018;12(1):45-53.

181. Moon HJ, Finney J, Ronnebaum T, et al. Human lysyl oxidase-like 2. *Bioorg Chem* 2014;57:231-41.

182. Borel A, Eichenberger D, Farjanel J, et al. Lysyl oxidase-like protein from bovine aorta. Isolation and maturation to an active form by bone morphogenetic protein-1. *J Biol Chem* 2001;276(52):48944-9.

183. Trackman PC. Lysyl Oxidase Isoforms and Potential Therapeutic Opportunities for Fibrosis and Cancer. *Expert Opin Ther Targets* 2016;20(8):935-45.

184. Knott L, Bailey AJ. Collagen cross-links in mineralizing tissues: a review of their chemistry, function, and clinical relevance. *Bone* 1998;22(3):181-7.

185. Eyre DR, Wu J-J. Collagen Cross-Links. In: Brinckmann J, Notbohm H, Müller PK (eds.) *Collagen: Primer in Structure, Processing and Assembly*. Berlin, Heidelberg: Springer Berlin Heidelberg; 2005 p207-29.

186. Nurminskaya MV, Belkin AM. Cellular functions of tissue transglutaminase. *Int Rev Cell Mol Biol* 2012;294:1-97.

187. Verderio EA, Johnson T, Griffin M. Tissue transglutaminase in normal and abnormal wound healing: review article. *Amino Acids* 2004;26(4):387-404.

188. Fulmer JD, Bienkowski RS, Cowan MJ, et al. Collagen concentration and rates of synthesis in idiopathic pulmonary fibrosis. *Am Rev Respir Dis* 1980;122(2):289-301.

189. Selman M, Montaño M, Ramos C, et al. Concentration, biosynthesis and degradation of collagen in idiopathic pulmonary fibrosis. *Thorax* 1986;41(5):355-9.

190. Kirk JM, Da Costa PE, Turner-Warwick M, et al. Biochemical evidence for an increased and progressive deposition of collagen in lungs of patients with pulmonary fibrosis. *Clin Sci (Lond)* 1986;70(1):39-45.

191. Last JA, King TE, Nerlich AG, et al. Collagen cross-linking in adult patients with acute and chronic fibrotic lung disease. Molecular markers for fibrotic collagen. *Am Rev Respir Dis* 1990;141(2):307-13.

192. van der Slot AJ, Zuurmond AM, van den Bogaerdt AJ, et al. Increased formation of pyridinoline cross-links due to higher telopeptide lysyl hydroxylase levels is a general fibrotic phenomenon. *Matrix Biol* 2004;23(4):251-7.

193. Aumiller V, Strobel B, Romeike M, et al. Comparative analysis of lysyl oxidase (like) family members in pulmonary fibrosis. *Sci Rep* 2017;7(1):149.

194. Chien JW, Richards TJ, Gibson KF, et al. Serum lysyl oxidase-like 2 levels and idiopathic pulmonary fibrosis disease progression. *Eur Respir J* 2014;43(5):1430-8.

195. Barry-Hamilton V, Spangler R, Marshall D, et al. Allosteric inhibition of lysyl oxidase-like-2 impedes the development of a pathologic microenvironment. *Nat Med* 2010;16(9):1009-17.

196. Shao S, Zhang X, Duan L, et al. Lysyl Hydroxylase Inhibition by Minoxidil Blocks Collagen Deposition and Prevents Pulmonary Fibrosis via TGF-β_1/Smad3 Signaling Pathway. *Med Sci Monit* 2018;24:8592-601.

197. Gjaltema RA, de Rond S, Rots MG, et al. Procollagen Lysyl Hydroxylase 2 Expression Is Regulated by an Alternative Downstream Transforming Growth Factor β-1 Activation Mechanism. *J Biol Chem* 2015;290(47):28465-76.

198. Song Y, Zheng S, Wang J, et al. Hypoxia-induced PLOD2 promotes proliferation, migration and invasion via PI3K/Akt signaling in glioma. *Oncotarget* 2017;8(26):41947-62.

199. Trapnell C, Williams BA, Pertea G, et al. Transcript assembly and quantification by RNA-Seq reveals unannotated transcripts and isoform switching during cell differentiation. *Nat Biotechnol* 2010;28(5):511-5.

200. Wang F, Flanagan J, Su N, et al. RNAscope: a novel in situ RNA analysis platform for formalin-fixed, paraffin-embedded tissues. *J Mol Diagn* 2012;14(1):22-9.

201. Conforti F, Davies ER, Calderwood CJ, et al. The histone deacetylase inhibitor, romidepsin, as a potential treatment for pulmonary fibrosis. *Oncotarget* 2017;8(30):48737-54.

202. Kemp SJ, Thorley AJ, Gorelik J, et al. Immortalization of human alveolar epithelial cells to investigate nanoparticle uptake. *Am J Respir Cell Mol Biol* 2008;39(5):591-7.

203. Coelho MA, de Carné Trécesson S, Rana S, et al. Oncogenic RAS Signaling Promotes Tumor Immunoresistance by Stabilizing PD-L1 mRNA. *Immunity* 2017;47(6):1083-99.e6.

204. Molina-Arcas M, Hancock DC, Sheridan C, et al. Coordinate direct input of both KRAS and IGF1 receptor to activation of PI3 kinase in KRAS-mutant lung cancer. *Cancer Discov* 2013;3(5):548-63.

205. Witherden IR, Vanden Bon EJ, Goldstraw P, et al. Primary human alveolar type II epithelial cell chemokine release: effects of cigarette smoke and neutrophil elastase. *Am J Respir Cell Mol Biol* 2004;30(4):500-9.

206. Dana H, Chalbatani GM, Mahmoodzadeh H, et al. Molecular Mechanisms and Biological Functions of siRNA. *Int J Biomed Sci* 2017;13(2):48-57.

207. Wenger RH, Kurtcuoglu V, Scholz CC, et al. Frequently asked questions in hypoxia research. *Hypoxia (Auckl)* 2015;3:35-43.

208. Wicks J, Haitchi HM, Holgate ST, et al. Enhanced upregulation of smooth muscle related transcripts by TGF beta2 in asthmatic (myo) fibroblasts. *Thorax* 2006;61(4):313-9.

209. Foldager CB, Munir S, Ulrik-Vinther M, et al. Validation of suitable house keeping genes for hypoxia-cultured human chondrocytes. *BMC Mol Biol* 2009;10:94.

210. Junqueira LC, Bignolas G, Brentani RR. Picrosirius staining plus polarization microscopy, a specific method for collagen detection in tissue sections. *Histochem J* 1979;11(4):447-55.

211. Lattouf R, Younes R, Lutomski D, et al. Picrosirius red staining: a useful tool to appraise collagen networks in normal and pathological tissues. *J Histochem Cytochem* 2014;62(10):751-8.

212. Sang-Won Lee and Jong-Min Lim and Seong-Hee Bhoo and Young-Sook Paik and Tae-Ryong H. Colorimetric determination of amino acids using genipin from Gardenia jasminoides. *Analytica Chimica Acta* 2003;480(2):267-74.

213. NEUMAN RE, LOGAN MA. The determination of hydroxyproline. *J Biol Chem* 1950;184(1):299-306.

214. Gomez B, Ardakani S, Evans BJ, et al. Monoclonal antibody assay for free urinary pyridinium cross-links. *Clin Chem* 1996;42(8 Pt 1):1168-75.

215. Yao C, Guan X, Carraro G, et al. Senescence of Alveolar Type 2 Cells Drives Progressive Pulmonary Fibrosis. *Am J Respir Crit Care Med* 2020.

216. Fernandez IE, Eickelberg O. The impact of TGF-β on lung fibrosis: from targeting to biomarkers. *Proc Am Thorac Soc* 2012;9(3):111-6.

217. Kubiczkova L, Sedlarikova L, Hajek R, et al. TGF-β - an excellent servant but a bad master. *J Transl Med* 2012;10:183.

218. Aquino-Gálvez A, González-Ávila G, Jiménez-Sánchez LL, et al. Dysregulated expression of hypoxia-inducible factors augments myofibroblasts differentiation in idiopathic pulmonary fibrosis. *Respir Res* 2019;20(1):130.

219. Gust L, D'journo XB. The use of correlation functions in thoracic surgery research. *J Thorac Dis* 2015;7(3):E11-5.

220. Wang Y, Zhong S, Schofield CJ, et al. Nuclear entry and export of FIH are mediated by HIF1α and exportin1, respectively. *J Cell Sci* 2018;131(22).

221. Befani C, Mylonis I, Gkotinakou IM, et al. Cobalt stimulates HIF-1-dependent but inhibits HIF-2-dependent gene expression in liver cancer cells. *Int J Biochem Cell Biol* 2013;45(11):2359-68.

222. Chan MC, Atasoylu O, Hodson E, et al. Potent and Selective Triazole-Based Inhibitors of the Hypoxia-Inducible Factor Prolyl-Hydroxylases with Activity in the Murine Brain. *PLoS One* 2015;10(7):e0132004.

223. Schietke R, Warnecke C, Wacker I, et al. The lysyl oxidases LOX and LOXL2 are necessary and sufficient to repress E-cadherin in hypoxia: insights into cellular transformation processes mediated by HIF-1. *J Biol Chem* 2010;285(9):6658-69.

224. Deng Z, Fear MW, Suk Choi Y, et al. The extracellular matrix and mechanotransduction in pulmonary fibrosis. *Int J Biochem Cell Biol* 2020:105802.

225. Saito H, Papaconstantinou J, Sato H, et al. Regulation of a novel gene encoding a lysyl oxidase-related protein in cellular adhesion and senescence. *J Biol Chem* 1997;272(13):8157-60.

226. Semenza GL, Nejfelt MK, Chi SM, et al. Hypoxia-inducible nuclear factors bind to an enhancer element located 3' to the human erythropoietin gene. *Proc Natl Acad Sci U S A* 1991;88(13):5680-4.

227. Maxwell PH, Pugh CW, Ratcliffe PJ. Inducible operation of the erythropoietin 3' enhancer in multiple cell lines: evidence for a widespread oxygen-sensing mechanism. *Proc Natl Acad Sci U S A* 1993;90(6):2423-7.

228. Wang GL, Jiang BH, Rue EA, et al. Hypoxia-inducible factor 1 is a basic-helix-loop-helix-PAS heterodimer regulated by cellular O2 tension. *Proc Natl Acad Sci U S A* 1995;92(12):5510-4.

229. Bruick RK, McKnight SL. A conserved family of prolyl-4-hydroxylases that modify HIF. *Science* 2001;294(5545):1337-40.

230. Ivan M, Haberberger T, Gervasi DC, et al. Biochemical purification and pharmacological inhibition of a mammalian prolyl hydroxylase acting on hypoxia-inducible factor. *Proc Natl Acad Sci U S A* 2002;99(21):13459-64.

231. Epstein AC, Gleadle JM, McNeill LA, et al. C. elegans EGL-9 and mammalian homologs define a family of dioxygenases that regulate HIF by prolyl hydroxylation. *Cell* 2001;107(1):43-54.

232. Mahon PC, Hirota K, Semenza GL. FIH-1: a novel protein that interacts with HIF-1alpha and VHL to mediate repression of HIF-1 transcriptional activity. *Genes Dev* 2001;15(20):2675-86.

233. Fallah J, Rini BI. HIF Inhibitors: Status of Current Clinical Development. *Curr Oncol Rep* 2019;21(1):6.

234. Jaakkola P, Mole DR, Tian YM, et al. Targeting of HIF-alpha to the von Hippel-Lindau ubiquitylation complex by O2-regulated prolyl hydroxylation. *Science* 2001;292(5516):468-72.

235. Lando D, Peet DJ, Whelan DA, et al. Asparagine hydroxylation of the HIF transactivation domain a hypoxic switch. *Science* 2002;295(5556):858-61.

236. Watts ER, Walmsley SR. Inflammation and Hypoxia: HIF and PHD Isoform Selectivity. *Trends Mol Med* 2019;25(1):33-46.

237. Appelhoff RJ, Tian YM, Raval RR, et al. Differential function of the prolyl hydroxylases PHD1, PHD2, and PHD3 in the regulation of hypoxia-inducible factor. *J Biol Chem* 2004;279(37):38458-65.

238. Meneses AM, Wielockx B. PHD2: from hypoxia regulation to disease progression. *Hypoxia (Auckl)* 2016;4:53-67.

239. Chan MC, Ilott NE, Schödel J, et al. Tuning the Transcriptional Response to Hypoxia by Inhibiting Hypoxia-inducible Factor (HIF) Prolyl and Asparaginyl Hydroxylases. *J Biol Chem* 2016;291(39):20661-73.

240. Groenman F, Rutter M, Caniggia I, et al. Hypoxia-inducible factors in the first trimester human lung. *J Histochem Cytochem* 2007;55(4):355-63.

241. Grover TR, Asikainen TM, Kinsella JP, et al. Hypoxia-inducible factors HIF-1alpha and HIF-2alpha are decreased in an experimental model of severe respiratory distress syndrome in preterm lambs. *Am J Physiol Lung Cell Mol Physiol* 2007;292(6):L1345-51.

242. van Tuyl M, Liu J, Wang J, et al. Role of oxygen and vascular development in epithelial branching morphogenesis of the developing mouse lung. *Am J Physiol Lung Cell Mol Physiol* 2005;288(1):L167-78.

243. Asikainen TM, Ahmad A, Schneider BK, et al. Effect of preterm birth on hypoxia-inducible factors and vascular endothelial growth factor in primate lungs. *Pediatr Pulmonol* 2005;40(6):538-46.

244. Shimoda LA, Semenza GL. HIF and the lung: role of hypoxia-inducible factors in pulmonary development and disease. *Am J Respir Crit Care Med* 2011;183(2):152-6.

245. Haase VH. Pathophysiological Consequences of HIF Activation: HIF as a modulator of fibrosis. *Ann N Y Acad Sci* 2009;1177:57-65.

246. Senavirathna LK, Huang C, Yang X, et al. Hypoxia induces pulmonary fibroblast proliferation through NFAT signaling. *Sci Rep* 2018;8(1):2709.

247. Tzouvelekis A, Harokopos V, Paparountas T, et al. Comparative expression profiling in pulmonary fibrosis suggests a role of hypoxia-inducible factor-1alpha in disease pathogenesis. *Am J Respir Crit Care Med* 2007;176(11):1108-19.

248. Madsen CD, Pedersen JT, Venning FA, et al. Hypoxia and loss of PHD2 inactivate stromal fibroblasts to decrease tumour stiffness and metastasis. *EMBO Rep* 2015;16(10):1394-408.

249. Stegen S, Laperre K, Eelen G, et al. HIF-1α metabolically controls collagen synthesis and modification in chondrocytes. *Nature* 2019;565(7740):511-15.

250. Gilkes DM, Bajpai S, Chaturvedi P, et al. Hypoxia-inducible factor 1 (HIF-1) promotes extracellular matrix remodeling under hypoxic conditions by inducing P4HA1, P4HA2, and PLOD2 expression in fibroblasts. *J Biol Chem* 2013;288(15):10819-29.

251. Wykoff CC, Beasley NJ, Watson PH, et al. Hypoxia-inducible expression of tumor-associated carbonic anhydrases. *Cancer Res* 2000;60(24):7075-83.

252. Jain M, Sznajder JI. Effects of hypoxia on the alveolar epithelium. *Proc Am Thorac Soc* 2005;2(3):202-5.

253. Höckel M, Vaupel P. Tumor hypoxia: definitions and current clinical, biologic, and molecular aspects. *J Natl Cancer Inst* 2001;93(4):266-76.

254. Mizuno S, Bogaard HJ, Voelkel NF, et al. Hypoxia regulates human lung fibroblast proliferation via p53-dependent and -independent pathways. *Respir Res* 2009;10:17.

255. Tian YM, Yeoh KK, Lee MK, et al. Differential sensitivity of hypoxia inducible factor hydroxylation sites to hypoxia and hydroxylase inhibitors. *J Biol Chem* 2011;286(15):13041-51.

256. Movafagh S, Crook S, Vo K. Regulation of hypoxia-inducible factor-1a by reactive oxygen species: new developments in an old debate. *J Cell Biochem* 2015;116(5):696-703.

257. Pan Y, Mansfield KD, Bertozzi CC, et al. Multiple factors affecting cellular redox status and energy metabolism modulate hypoxia-inducible factor prolyl hydroxylase activity in vivo and in vitro. *Mol Cell Biol* 2007;27(3):912-25.

258. Sonveaux P, Copetti T, De Saedeleer CJ, et al. Targeting the lactate transporter MCT1 in endothelial cells inhibits lactate-induced HIF-1 activation and tumor angiogenesis. *PLoS One* 2012;7(3):e33418.

259. Jung SY, Song HS, Park SY, et al. Pyruvate promotes tumor angiogenesis through HIF-1-dependent PAI-1 expression. *Int J Oncol* 2011;38(2):571-6.

260. Ravenna L, Salvatori L, Russo MA. HIF3α: the little we know. *FEBS J* 2016;283(6):993-1003.

261. Maynard MA, Qi H, Chung J, et al. Multiple splice variants of the human HIF-3 alpha locus are targets of the von Hippel-Lindau E3 ubiquitin ligase complex. *J Biol Chem* 2003;278(13):11032-40.

262. Mao P, Wu S, Li J, et al. Human alveolar epithelial type II cells in primary culture. *Physiol Rep* 2015;3(2).

263. Myllyharju J. Prolyl 4-hydroxylases, the key enzymes of collagen biosynthesis. *Matrix Biol* 2003;22(1):15-24.

264. Baader E, Tschank G, Baringhaus KH, et al. Inhibition of prolyl 4-hydroxylase by oxalyl amino acid derivatives in vitro, in isolated microsomes and in embryonic chicken tissues. *Biochem J* 1994;300 (Pt 2):525-30.

265. Gelse K, Pfander D, Obier S, et al. Role of hypoxia-inducible factor 1 alpha in the integrity of articular cartilage in murine knee joints. *Arthritis Res Ther* 2008;10(5):R111.

266. Falcon JM, Chirman D, Veneziale A, et al. DMOG Negatively Impacts Tissue Engineered Cartilage Development. *Cartilage* 2020:1947603520967060.

267. Basu RK, Hubchak S, Hayashida T, et al. Interdependence of HIF-1α and TGF-β/Smad3 signaling in normoxic and hypoxic renal epithelial cell collagen expression. *Am J Physiol Renal Physiol* 2011;300(4):F898-905.

268. Mingyuan X, Qianqian P, Shengquan X, et al. Hypoxia-inducible factor-1α activates transforming growth factor-β1/Smad signaling and increases collagen deposition in dermal fibroblasts. *Oncotarget* 2018;9(3):3188-97.

269. Qian F, He M, Duan W, et al. Cross regulation between hypoxia-inducible transcription factor-1α (HIF-1α) and transforming growth factor (TGF)-ß1 mediates nickel oxide nanoparticles (NiONPs)-induced pulmonary fibrosis. *Am J Transl Res* 2015;7(11):2364-78.

270. Ueno M, Maeno T, Nomura M, et al. Hypoxia-inducible factor-1α mediates TGF-β-induced PAI-1 production in alveolar macrophages in pulmonary fibrosis. *Am J Physiol Lung Cell Mol Physiol* 2011;300(5):L740-52.

271. Rosell-García T, Palomo-Álvarez O, Rodríguez-Pascual F. A hierarchical network of hypoxia-inducible factor and SMAD proteins governs procollagen lysyl hydroxylase 2 induction by hypoxia and transforming growth factor β1. *J Biol Chem* 2019;294(39):14308-18.

272. Trackman PC. Diverse biological functions of extracellular collagen processing enzymes. *J Cell Biochem* 2005;96(5):927-37.

273. Milkiewicz M, Pugh CW, Egginton S. Inhibition of endogenous HIF inactivation induces angiogenesis in ischaemic skeletal muscles of mice. *J Physiol* 2004;560(Pt 1):21-6.

274. Berra E, Benizri E, Ginouvès A, et al. HIF prolyl-hydroxylase 2 is the key oxygen sensor setting low steady-state levels of HIF-1alpha in normoxia. *EMBO J* 2003;22(16):4082-90.

275. Thoms BL, Murphy CL. Inhibition of hypoxia-inducible factor-targeting prolyl hydroxylase domain-containing protein 2 (PHD2) enhances matrix synthesis by human chondrocytes. *J Biol Chem* 2010;285(27):20472-80.

276. Cheng S, Aghajanian P, Pourteymoor S, et al. Prolyl Hydroxylase Domain-Containing Protein 2 (Phd2) Regulates Chondrocyte Differentiation and Secondary Ossification in Mice. *Sci Rep* 2016;6:35748.

277. Dai Z, Li M, Wharton J, et al. Prolyl-4 Hydroxylase 2 (PHD2) Deficiency in Endothelial Cells and Hematopoietic Cells Induces Obliterative Vascular Remodeling and Severe Pulmonary Arterial Hypertension in Mice and Humans Through Hypoxia-Inducible Factor-2α. *Circulation* 2016;133(24):2447-58.

278. Chowdhury R, Candela-Lena JI, Chan MC, et al. Selective small molecule probes for the hypoxia inducible factor (HIF) prolyl hydroxylases. *ACS Chem Biol* 2013;8(7):1488-96.

279. Ebihara T, Venkatesan N, Tanaka R, et al. Changes in extracellular matrix and tissue viscoelasticity in bleomycin-induced lung fibrosis. Temporal aspects. *Am J Respir Crit Care Med* 2000;162(4 Pt 1):1569-76.

280. Tanaka N, Kato H, Inose T, et al. Expression of carbonic anhydrase 9, a potential intrinsic marker of hypoxia, is associated with poor prognosis in oesophageal squamous cell carcinoma. *Br J Cancer* 2008;99(9):1468-75.

281. Zhang H, Qian DZ, Tan YS, et al. Digoxin and other cardiac glycosides inhibit HIF-1alpha synthesis and block tumor growth. *Proc Natl Acad Sci U S A* 2008;105(50):19579-86.

282. Wong CC, Zhang H, Gilkes DM, et al. Inhibitors of hypoxia-inducible factor 1 block breast cancer metastatic niche formation and lung metastasis. *J Mol Med (Berl)* 2012;90(7):803-15.

283. Kong D, Park EJ, Stephen AG, et al. Echinomycin, a small-molecule inhibitor of hypoxia-inducible factor-1 DNA-binding activity. *Cancer Res* 2005;65(19):9047-55.

284. Bailey CM, Liu Y, Peng G, et al. Liposomal formulation of HIF-1α inhibitor echinomycin eliminates established metastases of triple-negative breast cancer. *Nanomedicine* 2020;29:102278.

285. Wang Y, Liu Y, Bailey C, et al. Therapeutic targeting of TP53-mutated acute myeloid leukemia by inhibiting HIF-1α with echinomycin. *Oncogene* 2020;39(14):3015-27.

286. Chau NM, Rogers P, Aherne W, et al. Identification of novel small molecule inhibitors of hypoxia-inducible factor-1 that differentially block hypoxia-inducible factor-1 activity and hypoxia-inducible factor-1alpha induction in response to hypoxic stress and growth factors. *Cancer Res* 2005;65(11):4918-28.

287. Baker LC, Boult JK, Walker-Samuel S, et al. The HIF-pathway inhibitor NSC-134754 induces metabolic changes and anti-tumour activity while maintaining vascular function. *Br J Cancer* 2012;106(10):1638-47.

288. Carroll VA, Ashcroft M. Role of hypoxia-inducible factor (HIF)-1alpha versus HIF-2alpha in the regulation of HIF target genes in response to hypoxia, insulin-like growth factor-I, or loss of von Hippel-Lindau function: implications for targeting the HIF pathway. *Cancer Res* 2006;66(12):6264-70.

289. Jackson AL, Linsley PS. Recognizing and avoiding siRNA off-target effects for target identification and therapeutic application. *Nat Rev Drug Discov* 2010;9(1):57-67.

290. Jackson AL, Linsley PS. Noise amidst the silence: off-target effects of siRNAs? *Trends Genet* 2004;20(11):521-4.

291. Ran FA, Hsu PD, Wright J, et al. Genome engineering using the CRISPR-Cas9 system. *Nat Protoc* 2013;8(11):2281-308.

292. Piret JP, Mottet D, Raes M, et al. Is HIF-1alpha a pro- or an anti-apoptotic protein? *Biochem Pharmacol* 2002;64(5-6):889-92.

293. Yu T, Tang B, Sun X. Development of Inhibitors Targeting Hypoxia-Inducible Factor 1 and 2 for Cancer Therapy. *Yonsei Med J* 2017;58(3):489-96.

294. Zuurmond AM, van der Slot-Verhoeven AJ, van Dura EA, et al. Minoxidil exerts different inhibitory effects on gene expression of lysyl hydroxylase 1, 2, and 3: implications for collagen cross-linking and treatment of fibrosis. *Matrix Biol* 2005;24(4):261-70.

295. Olsen KC, Sapinoro RE, Kottmann RM, et al. Transglutaminase 2 and its role in pulmonary fibrosis. *Am J Respir Crit Care Med* 2011;184(6):699-707.

296. Simon DD, Niklason LE, Humphrey JD. Tissue Transglutaminase, Not Lysyl Oxidase, Dominates Early Calcium-Dependent Remodeling of Fibroblast-Populated Collagen Lattices. *Cells Tissues Organs* 2014;200(2):104-17.

297. Zonca S, Pinton G, Wang Z, et al. Tissue transglutaminase (TG2) enables survival of human malignant pleural mesothelioma cells in hypoxia. *Cell Death Dis* 2017;8(2):e2592.

298. Iommarini L, Porcelli AM, Gasparre G, et al. Non-Canonical Mechanisms Regulating Hypoxia-Inducible Factor 1 Alpha in Cancer. *Front Oncol* 2017;7:286.

299. Kottmann RM, Kulkarni AA, Smolnycki KA, et al. Lactic acid is elevated in idiopathic pulmonary fibrosis and induces myofibroblast differentiation via pH-dependent activation of transforming growth factor-β. *Am J Respir Crit Care Med* 2012;186(8):740-51.

300. Maher TM. Aerobic Glycolysis and the Warburg Effect. An Unexplored Realm in the Search for Fibrosis Therapies? *Am J Respir Crit Care Med* 2015;192(12):1407-9.

301. Xie N, Tan Z, Banerjee S, et al. Glycolytic Reprogramming in Myofibroblast Differentiation and Lung Fibrosis. *Am J Respir Crit Care Med* 2015;192(12):1462-74.

302. Cheresh P, Kim SJ, Tulasiram S, et al. Oxidative stress and pulmonary fibrosis. *Biochim Biophys Acta* 2013;1832(7):1028-40.

303. Hecker L. Mechanisms and consequences of oxidative stress in lung disease: therapeutic implications for an aging populace. *Am J Physiol Lung Cell Mol Physiol* 2018;314(4):L642-L53.

304. Masson N, Singleton RS, Sekirnik R, et al. The FIH hydroxylase is a cellular peroxide sensor that modulates HIF transcriptional activity. *EMBO Rep* 2012;13(3):251-7.

305. Cantin AM, North SL, Fells GA, et al. Oxidant-mediated epithelial cell injury in idiopathic pulmonary fibrosis. *J Clin Invest* 1987;79(6):1665-73.

306. Psathakis K, Mermigkis D, Papatheodorou G, et al. Exhaled markers of oxidative stress in idiopathic pulmonary fibrosis. *Eur J Clin Invest* 2006;36(5):362-7.

307. Strausz J, Müller-Quernheim J, Steppling H, et al. Oxygen radical production by alveolar inflammatory cells in idiopathic pulmonary fibrosis. *Am Rev Respir Dis* 1990;141(1):124-8.

308. Cantin AM, Hubbard RC, Crystal RG. Glutathione deficiency in the epithelial lining fluid of the lower respiratory tract in idiopathic pulmonary fibrosis. *Am Rev Respir Dis* 1989;139(2):370-2.

309. van der Vaart H, Postma DS, Timens W, et al. Acute effects of cigarette smoke on inflammation and oxidative stress: a review. *Thorax* 2004;59(8):713-21.

310. Chuang KJ, Chan CC, Su TC, et al. The effect of urban air pollution on inflammation, oxidative stress, coagulation, and autonomic dysfunction in young adults. *Am J Respir Crit Care Med* 2007;176(4):370-6.

311. McMahon S, Charbonneau M, Grandmont S, et al. Transforming growth factor beta1 induces hypoxia-inducible factor-1 stabilization through selective inhibition of PHD2 expression. *J Biol Chem* 2006;281(34):24171-81.

312. Görlach A, Diebold I, Schini-Kerth VB, et al. Thrombin activates the hypoxia-inducible factor-1 signaling pathway in vascular smooth muscle cells: Role of the p22(phox)-containing NADPH oxidase. *Circ Res* 2001;89(1):47-54.

313. Metzen E, Wolff M, Fandrey J, et al. Pericellular PO2 and O2 consumption in monolayer cell cultures. *Respir Physiol* 1995;100(2):101-6.

314. Sheta EA, Trout H, Gildea JJ, et al. Cell density mediated pericellular hypoxia leads to induction of HIF-1alpha via nitric oxide and Ras/MAP kinase mediated signaling pathways. *Oncogene* 2001;20(52):7624-34.

315. Philp CJ, Siebeke I, Clements D, et al. Extracellular Matrix Cross-Linking Enhances Fibroblast Growth and Protects against Matrix Proteolysis in Lung Fibrosis. *Am J Respir Cell Mol Biol* 2018;58(5):594-603.

316. Penumatsa KC, Toksoz D, Warburton RR, et al. Role of hypoxia-induced transglutaminase 2 in pulmonary artery smooth muscle cell proliferation. *Am J Physiol Lung Cell Mol Physiol* 2014;307(7):L576-85.

317. Kumar S, Mehta K. Tissue transglutaminase constitutively activates HIF-1α promoter and nuclear factor-κB via a non-canonical pathway. *PLoS One* 2012;7(11):e49321.

318. Kyung SY, Byun KH, Yoon JY, et al. Advanced glycation end-products and receptor for advanced glycation end-products expression in patients with idiopathic pulmonary fibrosis and NSIP. *Int J Clin Exp Pathol* 2014;7(1):221-8.

319. Matsuse T, Ohga E, Teramoto S, et al. Immunohistochemical localisation of advanced glycation end products in pulmonary fibrosis. *J Clin Pathol* 1998;51(7):515-9.

320. Gopal P, Gosker HR, Theije CC, et al. Effect of chronic hypoxia on RAGE and its soluble forms in lungs and plasma of mice. *Biochim Biophys Acta* 2015;1852(5):992-1000.

321. Gilkes DM, Xiang L, Lee SJ, et al. Hypoxia-inducible factors mediate coordinated RhoA-ROCK1 expression and signaling in breast cancer cells. *Proc Natl Acad Sci U S A* 2014;111(3):E384-93.

322. Herrera I, Cisneros J, Maldonado M, et al. Matrix metalloproteinase (MMP)-1 induces lung alveolar epithelial cell migration and proliferation, protects from apoptosis, and represses mitochondrial oxygen consumption. *J Biol Chem* 2013;288(36):25964-75.

323. Bonnans C, Chou J, Werb Z. Remodelling the extracellular matrix in development and disease. *Nat Rev Mol Cell Biol* 2014;15(12):786-801.

324. Chen CZ, Peng YX, Wang ZB, et al. The Scar-in-a-Jar: studying potential antifibrotic compounds from the epigenetic to extracellular level in a single well. *Br J Pharmacol* 2009;158(5):1196-209.

325. Good RB, Eley JD, Gower E, et al. A high content, phenotypic 'scar-in-a-jar' assay for rapid quantification of collagen fibrillogenesis using disease-derived pulmonary fibroblasts. *BMC Biomed Eng* 2019;1:14.

326. B Moore B, Lawson WE, Oury TD, et al. Animal models of fibrotic lung disease. *Am J Respir Cell Mol Biol* 2013;49(2):167-79.

327. Jenkins RG, Moore BB, Chambers RC, et al. An Official American Thoracic Society Workshop Report: Use of Animal Models for the Preclinical Assessment of Potential Therapies for Pulmonary Fibrosis. *Am J Respir Cell Mol Biol* 2017;56(5):667-79.

328. Moeller A, Ask K, Warburton D, et al. The bleomycin animal model: a useful tool to investigate treatment options for idiopathic pulmonary fibrosis? *Int J Biochem Cell Biol* 2008;40(3):362-82.

329. Rodriguez HM, Vaysberg M, Mikels A, et al. Modulation of lysyl oxidase-like 2 enzymatic activity by an allosteric antibody inhibitor. *J Biol Chem* 2010;285(27):20964-74.

330. Devkota AK, Veloria JR, Guo HF, et al. Development of a High-Throughput Lysyl Hydroxylase (LH) Assay and Identification of Small-Molecule Inhibitors against LH2. *SLAS Discov* 2019;24(4):484-91.